Spline and Finite Difference Based Schemes for Time-Fractional Initial Boundary Value Problems

THESIS

Submitted in partial fulfillment of the requirements

for the degree of

DOCTOR OF PHILOSOPHY

by

Renu Choudhary

ID No. 2020PHXF0048P

Under the Supervision of

Prof. Devendra Kumar

Birla Institute of Technology and Science, Pilani, Pilani Campus, India

BITS Pilani

Pilani | Dubai | Goa | H derabad | Mumbai

BIRLA INSTITUTE OF TECHNOLOGY AND SCIENCE, PILANI

Pilani Campus, Rajasthan, India

[2024]

BIRLA INSTITUTE OF TECHNOLOGY AND SCIENCE, PILANI

PILANI CAMPUS, RAJASTHAN, INDIA

CERTIFICATE

This is to certify that the thesis entitled, **"Spline and Finite Difference Based Schemes for Time-Fractional Initial Boundary Value Problems."** and submitted by **Ms. Renu Choudhary** ID No. **2020PHXF0048P** for the award of Ph.D. degree of the institute embodies original work done by her under my supervision.

_____

Signature of the Supervisor

Name : **Prof. Devendra Kumar**

Designation : **Professor, Department of Mathematics, BITS Pilani, Pilani Campus**

Date: __/__/____

Dedicated to
My Beloved Family

ACKNOWLEDGEMENTS

It is an easy and enjoyable journey when you have the support of many people. Many individuals have accompanied and encouraged me throughout my Ph.D. journey. It's a beautiful gift from God that I can thank them all for.

First and foremost, I want to convey my heartfelt thanks and gratitude to my thesis supervisor, Prof. Devendra Kumar, for his invaluable assistance and constant support during my Ph.D. journey. My cognitive processes and creative thinking evolved under his inspiring mentoring. His expertise and unending desire for greatness motivated me to strive harder. His simplicity and compassion, attention to detail, hard work, and patience have set an example I aim to emulate someday.

I am also grateful to BITS Pilani's Department of Mathematics teachers for their support and insightful ideas in my research effort. I thank my Doctoral Advisory Committee (DAC) members, Dr. Ashish Tiwari and Dr. Sangita Yadav, for their consistent encouragement and assistance in keeping my work on track. Their recommendations and opinions have helped me better my work at different levels.

I am also thankful to my senior, Mr. Satpal Singh, for his continuous support and guidance. He is my coauthor and has assisted me like a co-guide in my journey toward my Ph.D.

As everyone is thankful to their parents for giving birth and upbringing them, I am also grateful to my parents (Let. Raghuveer Prasad Choudhary and Mrs. Vimala Devi). I wish to thank my mother for believing in me more than I did. Their unwavering support and profound understanding motivated me throughout my Ph.D. and life. I also want to thank my brother, Mr. Vinod Kumar, for lending a sympathetic ear and supporting me. I am eternally grateful to my whole family for their faith in me, which gave me the enthusiasm to complete this happening. I am also thankful to the office personnel who assisted me with all the requirements.

I want to acknowledge the financial support from the Department of Science and Technology (DST), Ministry of Science and Technology, Government of India, and BITS Pilani, Pilani Campus.

Finally, I want to express my heartfelt thanks to Acharya Prashant, the founder of the Advait Foundation, who was never present with me but whose teachings are always with me to support me.

I regret mistakenly leaving out anybody who has offered encouragement or inspiration over this journey. Your gifts will not be forgotten.

Place: BITS Pilani, Pilani Campus
Date: __/__/____ **(Renu Choudhary)**

ABSTRACT

The characteristics of non-integer-order derivatives and integrals are discovered using fractional calculus. This topic has grown in popularity and relevance over the past few decades because of its use in several engineering sectors, including bioscience, finance, signal processing, viscoelasticity, and technology. The fundamental advantage of fractional derivatives over typical integer-order derivatives is that they consider memory and heredity aspects of different processes. On the other hand, such considerations are not taken into account. Thus, the properties of fractional derivatives inspired us to investigate and solve time-fractional partial differential equations. In most cases, an exact solution of the time-fractional partial differential equation is difficult to obtain; hence, an approximation or numerical solution is necessary to understand the behavior of such fractional equations.

In Chapter 1, we have given a basic overview of fractional calculus. Some fundamental features and definitions related to fractional derivatives have also been presented. A literature survey also includes the most recent findings and contributions in theory and methodology about our current study activity. A brief introduction to the subsequent chapters is provided.

Chapter 2 presents a numerical approach for a class of time-fractional convection-reaction-diffusion problems with a time lag. In the Caputo notion, time-fractional derivatives are examined. The numerical strategy uses Crank and Nicolson's discretization technique in the temporal direction and spline functions with a tension factor in the spatial direction. The scheme is conditionally stable, according to the Von-Neumann stability analysis. In addition, the Fourier series is used to offer a thorough convergence analysis. Two numerical test problems are addressed to validate the suggested numerical scheme's efficacy.

The third chapter concerns constructing and analyzing a higher-order stable numerical approximation for the time fractional Kuramoto-Sivashinsky (K-S) problem, a fourth-order nonlinear equation. In the studied issue, the fractional derivative of order $\gamma \in (0, 1)$ is taken into Caputo meaning and approximated using the $L1-2$ technique. To estimate the derivatives and solve the problem in space, the discretization technique employs quintic $\mathfrak{B}$-spline functions. We produced unconditional stability findings and rate of accuracy convergence $\mathcal{O}(h^2 + k^2)$, where h and k represent the space and time step sizes, respectively.

We have also seen that the linearized form of the K-S equation leads to $\mathcal{O}(h^2 + k^{3-\gamma})$ accuracy. The current method is also quite successful for solving the time-fractional Burgers equation. We demonstrated that the current strategy outperforms the L1 scheme with the exact computing cost for many linear and nonlinear problems with classical and fractional time derivatives.

The fourth chapter seeks a dependable numerical approach for solving the Allen-Cahn equation using the Caputo time-fractional derivative. The technique of fractional derivative semi-discretization utilizing second-order finite differences is presented first. The cubic B-spline collocation approach is applied to obtain a complete discretization. The conditional stability and convergence of the proposed technique are demonstrated. The method's efficiency is proven using numerical examples from two test issues. A numerical study validates the effectiveness of the methodology and the method's continuous accuracy.

Chapter 5 uses the generalized time-fractional Fisher's equation to illustrate the system's dynamics. The study of appropriate numerical techniques for this problem has significant scientific and practical significance. In that vein, this study offers a high-order numerical approach for the generalized time-fractional Fisher's equation and its design and analysis. The time-fractional derivative is computed in the Caputo sense and approximated via Euler backward discretization. To linearize the problem, the quasilinearization approach is employed, and then a compact finite difference scheme is proposed for discretizing the equation in the space direction. Our numerical technique is $O(k^{2-\alpha} + h^4)$ convergent, where h and k are stepped sizes in the spatial and temporal directions, respectively. Three issues are quantitatively tested using the suggested strategy, and the results show that the proposed method is appropriate for solving this problem.

The predictor-corrector method (PCM) is investigated in Chapter 6 to solve a nonlinear, two-dimensional fractional-order predator-prey model. This model's carrying capacity is one. The fractional order derivative (MABC derivative) resides above the modified Atangana-Baleanu fractional derivative in the Caputo sense. PCM has an edge over other approaches because of its smoothness and speed of implementation. The computational results correspond to two methods reported by Srivastava *et al.* . In [1], HPSTM, and HASTM, the computational results are graphed for various derivative values to show the variance of carnivore and pursued

populations.

In Chapter 7, we have discussed the conclusion of the thesis work and future dimensions in the numerical solutions of fractional partial differential equations and fractional order systems.

Contents

List of Tables

List of Figures

Chapter 1

Introduction

1.1 Fractional Calculus

Fractional calculus was developed in the 18th century by mathematicians such as Joseph Fourier and Augustin-Louis Cauchy. However, in the twentieth century, fractional calculus achieved widespread acceptance and began to be studied methodically. Fractional calculus, also known as fractional differentiation and integration or calculus of fractions, is a field of mathematics that extends the principles of differentiation and integration to non-integer or fractional orders. It is a sophisticated and adaptable mathematical instrument with applications in physics, engineering, economics, biology, and signal processing. The conventional calculus of Isaac Newton and Gottfried Wilhelm Leibniz concerns integer orders of differentiation and integration. Fractional calculus extends these ideas by allowing non-integer orders like $1/2$, $3/4$, or any other real or complex number. This addition enables describing and evaluating phenomena with complicated behavior, memory effects, and non-local interactions, which integer-order calculus frequently needs to address. There are two basic procedures in fractional calculus: fractional differentiation and fractional integration. Fractional differentiation extends integration to fractional orders by generalizing the notion of obtaining the nth derivative of a function. These processes have many applications, including long-term memory models, fractals, viscoelastic materials, and power-law systems.

Though fractional calculus has a long history and is as old as classical calculus, people only applied it to the problems arising in science and engineering for a short time. However, with its wide applications, fractional calculus began to attract the increasing attention of researchers and scientists in the last few decades. In 1695, Leibnitz devised both the notations $\frac{d^n}{dx^n}f(x)$ and $\int f(x)dx$; then L'Hospital asked Leibnitz, "What is the meaning of the notation $\frac{d^n}{dx^n}f(x)$ for $n = 1/2$?" In a September 30, 1695 letter, Leibniz wrote to L'Hospital, "This is an apparent paradox from which useful consequences will be drawn one day." After this, several prominent mathematicians, including Riemann and Liouville, were the first to lay the foundation of fractional calculus. The first book published in 1974 by Oldham and Spanier [2] is solely devoted to fractional calculus. They have observed that the derivatives and integrals of fractional orders are more valuable than the integer derivatives and integrals. It motivates them towards the fundamental mathematical properties of the fractional differential and integral operators and the applications of arbitrary order operators. Later, several authors, such as Kilbas *et al.* [3], Li and Zeng [4], Miller and Ross [5], and Podlubny [6], published several books on the theory and applications of fractional integrals and derivatives. For a good survey paper on applying fractional derivatives in modern mechanics, the readers are referred to [7]. Fractional calculus has proven its efficiency and aptitude to simulate anomalous behavior in several disciplines of science, engineering, and finance during the previous two decades. Many fractional calculus applications have emerged in recent years, some of which are listed below. Important phenomena in different areas like physics [8, 9], control theory [10], fluid mechanics [11, 12], chemistry and biology [13–15], and quantum mechanics [16] are modeled using the fractional order differential equations. For many more applications, we refer to [17–28]. Without using fractional calculus, one cannot model these problems appropriately. As a result, the theories and applications of the fractional differential and integral operators are well established, and their applicability to the problems arising in the areas mentioned above is being considered extensively. It has been shown that the fractional-order models are better than the integer models for complex systems with memory and genetic effects. The problems with fractional derivatives are mainly classified into two categories, namely, space-fractional and time-fractional.

Fractional calculus has been used in a variety of domains, including:

- **Physics:** It models anomalous diffusion, non-Newtonian fluids, and electrical circuits with fractal geometries.

- **Engineering:** Fractional calculus is used in control systems, signal processing, and investigating materials with memory qualities.

- **Biology:** It aids in simulating biological systems with long-term memory, such as disease propagation and population dynamics.

- **Economics:** Its applications include financial market simulation, stochastic process simulation, and time series analysis.

- **Medicine:** Fractional calculus is applied to describe physiological processes having memory effects, such as blood flow and medication dispersion.

- **Geophysics:** It is employed in analyzing seismic signals and the fractal features of geological formations.

To summarize, fractional calculus is a solid mathematical device that extends classical calculus principles to non-integer orders, enabling us to better comprehend and describe complicated events in various scientific and engineering areas. It has become an essential aspect of mathematical analysis and has significantly influenced many fields of study and technology.

1.2 Standard fractional models

- **Fractional conservation of mass:** A fractional conservation of mass equation is required to simulate fluid flow when the control volume is not big enough in comparison to the scale of heterogeneity and when the flux inside the control volume is nonlinear, as detailed by Wheatcraft and Meerschaert [29]. The fractional conservation of mass equation for fluid flow is given in the linked publication as follows:

$$-\sigma\left(\nabla^{\gamma}\cdot\vec{u}\right)=\Gamma(\gamma+1)\Delta x^{1-\gamma}\sigma\left(\delta_{s}+\phi\delta_{w}\right)\frac{\partial p}{\partial t},$$

where γ is fractional-flux, ϕ is porosity, σ is fluid density, δ_s is the coefficient of compressibility for the porous medium, and δ_w is the coefficient of compressibility of the water.

- **Electrochemical Analysis:** A voltage is provided at an electrode surface to force electron transport between the electrode and substrate while examining the redox behavior of a substrate in solution. The current generated as a result of the electron transfer is measured. The concentration of substrate at the electrode surface affects the current. Fick's law states that more substrate diffuses to the electrode when the substrate is used. Taking the Laplace transform of Fick's second law results in the following ordinary second-order differential equation in dimensionless form:

$$\frac{d^2}{dx^2}V(x,s) = sV(x,s).$$

Its solution $V(x,s)$ has a half-power dependency on s. Considering the derivative of $V(x,s)$ and then applying the inverse Laplace transform provides the following relationship:

$$\frac{\partial}{\partial x}V(x,t) = \frac{\partial^{\frac{1}{2}}}{\partial t^{\frac{1}{2}}}V(x,t).$$

It connects the concentration of substrates at the outermost layer of the electrode to the electrical current. In electrochemical kinetics, this relationship is used to deduce mechanistic behavior. It has been used to investigate the dimerization rate of substrates during electrochemical reduction[30].

- **Groundwater flow problem:** [31] discussed various groundwater flow issues utilizing the notion of derivative with fractional order in 2013–2014. The traditional Darcy law is generalized in these works by considering the water flow as a function of the piezometric head's non-integer-order derivative. This generalized law and the law of conservation of mass are then utilized to develop a new groundwater flow equation.

- **Fractional advection-dispersion equation:** This equation has proved helpful in simulating contaminant transport in heterogeneous porous media [18]. Atangana and Kilicman expanded the fractional advection-dispersion equation to a variable-order

equation. The hydrodynamic dispersion equation was expanded in their work by employing the idea of a variational order derivative. The Crank-Nicolson technique was used to solve the modified problem numerically. The modified equation's stability and convergence in numerical simulations show that it is more trustworthy than equations with constant fractional and integer derivatives in forecasting the movement of pollutants in deformable aquifers [32].

- **Time-space fractional diffusion equation models:** Fractional-order diffusion equation models may accurately describe anomalous diffusion processes in complicated media. The time derivative represents long-term heavy tail decay, while the spatial derivative represents diffusion nonlocality. The governing equation for time-space fractional diffusion is as follows:

$$\frac{\partial^{\gamma} u}{\partial t^{\gamma}} = -K(-\Delta)^{\delta} u.$$

  The variable-order fractional derivative is a simple modification of the fractional derivative in which γ and δ are converted into $\gamma(x,t)$ and $\delta(x,t)$. References may be obtained for its uses in anomalous diffusion modeling [32].

- **PID controllers:** The degrees of freedom of PID controllers can be increased by generalizing them to employ fractional orders. The revised equation linking the control variable $v(t)$ to a measured error value $e(t)$ is as follows:

$$v(t) = Pe(t) + ID_t^{-\gamma} e(t) + CD_t^{\delta} e(t),$$

  where γ and δ are positive fractional orders and P, I, and C are all non-negative, denote the coefficients for the proportional, integral, and derivative terms, respectively [33].

- **Acoustical wave equations for complex media:** Acoustic wave propagation in complex media, such as biological tissue, often indicates attenuation following a frequency power law. See Holm & Näsholm (2011) [33] citeHolm and its sources. Such models are connected to the widely accepted idea that numerous relaxation events cause attenuation in complex media. This connection is discussed further in Näsholm & Holm (2011) [34] and the survey study [35], as well as the acoustic attenuation article. For a

work comparing fractional wave equations that represent power-law attenuation, see Holm & Näsholm (2013) [36].

- **Fractional Schrödinger equation in quantum theory:** The fractional Schrödinger equation, a fundamental equation of fractional quantum mechanics, has the following form[37]:

$$i\hbar\frac{\partial\psi(\mathbf{r},t)}{\partial t} = D_\gamma\left(-\hbar^2\Delta\right)^{\frac{\gamma}{2}}\psi(\mathbf{r},t) + V(\mathbf{r},t)\psi(\mathbf{r},t)\,,$$

where, $\Delta = \frac{\partial^2}{\partial\mathbf{r}^2} = \frac{\partial^2}{\partial x_1^2} + \frac{\partial^2}{\partial x_2^2} + \ldots$ is the Laplace operator, D_γ is a scale constant, and the operator $(-\hbar^2\Delta)^{\gamma/2}$ is the 3-dimensional fractional quantum Riesz derivative defined by

$$(-\hbar^2\Delta)^{\frac{\gamma}{2}}\psi(\mathbf{r},t) = \frac{1}{(2\pi\hbar)^3}\int d^3p e^{\frac{i}{\hbar}\mathbf{p}\cdot\mathbf{r}}|\mathbf{p}|^\gamma\varphi(\mathbf{p},t).$$

The index γ in the fractional Schrödinger equation is the Levy index, $1 < \gamma \leq 2$.

- **Variable-order fractional Schrödinger equation:**

The variable-order fractional Schrödinger equation has been used to study fractional quantum phenomena as a natural generalization of the fractional Schrödinger equation [38].

$$i\hbar\frac{\partial\psi^{\gamma(\mathbf{r})}(\mathbf{r},t)}{\partial t^{\gamma(\mathbf{r})}} = \left(-\hbar^2\Delta\right)^{\frac{\delta(t)}{2}}\psi(\mathbf{r},t) + V(\mathbf{r},t)\psi(\mathbf{r},t),$$

where $\Delta = \frac{\partial^2}{\partial\mathbf{r}^2} = \frac{\partial^2}{\partial x_1^2} + \frac{\partial^2}{\partial x_2^2} + \ldots$ is the Laplace operator and the operator $(-\hbar^2\Delta)^{\delta(t)/2}$ is the variable-order fractional quantum Riesz derivative.

1.3 Preliminaries

Some of the critical mathematical definitions that will be utilized throughout this study are briefly presented in this section. Calculus, as we all know, is widely renowned for its integration and differentiation of ideas. Fractional integration and fractional differentiation are utilized in fractional calculus. To explain fractional integration, the Riemann-Liouville integral is utilized. However, many other forms of fractional derivatives may be used to describe fractional differentiation. In most cases, these definitions are different. Every formulation, however, is motivated by the need to retain the features of classical calculus.

Definition 1.3.1 (Caputo fractional derivative)**.** *[3] The Caputo fractional derivative of order γ (denoted by ${}_0^C D_t^\gamma$) of $w(t)$ is defined as*

$$ {}_0^C D_t^\gamma w(t) = \begin{cases} \dfrac{1}{\Gamma(n-\gamma)} \displaystyle\int_0^t \frac{w^{(n)}(s)}{(t-s)^{\gamma-n+1}}\, ds, & n-1 \le \gamma < n,\ n \in \mathbb{N} \\ w^{(n)}(t), & \gamma = n \in \mathbb{N}. \end{cases} $$

Definition 1.3.2 (Riemann-Liouville derivative)**.** *[3] The Riemann-Liouville derivative (denoted by ${}_0^{RL} D_t^\gamma$) of order γ of $w(t)$ is defined as*

$$ {}_0^{RL} D_t^\gamma w(t) = \begin{cases} \dfrac{1}{\Gamma(n-\gamma)} \dfrac{d^n}{dt^n} \displaystyle\int_0^t \frac{w(s)}{(t-s)^{\gamma-n+1}}\, ds, & n-1 < \gamma \le n,\ n \in \mathbb{N} \\ w^{(n)}(t), & \gamma = n \in \mathbb{N}, \end{cases} $$

where Γ represents the gamma function and defined for a complex number z with non-negative real part as

$$ \Gamma(z) = \int_0^\infty e^{-t} t^{z-1}\, dt. $$

Definition 1.3.3 (Riemann-Liouville fractional integral)**.** *[3] The definition of the Riemann-Liouville fractional integral of order $\gamma \in (0,1)$ is given by*

$$ {}^{RL} I_0^\gamma \omega(t) = \frac{1}{\Gamma(\gamma)} \int_0^t (t-s)^{\gamma-1} \omega(s)\, ds, $$

where $\omega(t)$ is real-valued function on $[0,1]$.

Definition 1.3.4 (The Mittag-Leffler function)**.** *[39] The Mittag-Leffler function in two parameters $\mathcal{E}_{p,q}(.)$ for $x \in \mathbb{R}$ and a matrix $\mathcal{A} \in \mathbb{R}^{m\times m}$ are defined respectively, by*

$$ \mathcal{E}_{p,q}(x) = \sum_{i=0}^{\infty} \frac{x^i}{\Gamma(pi+q)},\ p>0,\ q>0, $$

$$ \mathcal{E}_{p,q}(\mathcal{A}) = \sum_{i=0}^{\infty} \frac{\mathcal{A}^i}{\Gamma(pi+q)},\ p>0,\ q>0, $$

if $q = 1$, this function called one parameter Mittag-Leffler function $\mathcal{E}_p(.)$

Definition 1.3.5 (The Atangana-Baleanu fractional derivative)**.** *[39] The Atangana-Baleanu fractional derivative of Caputo sense (ABC derivative) of fractional order* $\gamma \in (0,1)$ *is described for* $\omega(t) \in H^1(0,T)$.

$$^{ABC}D_0^{\gamma}\omega(t) = \frac{N(\gamma)}{1-\gamma}\int_0^t \omega'(s)\mathcal{E}_{\gamma}\left(-\frac{\gamma}{1-\gamma}(t-s)^{\gamma}\right)ds,$$

where $H^1(0,T)$ *is a space of square-integrable functions and is defined as*

$$H^1(0,T) = \{\omega(t) \in L^2(0,T) | \omega'(t) \in L^2(0,T)\},$$

and $N(\gamma)$ *is a normalization function with* $N(0) = N(1) = 1$.

Definition 1.3.6 (The modified Atangana-Baleanu fractional derivative)**.** *[39] The modified Atangana-Baleanu fractional derivative of Caputo meaning (MABC derivative) of order* $\gamma \in (0,1)$ *is determined for* $\omega(t) \in L^1(0,T)$ *and given by*

$$\begin{aligned}{}^{MABC}D_0^{\gamma}\omega(t) =& \frac{N(\gamma)}{1-\gamma}\left[\omega(t) - \mathcal{E}_{\gamma}\left(-\frac{\gamma}{1-\gamma}t^{\gamma}\right)\omega(0)\right.\\ &\left. - \frac{\gamma}{1-\gamma}\int_0^t (t-s)^{\gamma-1}\mathcal{E}_{\gamma,\gamma}\left(-\frac{\gamma}{1-\gamma}(t-s)^{\gamma}\right)\omega(s)\,ds\right].\end{aligned}$$

Definition 1.3.7 (The generalization of the modified Atangana-Baleanu fractional derivative)**.** *[39] The MABC derivative of order* $\gamma \in (n-1,n),\ n \in \mathbb{N}$ *is defined for* $\omega(t) \in L^1(0,T)$ *and given by*

$$\begin{aligned}{}^{MABC}D_0^{\gamma}\omega(t) =& \frac{N(\delta)}{1-\delta}\left[\omega^{(n-1)}(t) - \mathcal{E}_{\delta}\left(-\frac{\delta}{1-\delta}t^{\delta}\right)\omega^{(n-1)}(0)\right.\\ &\left. - \frac{\delta}{1-\delta}\int_0^t (t-s)^{\delta-1}\mathcal{E}_{\delta,\delta}\left(-\frac{\delta}{1-\delta}(t-s)^{\delta}\right)\omega^{(n-1)}(s)\,ds\right],\end{aligned}$$

where $\gamma = n + \delta - 1$.

Definition 1.3.8 (The formula of pointwise error and the order of convergence)**.** *The double*

mesh principle to determine the errors in L_∞ and L_2-norms as follows:

$$\mathcal{E}_\infty^{N_x,M_t} = \max_{1\le n\le M_t}\left(\max_{1\le m\le N_x-1}|\widetilde{y}_i^j - \widetilde{y}_{2i}^{2j}|\right),$$
$$\mathcal{E}_2^{N_x,M_t} = \max_{1\le n\le M_t}\sqrt{\Delta x\sum_{m=1}^{N_x-1}(\widetilde{y}_i^j - \widetilde{y}_{2i}^{2j})^2},$$

where $\widetilde{y}_i^j$ and $\widetilde{y}_{2i}^{2j}$ are the numerical solutions obtained by using (N_x+1, M_t+1) and $(2N_x+1, 2M_t+1)$ points, respectively. We can also compute the corresponding orders of convergence using the formula

$$\mathcal{Q}_q^{N_x,M_t} = \log_2\left(\frac{\mathcal{E}_q^{N_x,M_t}}{\mathcal{E}_q^{2N_x,2M_t}}\right), \quad q = 2, \infty.$$

1.4 Fractional partial differential equation

In mathematics, PDEs are generally used to quantitatively solve physical and other issues involving the functions of numerous variables, such as heat or sound propagation, fluid movement, and eddy currents. A FPDE is a PDE that incorporates fractional derivatives of non-integer order. Its significant benefit is the nonlocality of a fractional derivative over an integer-order derivative. The former offers a mechanism for the internalization of memory as well as hereditary aspects of numerous events. FPDEs occur in diverse regions of science and engineering, such as physics, rheology, biology, control theory, viscoelasticity, systems identification, signal processing, and electrochemistry [2, 5, 6, 40–44]. Fractional partial differential equations (FPDEs) are a kind of partial differential equation (PDE) that involves fractional derivatives. While traditional PDEs use integer-order derivatives to explain the behavior of functions, FPDEs use non-integer fractional-order derivatives. These equations have acquired popularity in various scientific and technical domains due to their ability to represent complicated behavior in systems with memory and anomalous diffusion. There are several definitions of fractional derivatives, the most prominent being Riemann-Liouville and Caputo derivatives. The chosen definition has a significant influence on the characteristics and solutions of the resulting FPDEs. A general version of a fractional partial differential

equation can be stated as:

$$\mathcal{L}\{u(x,t)\} = f(x,t),$$

where $\mathcal{L}$ is a fractional differential operator, $u(x,t)$ denotes the unknown function, and $f(x,t)$ denotes a forcing or source term. Under the suitable boundary and beginning conditions, the solution $u(x,t)$ is sought.

Some essential considerations while working with FPDEs:

- **Non-local behavior:** Non-local behavior is introduced by fractional derivatives, which implies that the derivative at a location depends on the function throughout a range of values rather than only at the point itself.
- **Memory and Heredity effect:** FPDEs may represent systems with memory effects, in which a system's current behavior is determined by its prior history over a continuous time period.
- **Anomalous diffusion:** FPDEs are frequently used to represent anomalous diffusion processes in which the diffusion is described by a power-law behavior rather than a straightforward diffusion equation.
- **Numerical methods:** Numerical solutions to FPDEs can be complicated, and specialized numerical approaches are sometimes required. FPDEs can be solved using finite difference, finite element, collocation methods, and spectral approaches.
- **Applications:** FPDEs are employed in various disciplines, including physics, engineering, biology, and finance. They are instrumental in characterizing occurrences where traditional integer-order derivatives are insufficient.

FPDEs are mainly of two types: linear and nonlinear. The following FPDEs form the foundation of this thesis and aid in investigating additional FPDEs.

- The fractional partial differential equation with a time delay.
- Time-fractional nonlinear Kuramoto-Sivashinsky.
- Fractional order Allen-Cahn equation.

- Generalized time-fractional Fisher's equation.

1.5 Fractional order system

A fractional-order system can be defined as a dynamical system that may be described by a fractional differential equation, including non-integer-order derivatives in the domains of dynamical systems and control theory. These types of systems are considered to exhibit fractional dynamics. Derivatives and integrals of fractional orders are often employed to explain things with power-law nonlocality, power-law long-range dependency, or fractal features. Fractional-order systems are essential for understanding the abnormal behavior of dynamical systems in physics, electrochemistry, biology, viscoelasticity, and chaotic systems.

A fractional-order system, commonly called a fractional-order control system, is a form of dynamic system characterized by fractional-order differential equations. These systems are distinguished by non-integer-order derivatives or integrals in their mathematical models, frequently expressed by a fractional exponent. In contrast to traditional control systems, which employ integer-order differential equations, fractional-order systems can capture more complicated and non-integer behaviors commonly found in real-world systems. Engineering, physics, biology, and finance are the domains where fractional-order systems are used. Some of the significant traits and characteristics of fractional-order systems are:

- **Fractional-order dynamics, Memory and heredity:** Fractional derivatives, or integrals, formulate equations for fractional-order systems. Because they can model memory effects and long-term dependencies, these non-integer orders enable more flexible and diverse system behavior modeling. Memory in fractional-order systems extends beyond that of standard integer-order systems. The system's present behavior is heavily impacted by its previous states.

- **Complex dynamics:** Complex phenomena like power-law interactions, fractal patterns, and non-exponential decay or growth can be seen in fractional-order systems. These characteristics are frequently used to define real-world situations more precisely.

- **Control and optimization:** Various systems are regulated and stabilized using fractional-order controllers. They benefit from better transient responsiveness, resilience, and the

capacity to deal with systems with unknown parameters.

- **Challenges:** Because non-integer derivatives and integrals are involved, fractional-order systems can be more challenging to analyze and regulate than integer-order systems. Unique approaches and tools, such as fractional calculus, are utilized to overcome these issues.

Because of their capacity to more correctly describe and regulate complicated, nonlinear, and memory-dependent systems, fractional-order systems have attracted interest and focus in recent years. Researchers and engineers continue investigating their applications and creating tools and methods for adequately understanding and regulating these systems.

Fractional differentiation and integration have been utilized in various burning fields of mathematics, with a tremendous increase in developing further and modern models. In the literature, different fractional order differential operators possess Caputo, Caputo-Fabrizio, Riemann-Liouville, and Atangana-Baleanu, etc. [45–47]. Fractional-order differential equations exist as one of the additional favored instruments; they support complex dynamic systems from various domains. These contain electrochemistry [48], electricity [49], mechanics [50], economy [51], biology [52], and epidemiology [53]. Since fractional order derivatives have integer orders, fractional order differential equations are an abstraction of ordinary differential equations (ODEs). Systems modeled with fractional-order differential equations demonstrate real-life spectacles more accurately. Modeling with fractional-order derivatives describes the real-life system's behavior, and these are also helpful in analyzing the dynamical approaches. In modeling biological and physical procedures with longer-range interactivity, fractional differential equations are more appropriate than ordinary ones in time and space. Using fractional derivatives highlights the inherent non-local characteristic whereby the future state is contingent upon the current state and all previously recorded states. The systems with fractional derivatives that are multiplied together eventually become systems with integer-order derivatives. Thus, fractional calculus naturally results in various attachments, including the non-local nature of fractional derivative operators, an improved degree of freedom, a vast stability province, and maximal utilization of information. In the case of fractional order models, the majority of these characteristics and consequences

only manifest. The latter fractional order derivative is successfully utilized in nearly all experimental models, with particular mention of various directions of computational biology. In 2018, Evirgen and Yavuz [54] examined an alternative method for a nonlinear optimization problem, and Yavuz [55] examined a unique recursive approximation for nonlinear problems containing the Caputo-Fabrizio derivative. In their paper [56], Ghanbari and Cattani describe mutualistic predation in Lotka-Volterra models. A novel variable-order fractional tumor model is presented with an ideal control by Sweilam *et al.* [57]. In their study, Danane *et al.* [58] investigated the fractional model that describes the dynamics of the hepatitis B viral infection. Baleanu *et al.* [59] offered an unexplored fractional model of human life utilizing the Caputo-Fabrizio fractional derivative established on the exponential kernel—a novel fractional SIRS-SI malaria model transmission delivered by Kumar *et al.* [60]. In 2020, Singh *et al.* [61] conducted a study on the fractional fish farm system linked to the Mittag-Leffler-type kernel. The readers can be directed to [62, 63] for additional practical models concerning fractional order derivatives.

The following fractional order system forms the foundation of this thesis and aids in investigating additional fractional order systems.

- A two-dimensional predator-prey model of fractional order with one carrying capacity

1.6 Finite difference schemes for Caputo fractional derivative

The fractional derivative is discretized in finite difference methods for numerical solutions of fractional partial differential equations. Three fundamental discretizations of the Caputo fractional derivative are used as follows:

- The central difference scheme for Caputo fractional derivative.
- $L1$ scheme for Caputo fractional derivative.
- $L1-2$ scheme for Caputo fractional derivative.

Let $0 < \gamma < 1$ be an order of fractional derivative, then the central difference scheme has second-order accuracy, the $L1$ scheme has $(2-\gamma)$ order accuracy, and the $L1-2$ scheme

has $(3-\gamma)$ order accuracy. We will study these schemes in detail in the upcoming chapters. The L1 formula is constructed through a sequentially linear interpolation estimate for the integrand function for each very small interval. $L1-2$ scheme is a modification of $L1$ scheme (see [64] for more details).

1.7 Quasilinearization

The quasilinearization approach is a generalized Newton-Raphson technique for functional equations. If there is convergence at all, it converges quadratically to the exact solution, and it has monotone convergence. Let us consider nonlinear second-order differential the equation is as follows:

$$u''(x) = f(x, u(x)), \quad a \leq x \leq b \tag{1.7.1}$$

with the boundary conditions

$$u(a) = \alpha, \quad u(b) = \beta.$$

Choose an initial approximation $u_0(x)$ of the function $u(x)$, it may be $u_0(x) = \alpha$, for $a \leq x \leq b$. Using the Taylor series, the function f can now be expanded around the function $u_0(x)$. Consider

$$f(x, u(x)) \approx f(x, u_0(x)) + (u(x) - u_0(x)) f_u(x, u_0(x)), \tag{1.7.2}$$

where second and higher-order terms are ignored. Using (1.7.2) in (1.7.1), we get

$$u''(x) = f(x, u_0(x)) + (u(x) - u_0(x)) f_u(x, u_0(x)). \tag{1.7.3}$$

Solving (1.7.3) for $u(x)$, call it $u_1(x)$ and expand (1.7.1) about $u_1(x)$

$$u''(x) = f(x, u_1(x)) + (u(x) - u_1(x)) f_u(x, u_1(x)), \tag{1.7.4}$$

we obtain a third approximation for $u(x)$, call it $u_2(x)$. Assume the problem converges and continue the procedure to obtain the desired accuracy. The recurrence relationship is of the form

$$u''_{r+1}(x) = f(x, u_r(x)) + (u_{r+1}(x) - u_r(x))f_u(x, u_r(x)), \tag{1.7.5}$$

where $u_r(x)$ is known and can be used for obtaining $u_{r+1}(x)$. Equation (1.7.5) is always a linear differential equation and boundary conditions are

$$u_{r+1}(a) = \alpha, \quad u_{r+1}(b) = \beta. \tag{1.7.6}$$

Now consider the nonlinear second-order differential equation of the form

$$u''(x) = f(x, u(x), u'(x)). \tag{1.7.7}$$

Here, the first derivative, $u'(x)$ can be considered as another function and (1.7.7) can analogously be expressed as

$$\begin{aligned} u''_{r+1}(x) =& f(x, u_r(x), u'_r(x)) + (u_{r+1}(x) - u_r(x))f_u(x, u_r(x), u'_r(x)) \\ &+ (u'_{r+1}(x) - u'_r(x))f_{u'}(x, u_r(x), u'_r(x) \end{aligned}$$

with the same boundary conditions

$$u_{r+1}(a) = \alpha, \quad u_{r+1}(b) = \beta,$$

where f_u is differentiation of f with respect to u.

Similarly, one can follow the same procedure for higher-order nonlinear differential equations to obtain the recurrence relation.

1.8 Numerical Methods to solve FPDEs

In several scientific and technical domains, numerical techniques for solving fractional partial differential equations (FPDEs) are becoming increasingly significant. Because FPDEs

incorporate non-integer-order derivatives, they are more challenging to solve than ordinary PDEs. Here are some of the most common numerical approaches for solving FPDEs:

- **Finite Difference Method (FDM):** FDM is a simple and frequently used discretization technique for FPDEs. It makes use of finite difference approximations to approximate fractional derivatives. The fractional derivatives of Caputo or Riemann-Liouville can be discretized and solved using the usual time-stepping methods. For Riemann-Liouville derivatives, the Grünwald-Letnikov discretization is widely utilized.

- **Fractional Finite Element Method (FEM):** Another prominent approach for resolving FPDEs is FEM. It entails breaking down the issue domain into elements and building an algebraic equation system. Traditional FEM is adapted to handle fractional derivatives, utilizing weak formulations and variational techniques in fractional FEM.

- **Fractional Finite Volume Method (FVM):** FVM is a method for discretizing FPDEs that divides the domain into control volumes. Fractional FVM, like FEM, introduces fractional derivatives into the balance equations.

- **Method of Lines (MOL):** MOL is a technique for discretizing spatial derivatives, resulting in an ordinary differential equation (ODE) system. The temporal evolution of the issue can then be handled using numerical ODE solvers.

- **Spectral Methods:** The solution is expanded regarding orthogonal basis functions, such as Chebyshev or Legendre polynomials. In the spectrum domain, fractional derivatives may be determined analytically, which may be more efficient for particular tasks.

- **Laplace Transform Method:** This approach transforms the FPDE into a system of ODE in the Laplace domain. After solving the issue in the Laplace domain, the answer in the time domain is obtained using an inverse Laplace transform.

- **Adomian Decomposition Method (ADM):** ADM is a series-based, non-iterative approach for solving FPDEs. It decomposes the issue into components and iteratively finds approximations for each component.

- **Numerical Inversion of Laplace Transforms:** Some approaches concentrate on efficiently inverting Laplace transforms, a critical step in solving FPDEs. The Gaver-Stehfest algorithm, as well as other numerical inversion methods, can be employed.

- **Fractional Integral Equations:** Some FPDEs may be turned into fractional integral equations, which can then be solved using different integral equation numerical methods, such as the method of moments.

- **Meshless Methods:** Meshless approaches like the Radial Basis Function (RBF) do not need a set grid or mesh. By including fractional derivatives, they may be used to solve FPDEs.

- **Finite Difference Time-Domain (FDTD) Method:** The FDTD approach in electromagnetic simulations may be expanded to accommodate fractional derivatives to tackle fractional electromagnetic field issues.

The selection of the preferred approach is based on the specific characteristics of the FPDE, the field of application, and the computational resources at hand. When deciding on the best solution for a specific situation, examining various methods' accuracy, stability, and efficiency is critical. Additionally, software libraries and packages may be provided to aid in implementing these approaches.

Approximate solutions to fractional partial differential equations have been presented using numerical approaches. Many numerical methods have been established in the literature to solve fractional partial differential equations. Fourier techniques, energy estimates, the matrix eigenvalue approach, and mathematical induction are some of the conceptually analytical methods. The prominent numerical approaches for solving fractional partial differential equations are finite difference methods and series approximation methods. In [65], Wang devised a fourth-order compact finite difference approach for solving convection-diffusion wave equations with variable coefficients. Using the explicit finite difference approach, Yuste and Acedo [66] investigated the fractional diffusion equation. See also [67, 68]. The finite element method is also useful for solving fractional partial differential equations. It has been discovered that while finite element techniques allow for high-order precision, they have a

higher computational cost and depend more on mesh quality. Here are several articles that use the finite element approach. To obtain a solution to the fractional Bloch-Torrey equation, Dehghan and Abbaszadeh [69] employed finite difference techniques concerning temporal discretization and the Galerkin finite element approach for spatial discretization. To examine the multi-term time-fractional diffusion problem, Jin *et al.* [70] devised a numerical technique based on the Galerkin finite element method. Jiang and Ma [71] devised a finite element approach of high order for solving time fractional partial differential equations. For more study, readers can see [72, 73].

The numerical methods listed below form the basis of this thesis and help investigate further fractional-order partial differential equations.

- Tension spline collocation method
- Quintic B-spline collocation method
- Cubic B-spline collocation method
- The compact finite difference scheme

To examine the fractional diffusion problem, Baseri *et al.* [74] developed a collocation approach. For the collocation approach, they used a rational Chebyshev function in the temporal direction and shifted Chebyshev polynomials in the spatial direction. The authors of [75] solved the fractional diffusion and diffusion-wave equations using the collocation method using a cubic B-spline basis function. Nagy considers the time fractional nonlinear Klein-Gordon equation in [76] using the Sinc-Chebyshev collocation method. Zhou and Xu [77] investigated the time fractional diffusion-wave equation using the second kind of Chebyshev wavelet collocation technique. Pirkhedri and Javadi [78] used the Sinc-Haar collocation method to solve the time-fractional diffusion problem. The suggested approach is highly successful because of its high computing speed and exponential convergence rate.

1.9 The thesis Aims and Objectives

We only studied the solution in one spatial dimension in this thesis, but this study suggests developing numerical approaches for solving time-fractional PDEs. It will aid in developing

more efficient (less computationally intensive) ways for approximating the Caputo fractional derivatives while preserving accuracy. These approximation approaches will be coupled with the various spatial discretization methods outlined in the preceding section to help solve time-fractional PDEs more effectively. The benefits of such an approach are:

- The numerical approaches are more beneficial when the analytical technique is either unavailable or hard to assess.
- It will aid in the development of more computationally efficient approaches as well as the reduction of computing effort.

The objectives of this thesis are presented below and are based on numerical analysis for linear and nonlinear fractional partial differential equations.

- To provide innovative, precise numerical techniques for solving linear and nonlinear fractional partial differential equations.
- To look for a more efficient method of approximating fractional derivatives while maintaining accuracy.
- To determine various numerical systems' accuracy, convergence, and stability.

1.10 Overview of the Thesis

This thesis has been organized as follows: Chapter 2 suggests a second-order numerical scheme for the time-fractional partial differential equations with a time delay. Chapter 3 gives a higher-order stable numerical approximation for the time-fractional nonlinear Kuramoto-Sivashinsky equation based on quintic $\mathfrak{B}$-spline. Chapter 4 offers a collocation-based numerical simulation of the fractional-order Allen-Cahn equation. Chapter 5 delivers a high-order numerical technique for generalized time-fractional Fisher's equation. Chapter 6 offered a numerical method for solving the fractional-order predator-prey model.

Remark 1.10.1. *Throughout all Chapters, we take C as a positive generic constant that takes different values at different places.*

Chapter 2

A second-order numerical scheme for the time-fractional partial differential equations with a time delay

This work proposes a numerical scheme for a class of time-fractional convection-reaction-diffusion problems with a time lag. The time-fractional derivative is considered in the Caputo sense. The numerical method comprises the discretization technique given by Crank and Nicolson in the temporal direction, and spline functions with a tension factor are used in the spatial direction. Through the Von-Neumann stability analysis, the scheme is shown to be conditionally stable. Moreover, a rigorous convergence analysis is presented through the Fourier series. Two test problems are solved numerically to verify the effectiveness of the proposed numerical scheme.

2.1 Literature survey

In contrast to partial differential equations (PDEs), the physical problems for which the evolution depends not only on the present state of the system but also on the history are modeled

R. Choudhary, S. Singh, D. Kumar, A second-order numerical scheme for the time-fractional partial differential equations with a time delay, Comput. Appl. Math., 41 (2022), 114.

by delay partial differential equations (DPDEs) and time-fractional delay partial differential equations (TF-DPDEs). Often, in systems with subdiffusive processes, the future state is determined by their history, and delay terms must be addressed despite the whole history being considered by the fractional differential equations (FDEs). These equations frequently arise in many areas of science and engineering, such as time to maturity and incubation time, delayed feedback, time to transport, and the time lag for getting information. The three well-known derivatives of fractional order are widely used in the literature, namely, the Caputo derivative, the Riemann-Liouville derivative, and the Grünwald-Letnikov derivative. However, recently, two new fractional derivatives, namely, the Atangana-Baleanu-Caputo derivative [79] and the Caputo-Fabrizio derivative [80], have been introduced. For reference, we define the Caputo and Riemann-Liouville derivatives as follows:

Fractional partial differential equations (FPDEs) are those where a fractional derivative replaces the classical derivative. Because of the precise and powerful descriptions of a large variety of natural phenomena, many mathematicians and scientists are analyzing FPDEs with delay analytically as well as numerically [81–88]. The models containing the time delay can be seen in the automatic control systems [89, 90], random walk [91], and modeling HIV infection of $CD4^+$ T-cells [81, 92, 93]. An extensive study of delay differential equations (DDEs) in the context of ordinary differential equations (ODEs) can be seen in [94–98] and the references therein. Furthermore, the analytical solutions, including the spectral methods and the integral transform methods such as Laplace transforms, and Mellin transforms for FPDEs, can be seen in [3, 99–103]. On the other hand, the DPDEs and TF-DPDEs are less explored than DDEs and FPDEs.

Because the evolution of a dependent variable of TF-DPDEs at any time t not only depends on its value at $t - \tau$ (for some time delay τ) but also depends on all previous solutions. It is a difficult task to solve TF-PDEs with delay effectively and accurately. However, some analytical methods have been investigated to solve these problems. For instance, to obtain the actual solution to the TF-DPDEs, Prakash *et al.* [104] proposed the invariant subspace approach. For a detailed discussion on the asymptotic properties of the solution to DDEs, the readers are referred to [105, 106] whereas the existence of solutions is presented in [107]. Moreover, the stability bounds on the solution for the class of fractional delay difference

equations (FDDEs) can be found in [108–110]. For the finite-time stability of robotic systems where a time delay appears in PD^{γ} fractional control system, the readers are referred to [89, 111]. As a consequence, we look for numerical methods for TF-DPDEs. Some numerical methods have also been developed for these problems; for instance, for a numerical scheme for space-fractional diffusion equations with a delay in time, the readers are referred to Hao *et al.* [93]. They have used the Taylor series expansion to linearize the nonlinear term and weighted shifted Grünwald-Letnikov formula to approximate the space-fractional derivative. Rihan [112] extended the θ method to solve the TF-DPDEs of parabolic type in the Caputo sense. To test the BIBO stability of the system of TF-DDEs, Hwang, and Cheng [110] presented an effective numerical algorithm based on Cauchy's integral theorem. Mohebbi [87] constructed an efficient numerical method to solve the TF-DPDEs of convection-reaction-diffusion type with a nonlinear source term. The Chebyshev spectral collocation method and second-order finite difference approximations are used in spatial and temporal directions. Sakara *et al.* [85] presented a homotopy perturbation method for nonlinear TF-DPDEs. Zhang *et al.* [84] proposed a linearized compact finite difference method (FDM) for the semilinear TF-DPDEs. The compact finite difference approximation is used to discretize the spatial derivative, and the temporal derivative is discretized using the L_1 approximation. Through rigorous analysis, the method is shown as fourth-order convergent in space and of order $(2-\gamma)$ in time.

In this work, we consider the following TF-PDE with a time lag:

$$ {}_{0}^{C}D_{t}^{\gamma}y(x,t) - \frac{\partial^2 y(x,t)}{\partial x^2} + b(x,t)\frac{\partial y(x,t)}{\partial x} + c(x,t)y(x,t) = -d(x,t)y(x,t-\tau) + f(x,t), \tag{2.1.1a} $$

for all $(x,t) \in \mathfrak{D} \equiv \Omega \times \Lambda = (0,1) \times (0,\mathfrak{T}]$, with the following interval and boundary conditions

$$ y(x,t) = \psi_b(x,t), \quad (x,t) \in [0,1] \times [-\tau, 0], \tag{2.1.1b} $$

$$ y(0,t) = \psi_l(t), \quad y(1,t) = \psi_r(t), \quad t \in [0,\mathfrak{T}], \tag{2.1.1c} $$

where the fractional derivative of order $\gamma \in (0,1)$ is estimated in the Caputo sense. A hybrid scheme and a compact FDM have been investigated in [113, 114] for the classical integer order DPDEs that is the simplified form of the equation (2.1.1) for $\gamma = 1$. Several

numerical schemes have been developed (for $\gamma = 2$) when (2.1.1) is equivalent to the wave equation with delay, see e.g. [86, 88, 115]. Du *et al.* [116] developed a high-order difference method for the fractional diffusion-wave equation associated with $\gamma \in (1, 2)$ in (2.1.1) with constant coefficients and without the convective term. Li *et al.* [117] investigates a linearized FDM for the problem similar to (2.1.1) without the reaction term and non-linear source term. First, the original problem is transformed into an equivalent semi-linear fractional delay reaction-diffusion equation. Then, they used the central finite difference formula for the space derivative and L_1 approximation for the Caputo derivative. Finally, the inverse exponential recovery method is used to obtain the numerical solution.

2.2 Discretization of the problem

2.2.1 The time semi-discretization

To discretize the time domain, we use an equidistant mesh. Let $\Lambda_\tau^k = \{-\tau = t_{-k} < t_{-k+1} < \ldots < t_{-1} < t_0 = 0\}$ be the partition of $[-\tau, 0]$ divided into k sub-intervals using step size $\Delta t = \tau/k$. Then, using the mesh size Δt, we discretize $[0, \mathfrak{T}]$ into $M_t = \mathfrak{T}/\Delta t$ sub-intervals and denote by Λ^{M_t}, the collection of all nodal points of the domain $[0, \mathfrak{T}]$. Then

$$\Lambda^{M_t} = \{0 = t_0 < t_1 < \ldots < t_k = \tau < \ldots < t_{M_t-1} < t_{M_t} = \mathfrak{T}\}.$$

Now we semi-discretize the problem (2.1.1) on Λ^{M_t} as

$$-\frac{\partial^2 \widetilde{y}(x, t_{n+\frac{1}{2}})}{\partial x^2} + b(x, t_{n+\frac{1}{2}})\frac{\partial \widetilde{y}(x, t_{n+\frac{1}{2}})}{\partial x} + c(x, t_{n+\frac{1}{2}})\widetilde{y}(x, t_{n+\frac{1}{2}}) = -d(x, t_{n+\frac{1}{2}})\widetilde{y}(x, t_{n+\frac{1}{2}-k}) + f(x, t_{n+\frac{1}{2}}) - \frac{\partial^\gamma \widetilde{y}(x, t_{n+\frac{1}{2}})}{\partial t^\gamma}, \tag{2.2.1a}$$

for $n = 1, 2, \ldots, M_t - 1$ with

$$\widetilde{y}(x, t_{n+1}) = \psi_b(x, t_{n+1}), \text{ for } (x, t_{n+1}) \in [0, 1] \times \Lambda_\tau^k, \tag{2.2.1b}$$

$$\widetilde{y}(0, t_{n+1}) = \psi_l(t_{n+1}), \quad \widetilde{y}(1, t_{n+1}) = \psi_r(t_{n+1}), \ t_{n+1} \in \Lambda^{M_t}, \tag{2.2.1c}$$

where $\widetilde{y}$ represents the approximate solution to the problem (2.1.1). We approximate $\frac{\partial^\gamma \widetilde{y}(x,t_{n+1/2})}{\partial t^\gamma}$ at $(x, t_{n+1/2})$ using the following approach:

$$\begin{aligned}
\frac{\partial^\gamma \widetilde{y}(x,t_{n+1/2})}{\partial t^\gamma} &= \frac{1}{\Gamma(1-\gamma)} \int_0^{t_{n+1/2}} \widetilde{y}_t(x,t_{n+1/2})(t_{n+1/2}-s)^{-\gamma} ds \\
&= \frac{1}{\Gamma(1-\gamma)} \int_0^{t_n} \widetilde{y}_t(x,t_{n+1/2}) \left(\left(n+\frac{1}{2}\right)\Delta t - s\right)^{-\gamma} ds \\
&+ \frac{1}{\Gamma(1-\gamma)} \int_{t_n}^{t_{n+1/2}} \left[\frac{\widetilde{y}^{n+1}-\widetilde{y}^n}{\Delta t} + \mathcal{O}((\Delta t)^2)\right] \left(\left(n+\frac{1}{2}\right)\Delta t - s\right)^{-\gamma} ds \\
&= \frac{1}{\Gamma(1-\gamma)} \sum_{i=1}^{n} \int_{(i-1)\Delta t}^{i\Delta t} \left[\frac{\widetilde{y}^{i}-\widetilde{y}^{i-1}}{\Delta t} + \mathcal{O}((\Delta t)^2)\right] \left(\left(n+\frac{1}{2}\right)\Delta t - s\right)^{-\gamma} ds \\
&+ \frac{1}{\Gamma(1-\gamma)} \int_{n\Delta t}^{(n+1/2)\Delta t} \left[\frac{\widetilde{y}^{n+1}-\widetilde{y}^n}{\Delta t} + \mathcal{O}((\Delta t)^2)\right] \left(\left(n+\frac{1}{2}\right)\Delta t - s\right)^{-\gamma} ds. \\
&= \frac{1}{\Gamma(1-\gamma)} \sum_{i=1}^{n} \left(\frac{\widetilde{y}^{i}-\widetilde{y}^{i-1}}{\Delta t}\right) \int_{(i-1)\Delta t}^{i\Delta t} \left(\left(n+\frac{1}{2}\right)\Delta t - s\right)^{-\gamma} ds \\
&+ \frac{\mathcal{O}((\Delta t)^2)}{\Gamma(1-\gamma)} \sum_{i=1}^{n} \int_{(i-1)\Delta t}^{i\Delta t} \left(\left(n+\frac{1}{2}\right)\Delta t - s\right)^{-\gamma} ds \\
&+ \frac{1}{\Gamma(1-\gamma)} \int_{n\Delta t}^{(n+1/2)\Delta t} \left[\frac{\widetilde{y}^{n+1}-\widetilde{y}^n}{\Delta t} + \mathcal{O}((\Delta t)^2)\right] \left(\left(n+\frac{1}{2}\right)\Delta t - s\right)^{-\gamma} ds \\
&= \frac{1}{\Gamma(1-\gamma)} \frac{1}{(\Delta t)^\gamma (1-\gamma)} \sum_{i=1}^{n} \left[\widetilde{y}^{i}-\widetilde{y}^{i-1}\right] \left[\left(n-i+\frac{3}{2}\right)^{1-\gamma} - \left(n-i+\frac{1}{2}\right)^{1-\gamma}\right] \\
&+ \frac{1}{\Gamma(1-\gamma)} \frac{1}{(1-\gamma)} \sum_{i=1}^{n} \left[\left(n-i+\frac{3}{2}\right)^{1-\gamma} - \left(n-i+\frac{1}{2}\right)^{1-\gamma}\right] \mathcal{O}((\Delta t)^{3-\gamma}) \\
&+ \frac{1}{\Gamma(1-\gamma)} \frac{1}{(\Delta t)^\gamma (1-\gamma)} (\widetilde{y}^{n+1}-\widetilde{y}^{n}) \frac{1}{2^{1-\gamma}} + \frac{1}{\Gamma(1-\gamma)} \frac{1}{(1-\gamma)} \frac{1}{2^{1-\gamma}} \mathcal{O}((\Delta t)^{3-\gamma}).
\end{aligned}$$

Thus, we get

$$\begin{aligned}
\frac{\partial^\gamma \widetilde{y}(x,t_{n+1/2})}{\partial t^\gamma} &= \frac{1}{\Gamma(2-\gamma)} \frac{1}{(\Delta t)^\gamma} (\widetilde{y}^{n+1}-\widetilde{y}^{n}) \frac{1}{2^{1-\gamma}} \\
&+ \frac{1}{\Gamma(2-\gamma)} \frac{1}{(\Delta t)^\gamma} \sum_{i=1}^{n} \left[\widetilde{y}^{i}-\widetilde{y}^{i-1}\right] \left[\left(n-i+\frac{3}{2}\right)^{1-\gamma} - \left(n-i+\frac{1}{2}\right)^{1-\gamma}\right] \\
&+ \frac{1}{\Gamma(2-\gamma)} \sum_{i=1}^{n} \left[\left(n-i+\frac{3}{2}\right)^{1-\gamma} - \left(n-i+\frac{1}{2}\right)^{1-\gamma}\right] \mathcal{O}((\Delta t)^{3-\gamma}) \\
&+ \frac{1}{\Gamma(2-\gamma)} \frac{1}{2^{1-\gamma}} \mathcal{O}((\Delta t)^{3-\gamma}). \qquad (2.2.2)
\end{aligned}$$

Let $\sigma = \frac{1}{\Gamma(2-\gamma)}\frac{1}{(\Delta t)^{\gamma}}$, and $w_j = \left(j+\frac{1}{2}\right)^{1-\gamma} - \left(j-\frac{1}{2}\right)^{1-\gamma}$, so that $\sum_{j=1}^{n_1} w_j = \left(n_1+\frac{1}{2}\right)^{1-\gamma} - \left(\frac{1}{2}\right)^{1-\gamma}$. Substituting σ and w_j into (2.2.2), we get

$$\frac{\partial^{\gamma}\widetilde{y}(x,t_{n+1/2})}{\partial t^{\gamma}} = \sigma\left[w_1\widetilde{y}^n + \sum_{i=1}^{n-1}(w_{n-i+1}-w_{n-i})\widetilde{y}^i - w_n\widetilde{y}^0 + \frac{\widetilde{y}^{n+1}-\widetilde{y}^n}{2^{1-\gamma}}\right] + R_1 + R_2,$$

where

$$R_1 + R_2 = \frac{1}{\Gamma(2-\gamma)}\sum_{i=1}^{n} w_{n-i+1}\mathcal{O}((\Delta t)^{3-\gamma}) + \frac{1}{\Gamma(2-\gamma)}\frac{1}{2^{1-\gamma}}\mathcal{O}((\Delta t)^{3-\gamma}).$$

Let $j = n-i+1$, then

$$\begin{aligned}
R_1 + R_2 &= \frac{1}{\Gamma(2-\gamma)}\left[\sum_{j=1}^{n} w_j\mathcal{O}((\Delta t)^{3-\gamma}) + \frac{1}{2^{1-\gamma}}\mathcal{O}((\Delta t)^{3-\gamma})\right] \\
&= \frac{1}{\Gamma(2-\gamma)}\left[\left(n+\frac{1}{2}\right)^{1-\gamma} - \left(\frac{1}{2}\right)^{1-\gamma} + \frac{1}{2^{1-\gamma}}\right]\mathcal{O}((\Delta t)^{3-\gamma}) \\
&= \frac{1}{\Gamma(2-\gamma)}\left(n+\frac{1}{2}\right)^{1-\gamma}\mathcal{O}((\Delta t)^{3-\gamma}) \\
&= \frac{1}{\Gamma(2-\gamma)}\left(\frac{t_n}{\Delta t}+\frac{1}{2}\right)^{1-\gamma}\mathcal{O}((\Delta t)^{3-\gamma}) \\
&\leq C(\Delta t)^2.
\end{aligned}$$

Thus, we have the following approximation at $(x, t_{n+\frac{1}{2}})$

$$\frac{\partial^{\gamma}\widetilde{y}(x,t_{n+1/2})}{\partial t^{\gamma}} = \sigma\left[w_1\widetilde{y}^n + \sum_{i=1}^{n-1}(w_{n-i+1}-w_{n-i})\widetilde{y}^i - w_n\widetilde{y}^0 + \frac{\widetilde{y}^{n+1}-\widetilde{y}^n}{2^{1-\gamma}}\right] + \mathcal{O}((\Delta t)^2). \tag{2.2.3}$$

2.2.2 The spatial discretization

Let $\Omega^{N_x} = \{0 = x_0 < x_1 < \ldots < x_{N_x-1} < x_{N_x} = 1\}$ be the partition of $[0,1]$ divided into N_x sub-intervals each of width $\Delta x = \frac{1}{N_x}$. Let the function $\mathcal{S}(x,t,\delta)$ belongs to the class $C^2[0,1]$, which gives interpolation of $y(x,t)$ at the mesh point (x_m, t_n), where δ is termed as tension factor. As $\delta \to 0$ the function $\mathcal{S}(x,t,\delta)$ is turned to be parametric cubic spline in $[0,1]$. Let $\mathcal{S}_m^n$ be an approximation of $\widetilde{y}_m^n$ obtained by the segment of the functions passing

through the points $(x_m, \mathcal{S}_m^n)$ and $(x_{m+1}, \mathcal{S}_{m+1}^n)$. For $\delta > 0$, $\mathcal{S}_\pi(x, t_n, \delta)$ satisfies the following differential equation in the sub-interval $[x_m, x_{m+1}]$

$$\begin{aligned}\mathcal{S}_\pi''(x, t_n, \delta) - \delta\mathcal{S}_\pi(x, t_n, \delta) =&[\mathcal{S}_\pi''(x_m, t_n, \delta) - \delta\mathcal{S}_\pi(x_m, t_n, \delta)](x_{m+1} - x)/\Delta x \\ &+ [\mathcal{S}_\pi''(x_{m+1}, t_n, \delta) - \delta\mathcal{S}_\pi(x_{m+1}, t_n, \delta)](x - x_m)/\Delta x,\end{aligned} \tag{2.2.4}$$

with the following interpolation conditions

$$\mathcal{S}_\pi(x_m, t_n, \delta) = \widetilde{y}_m^n,\ \mathcal{S}_\pi(x_{m+1}, t_n, \delta) = \widetilde{y}_{m+1}^n. \tag{2.2.5}$$

The function derivative $y''(x_m, t_n)$ has the spline derivative approximation given by

$$\mathcal{S}_\pi''(x_m, t_n, \delta) = \mathcal{M}(x_m, t_n)\ ,\ \mathcal{S}_\pi''(x_{m+1}, t_n, \delta) = \mathcal{M}(x_{m+1}, t_n). \tag{2.2.6}$$

The solution of (2.2.4) with the interpolatory conditions (2.2.5) can be written as

$$\begin{aligned}\mathcal{S}_\pi(x, t_n, \delta) =&\frac{(\Delta x)^2}{\nu^2 \sinh(\nu)}\left[\mathcal{M}_{m+1}^n \sinh\frac{\nu(x - x_m)}{\Delta x} + \mathcal{M}_m^n \sinh\frac{\nu(x_{m+1} - x)}{\Delta x}\right] \\ &- \frac{(\Delta x)^2}{\nu^2}\left[\frac{(x - x_m)}{\Delta x}\left(\mathcal{M}_{m+1}^n - \frac{\nu^2}{(\Delta x)^2}\widetilde{y}_{m+1}^n\right) + \frac{(x_{m+1} - x)}{\Delta x}\left(\mathcal{M}_m^n - \frac{\nu^2}{(\Delta x)^2}\widetilde{y}_m^n\right)\right].\end{aligned} \tag{2.2.7}$$

Rewrite the equation (2.2.7) as follows

$$\mathcal{S}_\pi(x, t_n, \delta) = \mu\widetilde{y}_{m+1}^n + \overline{\mu}\widetilde{y}_m^n + (\Delta x)^2[g(\mu)\mathcal{M}_{m+1}^n + g(\overline{\mu})\mathcal{M}_m^n]/\nu^2, \tag{2.2.8}$$

where $\mu = (x - x_m)/\Delta x$, $\overline{\mu} = 1 - \mu$, $\nu = \Delta x\sqrt{\delta}$, $g(\mu) = \frac{\sinh(\nu\mu)}{\sinh(\nu)} - \mu$. Differentiating (2.2.8) and let $x \to x_m$ to get

$$\mathcal{S}_\pi'(x_m^+, t_n, \delta) = \frac{1}{\Delta x}(\widetilde{y}_{m+1}^n - \widetilde{y}_m^n) + \frac{\Delta x}{\nu^2}\left[\left(\frac{\nu}{\sinh(\nu)} - 1\right)\mathcal{M}_{m+1}^n + \left(1 - \frac{\nu\cosh(\nu)}{\sinh(\nu)}\right)\mathcal{M}_m^n\right]. \tag{2.2.9}$$

Similarly, we proceed for the interval $[x_{m-1}, x_m]$, to obtain

$$\mathcal{S}'_\pi(x_m^-, t_n, \delta) = \frac{1}{\Delta x}(\widetilde{y}_m^n - \widetilde{y}_{m-1}^n) + \frac{\Delta x}{\nu^2}\left[\left(1 - \frac{\nu}{\sinh(\nu)}\right)\mathcal{M}_{m-1}^n + \left(\frac{\nu\cosh(\nu)}{\sinh(\nu)} - 1\right)\mathcal{M}_m^n\right]. \tag{2.2.10}$$

The first derivative of $\mathcal{S}_\pi(x, t_n, \delta)$ is continuous at $x = x_m$, so $\mathcal{S}'_\pi(x_m^-, t_n, \delta) = \mathcal{S}'_\pi(x_m^+, t_n, \delta)$ for $m = 1, 2, \ldots, N_x - 1,\ n = 1, 2, \ldots, M_t$, which gives

$$\alpha\mathcal{M}_{m-1}^n + \beta\mathcal{M}_m^n + \alpha\mathcal{M}_{m+1}^n = \frac{1}{(\Delta x)^2}\left[\widetilde{y}_{m-1}^n - 2\widetilde{y}_m^n + \widetilde{y}_{m+1}^n\right], \tag{2.2.11}$$

where $\alpha = \frac{1}{\nu^2}\left(1 - \frac{\nu}{\sinh(\nu)}\right),\ \beta = \frac{2}{\nu^2}\left(\frac{\nu\cosh(\nu)}{\sinh(\nu)} - 1\right)$. Using (2.2.3), the equation (2.2.1a) (at (x_m, t_n)) can be written as

$$\begin{aligned}
&-\left(\frac{(\widetilde{y}_{xx})_m^n + (\widetilde{y}_{xx})_m^{n+1}}{2}\right) + b_m^{n+1/2}\left(\frac{(\widetilde{y}_x)_m^n + (\widetilde{y}_x)_m^{n+1}}{2}\right) + c_m^{n+1/2}\left(\frac{\widetilde{y}_m^n + \widetilde{y}_m^{n+1}}{2}\right)\\
&= -d_m^{n+1/2}\left(\frac{\widetilde{y}_m^{n-k} + \widetilde{y}_m^{n+1-k}}{2}\right) + f_m^{n+1/2} - \sigma\left(\frac{\widetilde{y}_m^{n+1} - \widetilde{y}_m^n}{2^{1-\gamma}}\right)\\
&-\sigma\left[w_1\widetilde{y}_m^n + \sum_{i=1}^{n-1}(w_{n-i+1} - w_{n-i})\widetilde{y}_m^i - w_n\widetilde{y}_m^0\right].
\end{aligned} \tag{2.2.12}$$

Now, on replacing the second order derivative in (2.2.12) by the tension spline function defined as

$$(y_{xx})_m^n = \mathcal{S}''(x_m, t_n) = \mathcal{M}_m^n + \mathcal{O}((\Delta x)^2), \tag{2.2.13}$$

we get

$$\begin{aligned}
\frac{\mathcal{M}_m^n + \mathcal{M}_m^{n+1}}{2} =& \sigma\left[w_1\widetilde{y}_m^n + \sum_{i=1}^{n-1}(w_{n-i+1} - w_{n-i})\widetilde{y}_m^i - w_n\widetilde{y}_m^0 + \frac{\widetilde{y}_m^{n+1} - \widetilde{y}_m^n}{2^{1-\gamma}}\right]\\
&+ b_m^{n+1/2}\left(\frac{(\widetilde{y}_x)_m^n + (\widetilde{y}_x)_m^{n+1}}{2}\right) + c_m^{n+1/2}\left(\frac{\widetilde{y}_m^n + \widetilde{y}_m^{n+1}}{2}\right)\\
&+ d_m^{n+1/2}\left(\frac{\widetilde{y}_m^{n-k} + \widetilde{y}_m^{n+1-k}}{2}\right) - f_m^{n+1/2} + \mathfrak{R}_m^{n+1/2}.
\end{aligned} \tag{2.2.14}$$

Rewriting (2.2.11) at $(n+1)$-th time-level as

$$\alpha\mathcal{M}_{m-1}^{n+1} + \beta\mathcal{M}_m^{n+1} + \alpha\mathcal{M}_{m+1}^{n+1} = \frac{1}{(\Delta x)^2}\left[\widetilde{y}_{m-1}^{n+1} - 2\widetilde{y}_m^{n+1} + \widetilde{y}_{m+1}^{n+1}\right], m = 1, 2, \ldots, N_x - 1,$$

$$n = 0, 1, \ldots, M_t - 1. \tag{2.2.15}$$

On adding (2.2.11) and (2.2.15), we get

$$\alpha\left(\frac{\mathcal{M}_{m-1}^{n}+\mathcal{M}_{m-1}^{n+1}}{2}\right)+\beta\left(\frac{\mathcal{M}_{m}^{n}+\mathcal{M}_{m}^{n+1}}{2}\right)+\alpha\left(\frac{\mathcal{M}_{m+1}^{n}+\mathcal{M}_{m+1}^{n+1}}{2}\right)$$
$$=\frac{1}{(\Delta x)^2}\left[\frac{\widetilde{y}_{m-1}^{n}+\widetilde{y}_{m-1}^{n+1}}{2}-\widetilde{y}_{m}^{n}-\widetilde{y}_{m}^{n+1}+\frac{\widetilde{y}_{m+1}^{n}+\widetilde{y}_{m+1}^{n+1}}{2}\right]. \tag{2.2.16}$$

A use of (2.2.14) in (2.2.16) yields

$$\left[\alpha\left(\frac{\sigma}{2^{1-\gamma}}-\frac{b_{m-1}^{n+1/2}}{2\Delta x}+\frac{c_{m-1}^{n+1/2}}{2}\right)-\frac{\beta b_{m}^{n+1/2}}{4\Delta x}-\frac{1}{2(\Delta x)^2}\right]\widetilde{y}_{m-1}^{n+1}+\left[\frac{\alpha b_{m-1}^{n+1/2}}{2(\Delta x)}+\beta\left(\frac{\sigma}{2^{1-\gamma}}+\frac{c_{m}^{n+1/2}}{2}\right)\right.$$
$$\left.-\frac{\alpha b_{m+1}^{n+1/2}}{2\Delta x}+\frac{1}{(\Delta x)^2}\right]\widetilde{y}_{m}^{n+1}+\left[\alpha\left(\frac{\sigma}{2^{1-\gamma}}+\frac{b_{m+1}^{n+1/2}}{2\Delta x}+\frac{c_{m+1}^{n+1/2}}{2}\right)+\frac{\beta b_{m}^{n+1/2}}{4\Delta x}-\frac{1}{2(\Delta x)^2}\right]\widetilde{y}_{m+1}^{n+1}$$
$$=\left[\alpha\left(\frac{\sigma}{2^{1-\gamma}}+\frac{b_{m-1}^{n+1/2}}{2\Delta x}-\frac{c_{m-1}^{n+1/2}}{2}\right)+\frac{\beta b_{m}^{n+1/2}}{4\Delta x}+\frac{1}{2(\Delta x)^2}\right]\widetilde{y}_{m-1}^{n}+\left[-\frac{\alpha b_{m-1}^{n+1/2}}{2\Delta x}\right.$$
$$\left.+\beta\left(\frac{\sigma}{2^{1-\gamma}}-\frac{c_{m}^{n+1/2}}{2}\right)+\frac{\alpha b_{m+1}^{n+1/2}}{2\Delta x}-\frac{1}{(\Delta x)^2}\right]\widetilde{y}_{m}^{n}+\left[\alpha\left(\frac{\sigma}{2^{1-\gamma}}-\frac{b_{m+1}^{n+1/2}}{2\Delta x}-\frac{c_{m+1}^{n+1/2}}{2}\right)\right.$$
$$\left.-\frac{\beta b_{m}^{n+1/2}}{4\Delta x}+\frac{1}{2(\Delta x)^2}\right]\widetilde{y}_{m+1}^{n}-\sigma w_1\left(\alpha\widetilde{y}_{m-1}^{n}+\beta\widetilde{y}_{m}^{n}+\alpha\widetilde{y}_{m+1}^{n}\right)+\sigma w_n\left(\alpha\widetilde{y}_{m-1}^{0}+\beta\widetilde{y}_{m}^{0}+\alpha\widetilde{y}_{m+1}^{0}\right)$$
$$-\sigma\sum_{q=1}^{n-1}(w_{n-q+1}-w_{n-q})\left(\alpha\widetilde{y}_{m-1}^{q}+\beta\widetilde{y}_{m}^{q}+\alpha\widetilde{y}_{m+1}^{q}\right)-\frac{1}{2}\left[\alpha d_{m-1}^{n+1/2}(\widetilde{y}_{m-1}^{n+1-k}+\widetilde{y}_{m-1}^{n-k})\right.$$
$$\left.+\beta d_{m}^{n+1/2}(\widetilde{y}_{m}^{n+1-k}+\widetilde{y}_{m}^{n-k})+\alpha d_{m+1}^{n+1/2}(\widetilde{y}_{m+1}^{n+1-k}+\widetilde{y}_{m+1}^{n-k})\right]$$
$$+\left(\alpha f_{m-1}^{n+1/2}+\beta f_{m}^{n+1/2}+\alpha f_{m+1}^{n+1/2}\right)+\mathfrak{T}_{m}^{n+1/2}, \tag{2.2.17}$$

where $\mathfrak{T}_{m}^{n+1/2}=\alpha\mathfrak{R}_{m-1}^{n+1/2}+\beta\mathfrak{R}_{m}^{n+1/2}+\alpha\mathfrak{R}_{m+1}^{n+1/2}$. We assume that Y_m^n is the approximate solution of $\widetilde{y}_m^n$ and omitting the truncation error from (2.2.17), we find the following numerical scheme for (2.1.1)

$$\left[\alpha\left(\frac{\sigma}{2^{1-\gamma}}-\frac{b_{m-1}^{n+1/2}}{2\Delta x}+\frac{c_{m-1}^{n+1/2}}{2}\right)-\frac{\beta b_{m}^{n+1/2}}{4\Delta x}-\frac{1}{2(\Delta x)^2}\right]Y_{m-1}^{n+1}+\left[\frac{\alpha b_{m-1}^{n+1/2}}{2\Delta x}+\alpha\left(\frac{\sigma}{2^{1-\gamma}}+\frac{c_{m}^{n+1/2}}{2}\right)\right.$$

$$
\begin{aligned}
&- \frac{\alpha b_{m+1}^{n+1/2}}{2\Delta x} + \frac{1}{(\Delta x)^2}\Bigg] Y_m^{n+1} + \left[\alpha\left(\frac{\sigma}{2^{1-\gamma}} + \frac{b_{m+1}^{n+1/2}}{2\Delta x} + \frac{c_{m+1}^{n+1/2}}{2}\right) + \frac{\beta b_m^{n+1/2}}{4\Delta x} - \frac{1}{2(\Delta x)^2}\right] Y_{m+1}^{n+1} \\
&= \left[\alpha\left(\frac{\sigma}{2^{1-\gamma}} + \frac{b_{m-1}^{n+1/2}}{2\Delta x} - \frac{c_{m-1}^{n+1/2}}{2}\right) + \frac{\beta b_m^{n+1/2}}{4\Delta x} + \frac{1}{2(\Delta x)^2}\right] Y_{m-1}^{n} + \Bigg[- \frac{\alpha b_{m-1}^{n+1/2}}{2\Delta x} \\
&+ \beta\left(\frac{\sigma}{2^{1-\gamma}} - \frac{c_m^{n+1/2}}{2}\right) + \frac{\alpha b_{m+1}^{n+1/2}}{2\Delta x} - \frac{1}{(\Delta x)^2}\Bigg] Y_m^n + \left[\alpha\left(\frac{\sigma}{2^{1-\gamma}} - \frac{b_{m+1}^{n+1/2}}{2\Delta x} - \frac{c_{m+1}^{n+1/2}}{2}\right)\right. \\
&\left. - \frac{\beta b_m^{n+1/2}}{4\Delta x} + \frac{1}{2(\Delta x)^2}\right] Y_{m+1}^n - \sigma w_1\left(\alpha Y_{m-1}^n + \beta Y_m^n + \alpha Y_{m+1}^n\right) \\
&+ \sigma w_n\left(\alpha Y_{m-1}^0 + \beta Y_m^0 + \alpha Y_{m+1}^0\right) - \sigma\sum_{q=1}^{n-1}(w_{n-q+1} - w_{n-q})\left(\alpha Y_{m-1}^q + \beta Y_m^q + \alpha Y_{m+1}^q\right) \\
&- \frac{1}{2}\left[\alpha d_{m-1}^{n+1/2}(Y_{m-1}^{n+1-k} + Y_{m-1}^{n-k}) + \beta d_m^{n+1/2}(Y_m^{n+1-k} + Y_m^{n-k}) + \alpha d_{m+1}^{n+1/2}(Y_{m+1}^{n+1-k} + Y_{m+1}^{n-k})\right] \\
&+ \left(\alpha f_{m-1}^{n+1/2} + \beta f_m^{n+1/2} + \alpha f_{m+1}^{n+1/2}\right), \quad m = 1, 2, \ldots, N_x - 1, \quad n = 0, 1, \ldots, M_t - 1,
\end{aligned}
\tag{2.2.18a}
$$

with the interval and boundary conditions

$$
Y_m^n = \psi_b(x_m, t_n), \quad 0 \le m \le N_x, \quad -k \le n \le 0, \tag{2.2.18b}
$$

$$
Y_0^{n+1} = \psi_l(t_{n+1}), \quad Y_{N_x}^{n+1} = \psi_r(t_{n+1}), \quad 0 \le n \le M_t - 1. \tag{2.2.18c}
$$

Let

$$
\begin{aligned}
E(m,n) &= \alpha\left(\frac{\sigma}{2^{1-\gamma}} - \frac{b_{m-1}^{n+1/2}}{2\Delta x} + \frac{c_{m-1}^{n+1/2}}{2}\right) - \frac{\beta b_m^{n+1/2}}{4\Delta x} - \frac{1}{2(\Delta x)^2}, \\
F(m,n) &= \frac{\alpha b_{m-1}^{n+1/2}}{2\Delta x} + \beta\left(\frac{\sigma}{2^{1-\gamma}} + \frac{c_m^{n+1/2}}{2}\right) - \frac{\alpha b_{m+1}^{n+1/2}}{2\Delta x} + \frac{1}{(\Delta x)^2}, \\
G(m,n) &= \alpha\left(\frac{\sigma}{2^{1-\gamma}} + \frac{b_{m+1}^{n+1/2}}{2\Delta x} + \frac{c_{m+1}^{n+1/2}}{2}\right) + \frac{\beta b_m^{n+1/2}}{4\Delta x} - \frac{1}{2(\Delta x)^2},
\end{aligned}
\tag{2.2.19}
$$

then we can write the system (2.2.18) in matrix form as

$$
AC^{n+1} = B^n,
$$

with the coefficient matrix

$$A = \begin{bmatrix} F(1,n) & G(1,n) & 0 & & & \\ E(2,n) & F(2,n) & G(2,n) & & & \\ \ddots & \ddots & \ddots & & & \\ & & \ddots & \ddots & \ddots & \\ & & E(N_x-2,n) & F(N_x-2,n) & G(N_x-2,n) & \\ & & 0 & E(N_x-1,n) & F(N_x-1,n) & \end{bmatrix}_{(N_x-1)\times(N_x-1)}.$$

2.3 Local truncation error

To find the local truncation error $\hat{\mathfrak{T}}_m^n$ of the proposed scheme, we replace $\mathcal{M}_{m-1}^n$, $\mathcal{M}_m^n$, and $\mathcal{M}_{m+1}^n$ by $\frac{\partial^2 \widetilde{y}_{m-1}^n}{\partial x^2}$, $\frac{\partial^2 \widetilde{y}_m^n}{\partial x^2}$, and $\frac{\partial^2 \widetilde{y}_{m+1}^n}{\partial x^2}$, respectively in (2.2.11), to get

$$\hat{\mathfrak{T}}_m^n = \alpha\frac{\partial^2 \widetilde{y}_{m-1}^n}{\partial x^2} + \beta\frac{\partial^2 \widetilde{y}_m^n}{\partial x^2} + \alpha\frac{\partial^2 \widetilde{y}_{m+1}^n}{\partial x^2} - \frac{1}{(\Delta x)^2}\left[\widetilde{y}_{m-1}^n - 2\widetilde{y}_m^n + \widetilde{y}_{m+1}^n\right] + \mathcal{O}((\Delta x)^p),\ p \geq 0.$$

Using Taylor series expansion for $\widetilde{y}_{m-1}^n$ and $\widetilde{y}_{m+1}^n$ in term of $\widetilde{y}_m^n$ and its derivatives, we get

$$\hat{\mathfrak{T}}_m^n = ((2\alpha+\beta)-1)\frac{\partial^2 \widetilde{y}_m^n}{\partial x^2} + (\Delta x)^2\left(\alpha - \frac{1}{12}\right)\frac{\partial^4 \widetilde{y}_m^n}{\partial x^4} + (\Delta x)^4\left(\frac{1}{360} - \frac{\alpha}{12}\right)\frac{\partial^6 \widetilde{y}_m^n}{\partial x^6} + \mathcal{O}((\Delta x)^p). \tag{2.3.1}$$

It is clear from (2.3.1) that for suitable arbitrary values of α ($\alpha \neq 1/12$) and β such that $2\alpha + \beta = 1$, the value of $p = 2$ is 2. Now, from (2.2.12) the local truncation error $\mathfrak{R}_m^{n+1/2}$ is

$$\begin{aligned} \mathfrak{R}_m^{n+1/2} =& -\sigma\left[w_1\widetilde{y}_m^n + \sum_{i=1}^{n-1}(w_{n-i+1} - w_{n-i})\widetilde{y}_m^i - w_n\widetilde{y}_m^0 + \frac{\widetilde{y}_m^{n+1} - \widetilde{y}_m^n}{2^{1-\gamma}}\right] \\ &+ b_m^{n+1/2}\left(\frac{(\widetilde{y}_x)_m^n + (\widetilde{y}_x)_m^{n+1}}{2}\right) + c_m^{n+1/2}\left(\frac{\widetilde{y}_m^n + \widetilde{y}_m^{n+1}}{2}\right) \\ &- d_m^{n+1/2}\left(\frac{\widetilde{y}_m^{n-k} + \widetilde{y}_m^{n+1-k}}{2}\right) + \mathcal{M}_m^{n+1/2} + f_m^{n+1/2} \\ =& \mathcal{O}((\Delta x)^2 + (\Delta t)^2). \end{aligned}$$

Thus, the local truncation error $\mathfrak{T}_m^{n+1/2}$ in (2.2.17) is given by

$$
\begin{aligned}
&\mathfrak{T}_m^{n+1/2} = \alpha\mathfrak{R}_{m-1}^{n+1/2} + \beta\mathfrak{R}_m^{n+1/2} + \alpha\mathfrak{R}_{m+1}^{n+1/2} \\
&= -\alpha\sigma\left[w_1\widetilde{y}_{m-1}^n + \sum_{i=1}^{n-1}(w_{n-i+1} - w_{n-i})\widetilde{y}_{m-1}^i - w_n\widetilde{y}_{m-1}^0 + \frac{\widetilde{y}_{m-1}^{n+1} - \widetilde{y}_{m-1}^n}{2^{1-\gamma}}\right] \\
&- \beta\sigma\left[w_1\widetilde{y}_m^n + \sum_{i=1}^{n-1}(w_{n-i+1} - w_{n-i})\widetilde{y}_m^i - w_n\widetilde{y}_m^0 + \frac{\widetilde{y}_m^{n+1} - \widetilde{y}_m^n}{2^{1-\gamma}}\right] \\
&- \alpha\sigma\left[w_1\widetilde{y}_{m+1}^n + \sum_{i=1}^{n-1}(w_{n-i+1} - w_{n-i})\widetilde{y}_{m+1}^i - w_n\widetilde{y}_{m+1}^0 + \frac{\widetilde{y}_{m+1}^{n+1} - \widetilde{y}_{m+1}^n}{2^{1-\gamma}}\right] \\
&+ \alpha\left[b_{m-1}^{n+1/2}\left(\frac{(\widetilde{y}_x)_{m-1}^n + (\widetilde{y}_x)_{m-1}^{n+1}}{2}\right) + c_{m-1}^{n+1/2}\left(\frac{\widetilde{y}_{m-1}^n + \widetilde{y}_{m-1}^{n+1}}{2}\right) - d_{m-1}^{n+1/2}\left(\frac{\widetilde{y}_{m-1}^{n-k} + \widetilde{y}_{m-1}^{n+1-k}}{2}\right)\right] \\
&+ \beta\left[b_m^{n+1/2}\left(\frac{(\widetilde{y}_x)_m^n + (\widetilde{y}_x)_m^{n+1}}{2}\right) + c_m^{n+1/2}\left(\frac{\widetilde{y}_m^n + \widetilde{y}_m^{n+1}}{2}\right) - d_m^{n+1/2}\left(\frac{\widetilde{y}_m^{n-k} + \widetilde{y}_m^{n+1-k}}{2}\right)\right] \\
&+ \alpha\left[b_{m+1}^{n+1/2}\left(\frac{(\widetilde{y}_x)_{m+1}^n + (\widetilde{y}_x)_{m+1}^{n+1}}{2}\right) + c_{m+1}^{n+1/2}\left(\frac{\widetilde{y}_{m+1}^n + \widetilde{y}_{m+1}^{n+1}}{2}\right) - d_{m+1}^{n+1/2}\left(\frac{\widetilde{y}_{m+1}^{n-k} + \widetilde{y}_{m+1}^{n+1-k}}{2}\right)\right] \\
&+ \left((\alpha\mathcal{M}_{m-1}^{n+1/2} + \beta\mathcal{M}_m^{n+1/2} + \alpha\mathcal{M}_{m+1}^{n+1/2}\right) + \left(\alpha f_{m-1}^{n+1/2} + \beta f_m^{n+1/2} + \alpha f_{m+1}^{n+1/2}\right) \\
&= (2\alpha + \beta)(\mathcal{O}(\Delta x)^2 + \mathcal{O}(\Delta t)^2) \\
&\leq C((\Delta x)^2 + (\Delta t)^2). \qquad (2.3.2)
\end{aligned}
$$

2.4 Stability analysis

In this section, we will discuss the stability of the numerical scheme (2.2.18) using the Von Neumann stability method. We write the numerical scheme in the following form

$$
\begin{aligned}
&E(m,n)Y_{m-1}^{n+1} + F(m,n)Y_m^{n+1} + G(m,n)Y_{m+1}^{n+1} = E_1(m,n)Y_{m-1}^n + F_1(m,n)Y_m^n \\
&+ G_1(m,n)Y_{m+1}^n - \sigma w_1\left(\alpha Y_{m-1}^n + \beta Y_m^n + \alpha Y_{m+1}^n\right) + \sigma w_n\left(\alpha Y_{m-1}^0 + \beta Y_m^0 + \alpha Y_{m+1}^0\right) \\
&- \sigma\sum_{q=1}^{n-1}(w_{n-q+1} - w_{n-q})\left(\alpha Y_{m-1}^q + \beta Y_m^q + \alpha Y_{m+1}^q\right) - \frac{1}{2}\Bigg[\alpha d_{m-1}^{n+1/2}(Y_{m-1}^{n+1-k} + Y_{m-1}^{n-k}) \\
&+ \beta d_m^{n+1/2}(Y_m^{n+1-k} + Y_m^{n-k}) + \alpha d_{m+1}^{n+1/2}(Y_{m+1}^{n+1-k} + Y_{m+1}^{n-k})\Bigg] \\
&+ \left(\alpha f_{m-1}^{n+1/2} + \beta f_m^{n+1/2} + \alpha f_{m+1}^{n+1/2}\right), \quad m = 1, 2, \ldots, N_x - 1, \quad n = 0, 1, \ldots, M_t - 1,
\end{aligned}
\qquad (2.4.1)
$$

where

$$E_1(m,n) = \alpha\left(\frac{\sigma}{2^{1-\gamma}} + \frac{b_{m-1}^{n+1/2}}{2\Delta x} - \frac{c_{m-1}^{n+1/2}}{2}\right) + \frac{\beta b_m^{n+1/2}}{4\Delta x} + \frac{1}{2(\Delta x)^2},$$
$$F_1(m,n) = -\frac{\alpha b_{m-1}^{n+1/2}}{2\Delta x} + \beta\left(\frac{\sigma}{2^{1-\gamma}} - \frac{c_m^{n+1/2}}{2}\right) + \frac{\alpha b_{m+1}^{n+1/2}}{2\Delta x} - \frac{1}{(\Delta x)^2},$$
$$G_1(m,n) = \alpha\left(\frac{\sigma}{2^{1-\gamma}} - \frac{b_{m+1}^{n+1/2}}{2\Delta x} - \frac{c_{m+1}^{n+1/2}}{2}\right) - \frac{\beta b_m^{n+1/2}}{4\Delta x} + \frac{1}{2(\Delta x)^2}.$$

Let $\hat{Y}_m^n$ be the approximate solution of the system (2.2.18) and $\xi_m^n = Y_m^n - \hat{Y}_m^n$. The error equation of (2.4.1) is

$$\begin{aligned}
&E(m,n)\xi_{m-1}^{n+1} + F(m,n)\xi_m^{n+1} + G(m,n)\xi_{m+1}^{n+1} = E_1(m,n)\xi_{m-1}^n + F_1(m,n)\xi_m^n + G_1(m,n)\xi_{m+1}^n \\
&- \sigma w_1(\alpha\xi_{m-1}^n + \beta\xi_m^n + \alpha\xi_{m+1}^n) + \sigma w_n(\alpha\xi_{m-1}^0 + \beta\xi_m^0 + \alpha\xi_{m+1}^0) \\
&- \sigma\sum_{q=1}^{n-1}(w_{n-q+1} - w_{n-q})\left(\alpha\xi_{m-1}^q + \beta\xi_m^q + \alpha\xi_{m+1}^q\right) \\
&- \frac{1}{2}\left[\alpha d_{m-1}^{n+1/2}(\xi_{m-1}^{n+1-k} + \xi_{m-1}^{n-k}) + \beta d_m^{n+1/2}(\xi_m^{n+1-k} + \xi_m^{n-k}) + \alpha d_{m+1}^{n+1/2}(\xi_{m+1}^{n+1-k} + \xi_{m+1}^{n-k})\right], \\
&\quad m = 1, 2, \ldots, N_x - 1, \quad n = 0, 1, \ldots, M_t - 1,
\end{aligned} \tag{2.4.2}$$

along with the conditions

$$\xi_0^n = \xi_{N_x}^n = 0,\ n = 0, 1, \ldots, M_t.$$

The grid functions

$$\xi^n(x) = \begin{cases} \xi_m^n, & x_m - \frac{\Delta x}{2} < x < x_m + \frac{\Delta x}{2},\ m = 1, 2, \ldots, N_x - 1, \\ 0, & 0 \le x \le \frac{\Delta x}{2} \text{ or } 1 - \frac{\Delta x}{2} \le x \le 1, \end{cases}$$

have the following Fourier series expansion

$$\xi^n(x) = \sum_{j=-\infty}^{\infty} \zeta^n(j) e^{i(2j\pi x)},\ n = 0, 1, \ldots, M_t,$$

where

$$\zeta^n(j) = \int_0^1 \xi^n(x) e^{-i(2j\pi x)} dx.$$

Using Parseval's identity in L_2-norm, we find

$$||\xi^n||_2^2 = \sum_{m=1}^{N_x-1} \Delta x |\xi_m^n|^2 = \int_0^1 |\xi^n(x)|^2 dx = \sum_{j=-\infty}^{\infty} |\zeta^n(j)|^2.$$

According to the above analysis, we can assume that

$$\xi_m^n = \zeta^n e^{i\theta m \Delta x},$$

where $i = \sqrt{-1}$ and θ is wave number, then from (2.4.2)

$$\begin{aligned}
&E(m,n)\zeta^{n+1}e^{i\theta(m-1)\Delta x} + F(m,n)\zeta^{n+1}e^{i\theta m\Delta x} + G(m,n)\zeta^{n+1}e^{i\theta(m+1)\Delta x} \\
&= E_1(m,n)\zeta^n e^{i\theta(m-1)\Delta x} + F_1(m,n)\zeta^n e^{i\theta m\Delta x} + G_1(m,n)\zeta^n e^{i\theta(m+1)\Delta x} \\
&- \sigma w_1 \left(\alpha\zeta^n e^{i\theta(m-1)\Delta x} + \beta\zeta^n e^{i\theta m\Delta x} + \alpha\zeta^n e^{i\theta(m+1)\Delta x}\right) \\
&+ \sigma w_n \left(\alpha\zeta^0 e^{i\theta(m-1)\Delta x} + \beta\zeta^0 e^{i\theta m\Delta x} + \alpha\zeta^0 e^{i\theta(m+1)\Delta x}\right) \\
&- \sigma \sum_{q=1}^{n-1} (w_{n-q+1} - w_{n-q}) \left(\alpha\zeta^q e^{i\theta(m-1)\Delta x} + \beta\zeta^q e^{i\theta m\Delta x} + \alpha\zeta^q e^{i\theta(m+1)\Delta x}\right) \\
&- \frac{1}{2}\left[\alpha d_{m-1}^{n+1/2}(\zeta^{n+1-k}e^{i\theta(m-1)\Delta x} + \zeta^{n-k}e^{i\theta(m-1)\Delta x}) + \beta d_m^{n+1/2}(\zeta^{n+1-k}e^{i\theta m\Delta x} + \zeta^{n-k}e^{i\theta m\Delta x})\right] \\
&- \frac{1}{2}\alpha d_{m+1}^{n+1/2}(\zeta^{n+1-k}e^{i\theta(m+1)\Delta x} + \zeta^{n-k}e^{i\theta(m+1)\Delta x}). \qquad (2.4.3)
\end{aligned}$$

Dividing both sides by $e^{i\theta m\Delta x}$, we obtain

$$\begin{aligned}
&\zeta^{n+1}[E(m,n)e^{-i\theta\Delta x} + F(m,n) + G(m,n)e^{i\theta\Delta x}] = \zeta^n \Big[E_1(m,n)e^{-i\theta\Delta x} + F_1(m,n) \\
&+ G_1(m,n)e^{i\theta\Delta x}\Big] - \sigma w_1 \zeta^n \left(\alpha e^{-i\theta\Delta x} + \beta + \alpha e^{i\theta\Delta x}\right) + \sigma w_n \zeta^0 \left(\alpha e^{-i\theta\Delta x} + \beta + \alpha e^{i\theta\Delta x}\right) \\
&- \sigma \sum_{q=1}^{n-1} (w_{n-q+1} - w_{n-q})\zeta^q \left(\alpha e^{-i\theta\Delta x} + \beta + \alpha e^{i\theta\Delta x}\right) \\
&- \frac{1}{2}(\zeta^{n+1-k} + \zeta^{n-k}) \left(\alpha d_{m-1}^{n+1/2} e^{-i\theta\Delta x} + \beta d_m^{n+1/2} - \alpha d_{m+1}^{n+1/2} e^{i\theta\Delta x}\right). \qquad (2.4.4)
\end{aligned}$$

After simplification for $n = 0, 1, \ldots, k-1$, we get the following form

$$\zeta^{n+1} = \left(\frac{U_1 - w_1 U}{U_2}\right)\zeta^n - \frac{U}{U_2}\left(\sum_{q=1}^{n-1}(w_{n-q+1} - w_{n-q})\zeta^q + w_n\zeta^0\right), \tag{2.4.5a}$$

and for $n = k, k+1, \ldots, M_t - 1$, we have

$$\begin{aligned}\zeta^{n+1} = &\left(\frac{U_1 - w_1 U}{U_2}\right)\zeta^n - \frac{U}{U_2}\left(\sum_{q=1}^{n-1}(w_{n-q+1} - w_{n-q})\zeta^q + w_n\zeta^0\right)\\ &- \frac{1}{2U_2}(\zeta^{n+1-k} + \zeta^{n-k})\left(\alpha d_{m-1}^{n+1/2}e^{-i\theta\Delta x} + \beta d_m^{n+1/2} - \alpha d_{m+1}^{n+1/2}e^{i\theta\Delta x}\right),\end{aligned} \tag{2.4.5b}$$

where

$$\begin{aligned}U &= \sigma(2\alpha\cos(\theta\Delta x) + \beta),\\ U_1 &= E_1(m,n)e^{-i\theta\Delta x} + F_1(m,n) + G_1(m,n)e^{i\theta\Delta x},\\ U_2 &= E(m,n)e^{-i\theta\Delta x} + F(m,n) + G(m,n)e^{i\theta\Delta x}.\end{aligned}$$

For stability of numerical scheme (2.2.18), we prove that $|\zeta^{n+1}| \le |\zeta^0|$ by use of mathematical induction. For $n = 0$, (2.4.5a) yields

$$\begin{aligned}|\zeta^1| &= \left|\left(\frac{U_1 - w_1 U}{U_2}\right)\zeta^0\right|\\ &= \left|\frac{(2\alpha\cos(\theta\Delta x) + \beta)\left(\frac{\sigma}{2^{1-\gamma}} - \sigma w_1\right) + (1 - \cos(\theta\Delta x))(-X_1) - X_2 - iX_3\sin(\theta\Delta x)}{(2\alpha\cos(\theta\Delta x) + \beta)\left(\frac{\sigma}{2^{1-\gamma}}\right) + (1 - \cos(\theta\Delta x))(X_1) + X_2 + iX_3\sin(\theta\Delta x)}\right||\zeta^0|\\ &\le \frac{\left|(2\alpha\cos(\theta\Delta x) + \beta)\left(\frac{\sigma}{2^{1-\gamma}} - \sigma w_1\right) + (1 - \cos(\theta\Delta x))(-X_1) - X_2\right| + X_3\sin(\theta\Delta x)}{\left|(2\alpha\cos(\theta\Delta x) + \beta)\left(\frac{\sigma}{2^{1-\gamma}}\right) + (1 - \cos(\theta\Delta x))(X_1) + X_2 + iX_3\sin(\theta\Delta x)\right|}|\zeta^0|\\ &= R|\zeta^0|,\end{aligned}$$

where

$$\begin{aligned}X_1 &= \frac{1}{(\Delta x)^2} + \frac{\alpha}{2\Delta x}b_{m-1}^{1/2} - \frac{\alpha}{2\Delta x}b_{m+1}^{1/2},\\ X_2 &= \frac{\beta}{2}c_m^{1/2} + \frac{\alpha\cos(\theta\Delta x)}{2}(c_{m-1}^{1/2} + c_{m+1}^{1/2}),\end{aligned}$$

$$X_3 = \frac{\beta}{2\Delta x} b_m^{1/2} + \frac{\alpha}{2\Delta x} b_{m-1}^{1/2} + \frac{\alpha}{2\Delta x} b_{m+1}^{1/2} - \frac{\alpha}{2} c_{m-1}^{1/2} + \frac{\alpha}{2} c_{m+1}^{1/2},$$
$$R = \frac{\left|(2\alpha\cos(\theta\Delta x)+\beta)\left(\frac{\sigma}{2^{1-\gamma}} - \sigma w_1\right) - (1-\cos(\theta\Delta x))X_1 - X_2\right| + X_3\sin(\theta\Delta x)}{\left|(2\alpha\cos(\theta\Delta x)+\beta)\left(\frac{\sigma}{2^{1-\gamma}}\right) + (1-\cos(\theta\Delta x))X_1 + X_2 + iX_3\sin(\theta\Delta x)\right|}.$$

To show that $R \leq 1$, we consider two cases.

Case 1. If $(2\alpha\cos(\theta\Delta x)+\beta)\left(\frac{\sigma}{2^{1-\gamma}} - \sigma w_1\right) - (1-\cos(\theta\Delta x))X_1 - X_2 \geq 0$. Then $R \leq 1$ gives,

$$\frac{\left|(2\alpha\cos(\theta\Delta x)+\beta)\left(\frac{\sigma}{2^{1-\gamma}} - \sigma w_1\right) - (1-\cos(\theta\Delta x))X_1 - X_2\right| + X_3\sin(\theta\Delta x)}{\left|(2\alpha\cos(\theta\Delta x)+\beta)\left(\frac{\sigma}{2^{1-\gamma}}\right) + (1-\cos(\theta\Delta x))X_1 + X_2 + iX_3\sin(\theta\Delta x)\right|} \leq 1,$$

which gives

$$(2\alpha\cos(\theta\Delta x)+\beta)\left(\frac{\sigma}{2^{1-\gamma}} - \sigma w_1\right) - (1-\cos(\theta\Delta x))X_1 - X_2 \leq (2\alpha\cos(\theta\Delta x)+\beta)\left(\frac{\sigma}{2^{1-\gamma}}\right) + (1-\cos(\theta\Delta x))X_1 + X_2,$$

if and only if

$$(2\alpha\cos(\theta\Delta x)+\beta)(\sigma w_1) + 2(1-\cos(\theta\Delta x))X_1 + 2X_2 \geq 0,$$

which is true for all θ and Δx.

Case 2. If $(2\alpha\cos(\theta\Delta x)+\beta)\left(\frac{\sigma}{2^{1-\gamma}} - \sigma w_1\right) - (1-\cos(\theta\Delta x))X_1 - X_2 \leq 0$. Then $R \leq 1$ gives

$$\frac{\left|(2\alpha\cos(\theta\Delta x)+\beta)\left(\frac{\sigma}{2^{1-\gamma}} - \sigma w_1\right) - (1-\cos(\theta\Delta x))X_1 - X_2\right| + X_3\sin(\theta\Delta x)}{\left|(2\alpha\cos(\theta\Delta x)+\beta)\left(\frac{\sigma}{2^{1-\gamma}}\right) + (1-\cos(\theta\Delta x))X_1 + X_2 + iX_3\sin(\theta\Delta x)\right|} \leq 1,$$

which gives

$$-(2\alpha\cos(\theta\Delta x)+\beta)\left(\frac{\sigma}{2^{1-\gamma}} - \sigma w_1\right) + (1-\cos(\theta\Delta x))X_1 + X_2 \leq (2\alpha\cos(\theta\Delta x)+\beta)\left(\frac{\sigma}{2^{1-\gamma}}\right) + (1-\cos(\theta\Delta x))X_1 + X_2,$$

which conclude that $w_1 \leq \frac{2}{2^{1-\gamma}}$, true for all values of γ. Now we assume that

$$|\zeta^j| \leq |\zeta^0|, \text{ for } j = 2, 3, \ldots, n. \tag{2.4.6}$$

We will prove that (2.4.6) holds for $j = n + 1$. The equation (2.4.5a) yields

$$\begin{aligned}
|\zeta^{n+1}| &\leq \left(\frac{|U_1 - w_1 U| + w_1|U|}{|U_2|}\right)|\zeta^0| \\
&= \left|\frac{(2\alpha\cos(\theta\Delta x) + \beta)\left(\frac{\sigma}{2^{1-\gamma}} - \sigma w_1\right) - (1 - \cos(\theta\Delta x))X_1 - X_2 - iX_3\sin(\theta\Delta x)}{(2\alpha\cos(\theta\Delta x) + \beta)\left(\frac{\sigma}{2^{1-\gamma}}\right) + (1 - \cos(\theta\Delta x))X_1 + X_2 + iX_3\sin(\theta\Delta x)}\right||\zeta^0| \\
&+ \frac{\sigma w_1(2\alpha\cos(\theta\Delta x) + \beta)}{\left|(2\alpha\cos(\theta\Delta x) + \beta)\left(\frac{\sigma}{2^{1-\gamma}}\right) + (1 - \cos(\theta\Delta x))X_1 + X_2 + iX_3\sin(\theta\Delta x)\right|}|\zeta^0| \\
&\leq \frac{\left|(2\alpha\cos(\theta\Delta x) + \beta)\left(\frac{\sigma}{2^{1-\gamma}} - \sigma w_1\right) - (1 - \cos(\theta\Delta x))X_1 - X_2\right| + X_3\sin(\theta\Delta x)}{\left|(2\alpha\cos(\theta\Delta x) + \beta)\left(\frac{\sigma}{2^{1-\gamma}}\right) + (1 - \cos(\theta\Delta x))X_1 + X_2 + iX_3\sin(\theta\Delta x)\right|}|\zeta^0| \\
&+ \frac{\sigma w_1(2\alpha\cos(\theta\Delta x) + \beta)}{\left|(2\alpha\cos(\theta\Delta x) + \beta)\left(\frac{\sigma}{2^{1-\gamma}}\right) + (1 - \cos(\theta\Delta x))X_1 + X_2 + iX_3\sin(\theta\Delta x)\right|}|\zeta^0|.
\end{aligned}$$

Again, there arise two cases.

Case 1. If $(2\alpha\cos(\theta\Delta x) + \beta)\left(\frac{\sigma}{2^{1-\gamma}} - \sigma w_1\right) - (1 - \cos(\theta\Delta x))X_1 - X_2 \geq 0$, then

$$\begin{aligned}
|\zeta^{n+1}| &\leq \frac{(2\alpha\cos(\theta\Delta x) + \beta)\left(\frac{\sigma}{2^{1-\gamma}}\right) - (1 - \cos(\theta\Delta x))X_1 - X_2 + X_3\sin(\theta\Delta x)}{\left|(2\alpha\cos(\theta\Delta x) + \beta)\left(\frac{\sigma}{2^{1-\gamma}}\right) + (1 - \cos(\theta\Delta x))X_1 + X_2 + iX_3\sin(\theta\Delta x)\right|}|\zeta^0| \\
&\leq |\zeta^0|.
\end{aligned}$$

Case 2. If $(2\alpha\cos(\theta\Delta x) + \beta)\left(\frac{\sigma}{2^{1-\gamma}} - \sigma w_1\right) - (1 - \cos(\theta\Delta x))X_1 - X_2 \leq 0$, then

$$|\zeta^{n+1}| \leq \frac{-(2\alpha\cos(\theta\Delta x) + \beta)\left(\frac{\sigma}{2^{1-\gamma}} - 2\sigma w_1\right) + (1 - \cos(\theta\Delta x))X_1 + X_2 + X_3\sin(\theta\Delta x)}{\left|(2\alpha\cos(\theta\Delta x) + \beta)\left(\frac{\sigma}{2^{1-\gamma}}\right) + (1 - \cos(\theta\Delta x))X_1 + X_2 + iX_3\sin(\theta\Delta x)\right|}|\zeta^0|.$$

Now for $|\zeta^{n+1}| \leq |\zeta^0|$, we have

$$\frac{-(2\alpha\cos(\theta\Delta x) + \beta)\left(\frac{\sigma}{2^{1-\gamma}} - 2\sigma w_1\right) + (1 - \cos(\theta\Delta x))X_1 + X_2 + X_3\sin(\theta\Delta x)}{\left|(2\alpha\cos(\theta\Delta x) + \beta)\left(\frac{\sigma}{2^{1-\gamma}}\right) + (1 - \cos(\theta\Delta x))X_1 + X_2 + iX_3\sin(\theta\Delta x)\right|} \leq 1,$$

that gives

$$-(2\alpha\cos(\theta\Delta x)+\beta)\left(\frac{\sigma}{2^{1-\gamma}}-2\sigma w_1\right)+(1-\cos(\theta\Delta x))X_1+X_2$$
$$\leq(2\alpha\cos(\theta\Delta x)+\beta)\left(\frac{\sigma}{2^{1-\gamma}}\right)+(1-\cos(\theta\Delta x))X_1+X_2.$$

Last inequality holds true when $\frac{1}{2^{1-\gamma}}\geq w_1$ or $3^\gamma\geq\frac{3}{2}$. Now for $n=k,k+1,\ldots,M_t-1$, the equation (2.4.5b) becomes

$$|\zeta^{n+1}|\leq\left(\frac{|U_1-w_1U|+w_1|U|+|\alpha d_{m-1}^{n+1/2}e^{-i\theta\Delta x}+\beta d_m^{n+1/2}-\alpha d_{m+1}^{n+1/2}e^{i\theta\Delta x}|}{|U_2|}\right)|\zeta^0|$$
$$=\left|\frac{(2\alpha\cos(\theta\Delta x)+\beta)\left(\frac{\sigma}{2^{1-\gamma}}-\sigma w_1\right)-(1-\cos(\theta\Delta x))X_1-X_2-iX_3\sin(\theta\Delta x)}{(2\alpha\cos(\theta\Delta x)+\beta)\left(\frac{\sigma}{2^{1-\gamma}}\right)+(1-\cos(\theta\Delta x))X_1+X_2+iX_3\sin(\theta\Delta x)}\right||\zeta^0|$$
$$+\frac{\sigma w_1(2\alpha\cos(\theta\Delta x)+\beta)+|\alpha d_{m-1}^{n+1/2}e^{-i\theta\Delta x}+\beta d_m^{n+1/2}-\alpha d_{m+1}^{n+1/2}e^{i\theta\Delta x}|}{\left|(2\alpha\cos(\theta\Delta x)+\beta)\left(\frac{\sigma}{2^{1-\gamma}}\right)+(1-\cos(\theta\Delta x))X_1+X_2+iX_3\sin(\theta\Delta x)\right|}|\zeta^0|.$$

It is clear from previous analysis and mathematical induction that as $\Delta x,\Delta t\to 0$, $|\zeta^{n+1}|\leq|\zeta^0|$ for each $n=0,1,\ldots,M_t-1$. Hence, the numerical scheme (2.2.18) is conditionally stable with the condition $3^\gamma\geq\frac{3}{2}$.

2.5 convergence analysis

To prove the convergence of the numerical scheme (2.2.18), we assume

$$E_m^n=\widetilde{y}_m^n-Y_m^n,\ m=0,1,\ldots,N_x,\ n=0,1,\ldots,M_t. \tag{2.5.1}$$

From (2.2.17) and (2.2.18), we obtain

$$E(m,n)E_{m-1}^{n+1}+F(m,n)E_m^{n+1}+G(m,n)E_{m+1}^{n+1}=E_1(m,n)E_{m-1}^n+F_1(m,n)E_m^n$$
$$+G_1(m,n)E_{m+1}^n-\sigma w_1\left(\alpha E_{m-1}^n+\beta E_m^n+\alpha E_{m+1}^n\right)+\sigma w_n\left(\alpha E_{m-1}^0+\beta E_m^0+\alpha E_{m+1}^0\right)$$
$$-\sigma\sum_{q=1}^{n-1}(w_{n-q+1}-w_{n-q})\left(\alpha E_{m-1}^q+\beta E_m^q+\alpha E_{m+1}^q\right)$$
$$-\frac{1}{2}\left[\alpha d_{m-1}^{n+1/2}(E_{m-1}^{n+1-k}+E_{m-1}^{n-k})+\beta d_m^{n+1/2}(E_m^{n+1-k}+E_m^{n-k})+\alpha d_{m+1}^{n+1/2}(E_{m+1}^{n+1-k}+E_{m+1}^{n-k})\right]$$

$$+\left(\alpha\mathfrak{R}_{m-1}^{n+1/2}+\beta\mathfrak{R}_{m}^{n+1/2}+\alpha\mathfrak{R}_{m+1}^{n+1/2}\right), \tag{2.5.2}$$

along with the conditions

$$E_0^n = E_{N_x}^n = 0, \text{ and } E_m^0 = 0,$$

where

$$|\mathfrak{R}_m^{n+1/2}| \leq C\mathfrak{T}_m^{n+1/2} \leq C((\Delta x)^2 + (\Delta t)^2). \tag{2.5.3}$$

The grid functions

$$E^n(x) = \begin{cases} E_m^n, & x_m - \frac{\Delta x}{2} < x < x_m + \frac{\Delta x}{2},\ m = 1, 2, \ldots, N_x - 1, \\ 0, & 0 \leq x \leq \frac{\Delta x}{2} \text{ or } 1 - \frac{\Delta x}{2} \leq x \leq 1, \end{cases}$$

and

$$\mathfrak{R}^{n+1/2}(x) = \begin{cases} \mathfrak{R}_m^{n+1/2}, & x_m - \frac{\Delta x}{2} < x < x_m + \frac{\Delta x}{2},\ m = 1, 2, \ldots, N_x - 1, \\ 0, & 0 \leq x \leq \frac{\Delta x}{2} \text{ or } 1 - \frac{\Delta x}{2} \leq x \leq 1, \end{cases}$$

have the following Fourier series expansions

$$E^n(x) = \sum_{j=-\infty}^{\infty} \chi^n(j) e^{i(2j\pi x)},\ n = 0, 1, \ldots, M_t,$$

and

$$\mathfrak{R}^{n+1/2}(x) = \sum_{j=-\infty}^{\infty} r^{n+1/2}(j) e^{i(2j\pi x)},\ n = 0, 1, \ldots, M_t,$$

respectively, where

$$\chi^n(j) = \int_0^1 E^n(x) e^{-i(2j\pi x)} dx,$$

and

$$r^{n+1/2}(j) = \int_0^1 \mathfrak{R}^{n+1/2}(x) e^{-i(2j\pi x)} dx.$$

Using Parseval's identity in L_2-norm, we find

$$||E^n||_2^2 = \sum_{m=1}^{N_x-1} \Delta x |E_m^n|^2 = \int_0^1 |E^n(x)|^2 dx = \sum_{j=-\infty}^{\infty} |\chi^n(j)|^2, \tag{2.5.4}$$

and

$$||\mathfrak{R}^{n+1/2}||_2^2 = \sum_{m=1}^{N_x-1} \Delta x |\mathfrak{R}_m^{n+1/2}|^2 = \int_0^1 |\mathfrak{R}^{n+1/2}(x)|^2 dx = \sum_{j=-\infty}^{\infty} |r^{n+1/2}(j)|^2. \tag{2.5.5}$$

Now, we assume that

$$E_m^n = \chi^n e^{i\theta m \Delta x}, \tag{2.5.6}$$

and

$$\mathfrak{R}_m^{n+1/2} = r^{n+1/2} e^{i\theta m \Delta x}, \tag{2.5.7}$$

where $\theta = 2\pi j$. Using equations (2.5.2) and (2.5.6) in (2.5.7) for $n = 0, 1, \ldots, k-1$, we have

$$\chi^{n+1} = \left(\frac{U_1 - w_1 U}{U_2}\right)\chi^n - \frac{U}{U_2}\left(\sum_{q=1}^{n-1}(w_{n-q+1} - w_{n-q})\chi^q + w_n\chi^0\right) + \frac{U r^{n+1/2}}{\sigma U_2}, \tag{2.5.8a}$$

and for $n = k, k+1, \ldots, M_t - 1$, we have

$$\begin{aligned}\chi^{n+1} = &\left(\frac{U_1 - w_1 U}{U_2}\right)\chi^n - \frac{U}{U_2}\left(\sum_{q=1}^{n-1}(w_{n-q+1} - w_{n-q})\chi^q + w_n\chi^0\right) \\ &- \frac{1}{2U_2}(\chi^{n+1-k} + \chi^{n-k})\left(\alpha d_{m-1}^{n+1/2} e^{-i\theta\Delta x} + \beta d_m^{n+1/2} - \alpha d_{m+1}^{n+1/2} e^{i\theta\Delta x}\right) + \frac{U r^{n+1/2}}{\sigma U_2}.\end{aligned} \tag{2.5.8b}$$

Proposition 2.5.1. *There exist a positive constant C such that $|\chi^{n+1}| \leq (1+C\Delta t)^{n+1}|r^{1/2}|$, $n = 0, 1, \ldots, M_t - 1$.*

Proof. Clearly $\chi^0 = \chi^0(j) = 0$ (as $E^0 = 0$). From the convergence of the series on the right-hand side of the equation (2.5.5), there exists a positive constant C such that

$|r^{n+1/2}| \leq C\Delta t|r^{1/2}|$, $n = 0, 1, \ldots, M_t - 1$. From (2.5.3) and (2.5.5), we get

$$||\Re^{n+1/2}||_2 = C((\Delta x)^2 + (\Delta t)^2),\ n = 0, 1, \ldots, M_t - 1,$$

by the use of mathematical induction, for $n = 0$, we have

$$\begin{aligned}|\chi^1| &= \left| \frac{(2\alpha\cos(\theta(\Delta x)) + \beta)r^{1/2}}{(2\alpha\cos(\theta(\Delta x)) + \beta)\left(\frac{\sigma}{2^{(1-\gamma)}}\right) + (1 - \cos(\theta(\Delta x)))X_1 + X_2 + iX_3\sin(\theta(\Delta x))} \right| \\ &\leq C\Delta t|r^{1/2}| \leq (1 + C\Delta t)|r^{1/2}|.\end{aligned}$$

Now assuming that

$$|\chi^{\wp}| \leq (1 + C\Delta t)^{\wp}|r^{1/2}|,\ \wp = 2, 3, \ldots, n, \tag{2.5.9}$$

we will prove that (2.5.9) is true for $\wp = n + 1$. Equation (2.5.8a) yields

$$\begin{aligned}|\chi^{n+1}| \leq &\left(\frac{|U_1 - w_1U| + w_1|U|}{|U_2|}\right)(1 + C\Delta t)^n|r^{1/2}| \\ &+ \left| \frac{(2\alpha\cos(\theta\Delta x) + \beta)r^{1/2}}{(2\alpha\cos(\theta\Delta x) + \beta)\left(\frac{\sigma}{2^{1-\gamma}}\right) + (1 - \cos(\theta\Delta x))X_1 + X_2 + iX_3\sin(\theta\Delta x)} \right|,\end{aligned}$$

based on proof of stability, it can be easily proven that

$$|\chi^{n+1}| \leq (1 + C\Delta t)^{n+1}|r^{1/2}| \text{ for } n = 0, 1, \ldots, k - 1.$$

For $n = k, k + 1, \ldots, M_t - 1$, equation (2.5.8b) yields

$$\begin{aligned}|\chi^{n+1}| \leq &\left(\frac{|U_1 - w_1U| + w_1|U| + |\alpha d_{m-1}^{n+1/2}e^{-i\theta\Delta x} + \beta d_m^{n+1/2} - \alpha d_{m+1}^{n+1/2}e^{i\theta\Delta x}|}{|U_2|}\right)(1 + C\Delta t)^n|r^{1/2}| \\ &+ \left| \frac{(2\alpha\cos(\theta\Delta x) + \beta)r^{1/2}}{(2\alpha\cos(\theta\Delta x) + \beta)\left(\frac{\sigma}{2^{1-\gamma}}\right) + (1 - \cos(\theta\Delta x))X_1 + X_2 + iX_3\sin(\theta\Delta x)} \right|.\end{aligned}$$

Similarly, as in the stability, we can prove that

$$|\chi^{n+1}| \leq (1 + C\Delta t)^{n+1}|r^{1/2}| \text{ for } n = k, k - 1, \ldots, M_t - 1.$$

Hence, by the mathematical induction we can say that $|\chi^n| \leq (1 + C\Delta t)^n |r^{1/2}|$ for $n = 1, 2, \ldots, M_t$. □

Theorem 2.5.1. *The numerical scheme* $(2.2.18)$ *is convergent and the solution satisfies*

$$||\widetilde{y}_m^n - Y_m^n||_2 \leq C((\Delta x)^2 + (\Delta t)^2),\ m = 1, 2, \ldots, N_x,\ n = 1, 2, \ldots, M_t,$$

where C *is a positive constant independent of* Δx *and* Δt.

Proof. From equations (2.5.4) and (2.5.5) and proposition (2.5.1), we obtain

$$||E^n||_2 \leq (1 + C\Delta t)^n ||R^{1/2}||_2 \leq Ce^{(Cn\Delta t)}((\Delta x)^2 + (\Delta t)^2),\ n = 1, 2, \ldots, M_t,$$

then

$$||E^n||_2 \leq C((\Delta x)^2 + (\Delta t)^2),\ n = 1, 2, \ldots, M_t.$$

Thus, the numerical scheme $(2.2.18)$ is second-order convergent. □

2.6 Numerical Illustrations

In this section, the efficiency and effectiveness of the proposed technique are demonstrated by implementing our numerical method on two test examples for the TF-DPDEs. The exact solutions to these problems are not available, so we employ the double mesh principle to determine the errors in L_∞ and L_2-norms. We also compute the corresponding orders of convergence using definition 1.3.8. We consider the following TF-DPDEs with $\tau = 1$ and suitable interval and boundary conditions.

Example 2.6.1.

$${}_0^C D_t^\gamma y - y_{xx} + (2 - x^2)y_x + xy = y(x, t - \tau) + 10t^2 e^{-t}(x - x^2),\ (x, t) \in (0, 1) \times (0, 2],$$
$$\psi_b(x, t) = 0,\ \psi_l(t) = 0,\ \psi_r(t) = 0.$$

Example 2.6.2.

$${}_0^C D_t^\gamma y - y_{xx} + e^x y_x + (x + 1)(t + 1)y = y(x, t - \tau) + 10t^2 e^{-t}(2x - x^2),$$

$$(x,t) \in (0,1) \times (0,2],\ \psi_b(x,t) = 0,\ \psi_l(t) = 0,\ \psi_r(t) = 0.$$

Replacing the γ order fractional derivative with the first-order integer derivative, we define the following problem

$$y_t - y_{xx} + b(x,t)y_x + c(x,t)y(x,t) = -d(x,t)y(x,t-\tau) + f(x,t), \tag{2.6.1}$$

where $b(x,t)$, $c(x,t)$, $d(x,t)$, $f(x,t)$, and the interval and boundary conditions are the same as defined in Examples 2.6.1 and 2.6.2.

We have shown the errors in L_2 and L_∞ norms for different values of γ, in Tables 2.1 and 2.3, for Examples 2.6.1 and 2.6.2, respectively. From these tables, it can be observed that as we increase N_x and M_t, the errors decrease and are in good agreement with the theoretical results. It confirms our theoretical estimates that the suggested scheme is second-order convergent. From Tables 2.2 and 2.4 one can observe that the errors in L_2 and L_∞ norms for Examples 2.6.1 and 2.6.2 approach to the errors for the problem (2.6.1) as γ approaches 1. In Figures 1 and 4, we portray the numerical solution profiles of Examples 2.6.1 and 2.6.2, respectively, for different values of γ. Figures 2 and 5 exhibit the graphs of the numerical solutions of Examples 2.6.1 and 2.6.2 at different time levels. Keeping γ fixed, Figures 3 ($\gamma = 0.9$) and 6 ($\gamma = 0.8$) show the decrease in the error when we increase the number of points in both directions.

Remark 2.6.1. *To draw the Figures 1, 2, 4, and 5, we have used* $N_x = M_t = 64$.

2.7 Concluding Remarks

This chapter suggests a numerical method comprising a Crank-Nicolson scheme with tension spline for TF-DPDEs. The Caputo fractional derivative is used to discretize the fractional-order time derivative. Using the Fourier series analysis, the method is proved to be conditionally stable. Moreover, through rigorous analysis, the method is shown as a second-order convergent for arbitrary suitable choices of α ($\alpha \neq 1/12$) and β with $2\alpha+\beta = 1$. The method is easy to apply to the problem (2.1.1) and can easily be manipulated in MATLAB software. Numerical examples demonstrate the effectiveness and adaptability of the suggested method.

Table 2.1: L_2 and L_∞ errors, and respective orders of convergence for Example 2.6.1

γ	Number of grid points Norms	N_x=16 M_t=16	N_x=32 M_t=32	N_x=64 M_t=64	N_x=128 M_t=128	N_x=256 M_t=256
0.2	L_2	$1.3267e-04$	$3.3053e-05$	$8.2474e-06$	$2.0583e-06$	$5.1364e-07$
		2.0050	2.0028	2.0025	2.0026	
	L_∞	$1.8951e-04$	$4.7303e-05$	$1.1806e-05$	$2.9472e-06$	$7.3548e-07$
		2.0023	2.0024	2.0021	2.0026	
0.4	L_2	$1.3441e-04$	$3.3361e-05$	$8.2804e-06$	$2.0516e-06$	$5.0684e-07$
		2.0104	2.0104	2.0130	2.0171	
	L_∞	$1.9222e-04$	$4.7819e-05$	$1.1871e-05$	$2.9427e-06$	$7.2719e-07$
		2.0071	2.0101	2.0122	2.0167	
0.6	L_2	$1.3624e-04$	$3.3525e-05$	$8.2014e-06$	$1.9837e-06$	$4.7076e-07$
		2.0228	2.0313	2.0477	2.0751	
	L_∞	$1.9512e-04$	$4.8151e-05$	$1.1787e-05$	$2.8537e-06$	$6.7834e-07$
		2.0187	2.0304	2.0463	2.0728	
0.8	L_2	$1.3928e-04$	$3.3929e-05$	$8.1226e-06$	$1.8761e-06$	$5.2160e-07$
		2.0374	2.0625	2.1142	1.8467	
	L_∞	$1.9977e-04$	$4.8835e-05$	$1.1707e-05$	$2.7112e-06$	$7.4798e-07$
		2.0324	2.0605	2.1104	1.8579	

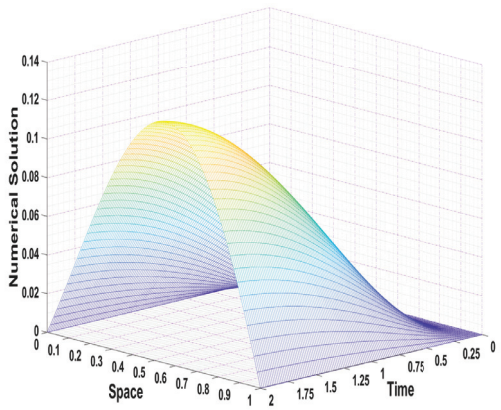

a $\gamma = 0.6$

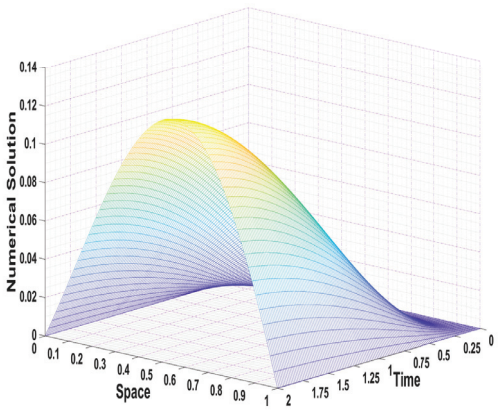

b $\gamma = 0.9$

Figure 1: Numerical solution for Example 2.6.1 for different values of γ.

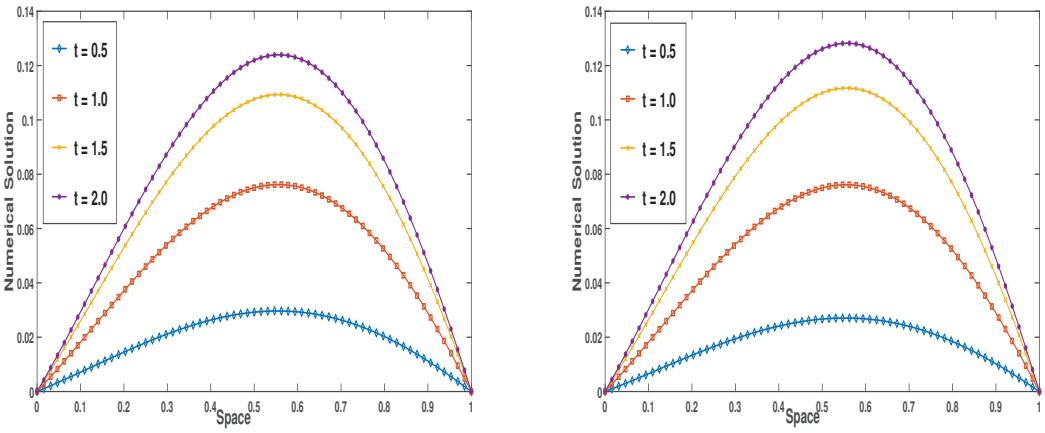

a $\gamma = 0.5$ b $\gamma = 0.9$

Figure 2: Graph of numerical solution for Example 2.6.1 at different time levels.

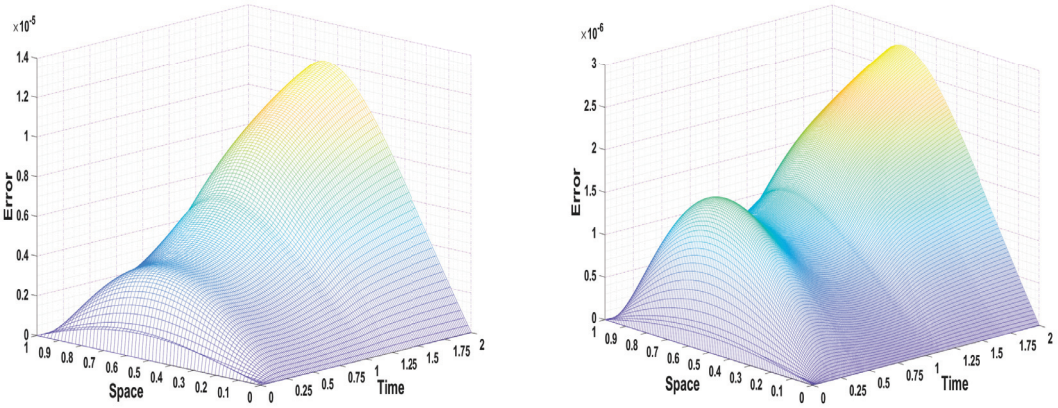

a $N_x = M_t = 64,\ \gamma = 0.9$ b $N_x = M_t = 128,\ \gamma = 0.9$

Figure 3: Absolute error for Example 2.6.1.

Table 2.2: Comparison of L_2 and L_∞ errors between Example 2.6.1 and problem (2.6.1)

γ	Number of grid points Norms	N_x=16 M_t=16	N_x=32 M_t=32	N_x=64 M_t=64	N_x=128 M_t=128	N_x=256 M_t=256
0.9	L_2	$1.4242e-04$	$3.4795e-05$	$8.3520e-06$	$1.9282e-06$	$5.2170e-07$
	L_∞	$2.0443e-04$	$5.0111e-05$	$1.2044e-05$	$2.7879e-06$	$7.4758e-07$
0.95	L_2	$1.4483e-04$	$3.5645e-05$	$8.6711e-06$	$2.0539e-06$	$4.5867e-07$
	L_∞	$2.0797e-04$	$5.1331e-05$	$1.2498e-05$	$2.9655e-06$	$6.6511e-07$
0.99	L_2	$1.4734e-04$	$3.6640e-05$	$9.0948e-06$	$2.2434e-06$	$5.4591e-07$
	L_∞	$2.1164e-04$	$5.2747e-05$	$1.3096e-05$	$3.2325e-06$	$7.8718e-07$
0.999	L_2	$1.4800e-04$	$3.6912e-05$	$9.2170e-06$	$2.3008e-06$	$5.7358e-07$
	L_∞	$2.1259e-04$	$5.3133e-05$	$1.3270e-05$	$3.3134e-06$	$8.2609e-07$
Error for (2.6.1)	L_2	$1.4807e-04$	$3.6944e-05$	$9.2313e-06$	$2.3075e-06$	$5.7686e-07$
	L_∞	$2.1270e-04$	$5.3178e-05$	$1.3291e-05$	$3.3230e-06$	$8.3072e-07$

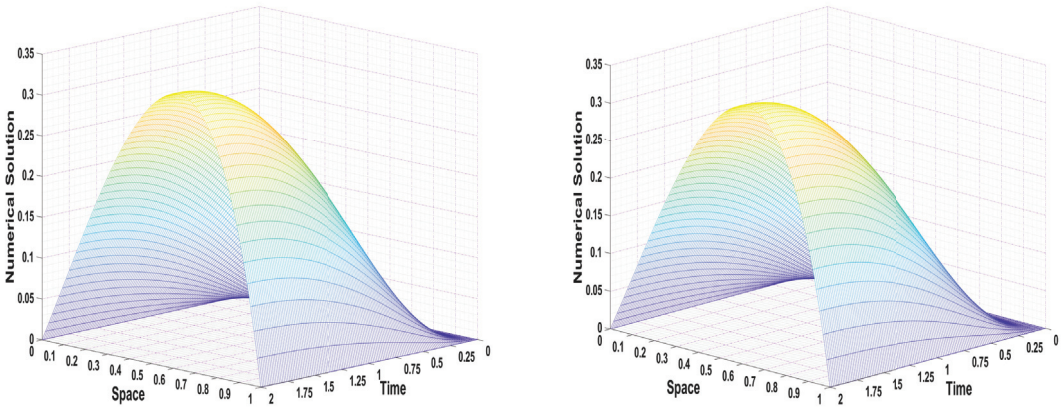

a $\gamma = 0.5$ b $\gamma = 0.75$

Figure 4: Numerical solution for Example 2.6.2 for different values of γ.

Table 2.3: L_2 and L_∞ errors, and respective orders of convergence for Example 2.6.2

	Number of grid points					
γ	Norms	N_x=16 M_t=16	N_x=32 M_t=32	N_x=64 M_t=64	N_x=128 M_t=128	N_x=256 M_t=256
0.2	L_2	$2.9711e-04$	$7.3928e-05$	$1.8478e-05$	$4.6247e-06$	$1.1581e-06$
		2.0068	2.0003	1.99984	1.9976	
	L_∞	$5.0981e-04$	$1.2674e-04$	$3.1686e-05$	$7.9297e-06$	$1.9846e-06$
		2.0081	2.0000	1.9985	1.9984	
0.4	L_2	$3.0021e-04$	$7.5004e-05$	$1.8847e-05$	$4.7512e-06$	$1.2015e-06$
		2.0009	1.9926	1.9880	1.9835	
	L_∞	$5.1291e-04$	$1.2785e-04$	$3.2107e-05$	$8.0725e-06$	$2.0342e-06$
		2.0043	1.9935	1.9918	1.9886	
0.6	L_2	$3.0453e-04$	$7.6757e-05$	$1.9566e-05$	$5.0474e-06$	$1.3232e-06$
		1.9882	1.9719	1.9547	1.9315	
	L_∞	$5.1731e-04$	$1.2970e-04$	$3.2937e-05$	$8.4153e-06$	$2.1767e-06$
		1.9959	1.9774	1.9686	1.9509	
0.8	L_2	$3.0740e-04$	$7.8291e-05$	$2.0832e-05$	$5.4693e-06$	$1.6242e-06$
		1.9732	1.9100	1.9294	1.7516	
	L_∞	$5.1996e-04$	$1.3144e-04$	$3.3870e-05$	$8.9166e-06$	$2.4352e-06$
		1.9840	1.9563	1.9254	1.8725	

Table 2.4: Comparison of L_2 and L_∞ errors between Example 2.6.2 and problem (2.6.1)

γ	Number of grid points Norms	N_x=16 M_t=16	N_x=32 M_t=32	N_x=64 M_t=64	N_x=128 M_t=128	N_x=256 M_t=256
0.9	L_2	$3.0553e-04$	$7.7633e-05$	$2.0176e-05$	$5.4251e-06$	$1.5731e-06$
	L_∞	$5.1757e-04$	$1.3058e-04$	$3.3620e-05$	$8.8625e-06$	$2.4413e-07$
0.95	L_2	$3.0278e-04$	$7.6379e-05$	$1.9605e-05$	$5.1654e-06$	$1.4239e-06$
	L_∞	$5.1432e-04$	$1.2904e-04$	$3.2942e-05$	$8.5509e-06$	$2.2979e-07$
0.99	L_2	$2.9943e-04$	$7.4708e-05$	$1.8784e-05$	$4.7614e-06$	$1.2242e-06$
	L_∞	$5.1033e-04$	$1.2713e-04$	$3.1960e-05$	$8.0674e-06$	$2.0570e-07$
0.999	L_2	$2.9850e-04$	$7.4230e-05$	$1.8545e-05$	$4.6416e-06$	$1.1638e-06$
	L_∞	$5.0925e-04$	$1.2658e-04$	$3.1672e-05$	$7.9235e-06$	$1.9851e-07$
Error for (2.6.1)	L_2	$2.9839e-04$	$7.4175e-05$	$1.8517e-05$	$4.6276e-06$	$1.1568e-06$
	L_∞	$5.0913e-04$	$1.2651e-04$	$3.1639e-05$	$7.9067e-06$	$1.9768e-07$

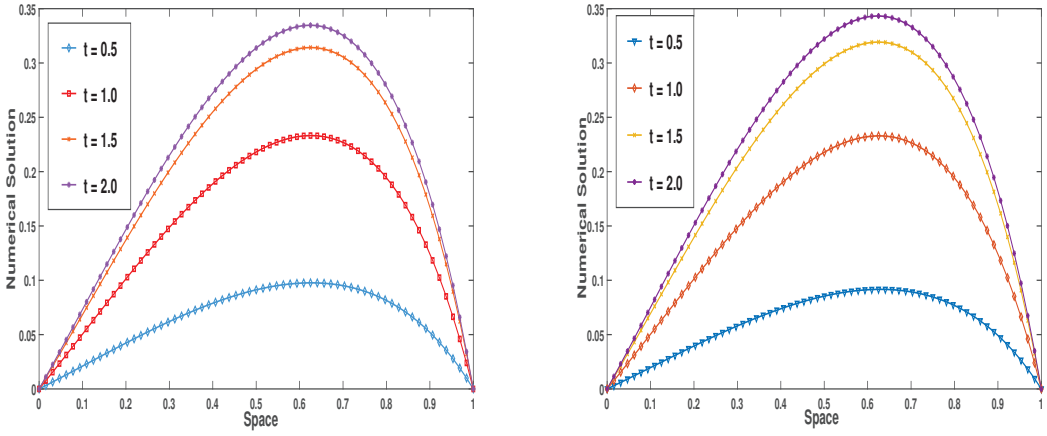

a $\gamma = 0.4$ b $\gamma = 0.8$

Figure 5: Graph of numerical solution for Example 2.6.2 at different time levels.

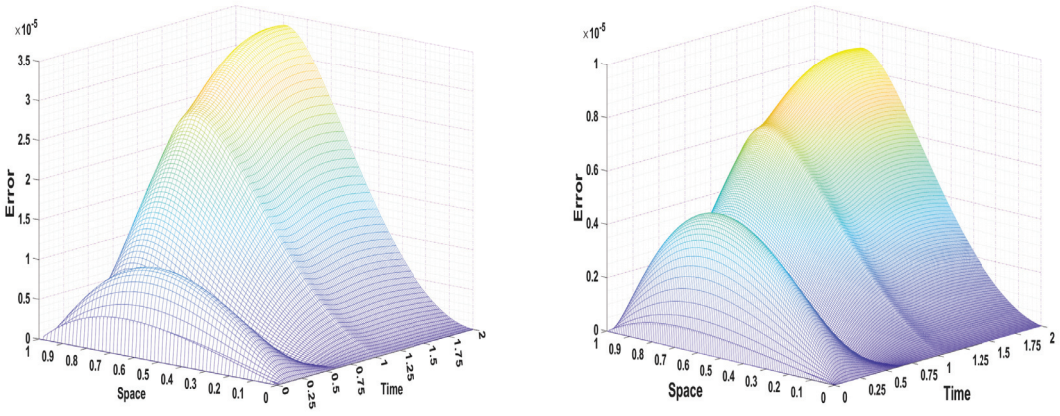

a $N_x = M_t = 64,\ \gamma = 0.8$ b $N_x = M_t = 128,\ \gamma = 0.8$

Figure 6: Absolute error for Example 2.6.2.

The proposed technique can be extended to the nonlinear TF-DPDEs and systems of FPDEs.

Chapter 3

A higher-order stable numerical approximation for time-fractional non-linear Kuramoto-Sivashinsky equation based on quintic $\mathfrak{B}$-spline

---

This chapter deals with designing and analyzing a higher-order stable numerical approximation for the time fractional Kuramoto-Sivashinsky (K-S) equation, which is a fourth-order non-linear equation. The fractional derivative of order $\gamma \in (0, 1)$ present in the considered problem is taken into Caputo sense and approximated using the $L1-2$ scheme. In the space direction, the discretization process uses quintic $\mathfrak{B}$-spline functions to approximate the derivatives and the problem's solution. We have established unconditional stability results and convergence of rate of accuracy $\mathcal{O}(h^2 + k^2)$, where h and k denote the space and time step sizes, respectively. We have also noted that the linearized version of the K-S equation leads the rate of accuracy to $\mathcal{O}(h^2 + k^{3-\gamma})$. The present approach is also highly effective for the time-fractional Burgers equation. We have shown that the current approach provides

R. Choudhary, D. Kumar, Numerical solution of linear time-fractional Kuramoto-Sivashinsky equation via quintic B-splines, Int. J. Comput. Math. , (2023), 1–20.

better accuracy than the $L1$ scheme with the same computational cost for several linear and nonlinear problems with classical and fractional time derivatives.

3.1 Literature survey

Nonlinear fractional order problems with nonlocal structures are frequent in several fields of engineering, physics, and applied mathematics. Analytical prospects of nonlinear problems like global wellposedness, local dynamics of periodic solutions, chaotic behavior, and nonlinear stability require a strong hypothesis, which is necessary for qualitative analysis of the problems. This is because highly accurate convergent approximations of the nonlocal problems are only sometimes straightforward when the nonlinearity appears in space. One can look into the complications involved in dealing with the existence and stability of symmetry-breaking bifurcations of solitons of vortex-soliton solutions and fractional N soliton solutions for nonlinear problems like fractional nonlinear Schrödinger equation, generalized time-fractional Benjamin Bona Mohany Burgers' equation, in the articles [118–121]. In the present work, we deal with the approximations of a nonlinear evolutionary Kuramoto-Sivashinsky (KS) equation which appears in the long waves from the interface between two viscous fluids, in unstable drift waves inside plasmas [122], etc. This equation is closely linked with the nonlinear KdV equation [123], which demonstrates the thin film dynamics down a wall, moving from the vertical to the horizontal side [124].

KS equation is a fourth-order nonlinear time-dependent PDE involving a second-order derivative that is accountable for instability at large scales, a fourth-order derivative in space that leads to damping at small scales, and a nonlinear term that stabilizes the problem by transferring energy from large to towards small scales. We consider the time derivative of the KS equation to be nonlocal so that the global behavior of the solution can be detected in practice. The present approach will also follow the standard KS equation where the time derivative is not of fractional order.

In the present work, we consider the following nonlinear Kuramoto-Sivashinsky (KS) equation with the Caputo type time fractional derivative of order $\gamma \in (0, 1)$

$$ {}_0^C D_t^\gamma u(s,t) + a_1(s,t)u(s,t)u_s(s,t) + a_2(s,t)u_{ss}(s,t) + a_3(s,t)u_{ssss}(s,t) = g(s,t), \quad (3.1.1a) $$

defined on $(0,1)\times(0,T]$ with the set of boundary conditions (BCs)

$$\begin{cases} u(0,t) = f_0(t),\ u(1,t) = f_1(t), \\ u_s(0,t) = 0,\ u_s(1,t) = 0, \end{cases} \tag{3.1.1b}$$

or

$$\begin{cases} u(0,t) = f_0(t),\ u(1,t) = f_1(t), \\ u_{ss}(0,t) = 0,\ u_{ss}(1,t) = 0, \end{cases} \tag{3.1.1c}$$

for $0 < t \leq T$, and the initial condition (IC)

$$u(s,0) = \phi(s),\ 0 \leq s \leq 1. \tag{3.1.1d}$$

$a_1(s,t)$, $a_2(s,t)$, and $a_3(s,t)$ are real-valued functions of s and t, $a_2(s,t)$ and $a_3(s,t)$ are connected to the growth of linear stability and surface tension [125], respectively. We have assumed that $a_1(s,t)$, $a_2(s,t)$, $a_3(s,t)$, $f(s,t)$, $\phi_0(s)$, $f_0(t)$, and $f_1(t)$ are sufficiently smooth functions. When $a_3(s,t)$ is zero, the surface tension term is terminated, and the Equation (3.1.1a) is reduced to the time-fractional Burger's equation. For Burger's equation involving classical time derivative, solutions based on traveling waves are well defined. However, in the absence of dispersive effects, complex dynamical behaviors like spatiotemporal chaos [126] appear when the term $a_3(s,t)$ is present and is not large enough. The linear version of the above time fractional problem will be of the following form

$${}_0^C D_t^\gamma u(s,t) + a_1(s,t)u_s(s,t) + a_2(s,t)u_{ss}(s,t) + a_3(s,t)u_{ssss}(s,t) = g(s,t), \quad (s,t) \in (0,1)\times(0,T], \tag{3.1.2}$$

with the same set of BCs ((3.1.1b) or (3.1.1c)) and IC ((3.1.1d)).

Note from the definition (1.3.1), the problem (3.1.1a) is nonlocal as time evolves. The approximation of this integral requires the storage of previous time information and hence increases the computational cost. In addition, this problem will behave like the Navier Stokes equation as the coefficient a_3 becomes small. In this case, the solution will have a large

front, varying in time (see, e.g., [127] for steady-state case). These time-varying solutions are challenging to detect if one uses standard approaches—the time fractional KS equation has all of these features in its dynamics. Correspondingly, the convergence of the approximations of this problem requires stepwise mathematical analysis, and the numerical approximations must detect those fronts, too.

In the present context, qualitative analysis, including the wellposedness of the KS equation, is well established in the literature. One can look into [128] for the existence and uniqueness of the modified versions of the KS equation. In the case of the ill-posed backward time KS equation, a regularization approach is necessary [129] and can be adapted using the concepts of control theory. The qualitative properties like the local dynamics of periodic traveling wave solutions and nonlinear stabilities are analyzed in [123]. An asymptotic analysis of the KS equation appearing in oscillatory core annular flow and the effect of background oscillations on the steady-state version of the KS equation and its chaotic states, time-periodic states, and nonlinear dispersive states are visible in [130]. Spectral and nonlinear modulational stabilities for the periodic solutions of the KS equation based on small perturbations are established in [131]. Spectral methods are also introduced for this equation in [132]. In the context of the nonlinear stochastic KS equation, surface roughness due to the multiple time and length scales can also be controlled periodically [133].

Numerical approximations of nonlinear problems are complicated and require linearization techniques to transform them into a system of algebraic equations (see [134, 135]). One can use low-order accurate upwind schemes when the time derivative is not of fractional form. In this case, several numerical approximation methods are available in the context of the KS equation. Spectral collocation methods based on Chebyshev approximations for higher order derivatives can be seen in [136] where the lower order derivative terms are approximated by integrating the higher order derivative approximations. Pseudo-spectral methods [126] in space with implicit explicit backward difference formula in time can also be used to obtain higher order accuracy for the KS equation. Collocation methods are also used in space based on polynomial scaling functions in [137] where the authors have used the Crank-Nicolson scheme [138] in time. Method of lines using radial basis functions are also considered for computational experiments of generalized KS equation in [139]. Compact

implicit schemes [140] on variable meshes are analyzed to deal with quasilinear biharmonic equations and KS equations with the time derivative of nonfractional order. In the context of linear problems, spline collocations are generally used to obtain higher-order approximations in space. For several types of KS equations and reduced Burgers equations, it is observed that the quintic $\mathfrak{B}$-spline [134] and exponential modified cubic $\mathfrak{B}$-spline [141], can detect the original solution behavior experimentally. However, these methods deal with local time behavior, and a rigorous mathematical convergence analysis behind the experiments is not available here.

For fractional differential equations, the wellposedness properties and the smoothness of the solution depend on the fractional derivative type and its order in the differential model. This observation can be made from [142, 143] for Caputo-type fractional problems and in [144] during approximations of variable order fractional systems. Fast numerical schemes for stochastic differential equations with Riemann Liouville-type fractional derivatives are also obtained in [145]. For time fractional problems, the reduced system of algebraic equations will not be tridiagonal, leading to higher computational costs. This cost increases for the system of problems, especially when the nonlinearity appears in space [127]. One can look into [146] on how to reduce the computational cost for the system of problems. In this chapter, we aim to obtain the space-time higher-order accurate approximations using a suitable linearization approach that maintains the higher-order accuracy in space and time. We consider the quintic $\mathfrak{B}$-spline approximation to obtain the higher order accuracy in space. Note that the definition (1.3.1) involves a weakly singular kernel, in addition to a differential term, which can be approximated by $L1$ discretization. This approximation leads to an order of accuracy between $(1, 2)$ if the fractional order γ lies in $(0, 1)$. In this work, we have considered a $L1 - 2$ approximation of the time derivative, which leads to the order of accuracy between $(2, 3)$ in time when $\gamma \in (0, 1)$.

3.2 Construction of numerical approximation

3.2.1 Time semi-discretization

For this, we consider a partition Ω_{M_t} of the time interval $[0, T]$ satisfying $\Omega_{M_t} \equiv \{0 = t_0 < t_1 < \cdots < t_{M_t-1} < t_{M_t} = T\}$ with equidistant points $t_j = jk$, $j = 0, 1, \ldots, M_t$, where $k = T/M_t$. For the rest of the numerical analysis, we consider the boundary condition (3.1.1b) as the similar analysis follows for (3.1.1a), (3.1.1d) with the boundary condition (3.1.1c).

Notion of $L1-2$ scheme: We start the discussion by defining the widely used $L1$ discretization [2] on a non-uniform mesh to approximate the time-fractional derivative (1.3.1) at $t = t_j$:

$$ {}_0^C D_t^\gamma u(s, t_j) = \frac{1}{\Gamma(1-\gamma)} \sum_{z=1}^{j} \frac{u(x, t_z) - u(x, t_{z-1})}{t_z - t_{z-1}} \int_{t_{z-1}}^{t_z} \frac{d\zeta}{(t_j - \zeta)^\gamma} + \mathfrak{r}^j, $$

where $\mathfrak{r}^j$ is the local truncation error (LTE). For the uniform mesh, the LTE is proved to be of $\mathcal{O}(k^{2-\gamma})$ (see [147, 148] for details). Therefore, the $L1$ approximation for Equation (1.3.1) at a nodal point t_j on the time mesh Ω_{M_t} is

$$ {}_0^C D_t^\gamma u(s, t_j) \approx \frac{1}{\Gamma(1-\gamma)} \sum_{z=1}^{j} \frac{u(x, t_z) - u(x, t_{z-1})}{t_z - t_{z-1}} \int_{t_{z-1}}^{t_z} \frac{d\zeta}{(t_j - \zeta)^\gamma}. $$

Now the sole idea of the $L1-2$ scheme consists of approximating the partial derivative $\dfrac{\partial u(s,\zeta)}{\partial \zeta}$ in two different ways in different partitions. In the subinterval $[t_0, t_1]$, the approximation uses the theory of linear interpolation and, for $[t_{z-1}, t_z]$, $z \geq 2$, the derivatives are approximated by quadratic interpolation. The process provides a modification in the $L1$ formula by adding a correction term with LTE of $\mathcal{O}(k^{3-\gamma})$ (see [64] for more details). By the use of this $L1-2$ scheme, the Caputo time-fractional derivative ${}_0^C D_t^\gamma u(s,t)$ is discretized as

$$ \begin{aligned} {}_0^C D_t^\gamma u(s, t_j) =& \frac{k^{-\gamma}}{\Gamma(2-\gamma)} \left[w_0^\gamma u(s, t_j) - \sum_{n=1}^{j-1} (w_{j-n-1}^\gamma - w_{j-n}^\gamma) u(s, t_n) - w_{j-1}^\gamma u(s, t_0) \right] \\ &+ \mathfrak{r}_1^j, \ j = 1, 2, \ldots, M_t, \end{aligned} \tag{3.2.1} $$

where the truncation error $\mathfrak{r}_1^j$ is of $\mathcal{O}(k^{3-\gamma})$. The coefficients appear in the Equation (3.2.1) are given by [64]

$$w_0^\gamma = 1, \text{ for } j = 1, \text{ and for } j \geq 2,\ w_n^\gamma = \begin{cases} b_0^\gamma + c_0^\gamma, & n = 0, \\ b_n^\gamma + c_n^\gamma - c_{n-1}^\gamma, & 1 \leq n \leq j-2, \\ b_n^\gamma - c_{n-1}^\gamma, & n = j-1. \end{cases} \tag{3.2.2}$$

In Equation (3.2.2)

$$b_n^\gamma = (n+1)^{1-\gamma} - n^{1-\gamma},\ 0 \leq n \leq j-1,$$

and

$$c_n^\gamma = \frac{1}{2-\gamma}[(n+1)^{2-\gamma} - n^{2-\gamma}] - \frac{1}{2}[(n+1)^{1-\gamma} + n^{1-\gamma}],\ 0 \leq n \leq j-2.$$

The following properties of the above constants will be used for stability analysis of the discrete problem. For $0 < \gamma < 1$, b_n^γ and w_n^γ $(0 \leq n \leq j-1,\ j \geq 3)$ satisfy (see [64])

$$\begin{aligned} &b_n^\gamma > 0,\ n \geq 0, \quad b_{n-1}^\gamma > b_n^\gamma,\ n \geq 1, \\ &w_0^\gamma > |w_1^\gamma|,\ w_n^\gamma > 0,\ n \neq 0, \\ &w_2^\gamma \geq w_3^\gamma \geq \cdots \geq w_{j-1}^\gamma, \quad w_0^\gamma > w_2^\gamma, \quad \text{and } \sum_{n=0}^{j-1} w_n^\gamma = j^{1-\gamma}. \end{aligned}$$

Using Equation (3.2.1) and denoting $u(s, t_j)$ as $u^j(s)$, at $t = t_j$ for $j = 1, 2, \ldots, M_t$, the semi-discrete form of given nonlinear KS equation (3.1.1a)-(3.1.1b) and (3.1.1d) can be expressed as

$$\begin{aligned} &\frac{k^{-\gamma}}{\Gamma(2-\gamma)}\left[w_0^\gamma u^j(s) - \sum_{n=1}^{j-1}(w_{j-n-1}^\gamma - w_{j-n}^\gamma)u^n(s) - w_{j-1}^\gamma u^0(s)\right] + a_1^j(s)u^j(s)u_s^j(s) \\ &+ a_2^j(s)u_{ss}^j(s) + a_3^j(s)u_{ssss}^j(s) = g^j(s) + \mathcal{O}(k^{3-\gamma}),\ 0 < s < 1, \end{aligned} \tag{3.2.3a}$$

with the BCs

$$u^j(0) = f_0^j,\ u^j(1) = f_1^j, \tag{3.2.3b}$$

and

$$u_s^j(0) = 0,\ u_s^j(1) = 0, \tag{3.2.3c}$$

and the IC

$$u^0(s) = \phi(s),\ 0 \le s \le 1. \tag{3.2.3d}$$

We consider linearization of the term $u^j(s)u_s^j(s)$ in Equation (3.2.3a) as follows [149]

$$(u^j(s)u_s^j(s))^{p+1} = (u^j(s))^{p+1}(u_s^{j-1}(s))^p + (u^{j-1}(s))^p(u_s^j(s))^{p+1} - (u^{j-1}(s)u_s^{j-1}(s))^p$$
$$p = 0, 1, 2, \ldots, \tag{3.2.4}$$

where p denotes the number of iterations. The truncation error of $\mathcal{O}(k^2)$ will be obtained in this process (see [149] for details). The initial guess $(u)^0$ is chosen in such a manner that the IC and BCs of (3.2.3) are satisfied. Putting this linearization from (3.2.4) in (3.2.3a) and rearrangement of the terms, provides

$$\begin{aligned}
&[\Lambda w_0^\gamma + a_1^j(s)(u_s^{j-1}(s))^p](u^j(s))^{p+1} + a_1^j(s)(u^{j-1}(s))^p(u_s^j(s))^{p+1} + a_2^j(s)(u_{ss}^j(s))^{p+1} \\
&+ a_3^j(s)(u_{ssss}^j(s))^{p+1} = g^j(s) + \Lambda\left[\sum_{n=1}^{j-1}(w_{j-n-1}^\gamma - w_{j-n}^\gamma)(u^n(s))^{p+1} + w_{j-1}^\gamma(u^0(s))^{p+1}\right] \\
&+ a_1^j(s)(u^{j-1}(s)u_s^{j-1}(s))^p + \mathcal{T}_k,\ 0 < s < 1,\ 0 < j \le M_t.
\end{aligned} \tag{3.2.5}$$

For simplicity, we denote $(u^j(s))^{p+1}$ and $(u^j(s))^p$ by $\widetilde{u}^j(s)$ and $u^{*j}(s)$, respectively. On simplification of (3.2.5), we get

$$\begin{aligned}
&[\Lambda w_0^\gamma + a_1^j(s)u_s^{*j-1}(s)]\widetilde{u}^j(s) + a_1^j(s)u^{*j-1}(s)\widetilde{u}_s^j(s) + a_2^j(s)\widetilde{u}_{ss}^j(s) + a_3^j(s)\widetilde{u}_{ssss}^j(s) \\
&= g^j(s) + \Lambda\left[\sum_{n=1}^{j-1}(w_{j-n-1}^\gamma - w_{j-n}^\gamma)\widetilde{u}^n(s) + w_{j-1}^\gamma\widetilde{u}^0(s)\right] + a_1^j(s)u^{*j-1}(s)u_s^{*j-1}(s) + \mathcal{T}_k,
\end{aligned} \tag{3.2.6}$$

where $\Lambda = \frac{k^{-\gamma}}{\Gamma(2-\gamma)}$ and $\mathcal{T}_k$ is truncation error given by

$$|\mathcal{T}_k| \le \mathcal{C}_{\widetilde{u}}k^{\min\{3-\gamma,2\}} = \mathcal{C}_{\widetilde{u}}k^2, \tag{3.2.7}$$

where $\mathcal{C}_{\widetilde{u}}$ is a constant, which depends only on $\widetilde{u}$. Equation (3.2.6) is the time semi-discretize form of Equation (3.1.1a), which, at each time level, is an ordinary differential equation that will be further discretized in a way so that higher order convergence is obtained in space for the proposed spline collocation technique.

3.2.2 Spatial discretization

To discretize the Equation (3.2.6) with BCs (3.2.3b)-(3.2.3c) and IC (3.2.3d) in space, we use a collocation approach by quintic $\mathfrak{B}$-spline basis functions. We create a uniform partition Π_{N_s} of space interval $[0,1]$ such that $\Pi_{N_s} = \{0 = s_0 < s_1 < \cdots < s_{N_s-1} < s_{N_s} = 1\}$ with mesh points $s_i = ih$, $i = 0, 1, \ldots, N_s$, and step size $h = 1/N_s$. First, we consider a space $\mathcal{S}_{5,\Pi^{N_s}} = \{\hat{r}(s) | \hat{r}(s) \in C^4[0,1]\}$. Using the results of [150], the basis for quintic $\mathfrak{B}$-spline functions $\mathfrak{B}_i(s)$ $(-2 \leq i \leq N_s + 2)$ are given as

$$\mathfrak{B}_i(s) = \frac{1}{h^5} \begin{cases} \varphi(s - s_{i-3}), & s \in [s_{i-3}, s_{i-2}), \\ \varphi(s - s_{i-3}) - 6\varphi(s - s_{i-2}), & s \in [s_{i-2}, s_{i-1}), \\ \varphi(s - s_{i-3}) - 6\varphi(s - s_{i-2}) + 15\varphi(s - s_{i-1}), & s \in [s_{i-1}, s_i), \\ \varphi(s_{i+3} - s) - 6\varphi(s_{i+2} - s) + 15\varphi(s_{i+1} - s), & s \in [s_i, s_{i+1}), \\ \varphi(s_{i+3} - s) - 6\varphi(s_{i+2} - s), & s \in [s_{i+1}, s_{i+2}), \\ \varphi(s_{i+3} - s), & s \in [s_{i+2}, s_{i+3}), \\ 0, & \text{otherwise}, \end{cases} \tag{3.2.8}$$

where $\varphi(s) = s^5$. To describe the quintic $\mathfrak{B}$-spline functions, we suggest 5 points on each side of the partition Π^{N_s} as $s_{-5} < s_{-4} < s_{-3} < s_{-2} < s_{-1} < s_0$ and $s_{N_s} < s_{N_s+1} < s_{N_s+2} < s_{N_s+3} < s_{N_s+4} < s_{N_s+5}$. It is straightforward to check that $\{\mathfrak{B}_i(s)\}_{i=-2}^{N_s+2}$ forms a basis on Π^{N_s} (see [151]). The values of each $\mathfrak{B}_i(s)$ and its first four derivatives are provided in Table 3.1. We will employ these quintic $\mathfrak{B}$-spline functions to approximate $\widetilde{u}_{ssss}$, $\widetilde{u}_{ss}$, $\widetilde{u}_s$ and $\widetilde{u}$ at the time level $t = t_j$.

Table 3.1: Values of $\mathfrak{B}_i(s)$, $\mathfrak{B}'_i(s)$, $\mathfrak{B}''_i(s)$, $\mathfrak{B}'''_i(s)$ and $\mathfrak{B}''''_i(s)$ at the node points

	Nodal points					
Functions	s_{i-2}	s_{i-1}	s_i	s_{i+1}	s_{i+2}	Otherwise
$\mathfrak{B}_i(s)$	1	26	66	26	1	0
$\mathfrak{B}'_i(s)$	$\frac{5}{h}$	$\frac{50}{h}$	0	$-\frac{50}{h}$	$-\frac{5}{h}$	0
$\mathfrak{B}''_i(s)$	$\frac{20}{h^2}$	$\frac{40}{h^2}$	$-\frac{120}{h^2}$	$\frac{40}{h^2}$	$\frac{20}{h^2}$	0
$\mathfrak{B}'''_i(s)$	$\frac{60}{h^3}$	$-\frac{120}{h^3}$	0	$\frac{120}{h^3}$	$-\frac{60}{h^3}$	0
$\mathfrak{B}''''_i(s)$	$\frac{120}{h^4}$	$-\frac{480}{h^4}$	$\frac{720}{h^4}$	$-\frac{480}{h^4}$	$\frac{120}{h^4}$	0

We desire an approximation of $\widetilde{u}^j(s)$ as

$$\widetilde{\mathcal{U}}^j(s) = \sum_{i=-2}^{N_s+2} \mathfrak{C}_i^j \mathfrak{B}_i(s), \tag{3.2.9}$$

where unknown scalars $\mathfrak{C}_i^j$'s depend on time which will be evaluated from the BCs and the collocation structure of the problem. Employing the quintic spline functions from (3.2.8) at nodal points s_i, we find

$$\widetilde{\mathcal{U}}^j(s_i) = \mathfrak{C}_{i+2}^j + 26\mathfrak{C}_{i+1}^j + 66\mathfrak{C}_i^j + 26\mathfrak{C}_{i-1}^j + \mathfrak{C}_{i-2}^j, \tag{3.2.10a}$$

$$\widetilde{\mathcal{U}}_s^j(s_i) = \frac{5}{h}(\mathfrak{C}_{i+2}^j + 10\mathfrak{C}_{i+1}^j - 10\mathfrak{C}_{i-1}^j - \mathfrak{C}_{i-2}^j), \tag{3.2.10b}$$

$$\widetilde{\mathcal{U}}_{ss}^j(s_i) = \frac{20}{h^2}(\mathfrak{C}_{i+2}^j + 2\mathfrak{C}_{i+1}^j - 6\mathfrak{C}_i^j + 2\mathfrak{C}_{i-1}^j + \mathfrak{C}_{i-2}^j), \tag{3.2.10c}$$

$$\widetilde{\mathcal{U}}_{sss}^j(s_i) = \frac{60}{h^3}(\mathfrak{C}_{i+2}^j - 2\mathfrak{C}_{i+1}^j + 2\mathfrak{C}_{i-1}^j - \mathfrak{C}_{i-2}^j), \tag{3.2.10d}$$

$$\widetilde{\mathcal{U}}_{ssss}^j(s_i) = \frac{120}{h^4}(\mathfrak{C}_{i+2}^j - 4\mathfrak{C}_{i+1}^j + 6\mathfrak{C}_i^j - 4\mathfrak{C}_{i-1}^j + \mathfrak{C}_{i-2}^j). \tag{3.2.10e}$$

Using the above expressions in the semi-discrete Equation (3.2.6), we get following system of algebraic equations

$$(\mathcal{P}_i^j - \mathcal{Q}_i^j + \mathcal{R}_i^j + \mathcal{S}_i^j)\mathfrak{C}_{i-2}^j + (26\mathcal{P}_i^j - 10\mathcal{Q}_i^j + 2\mathcal{R}_i^j - 4\mathcal{S}_i^j)\mathfrak{C}_{i-1}^j$$
$$+ (66\mathcal{P}_i^j - 6\mathcal{R}_i^j + 6\mathcal{S}_i^j)\mathfrak{C}_i^j + (26\mathcal{P}_i^j + 10\mathcal{Q}_i^j + 2\mathcal{R}_i^j - 4\mathcal{S}_i^j)\mathfrak{C}_{i+1}^j$$

$$+ (\mathcal{P}_i^j + \mathcal{Q}_i^j + \mathcal{R}_i^j + \mathcal{S}_i^j)\mathfrak{C}_{i+2}^j = \wp_i^j,\ i = 0, 1, \ldots, N_s,\ j = 1, 2, \ldots, M_t, \tag{3.2.11a}$$

where

$$\mathcal{P}_i^j = \Lambda w_0^\gamma + a_1^j(s_i)u_s^{*j-1}(s_i),\ \mathcal{Q}_i^j = \frac{5}{h}a_1^j(s_i)u^{*j-1}(s_i),$$
$$\mathcal{R}_i^j = \frac{20}{h^2}a_2^j(s_i),\ \mathcal{S}_i^j = \frac{120}{h^4}a_3^j(s_i),$$
$$\wp_i^j = g_i^j + \Lambda\left[\sum_{n=1}^{j-1}(w_{j-n-1}^\gamma - w_{j-n}^\gamma)\widetilde{\mathcal{U}}^n(s_i) + w_{j-1}^\gamma\widetilde{\mathcal{U}}^0(s_i)\right] + a_1^j(s_i)u^{*j-1}(s_i)u_s^{*j-1}(s_i).$$

The above notations are defined before (3.2.6). Now, in terms of quintic splines, the BCs ((3.2.3b) and (3.2.3c)) are expressed as

$$\widetilde{\mathcal{U}}^j(s_0) = \mathfrak{C}_{-2}^j + 26\mathfrak{C}_{-1}^j + 66\mathfrak{C}_0^j + 26\mathfrak{C}_1^j + \mathfrak{C}_2^j = f_0^j, \tag{3.2.11b}$$
$$\widetilde{\mathcal{U}}^j(s_{N_s}) = \mathfrak{C}_{N_s-2}^j + 26\mathfrak{C}_{N_s-1}^j + 66\mathfrak{C}_{N_s}^j + 26\mathfrak{C}_{N_s+1}^j + \mathfrak{C}_{N_s+2}^j = f_1^j, \tag{3.2.11c}$$

and

$$\widetilde{\mathcal{U}}_s^j(s_0) = -\mathfrak{C}_{-2}^j - 10\mathfrak{C}_{-1}^j + 10\mathfrak{C}_1^j + \mathfrak{C}_2^j = 0, \tag{3.2.11d}$$
$$\widetilde{\mathcal{U}}_s^j(s_{N_s}) = -\mathfrak{C}_{N_s-2}^j - 10\mathfrak{C}_{N_s-1}^j + 10\mathfrak{C}_{N_s+1}^j + \mathfrak{C}_{N_s+2}^j = 0. \tag{3.2.11e}$$

On eliminating $\mathfrak{C}_{-2}^j$, $\mathfrak{C}_{-1}^j$, $\mathfrak{C}_{N_s+2}^j$, and $\mathfrak{C}_{N_s+1}^j$ from the system (3.2.11b)-(3.2.11e) and substituting in (3.2.11a), we obtain an $(N_s+1)\times(N_s+1)$ penta-diagonal system of algebraic equations

$$\mathfrak{A}\mathcal{X}^j = \mathcal{Z}^j, \tag{3.2.12}$$

where

$$\mathfrak{A} = \begin{bmatrix} \mathfrak{A}_{11} & \mathfrak{A}_{12} & \mathfrak{A}_{13} & 0 & 0 & 0 & & & \\ \mathfrak{A}_{21} & \mathfrak{A}_{22} & \mathfrak{A}_{23} & \mathfrak{A}_{24} & 0 & 0 & & & \\ p_2^j & q_2^j & r_2^j & v_2^j & y_2^j & 0 & & & \\ & \ddots & \ddots & \ddots & \ddots & \ddots & & & \\ & & p_i^j & q_i^j & r_i^j & v_i^j & y_i^j & & \\ & & & \ddots & \ddots & \ddots & \ddots & \ddots & \\ & & 0 & p_{N_s-2}^j & q_{N_s-2}^j & r_{N_s-2}^j & v_{N_s-2}^j & y_{N_s-2}^j & \\ & & 0 & 0 & \mathfrak{A}_{N_s,N_s-2} & \mathfrak{A}_{N_s,N_s-1} & \mathfrak{A}_{N_s,N_s} & \mathfrak{A}_{N_s,N_s+1} & \\ & & 0 & 0 & 0 & \mathfrak{A}_{N_s+1,N_s-1} & \mathfrak{A}_{N_s+1,N_s} & \mathfrak{A}_{N_s+1,N_s+1} & \end{bmatrix}, \tag{3.2.13}$$

$$\mathcal{X}^j = \begin{bmatrix} \mathfrak{C}_0^j \\ \mathfrak{C}_1^j \\ \vdots \\ \mathfrak{C}_i^j \\ \vdots \\ \mathfrak{C}_{N_s-1}^j \\ \mathfrak{C}_{N_s}^j \end{bmatrix}, \quad \mathcal{Z}^j = \begin{bmatrix} 8\wp_0^j + (5p_0^j - q_0^j/2)f_0^j \\ 8\wp_1^j - p_1^j f_0^j/2 \\ \vdots \\ \wp_i^j \\ \vdots \\ 8\wp_{N_s-1}^j - y_{N_s-1}^j f_1^j/2 \\ 8\wp_{N_s}^j + (5y_{N_s}^j - v_{N_s}^j/2)f_1^j \end{bmatrix}. \tag{3.2.14}$$

The elements of the matrix $\mathfrak{A}$ are given by

$$\mathfrak{A}_{11} = 330p_0^j - 33q_0^j + 8r_0^j,\ \mathfrak{A}_{12} = 260p_0^j - 18q_0^j + 8v_0^j,\ \mathfrak{A}_{13} = 18p_0^j - q_0^j + 8y_0^j,$$

$$\mathfrak{A}_{21} = -33p_1^j + 8q_1^j,\ \mathfrak{A}_{22} = -18p_1^j + 8r_1^j,\ \mathfrak{A}_{23} = -p_1^j + 8v_1^j,\ \mathfrak{A}_{24} = 8y_1^j,$$

$$\mathfrak{A}_{N_s,N_s-2} = 8p_{N_s-1}^j,\ \mathfrak{A}_{N_s,N_s-1} = 8q_{N_s-1}^j - y_{N_s-1}^j,\ \mathfrak{A}_{N_s,N_s} = 8r_{N_s-1}^j - 18y_{N_s-1}^j,$$

$$\mathfrak{A}_{N_s,N_s+1} = 8v_{N_s-1}^j - 33y_{N_s-1}^j,\ \mathfrak{A}_{N_s+1,N_s-1} = 8p_{N_s}^j - v_{N_s}^j + 18y_{N_s}^j,$$

$$\mathfrak{A}_{N_s+1,N_s} = 8q_{N_s}^j - 18v_{N_s}^j + 260y_{N_s}^j,\ \mathfrak{A}_{N_s+1,N_s+1} = 8r_{N_s}^j - 33v_{N_s}^j + 330y_{N_s}^j,$$

$$p_i^j = \mathcal{P}_i^j - \mathcal{Q}_i^j + \mathcal{R}_i^j + \mathcal{S}_i^j,\ q_i^j = 26\mathcal{P}_i^j - 10\mathcal{Q}_i^j + 2\mathcal{R}_i^j - 4\mathcal{S}_i^j,\ r_i^j = 66\mathcal{P}_i^j - 6\mathcal{R}_i^j + 6\mathcal{S}_i^j,$$

$$v_i^j = 26\mathcal{P}_i^j + 10\mathcal{Q}_i^j + 2\mathcal{R}_i^j - 4\mathcal{S}_i^j,\ y_i^j = \mathcal{P}_i^j + \mathcal{Q}_i^j + \mathcal{R}_i^j + \mathcal{S}_i^j.$$

For initial time level $j = 0$, we determine $(\mathfrak{C}_0^0, \mathfrak{C}_1^0, \ldots, \mathfrak{C}_{N_s-1}^0, \mathfrak{C}_{N_s}^0)$ from the IC $\widetilde{\mathcal{U}}^0(s_i) = \phi(s_i)$. For this, we use BCs $\widetilde{\mathcal{U}}_s^0(s_0) = 0, \widetilde{\mathcal{U}}_s^0(s_{N_s}) = 0, \widetilde{\mathcal{U}}_{ss}^0(s_0) = 0$, and $\widetilde{\mathcal{U}}_{ss}^0(s_{N_s}) = 0$. After all these implementations, we obtain the required system $\mathcal{I}\mathcal{X}^0 = \mathcal{Z}^0$ having unknowns $\mathcal{X}^0$, where

$$\mathcal{I} = \begin{bmatrix} 54 & 60 & 6 & 0 & 0 & 0 & & \\ \frac{101}{4} & \frac{135}{2} & \frac{105}{4} & 1 & 0 & 0 & & \\ 1 & 26 & 66 & 26 & 1 & 0 & & \\ & \ddots & \ddots & \ddots & \ddots & \ddots & & \\ & & 1 & 26 & 66 & 26 & 1 & \\ & & & \ddots & \ddots & \ddots & \ddots & \ddots \\ & & 0 & 1 & 26 & 66 & 26 & 1 \\ & & 0 & 0 & 1 & \frac{105}{4} & \frac{135}{2} & \frac{101}{4} \\ & & 0 & 0 & 0 & 6 & 60 & 54 \end{bmatrix}, \quad \mathcal{X}^0 = \begin{bmatrix} \mathfrak{C}_0^0 \\ \mathfrak{C}_1^0 \\ \vdots \\ \mathfrak{C}_i^0 \\ \vdots \\ \mathfrak{C}_{N_s-1}^0 \\ \mathfrak{C}_{N_s}^0 \end{bmatrix}, \quad \mathcal{Z}^0 = \begin{bmatrix} \phi(s_0) \\ \phi(s_1) \\ \vdots \\ \phi(s_i) \\ \vdots \\ \phi(s_{N_s-1}) \\ \phi(s_{N_s}) \end{bmatrix}.$$

The corresponding numerical algorithm for the proposed approximation is given below:

Algorithm 1 Algorithm of Present Collocation Approach

Require: Fractional order (γ), Λ, Step sizes in Time and Space: (k and h, respectively), The number of partitions in time and space (M_t and N_s, respectively)
Ensure: Approximate Solution: $\widetilde{\mathcal{U}}_i^j$
Define the matrix $\mathcal{I}$ at initial time level
Calculate unknown $\mathcal{X}^0$ initially.
for $j = 1 : M_t$ **do**
Consider the unknowns $(\mathfrak{C}_i^j)_{i=-2}^{N_s+2}$ from (3.2.9)
Calculate p_i^j, q_i^j, r_i^j, v_i^j, y_i^j, $\wp_i^j$ from (3.2.13)
Calculate the matrix $\mathfrak{A}$ and column vector $\mathcal{Z}^j$ from (3.2.13) and (3.2.14)
Find $\mathcal{X}^j$ from (3.2.12)
Find the approximate solution $\widetilde{\mathcal{U}}$ as defined in Equation (3.2.10a)

3.3 Stability Analysis

In this province, we utilize the Von-Neumann procedure to test the stability of the present approach (3.2.11). To study this, we represent the discretized scheme in the subsequent

formation

$$p_m^j \mathfrak{C}_{m-2}^j + q_m^j \mathfrak{C}_{m-1}^j + r_m^j \mathfrak{C}_m^j + v_m^j \mathfrak{C}_{m+1}^j + y_m^j \mathfrak{C}_{m+2}^j = g_m^j + \Lambda \Bigg[\sum_{n=1}^{j-1} (w_{j-n-1}^\gamma - w_{j-n}^\gamma)(\mathfrak{C}_{m-2}^n + 26\mathfrak{C}_{m-1}^n + 66\mathfrak{C}_m^n + 26\mathfrak{C}_{m+1}^n + \mathfrak{C}_{m+2}^n) + w_{j-1}^\gamma (\mathfrak{C}_{m-2}^0 + 26\mathfrak{C}_{m-1}^0 + 66\mathfrak{C}_m^0 + 26\mathfrak{C}_{m+1}^0 + \mathfrak{C}_{m+2}^0) \Bigg] + a_1^j(s_m) u^{*j-1}(s_m) u_s^{*j-1}(s_m),\ m = 0, 1, \ldots, N_s,\ j = 1, 2, \ldots, M_t. \tag{3.3.1}$$

Suppose that $\tilde{\mathfrak{C}}_m^j$ be the perturbed solution of (3.2.11a), then the perturbation $\lambda_m^j = \mathfrak{C}_m^j - \tilde{\mathfrak{C}}_m^j$ satisfies

$$p_m^j \lambda_{m-2}^j + q_m^j \lambda_{m-1}^j + r_m^j \lambda_m^j + v_m^j \lambda_{m+1}^j + y_m^j \lambda_{m+2}^j = \Lambda \Bigg[\sum_{n=1}^{j-1} (w_{j-n-1}^\gamma - w_{j-n}^\gamma)(\lambda_{m-2}^n + 26\lambda_{m-1}^n + 66\lambda_m^n + 26\lambda_{m+1}^n + \lambda_{m+2}^n) + w_{j-1}^\gamma (\lambda_{m-2}^0 + 26\lambda_{m-1}^0 + 66\lambda_m^0 + 26\lambda_{m+1}^0 + \lambda_{m+2}^0) \Bigg],$$
$$m = 0, 1, \ldots, N_s,\ j = 1, 2, \ldots, M_t, \tag{3.3.2}$$

along with the requirements

$$\lambda_0^j = \lambda_{N_s}^j = 0,\ j = 0, 1, \ldots, M_t.$$

For the primary investigation, let us suppose that

$$\lambda_m^j = \zeta^j e^{i\theta m h},$$

where $i = \sqrt{-1}$ and θ is a wave number. Then, after simplification, (3.3.2) leads to

$$\zeta^j (p_m^j e^{-2i\theta h} + q_m^j e^{-i\theta h} + r_m^j + v_m^j e^{i\theta h} + y_m^j e^{2i\theta h}) = \Lambda \Bigg[\sum_{n=1}^{j-1} \zeta^n (w_{j-n-1}^\gamma - w_{j-n}^\gamma)(e^{-2i\theta h} + 26e^{-i\theta h} + 66 + 26e^{i\theta h} + e^{2i\theta h}) + w_{j-1}^\gamma \zeta^0 (e^{-2i\theta h} + 26e^{-i\theta h} + 66 + 26e^{i\theta h} + e^{2i\theta h}) \Bigg],$$
$$j = 1, 2, \ldots, M_t. \tag{3.3.3}$$

For stability investigation of the procedure presented in (3.2.11), we prove that $|\zeta^j| \leq |\zeta^0|$ by mathematical induction. For $j = 1$, Equation (3.3.3) yields

$$\zeta^1(p_m^1 e^{-2i\theta h}+q_m^1 e^{-i\theta h}+r_m^1+v_m^1 e^{i\theta h}+y_m^1 e^{2i\theta h}) = \Lambda w_0^\gamma \zeta^0(e^{-2i\theta h}+26e^{-i\theta h}+66+26e^{i\theta h}+e^{2i\theta h}),$$

and as for $j = 1$, $w_0^\gamma = 1$, we have

$$\begin{aligned}
&\zeta^1\Big((\mathcal{P}_m^1 - \mathcal{Q}_m^1 + \mathcal{R}_m^1 + \mathcal{S}_m^1)e^{-2i\theta h} + (26\mathcal{P}_m^1 - 10\mathcal{Q}_m^1 + 2\mathcal{R}_m^1 - 4\mathcal{S}_m^1)e^{-i\theta h} \\
&+ (66\mathcal{P}_m^1 - 6\mathcal{R}_m^1 + 6\mathcal{S}_m^1) + (26\mathcal{P}_m^1 + 10\mathcal{Q}_m^1 + 2\mathcal{R}_m^1 - 4\mathcal{S}_m^1)e^{i\theta h} + \\
&= (\mathcal{P}_m^1 + \mathcal{Q}_m^1 + \mathcal{R}_m^1 + \mathcal{S}_m^1)e^{2i\theta h}\Big)\Lambda\zeta^0(e^{-2i\theta h} + 26e^{-i\theta h} + 66 + 26e^{i\theta h} + e^{2i\theta h}). \quad (3.3.4)
\end{aligned}$$

After simplification, Equation (3.3.4) gives

$$|\zeta^1| = \left|\frac{\Lambda(2\cos(2\theta h) + 52\cos(\theta h) + 66)\zeta^0}{\mathcal{K}_m^1 + i\mathcal{L}_m^1}\right| = \frac{|\Lambda(2\cos(2\theta h) + 52\cos(\theta h) + 66)|}{\sqrt{(\mathcal{K}_m^1)^2 + (\mathcal{L}_m^1)^2}}|\zeta^0|, \quad (3.3.5)$$

where

$$\begin{aligned}
\mathcal{K}_m^1 &= \mathcal{P}_m^1(2\cos(2\theta h) + 52\cos(\theta h) + 66) + \mathcal{R}_m^1(2\cos(2\theta h) + 4\cos(\theta h) - 6) \\
&\quad + \mathcal{S}_m^1(2\cos(2\theta h) - 8\cos(\theta h) + 6), \\
\mathcal{L}_m^1 &= \mathcal{Q}_m^1(2\sin(2\theta h) + 20\sin(\theta h)).
\end{aligned}$$

After some simplifications, Replacing the values of $\mathcal{P}_m^1$, $\mathcal{R}_m^1$ and $\mathcal{S}_m^1$ as $h \to 0$ in Equation (3.3.5), we obtain

$$|\zeta^1| \leq |\zeta^0|. \quad (3.3.6)$$

Now let us assume the following before we proceed with mathematical induction

$$|\zeta^n| \leq |\zeta^0|, \text{ for } n = 2, 3, \ldots, j-1. \quad (3.3.7)$$

To confirm, (3.3.7) holds true for $n = j$, let us take Equation (3.3.3) in the simplified form

$$|\zeta^j| = \left| \frac{\Lambda \left[\sum_{n=1}^{j-1} \zeta^n (w_{j-n-1}^{\gamma} - w_{j-n}^{\gamma}) + w_{j-1}^{\gamma} \zeta^0 \right] (2\cos(2\theta h) + 52\cos(\theta h) + 66)}{\mathcal{K}_m^j + i\mathcal{L}_m^j} \right|$$
$$\leq \frac{\Lambda w_0^{\gamma} (2\cos(2\theta h) + 52\cos(\theta h) + 66)}{\sqrt{(\mathcal{K}_m^j)^2 + (\mathcal{L}_m^j)^2}} |\zeta^0|,$$

where

$$\mathcal{K}_m^j = \mathcal{P}_m^j (2\cos(2\theta h) + 52\cos(\theta h) + 66) + \mathcal{R}_m^j (2\cos(2\theta h) + 4\cos(\theta h) - 6)$$
$$+ \mathcal{S}_m^j (2\cos(2\theta h) - 8\cos(\theta h) + 6),$$
$$\mathcal{L}_m^j = \mathcal{Q}_m^j (2\sin(2\theta h) + 20\sin(\theta h)).$$

Replacing the values of $\mathcal{P}_m^j$, $\mathcal{R}_m^j$ and $\mathcal{S}_m^j$ and taking $h \to 0$ we acquire

$$|\zeta^j| \leq |\zeta^0|, \quad j = 1, 2, \ldots, M_t.$$

Therefore, the numerical scheme (3.2.11) is shown to be unconditionally stable.

3.4 Convergence analysis

Lemma 3.4.1. *The quintic $\mathfrak{B}$-spline functions $\mathfrak{B}_{-2}(s), \mathfrak{B}_{-1}(s), \mathfrak{B}_0(s), \ldots, \mathfrak{B}_{N_s+1}(s), \mathfrak{B}_{N_s+2}(s)$ satisfy the inequality*

$$\sum_{i=-2}^{N_s+2} |\mathfrak{B}_i(s)| \leq 186, \quad 0 \leq s \leq 1.$$

Proof. Note that

$$\sum_{i=-2}^{N_s+2} |\mathfrak{B}_i(s)| \leq 186, \quad 0 \leq s \leq 1.$$

At a mesh point $s = s_n$; $\mathfrak{B}_n(s_n)$ is nonzero at five mesh points $s_{n-2}, s_{n-1}, s_n, s_{n+1}$, and s_{n+2}. Therefore,

$$\sum_{i=-2}^{N_s+2} |\mathfrak{B}_i(s_n)| = |\mathfrak{B}_{n-2}(s_n)| + |\mathfrak{B}_{n-1}(s_n)| + |\mathfrak{B}_n(s_n)| + |\mathfrak{B}_{n+1}(s_n)| + |\mathfrak{B}_{n+2}(s_n)|$$

$$= 1 + 26 + 66 + 26 + 1 = 120.$$

If s is not a mesh point, then

$$\sum_{i=-2}^{N_s+2} |\mathfrak{B}_i(s)| = |\mathfrak{B}_{n-3}(s)| + |\mathfrak{B}_{n-2}(s)| + |\mathfrak{B}_{n-1}(s)| + |\mathfrak{B}_n(s)| + |\mathfrak{B}_{n+1}(s)| + |\mathfrak{B}_{n+2}(s)|$$

$$\leq 1 + 26 + 66 + 66 + 26 + 1 = 186.$$

Thus, the result is proved. □

Lemma 3.4.2. *If $\mathcal{V}^j(s)$ denote the unique quintic $\mathfrak{B}$-spline interpolant of $\widetilde{u}^j(s) \in C^6[0,1]$ at time $t = t_j$, then from [152, 153], we have*

$$\left\| \frac{\partial^n}{\partial s^n} \left(\mathcal{V}^j(s) - \widetilde{u}^j(s) \right) \right\|_\infty \leq c_n h^{6-n},\ n = 0, 1, 2, 3, 4,$$

for positive constants c_n.

Theorem 3.4.1. *If $\widetilde{\mathcal{U}}^j(s)$ be the quintic $\mathfrak{B}$-spline based approximation of $\widetilde{u}^j(s) \in C^6[0,1]$ at time $t = t_j$, then*

$$\|\widetilde{\mathcal{U}}^j(s) - \widetilde{u}^j(s)\|_\infty \leq Ch^2,$$

holds for some positive constant C and sufficiently small h.

Proof. If $\widetilde{\mathcal{U}}^j(s) = \sum_{i=-2}^{N_s+2} \mathfrak{C}_i^j \mathcal{B}_i(s)$ be the quintic $\mathfrak{B}$-spline approximation of $\widetilde{u}^j(s)$, which is the exact solution of the semi-discrete problem (3.2.6) at the j^{th} time level, and $\mathcal{V}^j(s) = \sum_{i=-2}^{N_s+2} \mathcal{D}_i^j \mathcal{B}_i(s)$ exist for the unique quintic $\mathfrak{B}$-spline interpolant. Now we want an estimate of $\|\widetilde{\mathcal{U}}^j(s) - \widetilde{u}^j(s)\|_\infty$ as

$$\|\widetilde{\mathcal{U}}^j(s) - \widetilde{u}^j(s)\|_\infty \leq \|\widetilde{\mathcal{U}}^j(s) - \mathcal{V}^j(s)\|_\infty + \|\mathcal{V}^j(s) - \widetilde{u}^j(s)\|_\infty.$$

We have

$$L\widetilde{\mathcal{U}}^j(s) = [\Lambda w_0^\gamma + a_1^j(s) u_s^{*j-1}(s)]\widetilde{\mathcal{U}}^j(s) + a_1^j(s) u^{*j-1}(s)\widetilde{\mathcal{U}}_s^j(s) + a_2^j(s)\widetilde{\mathcal{U}}_{ss}^j(s)$$

$$
\begin{aligned}
&+ a_3^j(s)\widetilde{\mathcal{U}}_{ssss}^j(s),\\
L(\widetilde{\mathcal{U}}^j(s) - \mathcal{V}^j(s)) = &\left(\Lambda w_0^\gamma + a_1(s,j)u^{*j-1}(s)\right)(\widetilde{\mathcal{U}}^j(s) - \mathcal{V}^j(s)) + a_1^j(s)u^{*j-1}(s)(\widetilde{\mathcal{U}}_s^j(s)\\
&- \mathcal{V}_s^j(s)) + a_2^j(s)(\widetilde{\mathcal{U}}_{ss}^j(s) - \mathcal{V}_{ss}^j(s)) + a_3^j(s))(\widetilde{\mathcal{U}}_{ssss}^j(s) - \mathcal{V}_{ssss}^j(s)).
\end{aligned} \tag{3.4.1}
$$

Using Lemma 3.4.2, we get

$$
\begin{aligned}
|L(\widetilde{\mathcal{U}}^j(s) - \mathcal{V}^j(s))| \leq &\left|\Lambda w_0^\gamma + a_1(s,j)u_s^{*j-1}(s)\right| c_0h^6 + |a_1^j(s)u^{*j-1}(s)|c_1h^5\\
&+ |a_2^j(s)|c_2h^4 + |a_3^j(s)|c_4h^2\\
\leq &K_1h^2,
\end{aligned} \tag{3.4.2}
$$

where

$$
K_1 = \left|\Lambda w_0^\gamma + a_1^j(s)u_s^{*j-1}(s)\right| c_0h^4 + |a_1^j(s)u^{*j-1}(s)|c_1h^3 + |a_2^j(s)|c_2h^2 + |a_3^j(s)|c_4.
$$

We have

$$
L\widetilde{\mathcal{U}}^j(s) = \mathfrak{A}\mathcal{X}^j,\ j = 1, 2, \ldots, M_t,
$$

and

$$
L\mathcal{V}^j(s) = \mathfrak{A}\mathcal{Y}^j,\ j = 1, 2, \ldots, M_t,
$$

where

$$
\mathcal{Y}^j = (\mathcal{D}_0^j, \mathcal{D}_1^j, \ldots, \mathcal{D}_{N_s-1}^j, \mathcal{D}_{N_s}^j)'.
$$

Note that the matrix $\mathfrak{A}$ is strictly diagonally dominant, which implies the invertibility of $\mathfrak{A}$. Now from Equation (3.4.2), we have

$$
\|\mathcal{X}^j - \mathcal{Y}^j\|_\infty \leq \|\mathfrak{A}^{-1}\|_\infty K_1h^2. \tag{3.4.3}
$$

Let $\rho_0, \rho_1, \ldots, \rho_{N_s}$ are row sums of $\mathfrak{A}$ at each time level and given by

$$
\rho_0 = 480\mathcal{R}_0^j + 840\mathcal{Q}_0^j,
$$

$$\begin{aligned}
\rho_1 &= 900\mathcal{P}_1^j + 60\mathcal{Q}_1^j - 60\mathcal{R}_1^j - 60\mathcal{S}_1^j,\\
\rho_i &= 120\mathcal{P}_i^j,\ 2 \le i \le N_s - 2,\\
\rho_{N_s-1} &= 900\mathcal{P}_{N_s-1}^j - 60\mathcal{Q}_{N_s-1}^j - 60\mathcal{R}_{N_s-1}^j - 60\mathcal{S}_{N_s-1}^j,\\
\rho_{N_s} &= 480\mathcal{R}_{N_s}^j + 840\mathcal{Q}_{N_s}^j.
\end{aligned}$$

Then, as a consequence

$$\|\mathfrak{A}^{-1}\|_\infty \le \frac{1}{\rho} \le \frac{1}{|\rho|}, \tag{3.4.4}$$

where $\rho = \min\{\rho_0, \rho_1, \ldots, \rho_{N_s}\}$. Now, we substitute Equation (3.4.4) into (3.4.3), to get

$$\|\mathcal{X}^j - \mathcal{Y}^j\|_\infty \le \frac{K_1 h^2}{|\rho|}. \tag{3.4.5}$$

Using Lemma 3.4.1 in Equation (3.4.5), it follows

$$\|\widetilde{\mathcal{U}}^j(s) - \mathcal{V}^j(s)\|_\infty = \left\| \sum_{i=-2}^{N_s+2} (\mathfrak{C}_i^j - \mathcal{D}_i^j)\mathcal{B}_i(s) \right\|_\infty \le \left| \sum_{i=-2}^{N_s+2} \mathcal{B}_i(s) \right| \|\mathcal{X}^j - \mathcal{Y}^j\|_\infty \le \frac{186K_1h^2}{|\rho|}, \tag{3.4.6}$$

and application of Lemma 3.4.2 gives

$$\|\mathcal{V}^j(s) - \widetilde{u}^j(s)\|_\infty \le c_0 h^6. \tag{3.4.7}$$

With the use of triangle inequality

$$\|\widetilde{\mathcal{U}}^j(s) - \widetilde{u}^j(s)\|_\infty \le \|\widetilde{\mathcal{U}}^j(s) - \mathcal{V}^j(s)\|_\infty + \|\mathcal{V}^j(s) - \widetilde{u}^j(s)\|_\infty,$$

and on adding equation (3.4.6) and (3.4.7), we deduce that

$$\|\widetilde{\mathcal{U}}^j(s) - \widetilde{u}^j(s)\|_\infty \le Ch^2,$$

where $C = c_0 h^4 + \frac{186K_1}{|\rho|}$. Hence, the theorem is proved. □

Theorem 3.4.2. *Let $\widetilde{\mathcal{U}}(s,t)$ and $u(s,t)$ denote $\mathfrak{B}$-spline approximation and exact solution of*

(3.1.1), resp.. Then, the proposed approximation satisfies the following convergence result

$$\|u - \widetilde{\mathcal{U}}\|_\infty \leq C(h^2 + k^2).$$

Following the approach for the nonlinear problems, the order of convergence for the linear problems (using (3.2.3a)) is given by the following results.

Lemma 3.4.3. *If $\mathcal{U}^j(s)$ denote the unique quintic $\mathfrak{B}$-spline interpolant of $\hat{u}^j(s) \in C^6[0,1]$, then from [152, 153], we have*

$$\left\| \frac{\partial^n}{\partial s^n} \left(\mathcal{U}^j(s) - \hat{u}^j(s) \right) \right\|_\infty \leq c_n h^{6-n},\ n = 0, 1, 2, 3, 4,$$

for positive constants c_n.

Theorem 3.4.3. *If $\widetilde{\mathcal{U}}^j(s)$ be the quintic $\mathfrak{B}$-spline approximation of $\hat{u}^j(s) \in C^6[0,1]$, then*

$$\|\widetilde{\mathcal{U}}^j(s) - \hat{u}^j(s)\|_\infty \leq Ch^2,$$

holds for positive constant C and sufficient small h.

Proof. The proof follows similar steps to the nonlinear KS equation. □

Theorem 3.4.4. *Let $\widetilde{\mathcal{U}}(s,t)$ and $u(s,t)$ denote $\mathfrak{B}$-spline approximation and exact solution of (3.1.2), resp. Then, the proposed approximation holds the following convergence result*

$$\|u - \widetilde{\mathcal{U}}\|_\infty \leq C(h^2 + k^{3-\gamma}).$$

Remark 3.4.1. *For the Burgers' equation (putting $a_3^j(s) = 0$ in Theorem 3.4.1) analysis remains same and the estimate $\|\widetilde{\mathcal{U}}^j(s) - \widetilde{u}^j(s)\|_\infty \leq Ch^4$ holds.*

3.5 Experimental Evidences

Now, we consider several types of nonlinear and linear problems for experimental evidence in favor of our theory. It will be easier to check the performance of our proposed approach if the exact solution is known. In general, the exact solutions to fractional problems are

more complex. Hence, for the problems with time-varying layers, we check the performance based on the available works for problems with classical time derivatives, as a limiting case of fractional order time derivatives. There are four types of problems considered here- Linear time fractional problem, Time fractional KS equation, Burgers equation with fractional derivative in time, and Classical KS equation with integer order derivative in time. The present approach provides higher-order convergence in all of the above cases.

The error estimates are calculated using the double mesh principle in the L_∞ and L_2-norms. The respective order of convergence is computed by using the definition 1.3.8

In all the tables, we provide CPU time to show the performance of the proposed technique. All computational results are obtained using MATLAB R2021 on Intel Core i7 (9th Gen).

Example 3.5.1. *Let us first check the effectiveness of the proposed approach for the linear problem*

$$ {}_0^C D_t^\gamma u(s,t) + 2u_s(s,t) + 4u_{ss}(s,t) + u_{ssss}(s,t) = g(s,t), \quad (s,t) \in (0,1) \times (0,1], $$

with the BCs

$$ \begin{cases} u(0,t) = 0, \ u(1,t) = 0, \ t \in [0,1], \\ u_{ss}(0,t) = 0, \ u_{ss}(1,t) = 0, \ t \in [0,1], \end{cases} $$

and the IC

$$ u(s,0) = 0, \ 0 \leq s \leq 1. $$

Source term $g(s,t)$ is calculated using the exact solution $u(s,t) = t^{4+\gamma} \sin(\pi s)$.

Example 3.5.2. *Next, consider the Caputo-type time fractional KS equation with constant coefficients-*

$$ {}_0^C D_t^\gamma u(s,t) + 2u(s,t)u_s(s,t) + 4u_{ss}(s,t) + u_{ssss}(s,t) = g(s,t), \quad (s,t) \in (0,1) \times (0,1], $$

with the BCs

$$\begin{cases} u(0,t) = 0,\ u(1,t) = 0,\ t \in [0,1], \\ u_s(0,t) = 0,\ u_s(1,t) = 0,\ t \in [0,1], \end{cases}$$

and the IC

$$u(s,0) = 0,\ 0 \le s \le 1.$$

Source term $g(s,t)$ is calculated using the exact solution $u(s,t) = s^2(s^3 - \frac{5}{2}s^2 + 2s - \frac{1}{2})t^4$.

Example 3.5.3. *Now, we consider the following Caputo-type time fractional variable coefficient nonlinear KS equation*

$${}_0^C D_t^\gamma u(s,t) + su(s,t)u_s(s,t) + su_{ss}(s,t) + u_{ssss}(s,t) = g(s,t), \quad (s,t) \in (0,1) \times (0,1],$$

with the BCs

$$\begin{cases} u(0,t) = 0,\ u(1,t) = 0,\ t \in [0,1], \\ u_{ss}(0,t) = 0,\ u_{ss}(1,t) = 0,\ t \in [0,1], \end{cases}$$

and the IC

$$u(s,0) = 0,\ 0 \le s \le 1.$$

Source term $g(s,t)$ is calculated using the exact solution $u(s,t) = t^4 \sin(\pi s)$.

Example 3.5.4. *Now let us consider the effectiveness of the present approach for Burgers' equation*

$${}_0^C D_t^\gamma u(s,t) + \exp(-20t)u(s,t)u_s(s,t) + (1+100s)u_{ss}(s,t) = g(s,t), \quad (s,t) \in (0,1)\times(0,1],$$

with the set of BCs

$$\begin{cases} u(0,t) = 0,\ u(1,t) = 0,\ t \in [0,1], \\ u_s(0,t) = 0,\ u_s(1,t) = 0,\ t \in [0,1], \end{cases}$$

and the IC

$$u(s,0) = 0,\ 0 \le s \le 1.$$

Source term $g(s,t)$ is calculated using the exact solution $u(s,t) = s^3(1-s)^3t^4$.

In general, the exact solution of the time-fractional nonlinear KS model is challenging to find out. Hence, motivated by the examples given in [134, 141] involving classical time derivatives, we took the time fractional KS equation in Example 3.5.5, whose solution will approach the time-varying layer originated to function as γ approaches 1.

Example 3.5.5. *Consider the time fractional nonlinear KS equation*

$${}_0^C D_t^\gamma u(s,t) + u(s,t)u_s(s,t) + u_{ss}(s,t) + u_{ssss}(s,t) = 0, \quad (s,t) \in (-30,30) \times (0,4],$$

with the BCs

$$\begin{cases} u(-30,t) = b + \frac{15}{19}\sqrt{\frac{11}{19}}\Big[-9\tanh(k_1(-30 - bt^\gamma - x_0)) + 11\tanh^3(k_1(-30 - bt^\gamma - x_0))\Big], \\ \ 0 \le t \le 4, \\ u(30,t) = b + \frac{15}{19}\sqrt{\frac{11}{19}}\Big[-9\tanh(k_1(30 - bt^\gamma - x_0)) + 11\tanh^3(k_1(30 - bt^\gamma - x_0))\Big], \\ \ 0 \le t \le 4, \\ u_{ss}(-30,t) = 0,\ u_{ss}(30,t) = 0,\ 0 \le t \le 4, \end{cases}$$

and the IC

$$u(s,0) = b + \frac{15}{19}\sqrt{\frac{11}{19}}\Big[-9\tanh(k_1(s - x_0)) + 11\tanh^3(k_1(s - x_0))\Big],\ -30 \le s \le 30,$$

where $b = 5$, $k_1 = \frac{1}{2}\sqrt{\frac{11}{19}}$, $x_0 = -12$.

The exact solution of Example 3.5.5 is unavailable. So, the double mesh principle [127] is used to compute the errors. Note that the solution at the initial time level has a sharp layer phenomenon that moves as time evolves. To compare the accurateness in terms of sharp layer

phenomena at the j-th time level, we calculate the Global Relative Error (GRE) as follows

$$\text{GRE} = \frac{\sum_i |\widetilde{\mathcal{U}}(s_i, t_j) - \widetilde{\mathcal{U}}(s_{2i-1}, t_j)|}{\sum_i \widetilde{\mathcal{U}}(s_i, t_j)}.$$

The following problem (at which time fractional derivative is substituted by 1st-order integer derivative) is considered to compare the results for the case when γ approaches 1 in the problem (3.1.1):

$$u_t(s,t) + a_1(s,t)u(s,t)u_s(s,t) + a_2(s,t)u_{ss}(s,t) + a_3(s,t)u_{ssss}(s,t) = g(s,t), \quad (3.5.1)$$

where $a_1(s,t)$, $a_2(s,t)$, $a_3(s,t)$, $g(s,t)$, and the IC and BCs take the same values as defined in Examples 3.5.2 and 3.5.3. Here, we use the Crank-Nicolson scheme for temporal discretization to maintain the temporal accuracy to the second order.

Now, we explain the experimental evidence in favor of our theory. In Tables 3.3 and 3.7, we present the outcomes of $E_\infty^{N_s,M_t}$, $E_2^{N_s,M_t}$, $\mathfrak{D}_2^{N_s,M_t}$, $\mathfrak{D}_\infty^{N_s,M_t}$ along with CPU time. It is easy to observe from tabulated results that the proposed numerical scheme provides second-order accuracy in space and time. The fractional order derivative increases the algorithm's complexity, but the proposed method handles this very well, and less computational time supports this analogy. We wanted to note that the computational time increases for time fractional problems compared to problems with classical time derivatives, as fractional derivatives involve integral approximations involving past data. In both the norms, we obtain good results matching theoretical claims. In addition, we produce the linear problem (3.5.1) to give an experimental comparison with the Examples 3.5.2 and 3.5.3 when γ approaches 1. It is evident from Tables 3.5 and 3.8 that the obtained results are close. The comparison of CPU times for both the problems (Time fractional KS Equation (3.1.1) and KS equation with classical time derivative (3.5.1)) justify the memory property of fractional derivatives, which uses additional storage of the system. Note that the computational cost for problems with classical time derivatives is lower than the cost for evaluating fractional time derivatives due to their nonlocal nature since the solutions at previous time levels need to be used to compute

the solution at present.

To show the better effectiveness of the present methodology based on the $L1-2$ scheme, we provide a comparison between $L1$ and $L1-2$ scheme in Table 3.6, which proves that the proposed scheme has a better rate of accuracy than $L1$ scheme. In addition, it should also be pointed out from this table that the higher order accuracy of the $L1-2$ scheme than the $L1$ scheme has been obtained with a similar computational cost. The present approach also performs well for the second-order Burgers' equation as given in Example 3.5.4 by putting $a_3(s,t)=0$. For the second-order problems, quintic $\mathfrak{B}$-splines provide fourth-order convergent results in space, and it is confirmed through Table 3.10 (see Remark 3.4.1). Tables 3.2, 3.4, and 3.9 confirm the quadratic accuracy in space and time separately by fixing the space (or time) steps and varying time (or space) steps, respectively. These tables confirm the accuracy of $\mathcal{O}(h^2+k^2)$ in both directions for the nonlinear KS equation and $\mathcal{O}(h^2+k^{3-\gamma})$ for the linear KS equation.

Graphically, one can observe that the approximate solutions of Examples 3.5.2 (Fig. 1) and 3.5.3 (Fig. 4) match with the exact one. The analytical and numerical solutions show a good match and can be confirmed by comparing them in a single plot (see Figures 3.2a and 3.5a). As the time step changes from the initial level to $t=1$, the solution changes accordingly, and in support of this argument, we plot Figs. 3.2b and 3.5b. Error plots (Fig. 3) are provided to demonstrate the error distribution at the nodal points.

Table 3.11 shows that the relative error associated with Example 3.5.5, evaluated by the double mesh principle, is negligible. In addition, the movement of layer behaviors is also visible in time for fractional order KS equations (refer to Fig. 6). This points out that the present approach can detect the sharpness of the layers. Furthermore, the boundary conditions involving derivatives are also satisfied as the solution is locally constant in a neighborhood of the boundaries. Note from Figure 6 that the present methodology works perfectly well when the fractional order γ approaches 1, as it matches with the exact solution given in [134, 141] for $\gamma=1$.

Table 3.2: Errors and order of convergence in spatial and time directions, for example, 3.5.1 in L_∞ norm

	Spatial direction (taking $M_t = 1000$)			Time direction (taking $N_s = 1000$)		
γ	N_s	Error	Order	M_t	Error	Order
0.5	4	$7.8758e-02$	1.9400	4	$2.3888e-03$	2.1215
	8	$2.0525e-02$	1.9848	8	$5.4895e-04$	2.2906
	16	$5.1857e-03$	1.9961	16	$1.1220e-04$	2.3508
	32	$1.2999e-03$	-	32	$2.1996e-05$	-
0.8	4	$7.7095e-02$	1.9420	4	$6.4762e-03$	1.8989
	8	$2.0065e-02$	1.9854	8	$1.7366e-03$	2.0257
	16	$5.0674e-03$	1.9963	16	$4.2649e-04$	2.2350
	32	$1.2701e-03$	-	32	$9.0598e-05$	-

Table 3.3: Errors, orders of convergence, and CPU time (in sec.) for Example 3.5.2 for different time fractional orders γ

	Norms	N_s=10 M_t=20	N_s=20 M_t=40	N_s=40 M_t=80	N_s=80 M_t=160	N_s=160 M_t=320
$\gamma = 0.3$	L_∞	$1.5603e-09$	$3.5878e-10$	$7.7052e-11$	$1.7191e-11$	$4.0055e-12$
		2.1207	2.2192	2.1642	2.1016	-
	L_2	$9.9903e-10$	$2.0688e-10$	$4.3001e-11$	$9.3373e-12$	$8.2604e-13$
		2.2717	2.2664	2.2033	2.1564	-
CPU Time		0.05768	0.2037	0.3330	2.1311	16.0248
$\gamma = 0.5$	L_∞	$4.2850e-09$	$8.6035e-10$	$1.7254e-10$	$3.4642e-11$	$7.3038e-12$
		2.3163	2.3180	2.3163	2.2458	-
	L_2	$2.7858e-09$	$5.5512e-10$	$1.0740e-10$	$2.0904e-11$	$9.0548e-12$
		2.3272	2.3698	2.3611	2.3086	-
CPU Time		0.0559	0.0840	0.3420	2.1214	16.1246
$\gamma = 0.8$	L_∞	$1.8388e-08$	$4.2561e-09$	$9.5043e-10$	$2.0983e-10$	$5.0390e-11$
		2.1112	2.1629	2.1794	2.0580	-
	L_2	$1.2157e-08$	$2.8081e-09$	$6.2613e-10$	$1.3803e-10$	$3.1675e-11$
		2.1141	2.1651	2.1815	2.1236	-
CPU Time		0.0623	0.0906	0.3514	2.3903	17.0300

Table 3.4: Errors and orders of convergence in spatial and temporal directions for Example 3.5.2 in L_∞ norm

	Spatial direction (taking $M_t = 512$)			Time direction (taking $N_s = 1024$)		
γ	N_s	Error	Rate	M_t	Error	Rate
0.5	4	$3.2790e-09$	2.1121	4	$5.4353e-07$	2.2211
	8	$7.5845e-10$	2.0303	8	$1.3440e-07$	2.2349
	16	$1.8567e-10$	2.0253	16	$3.1851e-08$	2.1038
	32	$4.5612e-11$	-	32	$7.4516e-09$	-
0.8	4	$2.7564e-08$	2.0878	4	$1.8495e-07$	2.0158
	8	$6.4841e-09$	2.0145	8	$3.9669e-08$	2.0771
	16	$1.6048e-09$	1.9693	16	$8.4273e-09$	2.0957
	32	$4.0983e-10$	-	32	$1.9606e-09$	-

Table 3.5: Comparison of errors, orders of convergence, and CPU time (in sec.) for Example 3.5.2 (as γ approaches 1) with Problem (3.5.1)

	N_s=10 M_t=20	N_s=20 M_t=40	N_s=40 M_t=80	N_s=80 M_t=160	N_s=160 M_t=320
$\gamma = 0.9$	$2.9339e-08$	$7.2312e-09$	$1.7215e-09$	$4.0527e-10$	$9.9665e-11$
	2.0205	2.0706	2.0867	2.0237	-
CPU Time	0.0641	0.0981	0.3319	2.1556	16.3124
$\gamma = 0.95$	$3.6933e-08$	$9.4043e-09$	$2.3143e-09$	$5.6346e-10$	$1.3772e-10$
	1.9735	2.0227	2.0382	2.0326	-
CPU Time	0.0523	0.0837	0.3249	2.1110	16.0089
$\gamma = 0.99$	$4.4329e-08$	$1.1590e-08$	$2.9297e-09$	$7.3329e-10$	$1.8407e-10$
	1.9354	1.9841	1.9983	1.9941	-
CPU Time	0.0661	0.0959	0.3393	2.1030	16.1969
$\gamma = 0.999$	$4.6179e-08$	$1.2146e-08$	$3.0890e-09$	$7.7790e-10$	$1.9558e-10$
	1.9268	1.9753	1.9895	1.9918	-
CPU Time	0.0652	0.0943	0.3444	2.1421	16.2448
$\gamma = 1$	$1.2166e-08$	$3.1440e-09$	$7.9259e-10$	$1.9863e-10$	$5.1888e-11$
	1.9522	1.9880	1.9965	1.9366	-
CPU Time	0.0690	0.0863	0.0780	0.1192	0.7122

Table 3.6: Comparison of errors, orders of convergence, and CPU time (in sec.) in $L1$ and $L1-2$ schemes for Example 3.5.2

	N_s=10 M_t=20	N_s=20 M_t=40	N_s=40 M_t=80	N_s=80 M_t=160	N_s=160 M_t=320
$\gamma = 0.5$					
$L1$ scheme	$6.5708e-08$	$2.5054e-08$	$9.1877e-09$	$3.3256e-09$	$1.1936e-09$
	1.3910	1.4473	1.4661	1.4783	-
CPU Time	0.0681	0.0989	0.3348	2.1385	16.0070
$L1-2$ scheme	$4.2850e-09$	$8.6035e-10$	$1.7254e-10$	$3.4642e-11$	$7.3038e-12$
	2.3163	2.3180	2.3163	2.2458	-
CPU Time	0.0559	0.0840	0.3420	2.1214	16.1246
$\gamma = 0.9$					
$L1$ scheme	$4.4770e-07$	$2.1955e-07$	$1.0426e-07$	$4.9126e-08$	$2.2992e-08$
	1.0280	1.0744	1.0856	1.0954	-
CPU Time	0.0619	0.0879	0.3228	2.0858	15.9919
$L1-2$ scheme	$2.9339e-08$	$7.2312e-09$	$1.7215e-09$	$4.0527e-10$	$9.9665e-11$
	2.0205	2.0706	2.0867	2.0237	-
CPU Time	0.0641	0.0981	0.3319	2.1556	16.3124

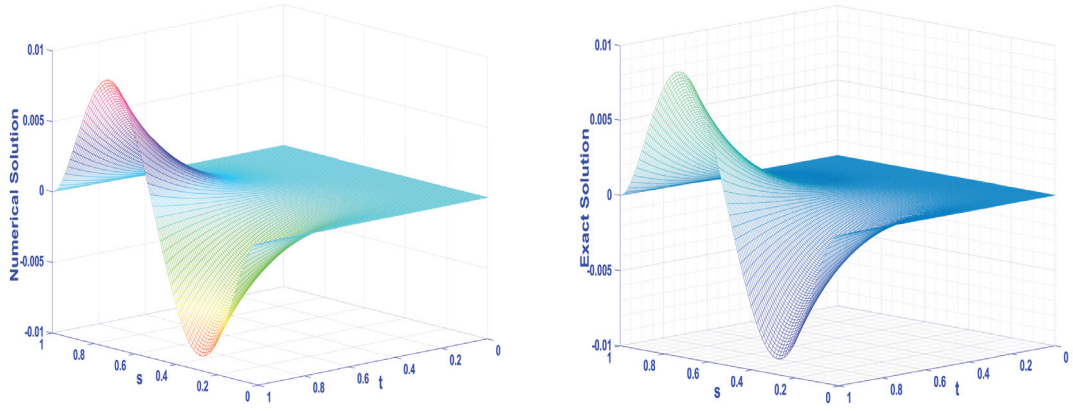

a Numerical solution

b Exact solution

Figure 1: Surface plots of exact and numerical solutions for Example 3.5.2 by taking $N_s = 80$, $M_t = 160$, $\gamma = 0.5$.

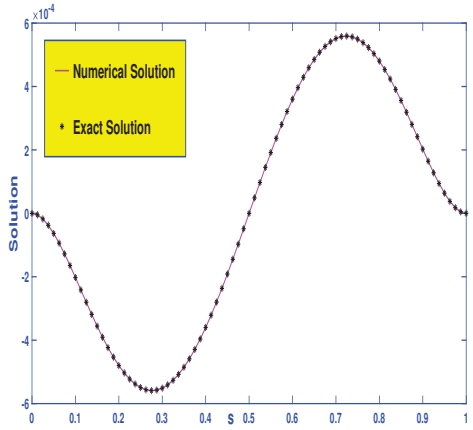

a Numerical and exact solutions at $t = 0.50$

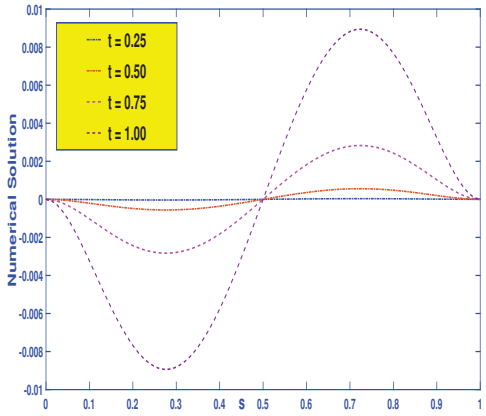

b Numerical solutions at different time levels

Figure 2: Plots of exact and numerical solutions at different time levels for Example 3.5.2 by taking $N_s = M_t = 80, \gamma = 0.75$.

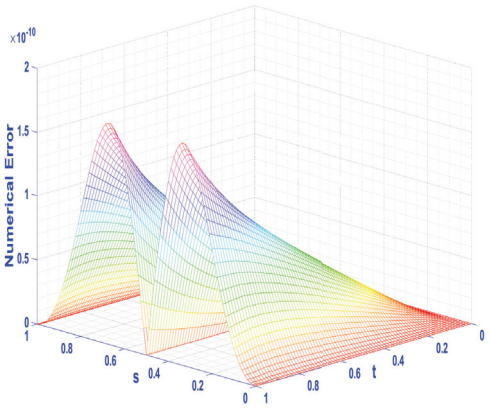

a Example 3.5.2

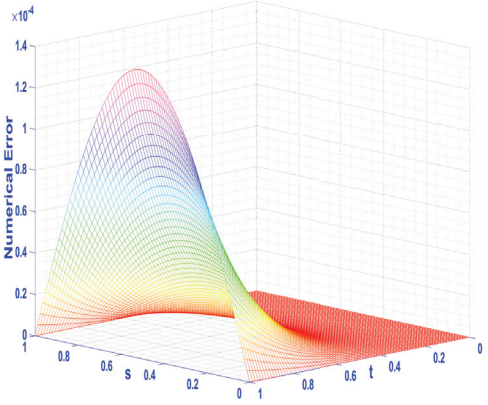

b Example 3.5.3

Figure 3: Error plots of numerical solution by taking $N_s = M_t = 80, \gamma = 0.5$.

Table 3.7: Errors, orders of convergence, and CPU time (in sec.) for Example 3.5.3 for different time fractional orders γ

	Norms	N_s=10 M_t=20	N_s=20 M_t=40	N_s=40 M_t=80	N_s=80 M_t=160	N_s=160 M_t=320
$\gamma = 0.3$	L_∞	$8.6359e-03$	$2.1680e-03$	$5.4275e-04$	$1.3576e-04$	$3.3946e-05$
		1.9940	1.9980	1.9992	1.9997	-
	L_2	$6.1079e-03$	$1.5334e-03$	$3.8388e-04$	$9.6022e-05$	$2.4010e-05$
		1.9939	1.9980	1.9992	1.9997	-
CPU Time		0.0568	0.0838	0.3207	2.1108	16.0575
$\gamma = 0.5$	L_∞	$8.5769e-03$	$2.1537e-03$	$5.3932e-04$	$1.3493e-04$	$3.3743e-05$
		1.9936	1.9976	1.9989	1.9996	-
	L_2	$6.0661e-03$	$1.5233e-03$	$3.8146e-04$	$9.5436e-05$	$2.3867e-05$
		1.9936	1.9976	1.9989	1.9996	-
CPU Time		0.0619	0.0846	0.3159	2.0585	15.8550
$\gamma = 0.8$	L_∞	$8.4195e-03$	$2.1149e-03$	$5.2990e-04$	$1.3266e-04$	$3.3195e-05$
		1.9931	1.9968	1.9980	1.9987	-
	L_2	$5.9548e-03$	$1.4959e-03$	$3.7480e-04$	$9.3827e-05$	$2.3479e-05$
		1.9930	1.9968	1.9980	1.9987	-
CPU Time		0.1197	0.0898	0.3266	2.1134	16.0571

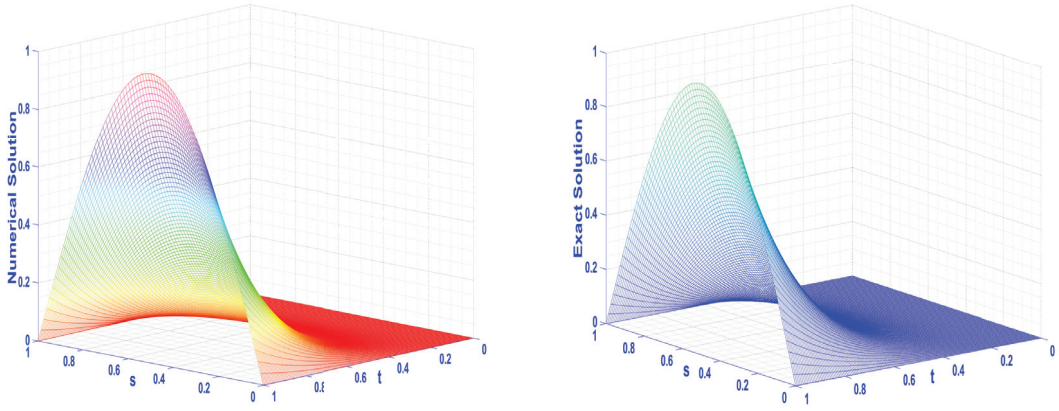

a Numerical solution

b Exact solution

Figure 4: Surface plots of exact and numerical solutions for Example 3.5.3 by taking $N_s = 80$, $M_t = 160$, $\gamma = 0.5$.

Table 3.8: Comparison of Errors, orders of convergence, and CPU time (in sec.) for Example 3.5.3 (γ approaches to 1) with the problem (3.5.1)

	N_s=10 M_t=20	N_s=20 M_t=40	N_s=40 M_t=80	N_s=80 M_t=160	N_s=160 M_t=320
$\gamma = 0.9$	$8.3315e-03$	$2.0920e-03$	$5.2406e-04$	$1.3118e-04$	$3.2827e-05$
	1.9937	1.9971	1.9982	1.9986	-
CPU Time	0.0763	0.1074	0.3434	2.1038	16.5623
$\gamma = 0.95$	$8.2765e-03$	$2.0771e-03$	$5.2013e-04$	$1.3016e-04$	$3.2562e-05$
	1.9945	1.9976	1.9986	1.9990	-
CPU Time	0.0585	0.0862	0.3316	2.1320	16.035357
$\gamma = 0.99$	$8.2258e-03$	$2.0631e-03$	$5.1633e-04$	$1.2914e-04$	$3.2292e-05$
	1.9953	1.9984	1.9994	1.9997	-
CPU Time	0.0813	0.1090	0.3498	2.1222	16.1849
$\gamma = 0.999$	$8.2135e-03$	$2.0596e-03$	$5.1537e-04$	$1.2888e-04$	$3.2222e-05$
	1.9956	1.9987	1.9996	1.9999	-
CPU Time	0.0785	0.1062	0.3426	2.1352	16.1141
$\gamma = 1$	$8.3218e-03$	$2.0861e-03$	$5.2188e-04$	$1.3049e-04$	$3.2622e-05$
	1.9961	1.9990	1.9998	2.0000	-
CPU Time	0.1026	0.0688	0.0786	0.1435	0.7781

Table 3.9: Errors and orders of convergence in spatial and time directions for Example 3.5.3 in L_∞ norm

	Spatial direction (taking $M_t = 1024$)			Time direction (taking $N_s = 1024$)		
γ	N_s	Error	Rate	M_t	Error	Rate
0.5	4	$5.2053e-02$	1.9746	4	$7.5669e-02$	2.1896
	8	$1.3244e-02$	1.9937	8	$1.6587e-02$	2.0581
	16	$3.3255e-03$	1.9984	16	$3.9832e-03$	2.0915
	32	$8.3230e-04$	-	32	$9.3463e-04$	-
0.8	4	$5.1507e-02$	1.9753	4	$7.4675e-02$	2.0384
	8	$1.3099e-02$	1.9939	8	$1.8179e-02$	2.0836
	16	$3.2887e-03$	1.9984	16	$4.2890e-03$	2.1010
	32	$8.2308e-04$	-	32	$9.9976e-04$	-

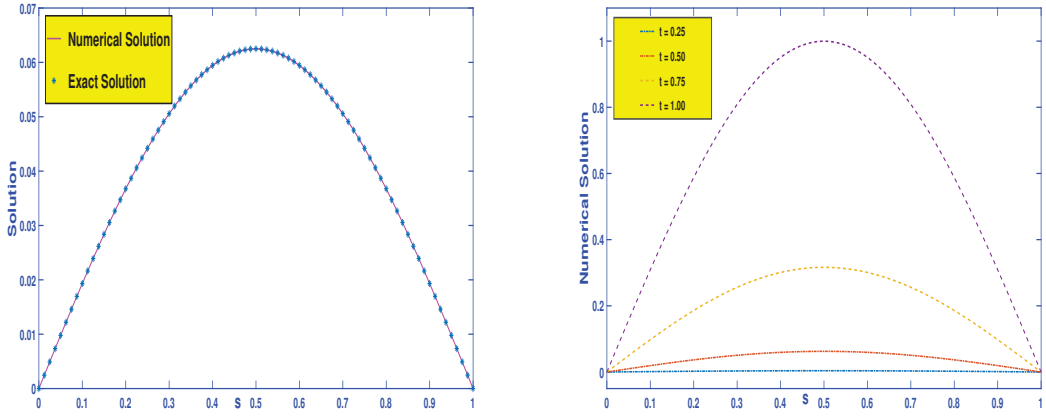

a Numerical and exact solutions at $t = 0.50$

b Numerical solutions at different time levels

Figure 5: Plots of exact and numerical solutions for Example 3.5.3 by taking $N_s = M_t = 80$, $\gamma = 0.75$.

Table 3.10: Spatial errors, orders of convergence, and CPU time (in sec.) in L_∞ norm for Example 3.5.4 by taking $M_t = 64$ and different values of γ

	$N_s = 8$	$N_s = 16$	$N_s = 32$	$N_s = 64$	$N_s = 128$
$\gamma = 0.6$	$2.5356e-05$	$1.6903e-06$	$1.0897e-07$	$6.8933e-09$	$4.2262e-10$
	3.9070	3.9553	3.9826	4.0278	-
CPU Time	0.1997	0.3069	0.5336	0.9916	2.0981
$\gamma = 0.8$	$2.5394e-05$	$1.6928e-06$	$1.0903e-07$	$6.8430e-09$	$3.9223e-10$
	3.9070	3.9566	3.9940	4.1249	-
CPU Time	0.2065	0.3149	0.5380	1.0114	2.0787
$\gamma = 0.95$	$2.5427e-05$	$1.6948e-06$	$1.0895e-07$	$6.7295e-09$	$3.3087e-10$
	3.9072	3.9594	4.0170	4.3462	-
CPU Time	0.2081	0.3073	0.5256	0.9780	2.0861

Table 3.11: Comparison of GRE at different time levels for Example 3.5.5 taking $M_t = 100$ and different fractional orders γ

γ	Time	$N_s = 200$	$N_s = 300$	$N_s = 400$
0.5	1	$4.5169e-06$	$1.9995e-06$	$1.1224e-06$
	2	$3.7078e-06$	$1.6410e-06$	$9.2107e-07$
	3	$3.7047e-06$	$1.6395e-06$	$9.2035e-07$
	4	$4.2209e-06$	$1.8690e-06$	$1.0493e-06$
0.8	1	$2.1890e-05$	$9.7642e-06$	$5.4943e-06$
	2	$6.3637e-06$	$2.8375e-06$	$1.5968e-06$
	3	$3.0069e-06$	$1.3394e-06$	$7.5383e-07$
	4	$2.2302e-06$	$9.9078e-07$	$5.5788e-07$
0.99	1	$1.4469e-04$	$6.4436e-05$	$3.6411e-05$
	2	$1.9996e-04$	$8.9104e-05$	$5.0228e-05$
	3	$2.4510e-04$	$1.0944e-04$	$6.1629e-05$
	4	$2.9015e-04$	$1.2948e-04$	$7.2939e-05$
0.999	1	$1.5276e-04$	$6.8299e-05$	$3.8451e-05$
	2	$2.2107e-04$	$9.9406e-05$	$5.5847e-05$
	3	$2.8232e-04$	$1.2626e-04$	$7.1144e-05$
	4	$3.4440e-04$	$1.5373e-04$	$8.6633e-05$
1 (Problem (3.5.1))	1	$1.6279e-04$	$7.2669e-05$	$4.0953e-05$
	2	$2.3549e-04$	$1.0493e-04$	$5.9247e-05$
	3	$3.0055e-04$	$1.3399e-04$	$7.5558e-05$
	4	$3.6829e-04$	$1.6391e-04$	$9.2450e-05$

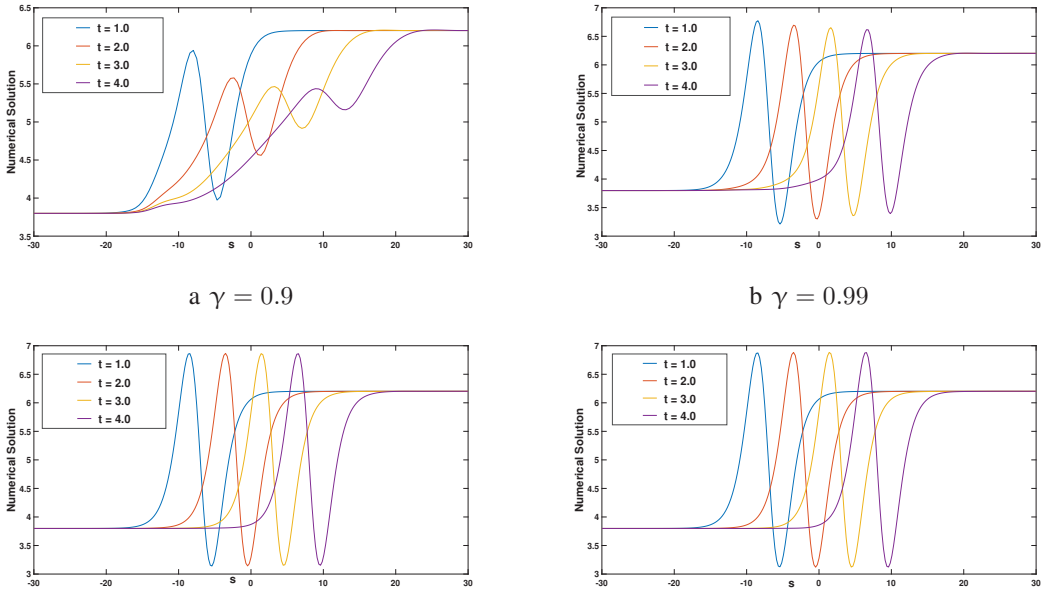

a $\gamma = 0.9$ b $\gamma = 0.99$

c $\gamma = 0.999$ d $\gamma = 1$ (Problem (3.5.1))

Figure 6: Layer movements in time for Example 3.5.5.

3.6 Conclusions

In the present work, we have proposed a highly accurate numerical approximation for Caputo-type time-fractional fourth-order nonlinear KS equation with several experimental observations in favor of our theory. The current $L1-2$ approximation in the temporal direction provides a better order of accuracy in time with the same computational cost as for the $L1$ approximation in the time direction. The space derivatives are approximated based on the quintic $\mathfrak{B}$-spline polynomials to maintain quadratic convergence in space. The present approach can also be used for linear problems as well as for Burgers equations, on which it leads to fourth-order accuracy in space. We have provided a concrete convergence analysis favoring our theory and experimental evidence.

Chapter 4

Collocation-based numerical simulation of fractional order Allen-Cahn equation

4.1 Introduction

This chapter looks for a reliable numerical technique to solve the Allen-Cahn equation using the Caputo time-fractional derivative. The fractional derivative semi-discretization approach using finite differences of the second order is shown first. The cubic B-spline collocation method is used to get a full discretization. We prove the conditional stability and convergence of the suggested approach. The technique's effectiveness is demonstrated with numerical examples using two test problems. Numerical analysis confirms the approach's efficiency and the method's continued correctness.

4.2 Literature survey

In demand to represent nonlinear physical marvels, acquiring exact solutions for nonlinear FPDEs is one of the numerous significant factors. Newly, several techniques have been involved in getting precise solutions of nonlinear FPDEs in the literature, such as the fractional

R. Choudhary, D. Kumar, Collocation-based numerical simulation of fractional order Allen–Cahn equation, J. Math. Chem. , (2023), https://doi.org/10.1007/s10910-023-01525-0.

sub-equation, the exp-function, the G'/G-expansion, first integral and Lie symmetry approach [154–159].

The phase-field models drew significant concentration in the domain of phase transitions [160]. The Allen-Cahn and Cahn-Hilliard models are the essential phase-field PDEs models. The Allen-Cahn equation (ACE) occurs in the motion of phase boundaries in crystalline solids[161], a mixture of two incompressible fluids[162], nucleation of solids[163], and vesicle membranes[164]. It also appears in numerous scientific applications such as mathematical biology, quantum mechanics, and plasma physics. In the literature, many researchers concentrated on analytical solutions of the time-fractional ACE. Esen *et al.* [165] presented the homotopy analysis method (HAM) to obtain the approximate analytical solutions of time-fractional damped Burger and ACE. Tariq and Akram [160] developed new exact analytical solutions for time-fractional ACE and time-fractional Phi-4 equation using the Tanh approach. Tascan and Bekir [166] employed the first integral method to assemble the ACE traveling wave solutions. In [167] Wazwaz offered the tanh-coth approach to emanate solitons and kink solutions for some of the famous nonlinear parabolic PDEs such as Newell-Whitehead equation, ACE, Fisher's equation, Fitz-Hugh-Nagumo equation, and the Burgers-Fisher equation. Jafari *et al.* [168] investigated the identical solution of space-time fractional order ACE by employing a fractional subdiffusion approach. In [169], Zhai *et al.* used a robust explicit operator splitting spectral method to decode the nonlocal fractional order ACE. Akagi *et al.* [170] examined the presence and essence of weak explanations for the fractional order ACE, Cahn-Hilliard equation, and absorbent medium equations. Liu *et al.* [171] studied a space-time fractional ACE and employed a fast Galerkin finite element technique to solve this equation. Huang and Stynes [172] presented optimal H^1 spatial convergence of a fully discrete finite element method for the time-fractional ACE. Ji *et al.* [173] suggested time-stepping methods for the time-fractional ACE with Caputo's derivative. Liu *et al.* [174] presented two accurate and efficient linear techniques for the time-fractional Cahn-Hilliard and ACE with known nonlinear bulk potential. Some numerical methods have also been invented for this problem, such as Hou *et al.* [175] found the numerical solution using the finite difference in temporal direction and the Crank-Nicolson method in spatial direction for space-fractional ACEs. Sakar *et al.* [176] suggested a numerical method established on the iterative reproducing kernel

method (IRKM) to examine the approximate solution of time-fractional ACE. With the finite-difference technique and the Fourier spectral method, Liu *et al.* [177] offered a numerical approach to decode time-fractional ACEs in one and two space dimensions. In 2018, Inc *et al.* [178] analyzed Lie symmetries and reduction for explicit resolutions, convergence investigation to the time-fractional ACE and time-fractional Klein-Gordon (KG) equations, and the fractional order derivative is taken Riemann-Liouville. Khalid *et al.* [179] proposed a collocation technique established on redefined cubic B-spline processes and finite difference method to examine the approximate explanation of time-fractional ACE.

In this work, we examine the following time-fractional ACE:

$$ {}_0^C D_t^{\gamma} v(y,t) - \frac{\partial^2 v(y,t)}{\partial y^2} + (v(y,t))^3 - v(y,t) = g(y,t),\ y \in (0,1),\ t \in (0,\mathcal{T}], \quad (4.2.1a) $$

subject to the boundary conditions

$$ v(0,t) = \Phi_l(t),\ v(1,t) = \Phi_r(t),\ t \in [0,\mathcal{T}], \quad (4.2.1b) $$

and the initial condition

$$ v(y,0) = \Phi_0(y),\ y \in [0,1], \quad (4.2.1c) $$

where $\Phi_l(t)$, $\Phi_r(t)$, and $\Phi_0(y)$ are presumed continuous functions with continuous first-order derivative. For compatible conditions, we assume that $\Phi_l(0) = \Phi_0(0)$ and $\Phi_r(0) = \Phi_0(1)$. The derivative of fractional order $\gamma \in (0,1)$ is accepted in the Caputo sence.

In this chapter, first, we employ the quasilinearization method to linearize the equation (4.2.1a). Then, we operate a cubic B-spline (CBS) function on the linearized equation for the numerical solution of time-fractional ACE. The Crank-Nicolson formula is used for discretizing the Caputo time-fractional derivative, whereas CBS functions are used to discretize spatial derivatives. Some nonlinear partial differential equations have also been solved using the CBS function. For example, Jiwari [180] employed modified CBS differential quadrature techniques in spatial direction for decoding hyperbolic partial differential equations. Mittal and Dahiya [181] operated the CBS differential quadrature approach for the numerical solution of the three-dimensional telegraphic equation. Mittal and Jain [182] employed the

cubic B-splines collocation technique for cracking nonlinear parabolic partial differential equations. Shukla and Tamsir [183] operated an extended, modified CBS algorithm for nonlinear Fisher's reaction-diffusion equation. Ramos *et al.* [184] used a CBS method to solve nonlinear partial differential equations. Jiwari *et al.* [185] developed a numerical technique established on trigonometric CBS functions for the numerical solution of nonlinear parabolic problems.

Following is how we structured this chapter: The Crank-Nicolson approach is used in Section 2 to semi-discretize the problem (4.2.1). To discretize spatial derivatives, CBS is also adopted in this province. After enforcing the wholly discretized method, we are given a system with $\mathcal{N}_y + 1$ unknowns at a specific time level. The stability analysis described in Section 3 ensures conditional stability. In Section 4, the suggested method is subjected to a thorough convergence study. By using a tabular examination of the suggested numerical examples, Section 5 validates the theoretical estimations. The study's future dimensions are discussed in Section 6, where we offer some concluding reflections.

4.3 Methodology

4.3.1 Temporal discretization

For a positive integer $\mathcal{M}_t$, let $\Upsilon^{\mathcal{M}_t}$ be the partition of the interval $[0, \mathcal{T}]$ described by $\Upsilon^{\mathcal{M}_t} = \{t_m | t_m = mk,\ 0 \leq m \leq \mathcal{M}_t\}$ where $k = \frac{\mathcal{T}}{\mathcal{M}_t}$ is temporal step size. The semi-discretized form of equation (4.2.1) at the $\left(m + \frac{1}{2}\right)$-th time-level is given by

$$\frac{\partial^\gamma \widetilde{v}(y, t_{m+\frac{1}{2}})}{\partial t^\gamma} - \frac{\partial^2 \widetilde{v}(y, t_{m+\frac{1}{2}})}{\partial y^2} + (\widetilde{v}(y, t_{m+\frac{1}{2}}))^3 - \widetilde{v}(y, t_{m+\frac{1}{2}}) = g(y, t_{m+\frac{1}{2}}),$$
$$m = 0, 1, 2, \ldots \mathcal{M}_t - 1, \tag{4.3.1a}$$

subject to the boundary conditions

$$\widetilde{v}(0, t_{m+1}) = \Phi_l(t_{m+1}),\ \widetilde{v}(1, t_{m+1}) = \Phi_r(t_{m+1}),\ m = 0, 1, \ldots \mathcal{M}_t - 1, \tag{4.3.1b}$$

and the initial condition

$$\widetilde{v}(y, t_0) = \Phi_0(y),\ y \in [0, 1]. \tag{4.3.1c}$$

To approximate $\frac{\partial^\gamma \widetilde{v}(y,t)}{\partial t^\gamma}$ at $(y, t_{m+\frac{1}{2}})$, if $\widetilde{v} \in C^4([0,1],[0,\mathcal{T}])$ then we make use of the following formula

$$\begin{aligned}\frac{\partial^\gamma \widetilde{v}(y,t_{m+1/2})}{\partial t^\gamma} &= \frac{1}{\Gamma(2-\gamma)}\frac{1}{k^\gamma}(\widetilde{v}^{m+1}-\widetilde{v}^m)\frac{1}{2^{1-\gamma}} \\ &+ \frac{1}{\Gamma(2-\gamma)}\frac{1}{k^\gamma}\sum_{j=1}^{m}\left[\widetilde{v}^j-\widetilde{v}^{j-1}\right]\left[\left(m-j+\frac{3}{2}\right)^{1-\gamma}-\left(j-m+\frac{1}{2}\right)^{1-\gamma}\right] \\ &+ \frac{1}{\Gamma(2-\gamma)}\sum_{j=1}^{m}\left[\left(m-j+\frac{3}{2}\right)^{1-\gamma}-\left(m-j+\frac{1}{2}\right)^{1-\gamma}\right]O(k^{3-\gamma}) \\ &+ \frac{1}{\Gamma(2-\gamma)}\frac{1}{2^{1-\gamma}}O(k^{3-\gamma}). \end{aligned} \tag{4.3.2}$$

Let $\rho = \frac{1}{\Gamma(2-\gamma)}\frac{1}{k^\gamma}$, and $\varpi_\imath = \rho((\imath+1/2)^{1-\gamma}-(\imath-1/2)^{1-\gamma})$, so that $\sum_{\imath=1}^{l_1}\varpi_\imath = \rho((l_1+\frac{1}{2})^{1-\gamma}-\frac{1}{2}^{1-\gamma})$. On substituting ρ and $\varpi_\imath$ into (4.3.2), we get

$$\frac{\partial^\gamma \widetilde{v}(y,t_{m+1/2})}{\partial t^\gamma} = \left[\varpi_1\widetilde{v}^m+\sum_{j=1}^{m-1}(\varpi_{m-j+1}-\varpi_{m-j})\widetilde{v}^j-\varpi_m\widetilde{v}^0+\rho\frac{(\widetilde{v}^{m+1}-\widetilde{v}^m)}{2^{1-\gamma}}\right]+R_1+R_2,$$

where

$$R_1+R_2 = \frac{1}{\rho\Gamma(2-\gamma)}\sum_{j=1}^{m}\varpi_{m-j+1}O(k^{3-\gamma})+\frac{1}{\Gamma(2-\gamma)}\frac{1}{2^{1-\gamma}}O(k^{3-\gamma}).$$

Let $\imath = m-j+1$, then

$$\begin{aligned} R_1+R_2 &= \frac{1}{\Gamma(2-\gamma)}\left[\frac{1}{\rho}\sum_{\imath=1}^{m}\varpi_\imath O(k^{3-\gamma})+\frac{1}{2^{1-\gamma}}O(k^{3-\gamma})\right] \\ &= \frac{1}{\Gamma(2-\gamma)}\left[\left(\left(m+\frac{1}{2}\right)^{1-\gamma}-\left(\frac{1}{2}\right)^{1-\gamma}\right)+\frac{1}{2^{1-\gamma}}\right]O(k^{3-\gamma}) \\ &= \frac{1}{\Gamma(2-\gamma)}\left(m+\frac{1}{2}\right)^{1-\gamma}O(k^{3-\gamma}) \\ &= \frac{1}{\Gamma(2-\gamma)}\left(\frac{t_{m+1/2}}{k}\right)^{1-\gamma}O(k^{3-\gamma}) \\ &\leq Ck^2. \end{aligned}$$

Thus, we get the following approximation of $\frac{\partial^\gamma \widetilde{v}(y,t)}{\partial t^\gamma}$ at $(y, t_{m+\frac{1}{2}})$

$$\frac{\partial^\gamma \widetilde{v}(y,t_{m+1/2})}{\partial t^\gamma} = \varpi_1 \widetilde{v}^m + \sum_{j=1}^{m-1}(\varpi_{m-j+1} - \varpi_{m-j})\widetilde{v}^j - \varpi_m \widetilde{v}^0 + \rho\frac{(\widetilde{v}^{m+1} - \widetilde{v}^m)}{2^{1-\gamma}} + O(k^2). \tag{4.3.3}$$

The resulting semi-discretized version of equation (4.3.1a) is obtained by using the approximation (4.3.3) in (4.3.1a) at the $(m + \frac{1}{2})$-th time level.

$$\left(\frac{\rho}{2^{1-\gamma}} - \frac{1}{2}\right)\widetilde{v}^{m+1} - \frac{1}{2}\widetilde{v}_{yy}^{m+1} + (\widetilde{v}^{m+\frac{1}{2}})^3 = \left(\frac{\rho}{2^{1-\gamma}} + \frac{1}{2}\right)\widetilde{v}^m + \frac{1}{2}\widetilde{v}_{yy}^m + g^{m+\frac{1}{2}} - \left[\varpi_1 \widetilde{v}^m + \sum_{j=1}^{m-1}(\varpi_{m-j+1} - \varpi_{m-j})\widetilde{v}^j - \varpi_m \widetilde{v}^0\right]. \tag{4.3.4}$$

The quasilinearization technique used in (4.3.4) for nonlinear term $(\widetilde{v}^{m+\frac{1}{2}})^3$ is as follows

$$((\widetilde{v}^{m+\frac{1}{2}})^i)^3 = \frac{1}{2}[-((\widetilde{v}^m)^{i-1})^3 + ((\widetilde{v}^m)^{i-1})^2(\widetilde{v}^{m+1})^i], \quad i = 1, 2, \ldots,$$

where i stands for the number of iterations and let $(\widetilde{v})^0$ is the initial guess that satisfies the initial and boundary conditions of the problem (4.2.1). We write the equation (4.3.4) at the i^{th} iteration as

$$\left(\frac{\rho}{2^{1-\gamma}} - \frac{1}{2}\right)(\widetilde{v}^{m+1})^i - \frac{1}{2}(\widetilde{v}_{yy}^{m+1})^i + \frac{1}{2}[-((\widetilde{v}^m)^{i-1})^3 + ((\widetilde{v}^m)^{i-1})^2(\widetilde{v}^{m+1})^i] = \left(\frac{\rho}{2^{1-\gamma}} + \frac{1}{2}\right)(\widetilde{v}^m)^i + \frac{1}{2}(\widetilde{v}_{yy}^m)^i + g^{m+\frac{1}{2}} - \left[\varpi_1(\widetilde{v}^m)^i + \sum_{j=1}^{m-1}(\varpi_{m-j+1} - \varpi_{m-j})(\widetilde{v}^j)^i - \varpi_m(\widetilde{v}^0)^i\right]. \tag{4.3.5}$$

Now, we replace $(\widetilde{v}^m)^i$ by $\widetilde{v}^m$ and $(\widetilde{v}^m)^{i-1}$ by V^m

$$\left(\frac{\rho}{2^{1-\gamma}} - \frac{1}{2} + \frac{3}{2}(V^m)^2\right)\widetilde{v}^{m+1} - \frac{1}{2}\widetilde{v}_{yy}^{m+1} = \left(\frac{\rho}{2^{1-\gamma}} + \frac{1}{2}\right)\widetilde{v}^m + \frac{1}{2}\widetilde{v}_{yy}^m + \frac{1}{2}(V^m)^3 + g^{m+\frac{1}{2}} - \left[\varpi_1 \widetilde{v}^m + \sum_{j=1}^{m-1}(\varpi_{m-j+1} - \varpi_{m-j})\widetilde{v}^j - \varpi_m \widetilde{v}^0\right], \tag{4.3.6}$$

$$\widetilde{v}(0,t_{m+1}) = \Phi_l(t_{m+1}),\ \widetilde{v}(1,t_{m+1}) = \Phi_r(t_{m+1}),\ m = 0,1,\ldots,\mathcal{M}_t - 1. \tag{4.3.7}$$

4.3.2 The spatial discretization: Cubic B-spline functions

For a positive integer $\mathcal{N}_y$, let $\Upsilon^{\mathcal{N}_y}$ be the partition of $[0,1]$ described by $\Upsilon^{\mathcal{N}_y} = \{y_n | y_n = nh,\ 0 \le n \le \mathcal{N}_y\}$ where $h = \frac{1}{\mathcal{N}_y}$ is the spatial step size. Let $\mathcal{B}_n(y)$ are the cubic B-spline functions defined on $[0,1]$, for forming cubic B-spline functions. We introduce four extra nodal points y_{-1}, y_{-2} on the left side of the partition $\Upsilon^{\mathcal{N}_y}$ and $y_{\mathcal{N}_y+1}$, $y_{\mathcal{N}_y+2}$ on the right side of the partition $\Upsilon^{\mathcal{N}_y}$. The functions $\mathcal{B}_n$, $n = -1,\ldots,\mathcal{N}_y+1$ are describe as follows:

$$\mathcal{B}_n(y) = \frac{1}{h^3}\begin{cases} (y - y_{n-2})^3, & y_{n-2} \le y \le y_{n-1}, \\ h^3 + 3h^2(y - y_{n-1}) + 3h(y - y_{n-1})^2 - 3(y - y_{n-1})^3, & y_{n-1} \le y \le y_n, \\ h^3 + 3h^2(y_{n+1} - y) + 3h(y_{n+1} - y)^2 - 3(y_{n+1} - y)^3, & y_n \le y \le y_{n+1}, \\ (y_{n+2} - y)^3, & y_{n+1} \le y \le y_{n+2}, \\ 0, & \text{otherwise.} \end{cases} \tag{4.3.8}$$

The definition shows that each B-spline is always zero and non-zero at three nodal points (Table 4.1). The following table displays the numerical value of each $\mathcal{B}_n(y)$ and its initial two derivatives.

Table 4.1: Values of $\mathcal{B}_n$, and its derivatives at nodal locations

	$j = n-1$	$j = n$	$j = n+1$	Otherwise
$\mathcal{B}_n(y_j)$	1	4	1	0
$\mathcal{B}'_n(y_j)$	$3/h$	0	$-3/h$	0
$\mathcal{B}''_n(y_j)$	$6/h^2$	$-12/h^2$	$6/h^2$	0

The set $\{\mathcal{B}_{-1}, \mathcal{B}_0, \ldots, \mathcal{B}_{\mathcal{N}_y}, \mathcal{B}_{\mathcal{N}_y+1}\}$ spans a family of polynomials ($B_3(\pi)$) of degree less than or equal to three on each of the subintervals $[y_n, y_{n+1}]$ (see [186]). We seek an approximation $\hat{v}(y,t_m) \in B_3(\pi)$ to the solution $\widetilde{v}(y,t_m)$, which use these cubic B-spline functions as follows

$$\hat{v}(y,t_m) = \sum_{n=-1}^{\mathcal{N}_y+1} \delta_n^m \mathcal{B}_n(y), \tag{4.3.9}$$

where δ_n^m's are the unknown time-dependent scalars. Using cubic spline functions for the approximated function $\hat{v}(y_n, t_m) = \hat{v}(n, m)$ in equation (4.3.9) with its first two derivatives, we get

$$\begin{cases} \hat{v}(n,m) = \delta_{n-1}^m + 4\delta_n^m + \delta_{n+1}^m, \\ h\hat{v}_y(n,m) = -3\delta_{n-1}^m + 3\delta_{n+1}^m, \\ h^2\hat{v}_{yy}(n,m) = 6\delta_{n-1}^m - 12\delta_n^m + 6\delta_{n+1}^m. \end{cases} \tag{4.3.10}$$

Using (4.3.10) in (4.3.6), we obtain following system of linear equations

$$P_n^m\delta_{n-1}^{m+1} + Q_n^m\delta_n^{m+1} + P_n^m\delta_{n+1}^{m+1} = \wp_n^m, \quad n = 0, 1, \ldots, \mathcal{N}_y, \quad m = 0, 1, \ldots, \mathcal{M}_t - 1, \tag{4.3.11a}$$

with

$$\delta_{-1}^{m+1} + 4\delta_0^{m+1} + \delta_1^{m+1} = \Phi_l(t_{m+1}), \quad m = 0, 1, \ldots, \mathcal{M}_t - 1, \tag{4.3.11b}$$

$$\delta_{\mathcal{N}_y-1}^{m+1} + 4\delta_{\mathcal{N}_y}^{m+1} + \delta_{\mathcal{N}_y+1}^{m+1} = \Phi_r(t_{m+1}), \quad m = 0, 1, \ldots, \mathcal{M}_t - 1, \tag{4.3.11c}$$

where

$$P_n^m = \frac{\rho}{2^{1-\gamma}} - \frac{1}{2} + \frac{3}{2}(V(n,m))^2 - \frac{3}{h^2},$$

$$Q_n^m = 4\left(\frac{\rho}{2^{1-\gamma}} - \frac{1}{2} + \frac{3}{2}(V(n,m))^2\right) + \frac{6}{h^2},$$

$$\wp_n^m = \left(\frac{\rho}{2^{1-\gamma}} + \frac{1}{2}\right)\hat{v}(n,m) + \frac{1}{2}\hat{v}_{yy}(n,m) + \frac{1}{2}(V(n,m))^3 + g_n^{m+\frac{1}{2}} - \left[\varpi_1\hat{v}(n,m) + \sum_{j=1}^{m-1}(\varpi_{m-j+1} - \varpi_{m-j})\hat{v}(n,j) - \varpi_m\hat{v}(n,0)\right].$$

Now on eliminating δ_{-1}^{m+1} and $\delta_{\mathcal{N}_y+1}^{m+1}$ from (4.3.11a)–(4.3.11c), we obtain following system of linear equations

$$\mathbf{A}\mathbf{C}^{m+1} = \mathbf{B}^m,$$

where

$$\mathbf{A} = \begin{bmatrix} Q_0^m - 4P_0^m & 0 & 0 & & \\ P_1^m & Q_1^m & P_1^m & & \\ \ddots & \ddots & \ddots & & \\ & \ddots & \ddots & \ddots & \\ & \ddots & \ddots & \ddots & \\ & & P_{\mathcal{N}_y-1}^m & Q_{\mathcal{N}_y-1}^m & P_{\mathcal{N}_y-1}^m \\ & & 0 & 0 & Q_{\mathcal{N}_y}^m - 4P_{\mathcal{N}_y}^m \end{bmatrix},$$

is a matrix of size $(\mathcal{N}_y + 1) \times (\mathcal{N}_y + 1)$ and

$$\mathbf{C}^{m+1} = \begin{bmatrix} \delta_0^{m+1} \\ \delta_1^{m+1} \\ \vdots \\ \delta_n^{m+1} \\ \vdots \\ \delta_{\mathcal{N}_y-1}^{m+1} \\ \delta_{\mathcal{N}_y}^{m+1} \end{bmatrix}_{(\mathcal{N}_y+1)\times 1}, \quad \mathbf{B}^m = \begin{bmatrix} \wp_0^m - \Phi_l(t_{m+1})P_0^m \\ \wp_1^m \\ \vdots \\ \wp_n^m \\ \vdots \\ \wp_{\mathcal{N}_y-1}^m \\ \wp_{\mathcal{N}_y}^m - \Phi_r(t_{m+1})P_{\mathcal{N}_y}^m \end{bmatrix}_{(\mathcal{N}_y+1)\times 1}.$$

4.4 The stability analysis

The Von-Neumann procedure-based stability study of the numerical approach (4.3.11) is presented in this section. We describe the discretized approach in the following structure to examine the stability.

$$\begin{aligned} P_n^m \delta_{n-1}^{m+1} + Q_n^m \delta_n^{m+1} + P_n^m \delta_{n+1}^{m+1} &= R_n^m \delta_{n-1}^m + S_n^m \delta_n^m + R_n^m \delta_{n+1}^m + \frac{1}{2}(V_n^m)^3 + g_n^{m+\frac{1}{2}} \\ &- \varpi_1 \left(\delta_{n-1}^m + 4\delta_n^m + \delta_{n+1}^m\right) - \sum_{j=1}^{m-1} (\varpi_{m-j+1} - \varpi_{m-j}) \left(\delta_{n-1}^j + 4\delta_n^j + \delta_{n+1}^j\right) \\ &+ \varpi_m \left(\delta_{n-1}^0 + 4\delta_n^0 + \delta_{n+1}^0\right), \; n = 0, 1, \ldots, \mathcal{N}_y, \; m = 0, 1, \ldots, \mathcal{M}_t - 1, \end{aligned} \tag{4.4.1}$$

where

$$R_n^m = \frac{\rho}{2^{1-\gamma}} + \frac{1}{2} + \frac{3}{h^2},$$

$$S_n^m = 4\left(\frac{\rho}{2^{1-\gamma}} + \frac{1}{2}\right) - \frac{6}{h^2}.$$

The round-off error is given by

$$\begin{aligned} P_n^m \Xi_{n-1}^{m+1} + Q_n^m \Xi_n^{m+1} + P_n^m \Xi_{n+1}^{m+1} = R_n^m \Xi_{n-1}^m + S_n^m \Xi_n^m + R_n^m \Xi_{n+1}^m - \varpi_1 \left(\Xi_{n-1}^m + 4\Xi_n^m + \Xi_{n+1}^m\right) \\ - \sum_{j=1}^{m-1} (\varpi_{m-j+1} - \varpi_{m-j}) \left(\Xi_{n-1}^j + 4\Xi_n^j + \Xi_{n+1}^j\right) \\ + \varpi_m \left(\Xi_{n-1}^0 + 4\Xi_n^0 + \Xi_{n+1}^0\right), \ n = 0, 1, \ldots, \mathcal{N}_y, \ m = 0, 1, \ldots, \mathcal{M}_t - 1, \end{aligned} \quad (4.4.2)$$

along with the constraints

$$\Xi_0^m = \Xi_{N_y}^m = 0, \ m = 0, 1, \ldots, \mathcal{M}_t.$$

Using the Fourier series expansion, the grid functions

$$\Xi^m(y) = \begin{cases} \Xi_n^m, & y_n - \frac{h}{2} < y < y_n + \frac{h}{2}, \ n = 1, 2, \ldots, \mathcal{N}_y - 1, \\ 0, & 0 \le y \le \frac{h}{2} \quad \text{or} \quad 1 - \frac{h}{2} \le y \le 1, \end{cases}$$

can be deduced into

$$\Xi^m(y) = \sum_{j=-\infty}^{\infty} \eta^m(j) e^{i(2j\pi y)}, \ m = 0, 1, \ldots, \mathcal{M}_t,$$

where

$$\eta^m(j) = \int_0^1 \Xi^m(y) e^{-i(2j\pi y)} dy.$$

Parseval's identity in the L_2-norm deduces

$$||\Xi^m||_2^2 = \sum_{n=1}^{\mathcal{N}_y - 1} h|\Xi_n^m|^2 = \int_0^1 |\Xi^m(y)|^2 dy = \sum_{j=-\infty}^{\infty} |\eta^m(j)|^2.$$

From the preceding analysis, we can assume that

$$\Xi_n^m = \eta^m e^{i\theta nh},$$

where $i = \sqrt{-1}$ and θ is a wave number. Then (4.4.2) gives

$$\eta^{m+1} = \left(\frac{(U_1)_n^m - \varpi_1 U}{(U_2)_n^m} \right) \eta^m - \frac{U}{(U_2)_n^m} \left(\sum_{q=1}^{m-1} (\varpi_{m-q+1} - \varpi_{m-q}) \eta^q + \varpi_m \eta^0 \right), \quad (4.4.3)$$

where

$$\begin{aligned} (U_1)_n^m &= 2R_n^m \cos(\theta h) + S_n^m, \\ (U_2)_n^m &= 2P_n^m \cos(\theta h) + Q_n^m, \\ U &= 2\cos(\theta h) + 4. \end{aligned}$$

For stability of numerical method (4.3.11), we demonstrate that $|\eta^{m+1}| \leq |\eta^0|$ using mathematical induction. For $m = 0$, (4.4.3) yields

$$\begin{aligned} |\eta^1| &= \left| \left(\frac{((U_1)_n^0 - \varpi_1 U}{(U_2)_n^0} \right) \eta^0 \right| \\ &= \frac{|2R_n^0 \cos(\theta h) + S_n^0 - \varpi_1 (2\cos(\theta h) + 4)|}{|2P_n^0 \cos(\theta h) + Q_n^0|} |\eta^0|. \end{aligned}$$

Putting the values R_n^0, S_n^0, P_n^0, and Q_n^0 after some simplification, we get

$$\begin{aligned} |\eta^1| &= \frac{\left| \left(\frac{\rho}{2^{1-\gamma}} + \frac{1}{2} - \varpi_1 \right) (\cos(\theta h) + 2) + \frac{3}{h^2} (\cos(\theta h) - 1) \right|}{\left| \left(\frac{\rho}{2^{1-\gamma}} - \frac{1}{2} + \frac{3}{2} (V_n^0)^2 \right) (\cos(\theta h) + 2) - \frac{3}{h^2} (\cos(\theta h) - 1) \right|} |\eta^0| \\ &= \frac{\left| \left(\frac{\rho}{2^{1-\gamma}} (2 - 3^{1-\gamma}) + \frac{1}{2} \right) (\cos(\theta h) + 2) + \frac{3}{h^2} (\cos(\theta h) - 1) \right|}{\left| \left(\frac{\rho}{2^{1-\gamma}} - \frac{1}{2} + \frac{3}{2} (V_n^0)^2 \right) (\cos(\theta h) + 2) - \frac{3}{h^2} (\cos(\theta h) - 1) \right|} |\eta^0|. \end{aligned}$$

To show $\dfrac{\left| \left(\frac{\rho}{2^{1-\gamma}} (2 - 3^{1-\gamma}) + \frac{1}{2} \right) (\cos(\theta h) + 2) + \frac{3}{h^2} (\cos(\theta h) - 1) \right|}{\left| \left(\frac{\rho}{2^{1-\gamma}} - \frac{1}{2} + \frac{3}{2} (V_n^0)^2 \right) (\cos(\theta h) + 2) - \frac{3}{h^2} (\cos(\theta h) - 1) \right|} \leq 1$, we look at two situations.

Case 1. If $\left(\frac{\rho}{2^{1-\gamma}}(2-3^{1-\gamma})+\frac{1}{2}\right)(\cos(\theta h)+2)+\frac{3}{h^2}(\cos(\theta h)-1)\geq 0$, then

$$\frac{\left|\left(\frac{\rho}{2^{1-\gamma}}(2-3^{1-\gamma})+\frac{1}{2}\right)(\cos(\theta h)+2)+\frac{3}{h^2}(\cos(\theta h)-1)\right|}{\left|\left(\frac{\rho}{2^{1-\gamma}}-\frac{1}{2}+\frac{3}{2}(V_n^0)^2\right)(\cos(\theta h)+2)-\frac{3}{h^2}(\cos(\theta h)-1)\right|}\leq 1,$$

iff

$$\left(\frac{\rho}{2^{1-\gamma}}(2-3^{1-\gamma})+\frac{1}{2}\right)(\cos(\theta h)+2)+\frac{3}{h^2}(\cos(\theta h)-1)\leq\left(\frac{\rho}{2^{1-\gamma}}-\frac{1}{2}+\frac{3}{2}(V_n^0)^2\right)(\cos(\theta h)+2)-\frac{3}{h^2}(\cos(\theta h)-1),$$

iff

$$\left(\frac{\rho}{2^{1-\gamma}}(1-3^{1-\gamma})+1-\frac{3}{2}(V_n^0)^2\right)(\cos(\theta h)+2)+\frac{3}{h^2}(\cos(\theta h)-1)\leq 0.$$

It is valid for all values of θ and h.

Case 2. If $\left(\frac{\rho}{2^{1-\gamma}}(2-3^{1-\gamma})+\frac{1}{2}\right)(\cos(\theta h)+2)+\frac{3}{h^2}(\cos(\theta h)-1)\leq 0$, then

$$\frac{\left|\left(\frac{\rho}{2^{1-\gamma}}(2-3^{1-\gamma})+\frac{1}{2}\right)(\cos(\theta h)+2)+\frac{3}{h^2}(\cos(\theta h)-1)\right|}{\left|\left(\frac{\rho}{2^{1-\gamma}}-\frac{1}{2}+\frac{3}{2}(V_n^0)^2\right)(\cos(\theta h)+2)-\frac{3}{h^2}(\cos(\theta h)-1)\right|}\leq 1,$$

iff

$$-\left(\frac{\rho}{2^{1-\gamma}}(2-3^{1-\gamma})+\frac{1}{2}\right)(\cos(\theta h)+2)-\frac{3}{h^2}(\cos(\theta h)-1)\leq\left(\frac{\rho}{2^{1-\gamma}}-\frac{1}{2}+\frac{3}{2}(V_n^0)^2\right)(\cos(\theta h)+2)-\frac{3}{h^2}(\cos(\theta h)-1),$$

iff

$$\left(-\frac{\rho}{2^{1-\gamma}}(3-3^{1-\gamma})-\frac{3}{2}(V_n^0)^2\right)(\cos(\theta h)+2)\leq 0.$$

It is valid for all values of θ and h. Now assuming

$$|\eta^j|\leq|\eta^0|,\ j=2,3,\ldots,m, \tag{4.4.4}$$

We shall demonstrate that it is true for $j = m + 1$. The equation (4.4.3) yields

$$|\eta^{m+1}| \leq \left(\frac{|(U_1)_n^m - \varpi_1 U| + \varpi_1 |U|}{|(U_2)_n^m|} \right) |\eta^0|.$$

Again, there are two cases.

Case 1. If $(U_1)_n^m - \varpi_1 U \geq 0$, then

$$\frac{|(U_1)_n^m - \varpi_1 U| + \varpi_1 |U|}{|(U_2)_n^m|} \leq 1,$$

iff

$$\frac{(U_1)_n^m}{(U_2)_n^m} \leq 1,$$

iff

$$\left(1 - \frac{3}{2}(V_n^m)^2\right)(\cos(\theta h) + \frac{6}{h^2}(\cos(\theta h) - 1) \leq 0,$$

which stands accurate for all θ as $h \to 0$.

Case 2. If $(U_1)_n^m - \varpi_1 U \leq 0$, then

$$\frac{|(U_1)_n^m - \varpi_1 U| + \varpi_1 |U|}{|(U_2)_n^m|} \leq 1,$$

iff

$$\frac{-(U_1)_n^m + 2\varpi_1 U}{(U_2)_n^m} \leq 1,$$

iff

$$-\left(\frac{\rho}{2^{1-\gamma}} + \frac{1}{2}\right)(\cos(\theta h) + 2) - \frac{3}{h^2}(\cos(\theta h) - 1) + 2\varpi_1(\cos(\theta h) + 2)$$
$$\leq \left(\frac{\rho}{2^{1-\gamma}} - \frac{1}{2} + \frac{3}{2}(V_n^m)^2\right)(\cos(\theta h) + 2) - \frac{3}{h^2}(\cos(\theta h) - 1),$$

iff

$$\left(- \frac{2\rho}{2^{1-\gamma}} + 2\varpi_1 - \frac{3}{2}(V_n^m)^2\right)(\cos(\theta h) + 2) \leq 0,$$
$$\left(- \frac{2\rho}{2^{1-\gamma}} + \frac{2\rho}{2^{1-\gamma}}(3^{1-\gamma} - 1) - \frac{3}{2}(V_n^m)^2\right)(\cos(\theta h) + 2) \leq 0,$$

$$\left(-\frac{2\rho}{2^{1-\gamma}}(2-3^{1-\gamma}) - \frac{3}{2}(V_n^m)^2 \right)(\cos(\theta h)+2) \leq 0,$$

iff

$$2-3^{1-\gamma} \geq 0 \Leftrightarrow 3^{\gamma} \geq \frac{3}{2}.$$

On merging further outcomes, we have established that $|\eta^{m+1}| \leq |\eta^0|$ for $m = 0, 1, 2, \ldots, \mathcal{M}_t - 1$ delivered $\frac{3}{2} \leq 3^{\gamma}$. Therefore, the scheme is conditionally stable.

4.5 Convergence analysis

Lemma 4.5.1. *The cubic B-spline will provide the following inequality functions* $\mathcal{B}_{-1}(y), \mathcal{B}_0(y), \ldots, \mathcal{B}_{\mathcal{N}_y+1}(y)$.

$$\sum_{n=-1}^{\mathcal{N}_y+1} |\mathcal{B}_n(y)| \leq 10, \quad y \in [0,1].$$

Proof. If y is a grid location *i.e.,* $y = y_r$, then

$$\sum_{n=-1}^{\mathcal{N}_y+1} |\mathcal{B}_n(y_r)| = |\mathcal{B}_{r-1}(y_r)| + |\mathcal{B}_r(y_r)| + |\mathcal{B}_{r+1}(y_r)| = 1+4+1 = 6.$$

Further, at any point $y \in [y_{r-1}, y_r]$, we have

$$\sum_{n=-1}^{\mathcal{N}_y+1} |\mathcal{B}_i(y)| = |\mathcal{B}_{r-2}(y)| + |\mathcal{B}_{r-1}(y)| + |\mathcal{B}_r(y)| + |\mathcal{B}_{r+1}(y)| \leq 1+4+4+1 = 10.$$

As a result, we have $\sum_{n=-1}^{\mathcal{N}_y+1} |\mathcal{B}_i(y)| \leq 10$ for every $y \in [0,1]$. □

Theorem 4.5.1. *Suppose that* $\hat{v}^{m+1}(y)$ *is the cubic* B*-spline approximation of the precise solution* $v^{m+1}(y) \in C^4([0,1])$ *of the problem (4.2.1) at the* $(m+1)$*-th time level. Then, there is a constant* C *that corresponds to*

$$\|\hat{v}^{m+1}(y) - v^{m+1}(y)\| \leq Ch^2.$$

Proof. Let $\hat{v}^{m+1}(y) = \sum_{n=-1}^{\mathcal{N}_y+1} \delta_n^{m+1} \mathcal{B}_n(y)$ be the cubic B-spline approximation to the exact

solution $v^{m+1}(y)$ and $\hat{V}^{m+1}(y) = \sum_{n=-1}^{\mathcal{N}_y+1} \hat{\delta}_n^{m+1}\mathcal{B}_n(y)$ be the unique cubic B-spline interpolation to the exact solution $v^{m+1}(y)$.

$$\|v^{m+1}(y) - \hat{v}^{m+1}(y)\| \leq \|v^{m+1}(y) - \hat{V}^{m+1}(y)\| + \|\hat{v}^{m+1}(y) - \hat{V}^{m+1}(y)\|. \tag{4.5.1}$$

With respect to $\hat{v}^{m+1}(y)$ and $\hat{V}^{m+1}(y)$, a system of linear equations is

$$\mathbf{A}\mathbf{C}^{m+1} = \mathbf{B}^m, \quad m = 0, 1, \ldots, \mathcal{M}_t - 1, \tag{4.5.2}$$

$$\mathbf{A}\hat{\mathbf{C}}^{m+1} = \hat{\mathbf{B}}^m, \quad m = 0, 1, \ldots, \mathcal{M}_t - 1, \tag{4.5.3}$$

respectively, where

$$\hat{\mathbf{C}}^{m+1} = (\hat{\delta}_0^{m+1}, \hat{\delta}_1^{m+1}, \ldots, \hat{\delta}_{\mathcal{N}_y-1}^{m+1}, \hat{\delta}_{\mathcal{N}_y}^{m+1})^T,$$

and

$$\hat{\mathbf{B}}^m = (\hat{\wp}(0,m) - \Phi_l(t_{m+1})P_0^m, \hat{\wp}(1,m), \ldots, \hat{\wp}(n,m), \ldots, \hat{\wp}(\mathcal{N}_y - 1, m), \hat{\wp}(\mathcal{N}_y, m) - \Phi_r(t_{m+1})P_{\mathcal{N}_y}^m)^T.$$

Subtracting (4.5.3) from (4.5.2), we find

$$\mathbf{A}(\mathbf{C}^{m+1} - \hat{\mathbf{C}}^{m+1}) = \mathbf{B}^m - \hat{\mathbf{B}}^m, \quad m = 0, 1, \ldots, \mathcal{M}_t - 1, \tag{4.5.4}$$

where

$$\begin{aligned}\mathbf{B}^m - \hat{\mathbf{B}}^m =& (\wp(0,m) - \hat{\wp}(0,m), \wp(1,m) - \hat{\wp}(1,m), \ldots, \wp(\mathcal{N}_y - 1, m) - \hat{\wp}(\mathcal{N}_y - 1, m), \\ & \wp(\mathcal{N}_y, m) - \hat{\wp}(\mathcal{N}_y, m))^T.\end{aligned}$$

Now, we can see that

$$\begin{aligned}|\wp(n,m) - \hat{\wp}(n,m)| \leq& \left(\frac{\rho}{2^{1-\gamma}} + \frac{1}{2}\right)|\hat{v}(y_n, t_m) - \hat{V}(y_n, t_m)| + \frac{1}{2}|\hat{v}_{yy}(y_n, t_m) - \hat{V}_{yy}(y_n, t_m)| \\ & + \varpi_1|\hat{v}_n^m - \hat{V}_n^m| + \sum_{j=1}^{m-1} |\varpi_{m-j+1} - \varpi_{m-j}||\hat{v}_n^j - \hat{V}_n^j| + \varpi_m|\hat{v}_n^0 - \hat{V}_n^0|.\end{aligned} \tag{4.5.5}$$

Using the result $\|(v^m(y) - \hat{v}^m(y))^{(\nu)}\| \leq c_\nu h^{4-\nu}$, $\nu = 0, 1, 2$, given in [153], we obtain

$$\begin{aligned}\|\mathbf{B}^m - \hat{\mathbf{B}}^m\| \leq & \left(\frac{\rho}{2^{1-\gamma}} + \frac{1}{2}\right)c_0 h^4 + \frac{1}{2}c_2 h^2 + \left(\varpi_1 + \sum_{j=1}^{m-1} |\varpi_{m-j+1} - \varpi_{m-j}| + \varpi_m\right)c_0 h^4 \\ \leq & M_1 h^2, \end{aligned} \tag{4.5.6}$$

where $M_1 = \left(\frac{\rho}{2^{1-\gamma}} + \frac{1}{2} + 2\varpi_1\right)c_0 h^2 + + \frac{1}{2}c_2$. The matrix $\mathbf{A}$ is invertible due to its rigorous diagonal dominance; as a result, from (4.5.4), we derive

$$\|\mathbf{C}^{m+1} - \hat{\mathbf{C}}^{m+1}\| \leq \|\mathbf{A}^{-1}\|\|\mathbf{B}^m - \hat{\mathbf{B}}^m\|. \tag{4.5.7}$$

Let the matrix $\mathbf{A}$'s row sums be $\sigma_0, \sigma_1, \ldots, \sigma_{\mathcal{N}_y}$. Then

$$\|\mathbf{A}^{-1}\| \leq \frac{1}{|\sigma|}, \tag{4.5.8}$$

where $\sigma = \min\{\sigma_0, \sigma_1, \ldots, \sigma_{\mathcal{N}_y}\}$. Thus, from (4.5.6), (4.5.7), and (4.5.8), we get

$$\|\mathbf{C}^{m+1} - \hat{\mathbf{C}}^{m+1}\| \leq \frac{M_1 h^2}{|\sigma|}. \tag{4.5.9}$$

Now, using Equation (4.5.9) and Lemma 4.5.1, we get

$$\|\hat{v}^{m+1}(y) - \hat{V}^{m+1}(y)\| = \left\|\sum_{n=-1}^{\mathcal{N}_y+1} (\delta_n^m - \hat{\delta}_n^m)\mathcal{B}_n(y)\right\| \leq \left|\sum_{n=-1}^{\mathcal{N}_y+1} \mathcal{B}_n(y)\right| \|\mathbf{C}^{m+1} - \hat{\mathbf{C}}^{m+1}\| \leq \frac{10M_1 h^2}{|\sigma|}.$$

Also, we have

$$\|v^{m+1}(y) - \hat{V}^{m+1}(y)\| \leq c_0 h^4.$$

Therefore, (4.5.1) gives

$$\|v^{m+1}(y) - \hat{v}^{m+1}(y)\| \leq Ch^2,$$

where $C = c_0 h^2 + \frac{10M_1}{|\sigma|}$. □

Theorem 4.5.2. *The solution to the problem (4.2.1a)-(4.2.1c) using the numerical approach (4.3.11) is second-order convergent.*

Proof. The relation (4.3.3) together with the theorem (4.5.1 gives the required result. □

4.6 Numerical Simulation

This section tests the proposed method's efficiency and accuracy (4.3.11) on two numerical problems for time-fractional ACE. The orders of convergence and errors in distinct norms are demonstrated in tables. As we deliver the exact solutions to both problems, we calculate the error in the L_2 and maximum norms by using the double mesh principle, and we calculate its order of convergence employing the definition 1.3.8.

Example 4.6.1. *We consider the time-fractional ACE*

$$ {}_0^C D_t^\gamma v(y,t) - \frac{\partial^2 v(y,t)}{\partial y^2} + (v(y,t))^3 - v(y,t) = \left(\frac{2e^y}{\Gamma(3-\gamma)} + \pi^2 t^2 - t^2 \right) \cos(\pi y) + t^6 \cos^3(\pi y), $$
$$ y \in (0,1),\ t \in (0,1], $$

with the initial condition

$$ v(y,0) = 0,\ y \in [0,1], $$

and the boundary conditions

$$ v(0,t) = t^2,\ v(1,t) = -t^2,\ t \in [0,1]. $$

The exact solution to the problem is $v(y,t) = t^2 \cos(\pi y)$.

Example 4.6.2. *We consider the time-fractional ACE*

$$ {}_0^C D_t^\gamma v(y,t) - \frac{\partial^2 v(y,t)}{\partial y^2} + (v(y,t))^3 - v(y,t) = \frac{2e^y t^{2-\gamma}}{\Gamma(3-\gamma)} - 2e^y t^2 + (e^y t^2)^3,\ y \in (0,1),\ t \in (0,1], $$

with the initial condition

$$ v(y,0) = 0,\ y \in [0,1], $$

and the boundary conditions

$$ v(0,t) = t^2,\ v(1,t) = et^2,\ t \in [0,1]. $$

The exact solution of the problem is $v(y,t) = e^y t^2$.

In Tables 4.2–4.5 we displayed the pointwise errors in the L_∞ and L_2 norms over a range of $gamma$ values for Examples 4.6.1 and 4.6.2.These statistics show that the errors decrease and are close to the theoretical results as the number of grid points increases in space and time. It supports the second-order convergent nature of the suggested approach as predicted by our theoretical study. Figures 1 and 4 depict the 3D numerical behavior of the solution to the problem evaluated in Examples 4.6.1 and 4.6.2, respectively. The numerical solution at different time levels (by taking different values of t_m ($m = \mathcal{M}_t/4,\ \mathcal{M}_t/2,\ 3\mathcal{M}_t/4,\ \mathcal{M}_t$)) are displayed in Figures 2 and 5 for Examples 4.6.1 and 4.6.2, respectively. Figures 3 and 6 are drawn to study the error behavior of the present scheme for Examples 4.6.1 and 4.6.2, respectively.

Table 4.2: Example 4.6.1: Pointwise errors and order of convergence for various values of the γ norm in the L_∞ norm

	Quantity of nodal points overall				
γ	$\mathcal{M}_t = 16$	$\mathcal{M}_t = 32$	$\mathcal{M}_t = 64$	$\mathcal{M}_t = 128$	$\mathcal{M}_t = 256$
	$\mathcal{N}_y = 10$	$\mathcal{N}_y = 20$	$\mathcal{N}_y = 40$	$\mathcal{N}_y = 80$	$\mathcal{N}_y = 160$
0.4	$1.37E-03$	$3.47E-04$	$8.84E-05$	$2.24E-05$	$5.68E-06$
	1.9812	1.9728	1.9805	1.9795	
0.6	$1.39E-03$	$3.58E-04$	$9.30E-05$	$2.43E-05$	$6.48E-06$
	1.9571	1.9447	1.9363	1.9069	
0.8	$1.41E-03$	$3.67E-04$	$9.86E-05$	$2.73E-05$	$7.94E-06$
	1.9418	1.8961	1.8527	1.7817	

Table 4.3: Example 4.6.1: Pointwise errors and order of convergence for various values of the γ norm in the L_2 norm

	Quantity of nodal points overall				
γ	$\mathcal{M}_t = 16$	$\mathcal{M}_t = 32$	$\mathcal{M}_t = 64$	$\mathcal{M}_t = 128$	$\mathcal{M}_t = 256$
	$\mathcal{N}_y = 10$	$\mathcal{N}_y = 20$	$\mathcal{N}_y = 40$	$\mathcal{N}_y = 80$	$\mathcal{N}_y = 160$
0.4	$9.97E-04$	$2.52E-04$	$6.35E-05$	$1.61E-05$	$4.08E-06$
	1.9842	1.9886	1.9797	1.9804	
0.6	$1.41E-03$	$2.59E-04$	$6.68E-05$	$1.75E-05$	$4.66E-06$
	1.9633	1.9550	1.9325	1.9090	
0.8	$1.02E-03$	$2.66E-04$	$7.09E-05$	$1.96E-05$	$5.71E-06$
	1.9391	1.9076	1.8549	1.7793	

Table 4.4: Example 4.6.2: Pointwise errors and order of convergence for various values of the γ norm in the L_∞ norm

	Quantity of nodal points overall				
γ	$\mathcal{M}_t = 16$	$\mathcal{M}_t = 32$	$\mathcal{M}_t = 64$	$\mathcal{M}_t = 128$	$\mathcal{M}_t = 256$
	$\mathcal{N}_y = 10$	$\mathcal{N}_y = 20$	$\mathcal{N}_y = 40$	$\mathcal{N}_y = 80$	$\mathcal{N}_y = 160$
0.4	$8.00E-03$	$1.99E-03$	$4.95E-04$	$1.23E-04$	$3.02E-05$
	2.0072	2.0073	2.0088	2.0260	
0.6	$7.75E-03$	$1.90E-03$	$4.62E-04$	$1.10E-04$	$2.55E-05$
	2.0282	2.0400	2.0704	2.1089	
0.8	$7.53E-03$	$1.81E-03$	$4.22E-04$	$9.20E-05$	$2.66E-05$
	2.0567	2.1007	2.1975	1.7902	

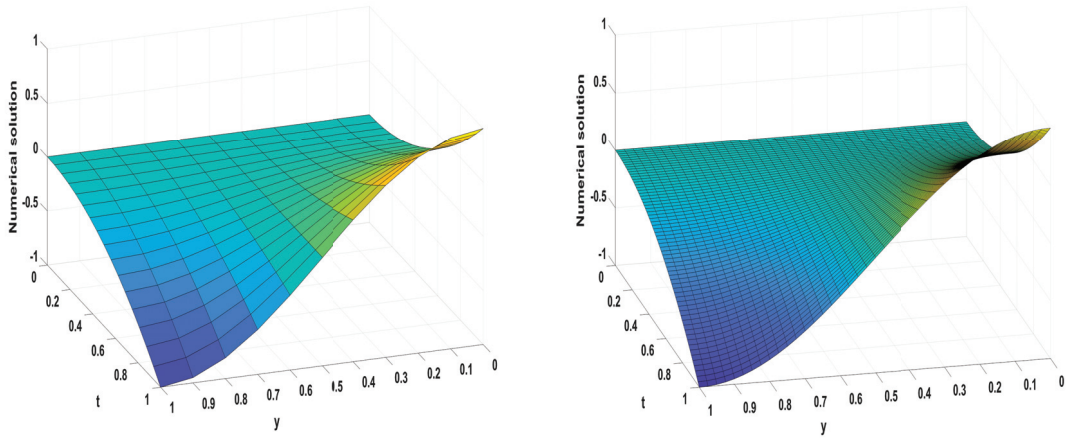

a $\mathcal{N}_y = 10,\ \mathcal{M}_t = 16$ b $\mathcal{N}_y = 40,\ \mathcal{M}_t = 64$

Figure 1: Example 4.6.1: Numerical Solution for $\gamma = 0.8$

Table 4.5: Example 4.6.2: Pointwise errors and order of convergence for various values of the γ norm in the L_2 norm

γ	Quantity of nodal points overall				
	$\mathcal{M}_t = 16$	$\mathcal{M}_t = 32$	$\mathcal{M}_t = 64$	$\mathcal{M}_t = 128$	$\mathcal{M}_t = 256$
	$\mathcal{N}_y = 10$	$\mathcal{N}_y = 20$	$\mathcal{N}_y = 40$	$\mathcal{N}_y = 80$	$\mathcal{N}_y = 160$
0.4	$5.83E-03$	$1.44E-03$	$3.58E-04$	$8.86E-05$	$2.18E-05$
	2.0174	2.0080	2.0146	2.0230	
0.6	$5.62E-03$	$1.37E-03$	$3.32E-04$	$7.87E-05$	$1.80E-05$
	2.0364	2.0449	2.0767	2.1284	
0.8	$5.44E-03$	$1.30E-03$	$2.99E-04$	$6.39E-05$	$1.94E-05$
	2.0651	2.1203	2.2263	1.7198	

4.7 Conclusion

This study presents a numerical technique for the time-fractional ACE, which combines the Crank-Nicolson method with cubic B-splines. To discretize the issue, we use consistent meshes in both directions. We have shown via thorough investigation that the offered strategy is conditionally stable and delivers satisfactory results for $\gamma \geq \log_3(3/2)$ and second-order convergent in every direction. Error estimates are given for the L_2 and L_∞ norms, despite the L_2--norm being used for error computation. The cubic B-spline technique is straightforward

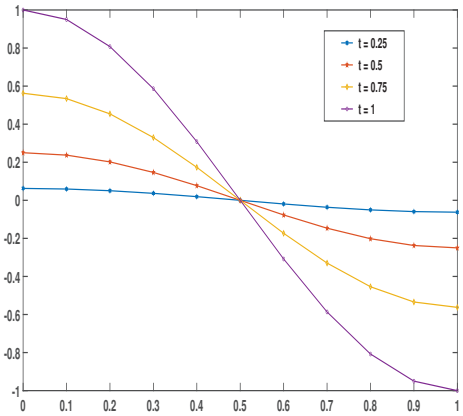

a $\mathcal{N}_y = 10,\ \mathcal{M}_t = 16$

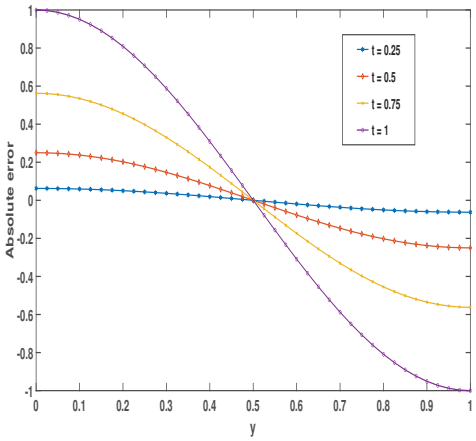

b $\mathcal{N}_y = 40,\ \mathcal{M}_t = 64$

Figure 2: Numerical solution for Example 4.6.1 at distinct time levels for $\gamma = 0.8$

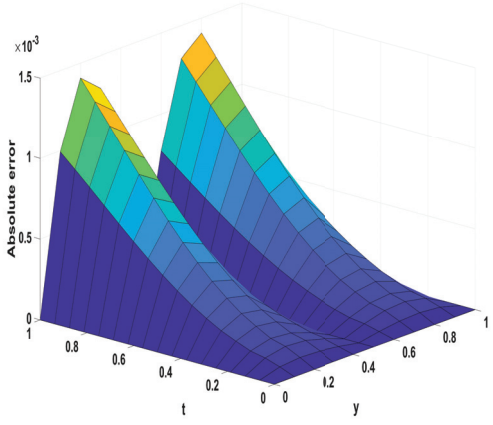

a $\mathcal{N}_y = 10,\ \mathcal{M}_t = 16$

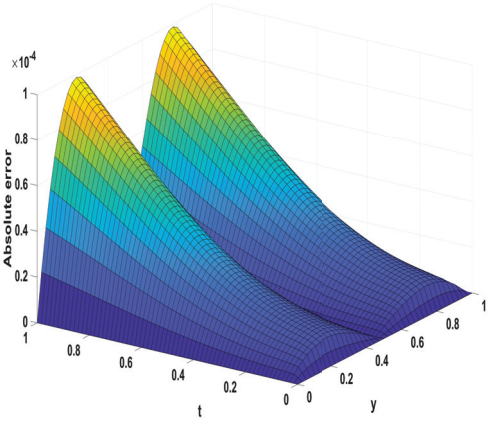

b $\mathcal{N}_y = 40,\ \mathcal{M}_t = 64$

Figure 3: Absolute errors for Example 4.6.1 for $\gamma = 0.8$

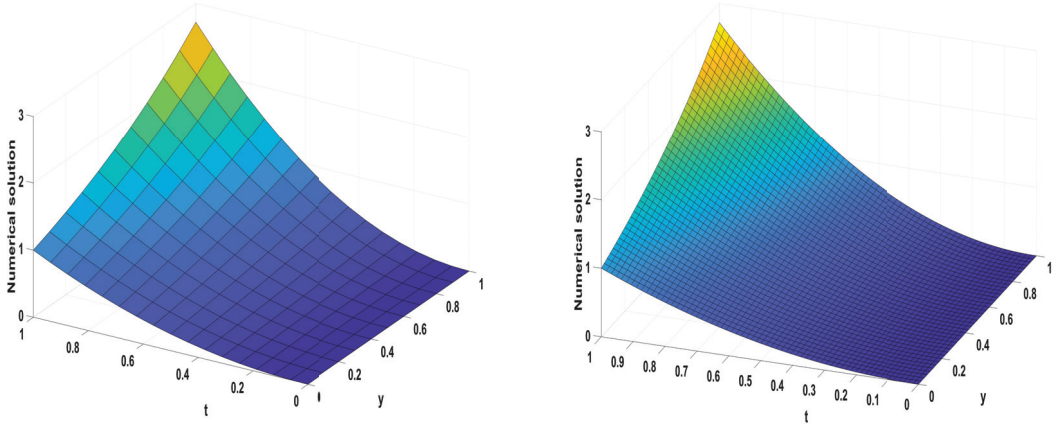

a $\mathcal{N}_y = 10,\ \mathcal{M}_t = 16$ b $\mathcal{N}_y = 40,\ \mathcal{M}_t = 64$

Figure 4: Numerical solution for Example 4.6.2 for $\gamma = 0.4$

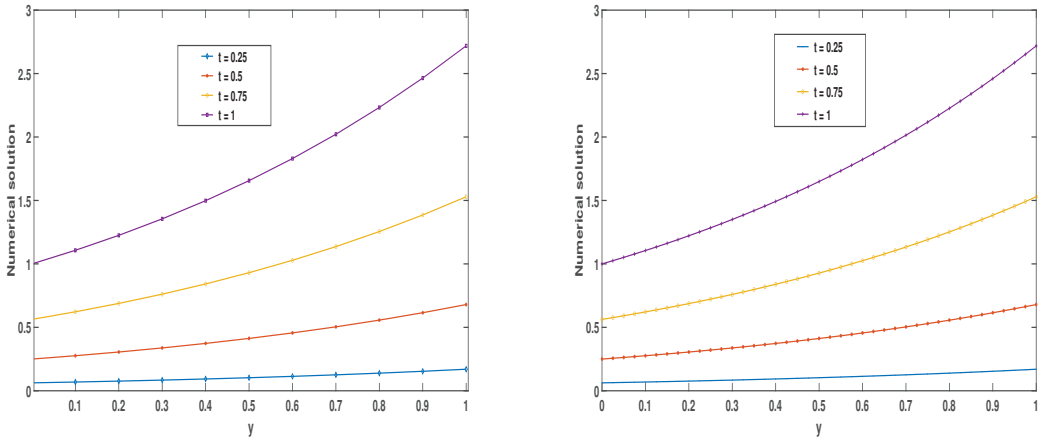

a $\mathcal{N}_y = 10,\ \mathcal{M}_t = 16$ b $\mathcal{N}_y = 40,\ \mathcal{M}_t = 64$

Figure 5: Numerical simulation for Example 4.6.2 at distinct time levels for $\gamma = 0.4$

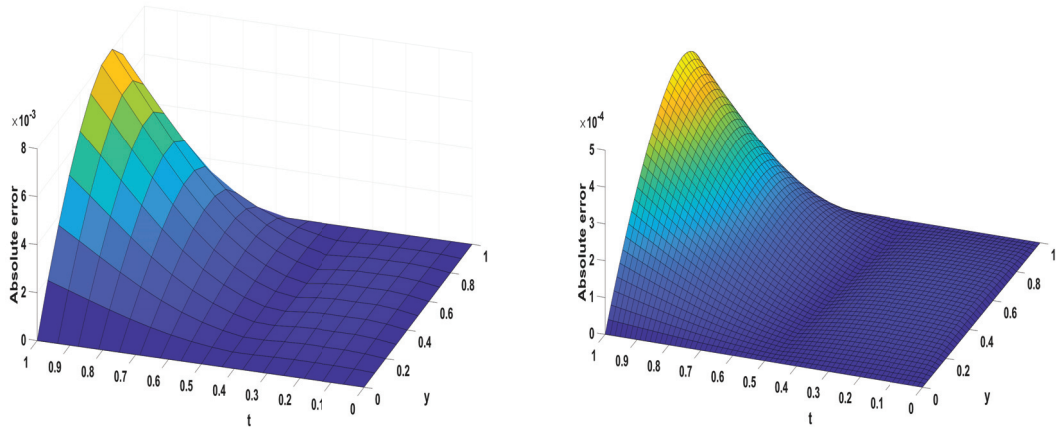

a $\mathcal{N}_y = 10,\ \mathcal{M}_t = 16$ b $\mathcal{N}_y = 40,\ \mathcal{M}_t = 64$

Figure 6: Absolute error for $\gamma = 0.4$ for Example 4.6.2

based on computational findings. Higher-order fractional partial differential equations could not be solved using the cubic B-spline approach.

Chapter 5

A high-order numerical technique for generalized time-fractional Fisher's equation

5.1 Introduction

The generalized time-fractional Fisher's equation is a substantial model for illustrating the system's dynamics. Studying effective numerical methods for this equation has considerable scientific importance and application value. In that direction, this chapter presents the design and analysis of a high-order numerical scheme for the generalized time-fractional Fisher's equation. The time-fractional derivative is taken in the Caputo sense and approximated using Euler backward discretization. The quasilinearization technique is used to linearize the problem, and then a compact finite difference scheme is considered for discretizing the equation in the space direction. Our numerical method is convergent of $O(k^{2-\alpha} + h^4)$, where h and k are stepped sizes in spatial and temporal directions, respectively. Three problems are tested numerically by implementing the proposed technique, and the acquired results reveal that the proposed method is suitable for solving this problem.

R. Choudhary, S. Singh, D. Kumar, A high-order numerical technique for generalized time-fractional Fisher's equation, Math. Methods Appl. Sci. , 46 (2023), 16050-–16071.

5.2 Literature survey

In recent years, most practical situations appearing in distinct fields of science have earned a great deal of curiosity and are modeled through nonlinear fractional order differential equations (FDEs). In mathematical modeling of these situations, the non-local property of the fractional derivative gives an extra edge over integer-order differential equations. Fractional derivatives deliver a unique mechanism for describing some phenomena with genetic and memory effects and redefine the flaws of integer-order derivatives. Again, this is the most substantial benefit of fractional-order systems compared to integer-order ones. Fractional calculus is a generalization of conventional calculus and deals with integrals and derivatives of arbitrary orders. The classical operators suggested by Leibniz more than three centuries ago have been developed for fractional systems in various formats. A special kernel characterizes each fractional operator's properties and can be employed in various individual problems (see [187]). Nonlinear partial differential equations (PDEs) are confronted in diverse domains of science. The generalized Fisher's equation [188] is highly significant for explaining various mechanisms. This chapter considers the following generalized time-fractional Fisher's Equation (GTFFE):

$$ {}_0^C D_t^{\alpha} u(x,t) - \mu_1 u_{xx}(x,t) - \mu_2 u(x,t)\left[1 - u^q(x,t)\right] = F(x,t),\ (x,t) \in (0,\mathcal{L}) \times (0,\mathcal{T}], \tag{5.2.1a} $$

subject to the initial condition

$$ u(x,0) = g_0(x),\ x \in [0,\mathcal{L}], \tag{5.2.1b} $$

and the boundary conditions

$$ u(0,t) = g_l(t),\ u(\mathcal{L},t) = g_r(t),\ t \in [0,\mathcal{T}], \tag{5.2.1c} $$

where $0 < \alpha \leq 1$, μ_1 and μ_2 are parameters, $F(x,t)$ is the source term, $q \in \mathbb{Z}^+$ (set of positive integers), and $g_0(x)$, $g_l(t)$, and $g_r(t)$ are known functions. For compatible conditions, we assume that $g_l(0) = g_0(0)$ and $g_r(0) = g_0(\mathcal{L})$. Taking $\alpha = 1$ and $q = 1$ in Equation

(5.2.1), we get an integer-order PDE considered by Fisher to study the propagation dynamics in the time-space direction of a virile gene in an infinite domain [189]. How a population grows between two competing processes can be defined through this equation. The proposed equation and its modified versions have appeared in flame propagation [190], neurophysiology [191], chemical kinetics [192], branching Brownian motion process [193], and many more areas (see [189] for the reference). Fisher's equation has become the center of interest for many researchers because of its widespread applications. Finding the exact solutions to a large class of time-fractional PDEs takes time and effort. Therefore, several numerical techniques are employed for approximating the solutions of Fisher's equation and similar problems. Gupta and Ray [194] proposed two reliable schemes based on Haar wavelets and homotopy asymptotic method for solving Burger's equation and GTFFE. Veeresha *et al.* [195] applied the q-homotopy analysis transform method (q-HATM) to the nonlinear Fishers's equation. Qurashi *et al.* [196] employed the residual power series technique by using Maclaurin expansion to solve the TFFE of integer order. Some other methods like Haar wavelets [197] and collocation using Jacobi wavelets [198], discontinuous local Galerkin method [199], cubic B-spline collocation [189] are also used for numerical studies of TFFEs of integer order. Recently, many articles came into existence for the numerical study of GTFFEs, like Majeed *et al.* [200] used cubic B-spline collocation technique to extend the previous study by adding source term and increasing the nonlinearity. They observed the accuracy of $O(\tau^{2-\alpha}+h^2)$. Qin *et al.* [201] proposed their study based on explicit and implicit difference schemes. They compared their results with the classical implicit difference scheme and showed that calculation cost was reduced by 60% using the proposed technique. In [202], Roul and Rohil presented a higher-order computational technique with an accuracy of $O(\tau^2+h^4)$, using $L1-2$ approximation for the time derivative and quintic B-splines for spatial derivatives. From previously cited literature, it is evident that most work is proposed for second-order accuracy in the spatial direction. In the proposed work, we intend to increase the accuracy in spatial direction by implementing a compact finite difference scheme (CFDS) (see [203, 204] for details).

The principal purpose of this work is to construct a higher-order (in space) effective numerical technique for the numerical solution of GTFFE defined in (5.2.1). We have used

the classical Euler backward technique to discretize the Caputo fractional derivative, while a compact finite difference scheme makes the space derivative's discretization. The nonlinearity is managed by using the well-known quasilinearization technique. We also present the computational time for the proposed method. To the author's knowledge, the suggested method has not been examined for the numerical study of the problem (5.2.1). This chapter is summarized as follows: First, in Section 2, we discretize the time-fractional derivative and apply quasilinearization to the considered problem. The time derivative shows the accuracy of $O(k^{2-\alpha})$. Then, we derived the CFDS and some other estimates required for convergence analysis. Section 3 deals with the convergence analysis, and we obtain the fourth-order convergence in the spatial direction. In Section 4, we provide a stability analysis of the proposed method. Three numerical experiments are executed in Section 5. We finish with a brief conclusion of the outcomes in Section 6.

5.3 Discretization of the problem

5.3.1 Temporal discretization

We utilize the Euler backward method to discretize the time-fractional derivative ${}_0^C D_t^\alpha u(x,t)$. For this, we split the time interval $[0,\mathcal{T}]$ employing the uniform step size $k=\mathcal{T}/M_t$, where M_t are the number of subintervals. Let $t_n = nk$, $n = 0,1,2,\ldots,M_t$ are the mesh points of the interval $[0,\mathcal{T}]$.

To discover the semidiscrete form of our problem, we rewrite the equation $(5.2.1)$ at the mesh point (x,t_{n+1}) as

$$\frac{\partial^\alpha \widetilde{u}(x,t_{n+1})}{\partial t^\alpha} - \mu_1 \widetilde{u}_{xx}(x,t_{n+1}) - \mu_2 \widetilde{u}(x,t_{n+1})\left[1-\widetilde{u}^q(x,t_{n+1})\right] = F(x,t_{n+1}),$$
$$x\in(0,\mathcal{L}),\ 0\le n\le M_t-1, \tag{5.3.1a}$$

with the initial condition

$$\widetilde{u}(x,0) = g_0(x),\ x\in[0,\mathcal{L}], \tag{5.3.1b}$$

and the boundary conditions

$$\widetilde{u}(0,t_{n+1}) = g_l(t_{n+1}),\ \widetilde{u}(\mathcal{L},t_{n+1}) = g_r(t_{n+1}),\ 0 \le n \le M_t - 1, \tag{5.3.1c}$$

where $\widetilde{u}$ denotes the approximated solution at the $(n+1)$-th time level. The Caputo time-fractional derivative in Equation (5.3.1) can be matched at the time point $t = t_n$ using the Euler backward method. Considering that the function $\widetilde{u}$ is three times differentiable, the Taylor expansion for $\frac{\partial \widetilde{u}(x,s)}{\partial t}$ for $s \in (t_n, t_{n+1})$ around t_n is given as

$$\begin{aligned}\frac{\partial \widetilde{u}(x,s)}{\partial t} &= \frac{\partial \widetilde{u}(x,t_n)}{\partial t} + (s-t_n)\frac{\partial^2 \widetilde{u}(x,t_n)}{\partial t^2} + O((s-t_n)^2) \\ &= \frac{\widetilde{u}(x,t_{n+1}) - \widetilde{u}(x,t_n)}{k} - \frac{1}{2}\frac{\partial^2 \widetilde{u}(x,t_n)}{\partial t^2}(t_{n+1}+t_n-2s) + O((s-t_n)^2). \end{aligned} \tag{5.3.2}$$

Since

$$\frac{\partial \widetilde{u}(x,t_n)}{\partial t} = \frac{\widetilde{u}(x,t_{n+1}) - \widetilde{u}(x,t_n)}{k} - \frac{k}{2!}\frac{\partial^2 \widetilde{u}(x,t_n)}{\partial t^2} + O(k^2),$$

therefore

$$\begin{aligned}{}_0^C D_t^\alpha \widetilde{u}(x,t_{n+1}) &= \frac{1}{\Gamma(1-\alpha)}\int_0^{t_{n+1}} \frac{\partial \widetilde{u}(x,s)}{\partial t}\frac{ds}{(t_{n+1}-s)^\alpha} \\ &= \frac{1}{\Gamma(1-\alpha)}\sum_{j=0}^{n}\int_{t_j}^{t_{j+1}} \frac{\partial \widetilde{u}(x,s)}{\partial t}\frac{ds}{(t_{n+1}-s)^\alpha} \\ &= \frac{1}{\Gamma(1-\alpha)}\sum_{j=0}^{n}\frac{\widetilde{u}(x,t_{j+1}) - \widetilde{u}(x,t_j)}{k}\int_{t_j}^{t_{j+1}}\frac{ds}{(t_{n+1}-s)^\alpha} + \mathcal{R}^{n+1} \\ &= \frac{1}{\Gamma(1-\alpha)}\sum_{j=0}^{n}\frac{\widetilde{u}(x,t_{j+1}) - \widetilde{u}(x,t_j)}{k}\frac{1}{(1-\alpha)}k^{1-\alpha}((n-j+1)^{1-\alpha} \\ &\quad - (n-j)^{1-\alpha}) + \mathcal{R}^{n+1} \qquad (5.3.3) \\ &= \frac{1}{\Gamma(2-\alpha)}\sum_{j=0}^{n}(\widetilde{u}(x,t_{j+1}) - \widetilde{u}(x,t_j))\sigma_{n-j} + \mathcal{R}^{n+1}, \qquad (5.3.4)\end{aligned}$$

where $\sigma_i = \dfrac{(i+1)^{1-\alpha} - i^{1-\alpha}}{k^\alpha}$ and the truncation error $\mathcal{R}^{n+1}$ is given as

$$\mathcal{R}^{n+1} = \frac{1}{\Gamma(1-\alpha)}\sum_{j=0}^{n}\int_{t_j}^{t_{j+1}}\left(-\frac{1}{2}\frac{\partial^2 \widetilde{u}(x,t_j)}{\partial t^2}(t_{j+1}+t_j-2s)\right)\frac{ds}{(t_{n+1}-s)^\alpha}$$

$$= \mathcal{C}_{\widetilde{u}} \left[\frac{1}{\Gamma(1-\alpha)} \sum_{j=0}^{n} \int_{t_j}^{t_{j+1}} \frac{t_{j+1} + t_j - 2s}{(t_{n+1} - s)^{\alpha}} ds \right], \tag{5.3.5}$$

where $\mathcal{C}_{\widetilde{u}}$ is a constant that depends only on $\widetilde{u}$.

Now, we have

$$\begin{aligned}
&\frac{1}{\Gamma(1-\alpha)} \sum_{j=0}^{n} \int_{t_j}^{t_{j+1}} \frac{t_{j+1} + t_j - 2s}{(t_{n+1} - s)^{\alpha}} ds \\
&= -\frac{1}{\Gamma(1-\alpha)} \sum_{j=0}^{n} \left[\frac{1}{1-\alpha} (2j+1) k^{2-\alpha} [(n-j)^{1-\alpha} - (n-j+1)^{1-\alpha}] \right. \\
&+ \frac{2}{1-\alpha} k^{2-\alpha} [(j+1)(n-j)^{1-\alpha} - j(n+1-j)^{1-\alpha}] \\
&\left. + \frac{2}{(1-\alpha)(2-\alpha)} k^{2-\alpha} [(n-j)^{2-\alpha} - (n-j+1)^{2-\alpha}] \right] \\
&= \frac{k^{2-\alpha}}{\Gamma(2-\alpha)} \left[(n+1)^{1-\alpha} + 2(n^{1-\alpha} + (n-1)^{1-\alpha} + (n-2)^{1-\alpha} + \cdots + 1^{1-\alpha}) \right] \\
&- \frac{2k^{2-\alpha}}{\Gamma(3-\alpha)} (j+1)^{2-\alpha} \\
&= \frac{k^{2-\alpha}}{\Gamma(2-\alpha)} \left[(n+1)^{1-\alpha} + 2(n^{1-\alpha} + (n-1)^{1-\alpha} + (n-2)^{1-\alpha} + \cdots + 1^{1-\alpha}) \right. \\
&\left. - \frac{2}{2-\alpha} (n+1)^{2-\alpha} \right].
\end{aligned} \tag{5.3.6}$$

If we take $\mathcal{S}(n) = (n+1)^{1-\alpha} + 2[n^{1-\alpha} + (n-1)^{1-\alpha} + (n-2)^{1-\alpha} + \cdots + 1^{1-\alpha}] - \frac{2}{2-\alpha}(n+1)^{2-\alpha}$, then the following lemma shows that $\mathcal{S}(n)$ is bounded for all n.

Lemma 5.3.1. *For all $n \geq 1$ and $\alpha \in (0,1)$,*

$$|\mathcal{S}(n)| \leq C,$$

where C is a constant independent of α and n.

Proof. We can easily check that

$$\begin{aligned}
\mathcal{S}(n) &= (n+1)^{1-\alpha} + 2[n^{1-\alpha} + (n-1)^{1-\alpha} + (n-2)^{1-\alpha} + \cdots + 1^{1-\alpha}] - \frac{2}{2-\alpha}(n+1)^{2-\alpha}, \\
&= \sum_{j=0}^{n} a_j,
\end{aligned}$$

where $a_j = (j+1)^{1-\alpha} + j^{1-\alpha} - \frac{2}{2-\alpha}[(j+1)^{2-\alpha} - j^{2-\alpha}]$. To prove the result, we will prove that $\sum_{j=0}^{n} a_j$ is convergent, which can be demonstrated by offering that $|a_j| \leq \frac{1}{j^{1+\alpha}}$ for large enough j. We have

$$
\begin{aligned}
|a_j| &= j^{1-\alpha}\left|\left(1+\frac{1}{j}\right)^{1-\alpha} + 1 - \frac{2j}{2-\alpha}\left(\left(1+\frac{1}{j}\right)^{2-\alpha} - 1\right)\right| \\
&= j^{1-\alpha}\Bigg|1 + 1 + (1-\alpha)\frac{1}{j} + \frac{(1-\alpha)(-\alpha)}{2!}\frac{1}{j^2} + \frac{(1-\alpha)(-\alpha)(-\alpha-1)}{3!}\frac{1}{j^3} + \cdots \\
&\quad - \frac{2j}{2-\alpha}\left(-1 + 1 + (2-\alpha)\frac{1}{j} + \frac{(2-\alpha)(1-\alpha)}{2!}\frac{1}{j^2} + \frac{(2-\alpha)(1-\alpha)(-\alpha)}{3!}\frac{1}{j^3} + \cdots\right)\Bigg| \\
&= j^{1-\alpha}\left|\left(\frac{1}{2!} - \frac{2}{3!}\right)(1-\alpha)(-\alpha)\frac{1}{j^2} + \left(\frac{1}{3!} - \frac{2}{4!}\right)(1-\alpha)(-\alpha)(-\alpha-1)\frac{1}{j^3} + \cdots\right| \\
&\leq j^{1-\alpha}\frac{1}{3!}(1-\alpha)\alpha\frac{1}{j^2}\left(1 + \frac{2(\alpha+1)}{4}\frac{1}{j} + \frac{3(\alpha+1)(\alpha+2)}{20}\frac{1}{j^2} + \cdots\right) \\
&\leq \frac{1}{3!}(1-\alpha)\alpha\frac{1}{j^{1+\alpha}}\left(1 + \frac{1}{j} + \frac{1}{j^2} + \cdots\right) \\
&\leq \frac{2}{3!}(1-\alpha)\alpha\frac{1}{j^{1+\alpha}} \\
&\leq \frac{1}{j^{1+\alpha}},
\end{aligned}
$$

which implies that $|\mathcal{S}(n)|$ is bounded for all $n \geq 1$ and $\alpha \in (0,1)$. □

Using Lemma 5.3.1 and Equation (5.3.6) in Equation (5.3.5), we can find that

$$
\begin{aligned}
|\mathcal{R}^{n+1}| &\leq \mathcal{C}_{\widetilde{u}}(C)k^{2-\alpha} \\
&\leq Ck^{2-\alpha},
\end{aligned} \tag{5.3.7}
$$

where C is a constant. Thus, the approximation of ${}_0^C D_t^\alpha u(x,t)$ at (x, t_{n+1}) is

$${}_0^C D_t^\alpha u(x,t_{n+1}) = \frac{1}{\Gamma(2-\alpha)}\sum_{j=0}^{n}(\widetilde{u}(x,t_{j+1}) - \widetilde{u}(x,t_j))\sigma_{n-j} + O(k^{2-\alpha}). \tag{5.3.8}$$

From Equations (5.3.8) and (5.3.1a), we have the following semi-discretized form of GTFFE

$$\frac{1}{\Gamma(2-\gamma)}\left[\sigma_0\widetilde{u}(x,t_{n+1}) - \sigma_n\widetilde{u}(x,t_0) - \sum_{j=1}^{n}\widetilde{u}(x,t_j)(\sigma_{n-j} - \sigma_{n-j+1})\right]$$

$$-\mu_1\widetilde{u}_{xx}(x,t_{n+1})-\mu_2\widetilde{u}(x,t_{n+1})\left[1-\widetilde{u}^q(x,t_{n+1})\right]=F(x,t_{n+1})+\mathcal{R}^{n+1}. \tag{5.3.9}$$

5.3.2 The derivation of the compact finite difference scheme

For full discretization of Equation (5.3.9), we operate a compact finite difference scheme; first, we split the spatial domain $[0,\mathcal{L}]$ into N_x sub-intervals to get a partition of $[0,\mathcal{L}]$ of equidistant mesh with the step size $h=\mathcal{L}/N_x$. Let $x_m=mh,\ m=0,1,2,\ldots,N_x$ are the grid points of the interval $[0,\mathcal{L}]$. Let $\widetilde{u}_m^n=\widetilde{u}(x_m,t_n),\ m=0,1,2,\ldots,N_x,\ n=0,1,2,\ldots,M_t$, and here we introduce some notations

$$\delta_x\widetilde{u}_m^n=\frac{1}{2h}(\widetilde{u}_{m+1}^n-\widetilde{u}_{m-1}^n),\ \delta_x^2\widetilde{u}_m^n=\frac{1}{h^2}(\widetilde{u}_{m-1}^n-2\widetilde{u}_m^n+\widetilde{u}_{m+1}^n),$$

$$\mathcal{A}\widetilde{u}_{xx}(x_m,t_n)=\frac{1}{12}\left[\widetilde{u}_{xx}(x_{m-1},t_n)+10\widetilde{u}_{xx}(x_m,t_n)+\widetilde{u}_{xx}(x_{m+1},t_n)\right],$$

$$\mathcal{A}\widetilde{u}_m^n=\frac{1}{12}(\widetilde{u}_{m-1}^n+10\widetilde{u}_m^n+\widetilde{u}_{m+1}^n),\ m=1,2,\ldots,N_x-1,\ n=0,1,2,\ldots,M_t.$$

The following lemmas are helpful in the derivation of the compact finite difference scheme whose proofs can be seen in [205] and [206], respectively.

Lemma 5.3.2. *For* $0<\alpha<1$,

- $\sigma_j\geq 0,\ j=0,1,2,\ldots,n,$
- $\sigma_0\geq\sigma_1\geq\sigma_2\geq\cdots\geq\sigma_n,$
- $\sigma_n+\sum_{j=1}^{n}(\sigma_{n-j}-\sigma_{n-j+1})=\sigma_0.$

Lemma 5.3.3. *Suppose* $v(x)\in C^6[x_{m-1},x_{m+1}]$ *and* $x_{m+1}=x_m+h,\ x_{m-1}=x_m-h$. *Then*

$$\frac{1}{12}\left[v''(x_{m-1})+10v''(x_m)+v''(x_{m+1})\right]-\frac{1}{h^2}\left[v(x_{m-1})-2v(x_m)+v(x_{m+1})\right]=\frac{h^4}{240}v^{(6)}(\kappa_m),$$

for some $\kappa_m\in(x_{m-1},x_{m+1})$.

Now, the Equation (5.3.9) at the point (x_m, t_{n+1}) gives

$$\frac{1}{\Gamma(2-\gamma)}\left[(\sigma_0-\Gamma(2-\gamma)\mu_2)\widetilde{u}_m^{n+1}-\sigma_n\widetilde{u}_m^0-\sum_{j=1}^{n}\widetilde{u}_m^j(\sigma_{n-j}-\sigma_{n-j+1})\right] - \mu_1\widetilde{u}_{xx}(x_m,t_{n+1})+\mu_2(\widetilde{u}_m^{n+1})^{q+1}=F(x_m,t_{n+1})+\mathcal{R}_m^{n+1}. \tag{5.3.10}$$

Making use of quasilinearization technique in Equation (5.3.10) for nonlinear term $(\widetilde{u}_m^{n+1})^{q+1}$, we get

$$((\widetilde{u}_m^{n+1})^{q+1})^{i+1}=(q+1)((\widetilde{u}_m^n)^q)^i(\widetilde{u}_m^{n+1})^{i+1}-q((\widetilde{u}_m^n)^{q+1})^i,\ i=1,2,\ldots \tag{5.3.11}$$

where i stands for the number of iterations and let $(\widetilde{u})^1$ is the initial guess that satisfies the initial and boundary conditions. We write the Equation (5.3.10) at the $(i+1)^{\text{th}}$ iteration as

$$\begin{aligned}&\frac{1}{\Gamma(2-\gamma)}\left[(\sigma_0-\Gamma(2-\gamma)\mu_2)\widetilde{u}_m^{n+1}-\sigma_n\widetilde{u}_m^0-\sum_{j=1}^{n}\widetilde{u}_m^j(\sigma_{n-j}-\sigma_{n-j+1})\right]^{i+1}\\&-\mu_1(\widetilde{u}_{xx}(x_m,t_{n+1}))^{i+1}+\mu_2((q+1)((\widetilde{u}_m^n)^q)^i(\widetilde{u}_m^{n+1})^{i+1})\\&=F(x_m,t_{n+1})+\mathcal{R}_m^{n+1}+\mu_2q((\widetilde{u}_m^n)^{q+1})^i.\end{aligned} \tag{5.3.12}$$

Now, for simplicity we denote $(\widetilde{u}_m^n)^{i+1}$ by $\widetilde{U}_m^n$ and $(\widetilde{u}_m^n)^i$ by U_m^n to get

$$\begin{aligned}&\frac{1}{\Gamma(2-\gamma)}\left[(\sigma_0-\Gamma(2-\gamma)\mu_2)\widetilde{U}_m^{n+1}-\sigma_n\widetilde{U}_m^0-\sum_{j=1}^{n}\widetilde{U}_m^j(\sigma_{n-j}-\sigma_{n-j+1})\right]\\&-\mu_1\widetilde{U}_{xx}(x_m,t_{n+1})+\mu_2(q+1)(U_m^n)^q\widetilde{U}_m^{n+1}\\&=F(x_m,t_{n+1})+\mathcal{R}_m^{n+1}+\mu_2q(U_m^n)^{q+1}.\end{aligned} \tag{5.3.13}$$

From Lemma 5.3.3, we can conclude that

$$\mathcal{A}\widetilde{u}_{xx}(x_m,t_{n+1})=\delta_x^2\widetilde{U}_m^{n+1}+\frac{h^4}{240}\frac{\partial^6\widetilde{U}}{\partial x^6}(\kappa_m,t_{n+1}),\ \kappa_m\in(x_{m-1},x_{m+1}).$$

Operating $\mathcal{A}$ on the both sides of Equation (5.3.13), we find

$$\begin{aligned}
&\frac{1}{\Gamma(2-\gamma)}\mathcal{A}\Bigg[(\sigma_0-\Gamma(2-\gamma)\mu_2)\widetilde{U}_m^{n+1}-\sigma_n\widetilde{U}_m^0-\sum_{j=1}^{n}\widetilde{U}_m^j(\sigma_{n-j}-\sigma_{n-j+1})\Bigg]\\
&-\mu_1\delta_x^2\widetilde{U}_m^{n+1}+\mu_2(q+1)\mathcal{A}(U_m^n)^q\mathcal{A}\widetilde{U}_m^{n+1}\\
&=\mathcal{A}F(x_m,t_{n+1})+\mu_2 q\mathcal{A}(U_m^n)^{q+1}+\mathfrak{R}_m^{n+1},
\end{aligned}\tag{5.3.14}$$

where

$$\begin{aligned}
\mathfrak{R}_m^{n+1}&=\mathcal{A}\mathcal{R}_m^{n+1}+\mu_1\frac{h^4}{240}\frac{\partial^6\widetilde{U}}{\partial x^6}(\kappa_m,t_{n+1})\\
&=\frac{1}{12}(\mathcal{R}_{m-1}^{n+1}+10\mathcal{R}_m^{n+1}+\mathcal{R}_{m+1}^{n+1})+\mu_1\frac{h^4}{240}\frac{\partial^6\widetilde{U}}{\partial x^6}(\kappa_m,t_{n+1}).
\end{aligned}\tag{5.3.15}$$

From (5.3.7), we can find that

$$|\mathfrak{R}_m^{n+1}|\le\mathcal{C}(k^{2-\alpha}+h^4),\tag{5.3.16}$$

where

$$\mathcal{C}=C+\mu_1\frac{1}{240}\frac{\partial^6\widetilde{U}}{\partial x^6}(\kappa_m,t_{n+1}),$$

is independent of k and h. thus, we get the following numerical scheme

$$\begin{aligned}
&\left[\left(\frac{\sigma_0}{\Gamma(2-\gamma)}-\mu_2\right)+\mu_2(q+1)\mathcal{A}(U_m^n)^q\right]\mathcal{A}\hat{u}_m^{n+1}-\mu_1\delta_x^2\hat{u}_m^{n+1}=\mathcal{A}F_m^{n+1}+\mu_2 q\mathcal{A}(U_m^n)^{q+1}\\
&+\frac{1}{\Gamma(2-\gamma)}\mathcal{A}\Bigg[\sigma_n\hat{u}_m^0+\sum_{j=1}^{n}\hat{u}_m^j(\sigma_{n-j}-\sigma_{n-j+1})\Bigg],
\end{aligned}\tag{5.3.17a}$$

with

$$\hat{u}_m^0=g_0(x_m),\ m=0,1,2,\ldots,N_x,\tag{5.3.17b}$$

and

$$\hat{u}_0^{n+1}=g_l(t_{n+1}),\ \hat{u}_{N_x}^{n+1}=g_r(t_{n+1}),\ n=0,1,\ldots,M_t-1.\tag{5.3.17c}$$

In matrix form, this numerical scheme can be written as

$$B\hat{U}^{n+1} = V^n,$$

where

$$B = \begin{bmatrix} d_1^{n+1} & e_1^{n+1} & 0 & & \\ f_2^{n+1} & d_2^{n+1} & e_2^{n+1} & & \\ \ddots & \ddots & \ddots & & \\ & \ddots & \ddots & \ddots & \\ & \ddots & \ddots & \ddots & \\ & & f_{N_x-2}^{n+1} & d_{N_x-2}^{n+1} & e_{N_x-2}^{n+1} \\ & & 0 & f_{N_x-1}^{n+1} & d_{N_x-1}^{n+1} \end{bmatrix},$$

is a matrix of size $(N_x - 1) \times (N_x - 1)$ and

$$\hat{U}^{n+1} = \begin{bmatrix} \hat{u}_1^{n+1} \\ \hat{u}_2^{n+1} \\ \vdots \\ \hat{u}_m^{n+1} \\ \vdots \\ \hat{u}_{N_x-2}^{n+1} \\ \hat{u}_{N_x-1}^{n+1} \end{bmatrix}_{(N_x-1)\times 1}, \quad V^n = \begin{bmatrix} z_1^{n+1} - g_l(t_{n+1}) f_1^{n+1} \\ z_2^{n+1} \\ \vdots \\ z_m^{n+1} \\ \vdots \\ z_{N_x-2}^{n+1} \\ z_{N_x-1}^{n+1} - g_r(t_{n+1}) e_{N_x-1}^{n+1} \end{bmatrix}_{(N_x-1)\times 1},$$

where

$$d_m^{n+1} = \frac{5}{6}\left(\frac{\sigma_0}{\Gamma(2-\gamma)} - \mu_2\right) + \frac{2\mu_1}{h^2} + \frac{5\mu_2(q+1)}{6}\mathcal{A}(U_m^n)^q,$$

$$e_m^{n+1} = \frac{1}{12}\left(\frac{\sigma_0}{\Gamma(2-\gamma)} - \mu_2\right) - \frac{\mu_1}{h^2} + \frac{\mu_2(q+1)}{12}\mathcal{A}(U_m^n)^q,$$

$$f_m^{n+1} = \frac{1}{12}\left(\frac{\sigma_0}{\Gamma(2-\gamma)} - \mu_2\right) - \frac{\mu_1}{h^2} + \frac{\mu_2(q+1)}{12}\mathcal{A}(U_m^n)^q,$$

$$z_m^{n+1} = \mathcal{A}F_m^{n+1} + \mu_2 q \mathcal{A}(U_m^n)^{q+1} + \frac{1}{\Gamma(2-\gamma)}\mathcal{A}\left[\sigma_n \hat{u}_m^0 + \sum_{j=1}^{n} \hat{u}_m^j(\sigma_{n-j} - \sigma_{n-j+1})\right].$$

5.4 Convergence Analysis

Let $W = \{w \mid w = (w_0, w_1, \ldots, w_{N_x}),\ w_0 = 0,\ w_{N_x} = 0\}$ be a grid function. For any $w, w' \in W$, we introduce the inner product and norms as follows

$$\langle w, w' \rangle = h \sum_{m=0}^{N_x-1} \left(\delta_x w_{m+\frac{1}{2}}\right) \left(\delta_x w'_{m+\frac{1}{2}}\right) - \frac{h^2}{12} h \sum_{m=0}^{N_x-1} \left(\delta_x^2 w_m\right) \left(\delta_x^2 w'_m\right),$$

$$|w|_1 = \sqrt{h \sum_{m=0}^{N_x} \left(\delta_x w_{m-\frac{1}{2}}\right)^2}, \quad \|w\| = \sqrt{h \sum_{m=0}^{N_x-1} (w_m)^2}, \quad \|w\|_\infty = \max_{1 \le m \le N_x-1} |w_m|.$$

The following lemmas will be used for convergence analysis of the scheme (5.3.17).

Lemma 5.4.1. *[207] For any $w \in W$, it holds that*

$$\frac{2}{3}|w|_1^2 \le \langle w, w \rangle \le |w|_1^2,$$
$$\|w\|_\infty \le \frac{\sqrt{\mathcal{L}}}{2}|w|_1,$$
$$\|w\| \le \frac{\mathcal{L}}{\sqrt{6}}|w|_1.$$

Lemma 5.4.2. *For any $w \in W$, $\|w\|^2 \le \frac{\mathcal{L}^2}{4}\langle w, w \rangle$, and $\|w\|_\infty^2 \le \frac{3\mathcal{L}}{8}\langle w, w \rangle$.*

Proof. This Lemma can easily be proved using Lemma 5.4.1. □

Lemma 5.4.3. *[208] For any $w, w' \in W$, it holds that*

$$-h \sum_{m=0}^{N_x-1} \left(\delta_x^2 w_m\right) w'_m = h \sum_{m=0}^{N_x} \left(\delta_x w_{m-\frac{1}{2}}\right) \left(\delta_x w'_{m-\frac{1}{2}}\right).$$

Lemma 5.4.4. *[209] For any $w \in W$, it holds that $\|\mathcal{A}w\|^2 \le \|w\|^2$.*

Lemma 5.4.5. *Let $\{a_l\}$ and $\{b_l\}$ are two non negative sequences and $\mathcal{K}$ is a non negative constant. If $a_l \le \mathcal{K} + \sum_{i=0}^{l} b_i a_i,\ l \ge 0$, then $a_l \le \mathcal{K} \exp\left(\sum_{i=0}^{l} b_i\right)$.*

Proof. We have

$$a_l \le \mathcal{K} + \sum_{i=0}^{l} b_i a_i,\ l \ge 0$$

$$
\begin{aligned}
&\leq \mathcal{K} + \sum_{i=0}^{l} \mathcal{K} b_i \prod_{i<j}^{l} (1 + b_j), \text{ (using sharp Gronwall's inequality [210])} \\
&= \mathcal{K} + \mathcal{K} \sum_{i=0}^{l} \left\{ \prod_{i \leq j}^{l} (1 + b_j) - \prod_{i+1 \leq j}^{l} (1 + b_j) \right\} \\
&= \mathcal{K} + \mathcal{K} \left\{ \prod_{j \geq 0}^{l} (1 + b_j) - \prod_{l+1 \leq j}^{l} (1 + b_j) \right\} \\
&= \mathcal{K} \prod_{j \geq 0}^{l} (1 + b_j) \leq \mathcal{K} \exp\left(\sum_{i=0}^{l} b_i \right), \text{ (since } 1 + b_i \leq \exp(b_i)). \qquad \square
\end{aligned}
$$

Theorem 5.4.1. *Let $u(x,t) \in C^{(6,2)}([0,\mathcal{L}] \times [0,\mathcal{T}])$ be the solution of the problem (5.2.1), and $\hat{u}_m^n$ be the solution of the difference scheme (5.3.17), and let $E_m^n = u(x_m, t_n) - \hat{u}_m^n$. Then, we have*

$$
\|E^n\| \leq C(k^{2-\alpha} + h^4), \quad \|E^n\|_\infty \leq C(k^{2-\alpha} + h^4), \quad 1 \leq n \leq M_t.
$$

Proof. Subtract Equation (5.3.17) from Equation (5.3.13) to get the following error equation for the difference scheme (5.3.17)

$$
\begin{aligned}
\left[\left(\frac{\sigma_0}{\Gamma(2-\gamma)} - \mu_2 \right) + \mu_2 (q+1) \mathcal{A} (U_m^n)^q \right] \mathcal{A} E_m^{n+1} &= \mu_1 \delta_x^2 E_m^{n+1} \\
&+ \frac{1}{\Gamma(2-\gamma)} \sum_{j=1}^{n} (\sigma_{n-j} - \sigma_{n-j+1}) \mathcal{A} E_m^j + \mathfrak{R}_m^{n+1},
\end{aligned} \tag{5.4.1a}
$$

with the errors at the initial time and boundaries

$$
E_m^0 = 0, \ m = 0, 1, \ldots, N_x, \tag{5.4.1b}
$$

and

$$
E_0^{n+1} = 0, \ E_{N_x}^{n+1} = 0, \ n = 0, 1, \ldots, M_t - 1. \tag{5.4.1c}
$$

Multiplying Equation (5.4.1a) by $-h(\delta_x^2 E_m^{n+1})$ and summing up for m from 1 to $N_x - 1$, we

get

$$-h\sum_{m=1}^{N_x-1}\left[\left(\frac{\sigma_0}{\Gamma(2-\gamma)}-\mu_2\right)+\mu_2(q+1)\mathcal{A}(U_m^n)^q\right](\mathcal{A}E_m^{n+1})(\delta_x^2E_m^{n+1})=-\mu_1||\delta_x^2E^{n+1}||^2$$
$$-h\frac{1}{\Gamma(2-\gamma)}\sum_{m=1}^{N_x-1}\sum_{j=1}^{n}(\sigma_{n-j}-\sigma_{n-j+1})(\mathcal{A}E_m^j)(\delta_x^2E_m^{n+1})-h\sum_{m=1}^{N_x-1}(\mathfrak{R}_m^{n+1})(\delta_x^2E_m^{n+1}). \tag{5.4.2}$$

Let $U_{m_*}^n=\min\{U_m^n|m=1,2,\ldots,N_x-1\}$, then

$$-h\left[\left(\frac{\sigma_0}{\Gamma(2-\gamma)}-\mu_2\right)+\mu_2(q+1)\mathcal{A}(U_{m_*}^n)^q\right]\sum_{m=1}^{N_x-1}(\mathcal{A}E_m^{n+1})(\delta_x^2E_m^{n+1})\leq-\mu_1||\delta_x^2E^{n+1}||^2$$
$$-h\frac{1}{\Gamma(2-\gamma)}\sum_{m=1}^{N_x-1}\sum_{j=1}^{n}(\sigma_{n-j}-\sigma_{n-j+1})(\mathcal{A}E_m^j)(\delta_x^2E_m^{n+1})-h\sum_{m=1}^{N_x-1}(\mathfrak{R}_m^{n+1})(\delta_x^2E_m^{n+1}). \tag{5.4.3}$$

Now from Lemma 5.4.3

$$-h\sum_{m=1}^{N_x-1}(\mathcal{A}E_m^{n+1})(\delta_x^2E_m^{n+1})=-h\sum_{m=1}^{N_x-1}\frac{1}{12}(E_{m-1}^{n+1}+10E_m^{n+1}+E_{m+1}^{n+1})(\delta_x^2E_m^{n+1})$$
$$=h\frac{10}{12}\sum_{m=0}^{N_x-1}(\delta_xE_{m+\frac{1}{2}}^{n+1})(\delta_xE_{m+\frac{1}{2}}^{n+1})-\frac{h}{12}\sum_{m=1}^{N_x-1}(\delta_x^2E_m^{n+1})(E_{m-1}^{n+1}+E_{m+1}^{n+1}),$$

and we know that

$$E_{m-1}^{n+1}+E_{m+1}^{n+1}=h^2\delta_x^2E_m^{n+1}+2E_m^{n+1},$$

thus

$$-h\sum_{m=1}^{N_x-1}(\mathcal{A}E_m^{n+1})(\delta_x^2E_m^{n+1})=h\sum_{m=0}^{N_x-1}(\delta_xE_{m+\frac{1}{2}}^{n+1})(\delta_xE_{m+\frac{1}{2}}^{n+1})-\frac{h^2}{12}h\sum_{m=1}^{N_x-1}(\delta_x^2E_m^{n+1})(\delta_x^2E_m^{n+1})$$
$$=\langle E^{n+1},E^{n+1}\rangle. \tag{5.4.4}$$

Similarly,

$$-h\sum_{m=1}^{N_x-1}\sum_{j=1}^{n}(\sigma_{n-j}-\sigma_{n-j+1})(\mathcal{A}E_m^j)(\delta_x^2E_m^{n+1})=\sum_{j=1}^{n}(\sigma_{n-j}-\sigma_{n-j+1})\langle E^{n+1},E^j\rangle. \quad (5.4.5)$$

The inequality $\sum_{j=1}^{n}(\sigma_{n-j}-\sigma_{n-j+1})\langle(E^{n+1}-E^j),(E^{n+1}-E^j)\rangle\geq 0$ implies that

$$\begin{aligned}\sum_{j=1}^{n}(\sigma_{n-j}-\sigma_{n-j+1})\langle E^{n+1},E^j\rangle &\leq \frac{1}{2}(\sigma_0-\sigma_n)\langle E^{n+1},E^{n+1}\rangle+\frac{1}{2}\sum_{j=1}^{n}(\sigma_{n-j}-\sigma_{n-j+1})\langle E^j,E^j\rangle\\ &\leq \frac{1}{2}\langle E^{n+1},E^{n+1}\rangle+\frac{1}{2}\sum_{j=1}^{n}(\sigma_{n-j}-\sigma_{n-j+1})\langle E^j,E^j\rangle,\end{aligned} \quad (5.4.6)$$

and the inequality $h\sum_{m=1}^{N_x-1}\left(\frac{1}{\sqrt{\mu_1}}\mathfrak{R}_m^{n+1}-\sqrt{\mu_1}\delta_x^2E_m^{n+1}\right)^2\geq 0$ implies that

$$\begin{aligned}-h\sum_{m=1}^{N_x-1}(\mathfrak{R}_m^{n+1})(\delta_x^2E_m^{n+1}) &\leq \frac{\mu_1}{2}\|\delta_x^2E^{n+1}\|^2+\frac{1}{2\mu_1}\|\mathfrak{R}^{n+1}\|^2\\ &\leq \mu_1\|\delta_x^2E^{n+1}\|^2+\frac{1}{2\mu_1}\|\mathfrak{R}^{n+1}\|^2.\end{aligned} \quad (5.4.7)$$

Substituting Equations (5.4.4), (5.4.5), (5.4.6), and (5.4.7) in Equation (5.4.3), we get

$$\begin{aligned}\left[\left(\frac{1}{2\Gamma(2-\gamma)}-\mu_2\right)+\mu_2(q+1)\mathcal{A}(U_{m_*}^n)^q\right]\langle E^{n+1},E^{n+1}\rangle &\leq \frac{1}{2}\sum_{j=1}^{n}(\sigma_{n-j}-\sigma_{n-j+1})\langle E^j,E^j\rangle\\ &\quad+\frac{1}{2\mu_1}\|\mathfrak{R}^{n+1}\|^2,\end{aligned}$$

now with the use of Equation (5.3.16) and $\lambda=\Gamma(2-\gamma)$

$$\begin{aligned}&\left[(1-2\lambda\mu_2)+2\lambda\mu_2(q+1)\mathcal{A}(U_{m_*}^n)^q\right]\langle E^{n+1},E^{n+1}\rangle\leq\lambda\sum_{j=1}^{n}(\sigma_{n-j}-\sigma_{n-j+1})\langle E^j,E^j\rangle\\ &+\frac{\lambda}{\mu_1}(\mathcal{C}(k^{2-\alpha}+h^4))^2\langle E^{n+1},E^{n+1}\rangle\leq\frac{\lambda}{(1-2\lambda\mu_2)+2\lambda\mu_2(q+1)\mathcal{A}(U_{m_*}^n)^q}\end{aligned}$$

$$\left[\sum_{j=1}^{n}(\sigma_{n-j}-\sigma_{n-j+1})\langle E^j,E^j\rangle+\frac{\mathcal{C}^2}{\mu_1}(k^{2-\alpha}+h^4)^2\right],$$

here we use Lemma 5.4.5

$$\begin{aligned}\langle E^{n+1},E^{n+1}\rangle &\le \frac{\lambda}{(1-2\lambda\mu_2)+2\lambda\mu_2(q+1)\mathcal{A}(U^n_{m_*})^q}\frac{\mathcal{C}^2}{\mu_1}(k^{2-\alpha}+h^4)^2\\ &\quad \exp\sum_{j=1}^{n}(\sigma_{n-j}-\sigma_{n-j+1})\langle E^j,E^j\rangle\\ &\le \frac{\lambda}{(1-2\lambda\mu_2)+2\lambda\mu_2(q+1)\mathcal{A}(U^n_{m_*})^q}\frac{\mathcal{C}^2}{\mu_1}(k^{2-\alpha}+h^4)^2(\sigma_0-\sigma_n)\\ &\le C^2(k^{2-\alpha}+h^4)^2. \end{aligned}\tag{5.4.8}$$

Using Lemma 5.4.2, we obtain

$$\|E^{n+1}\|\le C(k^{2-\alpha}+h^4),\quad \|E^{n+1}\|_\infty\le C(k^{2-\alpha}+h^4).\qquad\square$$

5.5 Stability Analysis

The numerical scheme (5.3.17) is numerically stable if a small perturbation to the initial solution gives a small perturbation in the numerical solution. Let $\{\nu^{n+1}_m|0\le m\le N_x,\ 0\le n\le M_t-1\}$ be the solution of

$$\begin{aligned}&\left[\left(\frac{\sigma_0}{\Gamma(2-\gamma)}-\mu_2\right)+\mu_2(q+1)\mathcal{A}(U^n_m)^q\right]\mathcal{A}\nu^{n+1}_m-\mu_1\delta_x^2\nu^{n+1}_m=\mathcal{A}F^{n+1}_m+\mu_2q\mathcal{A}(U^n_m)^{q+1}\\ &+\frac{1}{\Gamma(2-\gamma)}\mathcal{A}\left[\sigma_n\nu^0_m+\sum_{j=1}^{n}\nu^j_m(\sigma_{n-j}-\sigma_{n-j+1})\right],\end{aligned}\tag{5.5.1a}$$

with

$$\nu^0_m=g_0(x_m)+\psi^0_m,\ m=0,1,2\ldots,N_x,\tag{5.5.1b}$$

and

$$\nu^{n+1}_0=g_l(t_{n+1}),\ \nu^{n+1}_{N_x}=g_r(t_{n+1}),\ n=0,1,\ldots,M_t-1,\tag{5.5.1c}$$

where ψ_m^0 is a small perturbation of $g_0(x_m)$. Let

$$\varepsilon_m^n = \hat{u}_m^n - \nu_m^n,\ m = 0, 1, 2 \ldots, N_x,\ n = 0, 1, \ldots, M_t.$$

Theorem 5.5.1. *The numerical scheme (5.3.17a)-(5.3.17c) is stable if the discrete numerical solutions $\hat{u}_m^n$ satisfying (5.3.17) and ν_m^n satisfying (5.5.1) are such that $\|\varepsilon^{n+1}\|_\infty \leq C|\psi^0|_1$.*

Proof. To find error equation for compact difference scheme (5.3.17), we subtract (5.3.17) from (5.5.1)

$$\left[\left(\frac{\sigma_0}{\Gamma(2-\gamma)} - \mu_2\right) + \mu_2(q+1)\mathcal{A}(U_m^n)^q\right]\mathcal{A}\varepsilon_m^{n+1} = \mu_1\delta_x^2\varepsilon_m^{n+1} + \frac{1}{\Gamma(2-\gamma)}\left[\sigma_n\varepsilon_m^0 + \sum_{j=1}^{n}\varepsilon_m^j(\sigma_{n-j} - \sigma_{n-j+1})\right], \tag{5.5.2a}$$

with

$$\varepsilon_m^0 = \psi_m^0,\ m = 0, 1, 2, \ldots, N_x, \tag{5.5.2b}$$

and

$$\varepsilon_0^{n+1} = 0,\ \varepsilon_{N_x}^{n+1} = 0,\ n = 0, 1, \ldots, M_t - 1. \tag{5.5.2c}$$

Multiplying Equation (5.5.2a) by $-h(\delta_x^2\varepsilon_m^{n+1})$ and summing up for m from 1 to $N_x - 1$, to get

$$-h\sum_{m=1}^{N_x-1}\left[\left(\frac{\sigma_0}{\Gamma(2-\gamma)} - \mu_2\right) + \mu_2(q+1)\mathcal{A}(U_m^n)^q\right](\mathcal{A}\varepsilon_m^{n+1})(\delta_x^2\varepsilon_m^{n+1}) =$$
$$-h\mu_1\sum_{m=1}^{N_x-1}(\delta_x^2\varepsilon_m^{n+1})(\delta_x^2\varepsilon_m^{n+1}) - h\frac{1}{\Gamma(2-\gamma)}\sum_{m=1}^{N_x-1}\mathcal{A}\left[\sigma_n\varepsilon_m^0 + \sum_{j=1}^{n}\varepsilon_m^j(\sigma_{n-j} - \sigma_{n-j+1})\right](\delta_x^2\varepsilon_m^{n+1}),$$

which gives

$$-h\left[\left(\frac{\sigma_0}{\Gamma(2-\gamma)} - \mu_2\right) + \mu_2(q+1)\mathcal{A}(U_{m_*}^n)^q\right]\sum_{m=1}^{N_x-1}(\mathcal{A}\varepsilon_m^{n+1})(\delta_x^2\varepsilon_m^{n+1}) \leq$$

$$- h\mu_1 \sum_{m=1}^{N_x-1} (\delta_x^2 \varepsilon_m^{n+1})(\delta_x^2 \varepsilon_m^{n+1}) - h\frac{1}{\Gamma(2-\gamma)} \sum_{m=1}^{N_x-1} \mathcal{A}\left[\sigma_n \varepsilon_m^0 + \sum_{j=1}^{n} \varepsilon_m^j (\sigma_{n-j} - \sigma_{n-j+1})\right](\delta_x^2 \varepsilon_m^{n+1}). \tag{5.5.3}$$

Use of Equations (5.4.4) and (5.4.5) in (5.5.3) yields

$$\left[\left(\frac{\sigma_0}{\Gamma(2-\gamma)} - \mu_2\right) + \mu_2(q+1)\mathcal{A}(U_{m_*}^n)^q\right]\langle \varepsilon^{n+1}, \varepsilon^{n+1}\rangle \leq \frac{1}{\Gamma(2-\gamma)} \sum_{j=1}^{n} (\sigma_{n-j} - \sigma_{n-j+1})\langle \varepsilon^j, \varepsilon^{n+1}\rangle + \frac{\sigma_n}{\Gamma(2-\gamma)}\langle \varepsilon^0, \varepsilon^{n+1}\rangle - \mu_1 \|\delta_x^2 \varepsilon^{n+1}\|^2. \tag{5.5.4}$$

Now the inequality $\sum_{j=1}^{n} (\sigma_{n-j} - \sigma_{n-j+1})\langle (\varepsilon^{n+1} - \varepsilon^j), (\varepsilon^{n+1} - \varepsilon^j)\rangle \geq 0$ implies that

$$\sum_{j=1}^{n} (\sigma_{n-j} - \sigma_{n-j+1})\langle \varepsilon^j, \varepsilon^{n+1}\rangle \leq \frac{1}{2}(1-\sigma_n)\langle \varepsilon^{n+1}, \varepsilon^{n+1}\rangle + \frac{1}{2}\sum_{j=1}^{n} (\sigma_{n-j} - \sigma_{n-j+1})\langle \varepsilon^j, \varepsilon^j\rangle, \tag{5.5.5}$$

and the inequality $\langle (\varepsilon^{n+1} - \varepsilon^0), (\varepsilon^{n+1} - \varepsilon^0)\rangle \geq 0$ implies that

$$\langle \varepsilon^0, \varepsilon^{n+1}\rangle \leq \frac{1}{2}\langle \varepsilon^{n+1}, \varepsilon^{n+1}\rangle + \frac{1}{2}\langle \varepsilon^0, \varepsilon^0\rangle. \tag{5.5.6}$$

Substituting Equation (5.5.6) and (5.5.5) in Equation (5.5.4), and put $\lambda = \Gamma(2-\gamma)$, we get

$$\left[(1-\lambda\mu_2) + \lambda\mu_2(q+1)\mathcal{A}(U_{m_*}^n)^q\right]\langle \varepsilon^{n+1}, \varepsilon^{n+1}\rangle \leq \frac{1}{2}\langle \varepsilon^{n+1}, \varepsilon^{n+1}\rangle + \frac{1}{2}\sum_{j=1}^{n} (\sigma_{n-j} - \sigma_{n-j+1})\langle \varepsilon^j, \varepsilon^j\rangle + \frac{\sigma_n}{2}\langle \varepsilon^0, \varepsilon^0\rangle - \lambda\mu_1 \|\delta_x^2 \varepsilon^{n+1}\|^2,$$

or

$$\left[(1-2\lambda\mu_2) + 2\lambda\mu_2(q+1)\mathcal{A}(U_{m_*}^n)^q\right]\langle \varepsilon^{n+1}, \varepsilon^{n+1}\rangle \leq \sum_{j=1}^{n} (\sigma_{n-j} - \sigma_{n-j+1})\langle \varepsilon^j, \varepsilon^j\rangle + \sigma_n\langle \varepsilon^0, \varepsilon^0\rangle,$$

or

$$\left[(1-2\lambda\mu_2)+2\lambda\mu_2(q+1)\mathcal{A}(U_{m_*}^n)^q\right]\langle\varepsilon^{n+1},\varepsilon^{n+1}\rangle \leq \sum_{j=1}^{n}(\sigma_{n-j}-\sigma_{n-j+1})\langle\varepsilon^j,\varepsilon^j\rangle+\sigma_0\langle\varepsilon^0,\varepsilon^0\rangle. \tag{5.5.7}$$

An application of Lemma 5.4.5 yields

$$\begin{aligned}\left[(1-2\lambda\mu_2)+2\lambda\mu_2(q+1)\mathcal{A}(U_{m_*}^n)^q\right]\langle\varepsilon^{n+1},\varepsilon^{n+1}\rangle &\leq \sigma_0\langle\varepsilon^0,\varepsilon^0\rangle\exp(\sigma_0-\sigma_j)\\ &\leq \sigma_0\langle\varepsilon^0,\varepsilon^0\rangle\exp(1),\end{aligned}$$

or

$$\langle\varepsilon^{n+1},\varepsilon^{n+1}\rangle \leq \frac{\sigma_0\exp(1)}{(1-2\lambda\mu_2)+2\lambda\mu_2(q+1)\mathcal{A}(U_{m_*}^n)^q}\langle\varepsilon^0,\varepsilon^0\rangle. \tag{5.5.8}$$

Again using Lemmas 5.4.1 and 5.4.2 in Equation (5.5.8), we get

$$\|\varepsilon^{n+1}\|_\infty^2 \leq \frac{3\mathcal{L}}{8}\langle\varepsilon^{n+1},\varepsilon^{n+1}\rangle \leq \frac{3\mathcal{L}}{8}\frac{\sigma_0\exp(1)}{(1-2\lambda\mu_2)+2\lambda\mu_2(q+1)\mathcal{A}(U_{m_*}^n)^q}(|\psi^0|_1)^2,$$

that is

$$\|\varepsilon^{n+1}\|_\infty \leq C|\psi^0|_1,$$

where $C=\sqrt{\frac{3\mathcal{L}}{8}\frac{\sigma_0\exp(1)}{(1-2\lambda\mu_2)+2\lambda\mu_2(q+1)\mathcal{A}(U_{m_*}^n)^q}}$. □

5.6 Numerical Illustrations and Applications

In this section, three test examples are taken to demonstrate the proposed method's efficiency, computational complexity, and accuracy. We calculate numerical solutions and tabulate for various values of parameters μ_1, μ_2, and α. We also portray the numerical solution graphically to compare with the exact solution to represent the solution's nature for varying the parametric values. Using the double mesh principle, we find error estimates in L_∞-norm, the respective order of convergence is calculated by using the definition 1.3.8.

In a specific direction (space or time), the order of convergence is calculated by

$$d^{N_x,M_t,x} = \frac{\log\left(\frac{\mathcal{E}^{N_x,M_t}}{\mathcal{E}^{2N_x,M_t}}\right)}{\log 2},\ d^{N_x,M_t,t} = \frac{\log\left(\frac{\mathcal{E}^{N_x,M_t}}{\mathcal{E}^{N_x,2M_t}}\right)}{\log 2}.$$

The CPU time is also measured to further investigate the technique's performance. All examples are coded by MATLAB R2021b and performed on Intel Core i7 (9th Gen) with a memory of 16GB.

Example 5.6.1. *First, we consider the problem (5.2.1) defined on* $(0,1)\times(0,1]$ *with* $F(x,t) = 2x^2\dfrac{t^{2-\alpha}}{\Gamma(3-\alpha)} - 2\mu_1(1+t^2) - \mu_2 x^2(1+t^2)\left(1-(x^2(1+t^2))^q\right)$ *with the initial and boundary conditions*

$$u(x,0) = x^2,\ x\in[0,1],\quad u(0,t) = 0,\quad u(1,t) = 1+t^2,\ t\in[0,1].$$

The exact solution to this problem is $u(x,t) = x^2(1+t^2)$.

Example 5.6.2. *Next, we consider the problem (5.2.1) defined on* $(0,1)\times(0,1]$ *with* $F(x,t) = t^{\frac{3}{2}-\alpha}\dfrac{\Gamma(5/2)}{\Gamma(5/2-\alpha)}\sin\left(\dfrac{3\pi}{2}x\right)+\mu_1\dfrac{9\pi^2}{4}t^{3/2}\sin\left(\dfrac{3\pi}{2}x\right)-\mu_2 t^{3/2}\sin\left(\dfrac{3\pi}{2}x\right)\left(1-\left(t^{3/2}\sin\left(\dfrac{3\pi}{2}x\right)\right)^q\right)$ *with the initial and boundary conditions*

$$u(x,0) = 0,\ x\in[0,1],\quad u(0,t) = 0,\quad u(1,t) = -t^{3/2},\ t\in[0,1].$$

The exact solution to this problem is $u(x,t) = t^{3/2}\sin\left(\dfrac{3\pi}{2}x\right)$.

Example 5.6.3. *Finally, we consider the problem (5.2.1) defined on* $(0,1)\times(0,1]$ *with* $F(x,t) = t\Gamma(\alpha+2)(1-x^2)\cos(3\pi x)-\mu_1 t^{1+\alpha}\left(12\pi x\sin(3\pi x)+(9\pi^2x^2-9\pi^2-2)\cos(3\pi x)\right)-\mu_2 t^{1+\alpha}(1-x^2)\cos(3\pi x)\left(1-\left(t^{1+\alpha}(1-x^2)\cos(3\pi x)\right)^q\right)$ *with the initial and boundary conditions*

$$u(x,0) = 0,\ x\in[0,1],\quad u(0,t) = t^{2\alpha},\quad u(1,t) = 0,\ t\in[0,1].$$

The exact solution to this problem is $u(x,t) = t^{1+\alpha}(1-x^2)\cos(3\pi x)$.

In Table 5.1, we find $\mathcal{E}^{N_x,M_t}$, d^{N_x,M_t} for different values of α and fixed $q = 3$. It confirms the order of convergence $2 - \alpha$ in the temporal direction. The CPU time is also given for each α, which is quite reasonable as the number of points increases. The similar analogy one can see in Tables 5.4 and 5.7 for Examples 5.6.2 and 5.6.3, respectively (for different values of μ_1 and μ_2). In Tables 5.2, 5.5, and 5.8, we provide pointwise errors and orders of convergence in spatial direction for the same set of α values as in Tables 5.1, 5.4, and 5.7, keeping $M_t = 160$. The obtained numerical order of convergence agrees with the theoretical one derived in convergence analysis. We also deliver the CPU time in the same tables, which assures the computational efficiency of the proposed technique. Keeping α fixed and varying the values of q, we get order of convergence $2 - \alpha$ in Tables 5.3, 5.6, and 5.9.

To bring a clear sight of the real-time nature of the solution, the surface plots of the numerical and exact solutions are given in Figures 1, 4, 7 for the Examples 5.6.1, 5.6.2, and 5.6.3, respectively. One can easily see that the surface plots of these solutions are almost identical. We confirm this analogy by plotting the exact and numerical solutions at a fixed time level in Figures 5.2b, 5.5b, and 5.8b. The solution changes with each time level as we approach from lower to higher time levels. For this, we have drawn the numerical solution at different time levels (see Figures 5.2a, 5.5a, and 5.8a). Contour plots and 3D views of numerical solutions are provided for Examples 5.6.1 and 5.6.2 in Figures 3 and 6, respectively. For Example, 5.6.3, Figure 9 shows how the solution changes with respect to α?

5.7 Conclusions

This chapter suggests a higher-order numerical technique in spatial direction for the generalized time-fractional Fisher's equation with significantly less computational time. The discretization process for the time-fractional derivative uses the standard Euler Backward technique, while in the spatial direction, we employed CFDS. The proposed numerical scheme solves the GTFFE very efficiently and produces accurate solutions with less computational error for both directions. The graphical results reveal that the present approach for finding the numerical solution of GTFFE agrees well with the exact solution. The tabular results strongly confirm the theoretical aspects of orders of convergence in the spatial and temporal directions.

Table 5.1: $\mathcal{E}^{N_x,M_t}$, d^{N_x,M_t}, and CPU time (in sec.) for Example 5.6.1 taking $q = 3$, $\mu_1 = \mu_2 = 0.5$

α	N_x=16 M_t=20	N_x=32 M_t=40	N_x=64 M_t=80	N_x=128 M_t=160	N_x=256 M_t=320
0.2	$1.0983e-03$	$3.1510e-04$	$8.9685e-05$	$2.5598e-05$	$7.3675e-06$
	1.2768	1.4886	1.8088	1.7968	-
CPU Time	0.0617	0.1031	0.4648	3.2660	25.1628
0.5	$2.0294e-03$	$6.8669e-04$	$2.3369e-04$	$8.0328e-05$	$2.7829e-05$
	1.5633	1.5551	1.5406	1.5293	-
CPU Time	0.0774	0.1069	0.4655	3.2648	25.1729
0.8	$7.3508e-03$	$3.1916e-03$	$1.3826e-03$	$6.0009e-04$	$2.6073e-04$
	1.2036	1.2069	1.2041	1.2026	-
CPU Time	0.0616	0.1022	0.4677	3.3133	25.0789
0.95	$1.4228e-02$	$6.9107e-03$	$3.3369e-03$	$1.6113e-03$	$7.7815e-04$
	1.0418	1.0503	1.0503	1.0501	-
CPU Time	0.0553	0.1045	0.4663	3.3770	25.3164

Table 5.2: Pointwise errors, CPU time (in sec.), and orders of convergence in space for Example 5.6.1 taking $q = 3$, $\mu_1 = \mu_2 = 0.5$

	N_x				
α	16	32	64	128	256
0.2	$1.0500e-08$	$6.7182e-10$	$4.2503e-11$	$2.6643e-12$	$1.6689e-13$
	3.9662	3.9824	3.9957	3.9968	-
CPU Time	1.2870	2.5457	5.0066	9.6239	19.9678
0.5	$1.8176e-08$	$1.1752e-09$	$7.4135e-11$	$4.6405e-12$	$3.3107e-13$
	3.9511	3.9866	3.9978	3.8091	-
CPU Time	1.2690	2.5128	4.9514	9.8175	19.8542
0.8	$2.7406e-07$	$2.7319e-08$	$1.7580e-09$	$1.1088e-10$	$6.9803e-12$
	3.3265	3.9579	3.9869	3.9896	-
CPU Time	1.2972	2.5399	4.9081	9.7731	20.0414
0.95	$2.0146e-06$	$1.3063e-07$	$9.4002e-09$	$6.0389e-10$	$3.8496e-11$
	3.9469	3.7967	3.9603	3.9715	-
CPU Time	1.2667	2.4711	4.9423	9.8052	19.6993

Table 5.3: $\mathcal{E}^{N_x,M_t}$, d^{N_x,M_t}, and CPU time (in sec.) for Example 5.6.1 taking $\alpha = 0.7$, $\mu_1 = \mu_2 = 1$

q	N_x=16 M_t=20	N_x=32 M_t=40	N_x=64 M_t=80	N_x=128 M_t=160	N_x=256 M_t=320
2	$4.6149e-03$	$1.8808e-03$	$7.6294e-04$	$3.0951e-04$	$1.2559e-04$
	1.2950	1.3017	1.3016	1.3013	-
CPU Time	0.0575	0.1075	0.4659	3.3237	25.2550
4	$4.9565e-03$	$1.9269e-03$	$7.6275e-04$	$3.0467e-04$	$1.2249e-04$
	1.3630	1.3370	1.3240	1.3146	-
CPU Time	0.0571	0.1021	0.4755	3.3456	25.1361
5	$5.0677e-03$	$1.9091e-03$	$7.7161e-04$	$3.0355e-04$	$1.2199e-04$
	1.4084	1.3069	1.3459	1.3152	-
CPU Time	0.0557	0.1044	0.4642	3.2964	25.2418

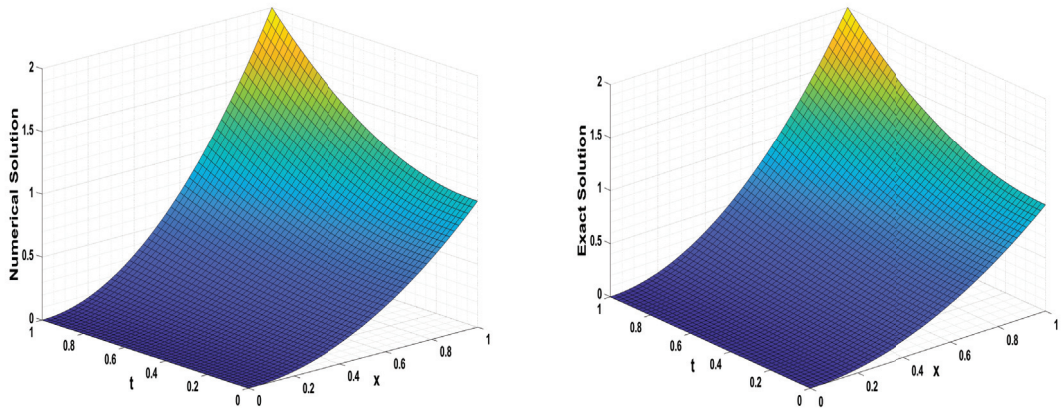

a Numerical solution

b Exact solution

Figure 1: Surface plots of exact and numerical solutions for Example 5.6.1 by taking $N_x = M_t = 50$, $\alpha = 0.8$, $q = 3$, and $\mu_1 = \mu_2 = 1$.

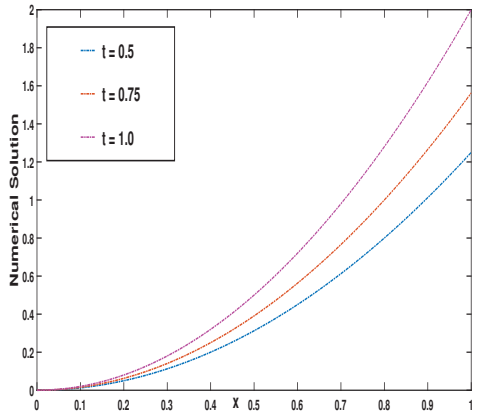

a Numerical solution at different time levels

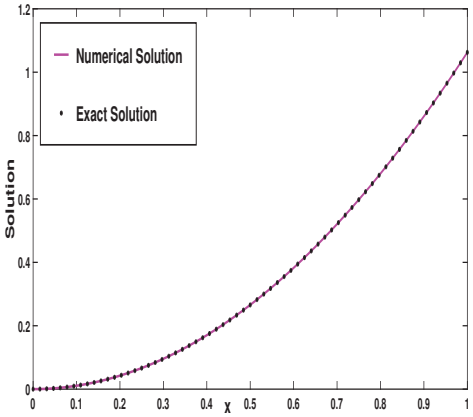

b Exact and numerical solution at $t = 0.25$

Figure 2: Plots of exact and numerical solutions for Example 5.6.1 by taking $N_x = M_t = 64$, $\alpha = 0.75$, $q = 3$, and $\mu_1 = \mu_2 = 1$.

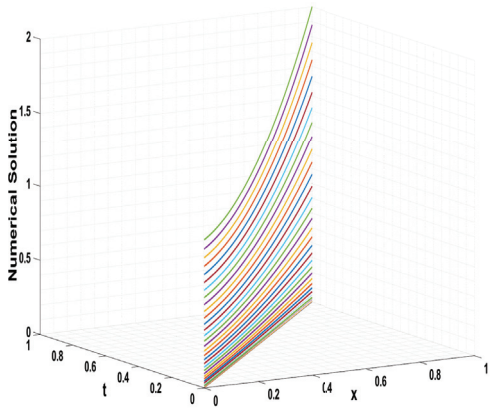

a 3D view of numerical solution

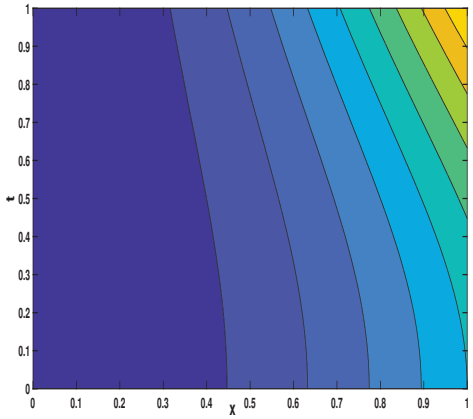

b Contour plot of numerical solution

Figure 3: Plots of numerical solution for Example 5.6.1 by taking $N_x = M_t = 32$, $\alpha = 0.5$, $q = 2$, and $\mu_1 = \mu_2 = 1$.

Table 5.4: $\mathcal{E}^{N_x,M_t}$, d^{N_x,M_t}, and CPU time (in sec.) for Example 5.6.2 taking $q = 3$, $\mu_1 = \mu_2 = 1$

α	N_x=16 M_t=20	N_x=32 M_t=40	N_x=64 M_t=80	N_x=128 M_t=160	N_x=256 M_t=320
0.4	$1.6392e-03$	$5.9534e-04$	$2.1451e-04$	$7.7025e-05$	$2.7556e-05$
	1.46142	1.4727	1.4776	1.4830	-
CPU Time	0.0776	0.1144	0.4828	3.2591	25.1628
0.6	$4.5193e-03$	$1.7498e-03$	$6.7151e-04$	$2.5688e-04$	$9.8051e-05$
	1.3689	1.3817	1.3863	1.3895	-
CPU Time	0.06730	0.1142	0.4647	3.2404	24.9058
0.8	$1.2096e-02$	$5.4119e-03$	$2.3959e-03$	$1.0545e-03$	$4.6247e-04$
	1.1603	1.1756	1.1840	1.1891	-
CPU Time	0.0678	0.1132	0.4835	3.2275	24.8066
0.95	$2.4003e-02$	$1.1951e-02$	$5.8852e-03$	$2.8796e-03$	$1.4033e-03$
	1.0061	1.0220	1.0312	1.0370	-
CPU Time	0.0662	0.1114	0.4828	3.2591	24.9153

Table 5.5: Pointwise errors, CPU time (in sec.), and orders of convergence in space for Example 5.6.2 taking $q = 3$, $\mu_1 = \mu_2 = 1$

	N_x				
α	16	32	64	128	256
0.4	$1.3322e-05$	$8.3713e-07$	$5.2285e-08$	$3.2673e-09$	$2.0420e-10$
	3.9922	4.0010	4.0002	4.0000	-
CPU Time	1.2757	2.4868	4.9491	9.6267	19.5583
0.6	$1.2194e-05$	$7.6523e-07$	$4.7795e-08$	$2.9872e-09$	$1.8671e-10$
	3.9941	4.0010	4.000	3.9999	-
CPU Time	1.2747	2.4904	4.9083	9.7121	19.5783
0.8	$1.0996e-05$	$6.8916e-07$	$4.3044e-08$	$2.6912e-09$	$1.6818e-10$
	3.9960	4.0010	3.9995	4.0002	-
CPU Time	1.3470	2.6052	5.2264	10.7367	21.7518
0.95	$1.0070e-05$	$8.2341e-07$	$5.9205e-08$	$3.8047e-09$	$2.4250e-10$
	3.6123	3.7978	3.9599	3.9717	-
CPU Time	1.2863	2.5494	5.2532	10.6452	21.4630

Table 5.6: $\mathcal{E}^{N_x,M_t}$, d^{N_x,M_t}, and CPU time (in sec.) for Example 5.6.2 taking $\alpha = 0.75$, and $\mu_1 = \mu_2 = 1$ and different values of q

q	N_x=16 M_t=20	N_x=32 M_t=40	N_x=64 M_t=80	N_x=128 M_t=160	N_x=256 M_t=320
2	$5.6723e-03$	$2.4734e-03$	$1.0628e-03$	$4.5410e-04$	$1.9305e-04$
	1.1974	1.2186	1.2268	1.2340	-
CPU Time	0.1019	0.1159	0.5342	3.5703	28.4285
4	$5.6717e-03$	$2.4748e-03$	$1.0636e-03$	$4.5444e-04$	$1.9319e-04$
	1.1965	1.2184	1.2268	1.2341	-
CPU Time	0.0646	0.1186	0.5323	3.5737	27.6741
5	$5.7242e-03$	$2.4747e-03$	$1.0636e-03$	$4.5445e-04$	$1.9319e-04$
	1.2098	1.2183	1.2268	1.2341	-
CPU Time	0.0862	0.1169	0.4753	3.3195	27.1765

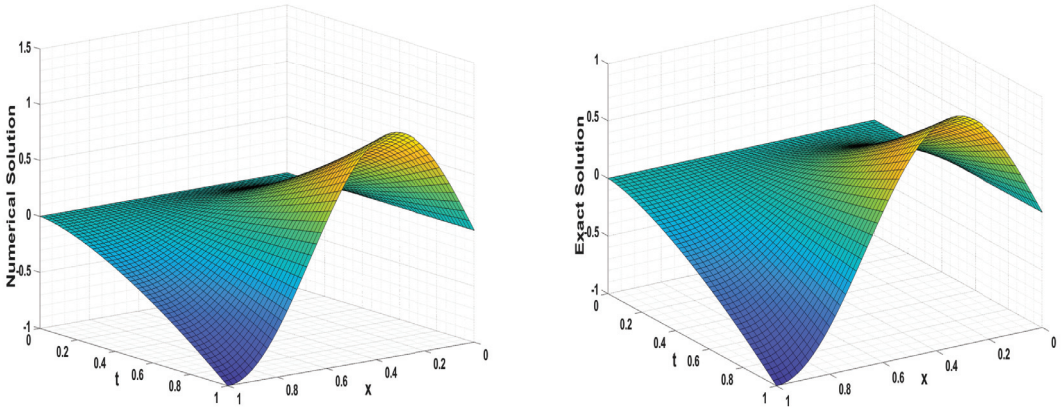

a Numerical solution

b Exact solution

Figure 4: Surface plots of exact and numerical solutions for Example 5.6.2 by taking $N_x = M_t = 50$, $\alpha = 0.8$, $q = 2$, and $\mu_1 = \mu_2 = 1$.

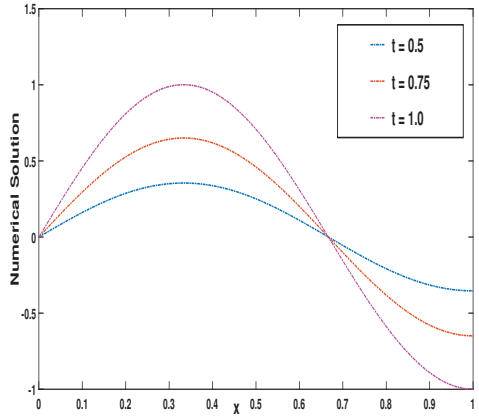

a Numerical solution at different time levels

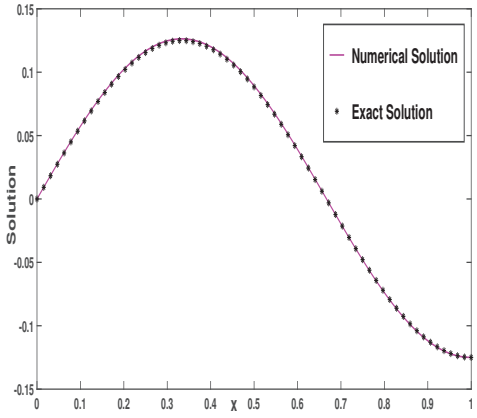

b Exact and numerical solution at $t = 0.25$

Figure 5: Plots of exact and numerical solutions for Example 5.6.2 by taking $N_x = M_t = 64$, $\alpha = 0.75$, $q = 2$, and $\mu_1 = \mu_2 = 1$.

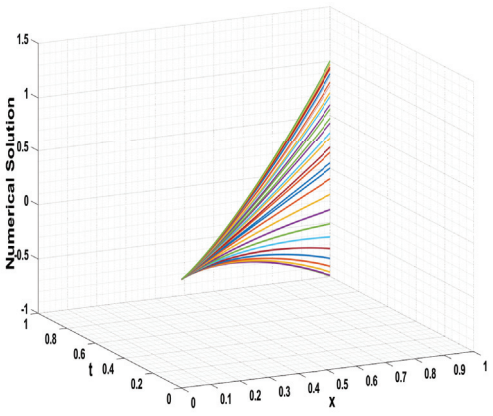

a 3D view of numerical solution

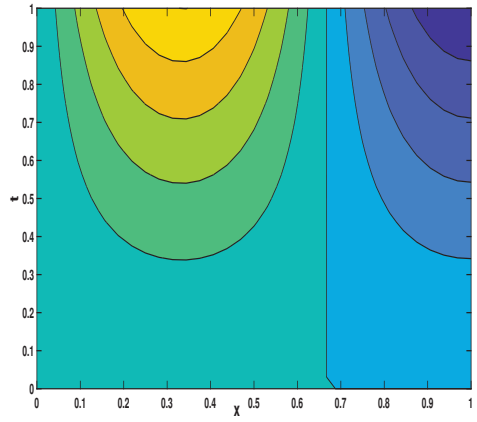

b Contour plot of numerical solution

Figure 6: Plots of numerical solutions for Example 5.6.2 by taking $N_x = M_t = 32$, $\alpha = 0.5$, $q = 2$, and $\mu_1 = \mu_2 = 1$.

Table 5.7: $\mathcal{E}^{N_x,M_t}$, d^{N_x,M_t}, and CPU time (in sec.) for Example 5.6.3 taking $q = 3$, $\mu_1 = \mu_2 = 0.009$

α	N_x=16 M_t=20	N_x=32 M_t=40	N_x=64 M_t=80	N_x=128 M_t=160	N_x=256 M_t=320
0.45	$1.4650e-03$	$5.6737e-04$	$2.2164e-04$	$8.4698e-05$	$3.2081e-05$
	1.3685	1.3561	1.3878	1.4006	-
CPU Time	0.0650	0.1126	0.4852	3.3066	25.2482
0.65	$4.3849e-03$	$1.6841e-03$	$6.7022e-04$	$2.6451e-04$	$1.0421e-04$
	1.3806	1.3293	1.3413	1.3438	-
CPU Time	0.0699	0.1119	0.4833	3.2947	25.6117
0.85	$1.3914e-02$	$6.2904e-03$	$2.8721e-03$	$1.2982e-03$	$5.8602e-04$
	1.1453	1.1310	1.1456	1.1475	-
CPU Time	0.0672	0.1151	0.4752	3.3361	25.2517
0.99	$2.8874e-02$	$1.4412e-02$	$7.2363e-03$	$3.5986e-03$	$1.7883e-03$
	1.0025	0.9939	1.0078	1.0088	-
CPU Time	0.0653	0.1112	0.4876	3.3159	25.3494

Table 5.8: Pointwise errors, CPU time (in sec.), and orders of convergence in space for Example 5.6.3 taking $q = 3$, and $\mu_1 = \mu_2 = 0.009$

	N_x				
α	16	32	64	128	256
0.45	$2.1570e-04$	$1.3307e-05$	$8.3738e-07$	$5.2292e-08$	$3.2676e-09$
	4.0188	3.9902	4.0012	4.0003	-
CPU Time	1.2697	2.4921	4.9558	9.8184	19.7032
0.65	$1.8678e-04$	$1.1524e-05$	$7.2429e-07$	$4.5230e-08$	$2.8269e-09$
	4.0186	3.9919	4.0012	4.0000	-
CPU Time	1.2981	2.5283	4.9520	9.7569	19.8107
0.85	$1.5596e-04$	$9.6220e-06$	$6.0412e-07$	$3.7726e-08$	$2.3586e-09$
	4.0187	3.9934	4.0012	3.9996	-
CPU Time	1.2946	2.5006	4.9340	9.7830	19.5258
0.99	$1.3445e-04$	$8.2950e-06$	$5.2048e-07$	$3.2503e-08$	$2.0324e-09$
	4.0187	3.9943	4.0012	3.9993	-
CPU Time	1.2833	2.5185	4.9685	9.6940	19.8018

Table 5.9: $\mathcal{E}^{N_x,M_t}$, d^{N_x,M_t}, and CPU time (in sec.) for Example 5.6.3 taking $\alpha = 0.75$, $\mu_1 = \mu_2 = 0.009$

q	N_x=16 M_t=20	N_x=32 M_t=40	N_x=64 M_t=80	N_x=128 M_t=160	N_x=256 M_t=320
2	$7.9444e-03$	$3.3151e-03$	$1.4104e-03$	$5.9474e-04$	$2.5052e-04$
	1.2609	1.2329	1.2458	1.2473	-
CPU Time	0.0595	0.1011	0.4597	3.2133	25.0561
4	$7.9663e-03$	$3.3220e-03$	$1.4127e-03$	$5.9549e-04$	$2.5078e-04$
	1.2619	1.2336	1.2463	1.2477	-
CPU Time	0.0546	0.1043	0.4567	3.2333	24.9164
5	$7.9299e-03$	$3.3212e-03$	$1.4166e-03$	$5.9828e-04$	$2.5226e-04$
	1.2556	1.2293	1.2435	1.2459	-
CPU Time	0.0594	0.1066	0.4760	3.2565	24.9839

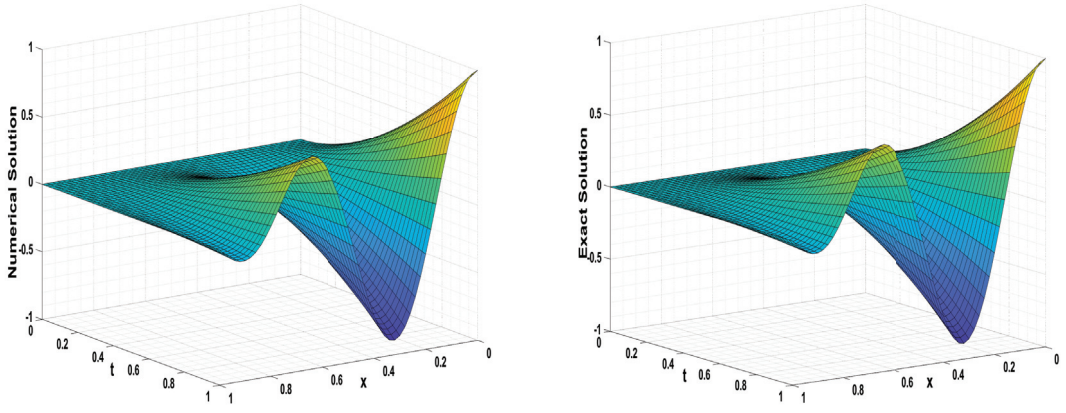

a Numerical solution

b Exact solution

Figure 7: Surface plots of exact and numerical solutions for Example 5.6.3 by taking $N_x = M_t = 50$, $\alpha = 0.8$, $q = 2$, and $\mu_1 = \mu_2 = 1$.

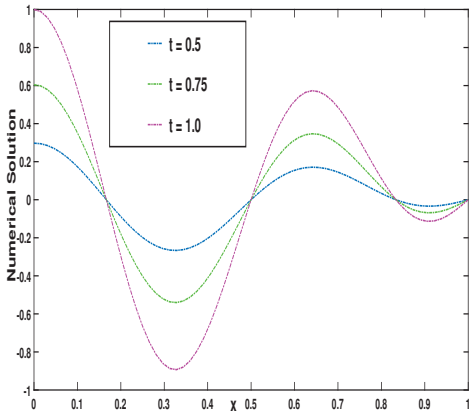

a Numerical solution at different time levels

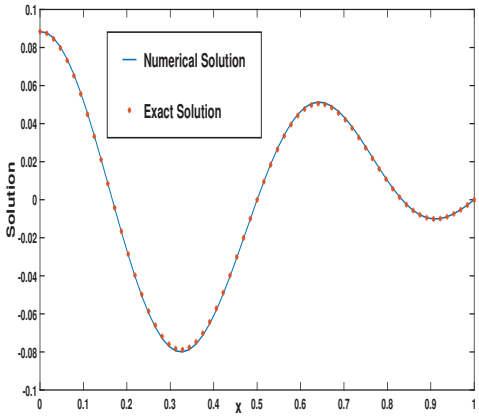

b Exact and numerical solution at $t = 0.25$

Figure 8: Plots of exact and numerical solutions for Example 5.6.3 by taking $N_x = M_t = 64$, $\alpha = 0.75$, $q = 2$, and $\mu_1 = \mu_2 = 1$.

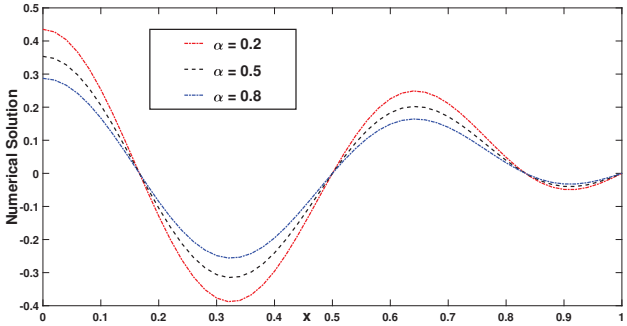

Figure 9: Plots of numerical solution of Example 5.6.3 for different values of α by taking $N_x = M_t = 50$, $q = 2$, and $\mu_1 = \mu_2 = 1$.

Chapter 6

A numerical method for solving the fractional-order predator-prey model

6.1 Introduction

This chapter explores the Predictor-Corrector Method (PCM) to solve a nonlinear two-dimensional fractional-order predator-prey model with carrying capacity. The derivative of fractional order abodes the modified Atangana-Baleanu fractional derivative of Caputo sense (MABC derivative). Due to the smoothness and fast implementation, PCM is advantageous over other methods. The computational outcomes match with two methods, the homotopy perturbation Sumudu transform method (HPSTM) and the homotopy analysis Sumudu transform method (HASTM), presented by Srivastava *et al.* in [1]. The computational results are drawn graphically for different values of derivatives to illustrate the variations of carnivore and chased populations.

6.2 Literature survey

In both ecology and biology, the dynamics of relationships between species are heavily entwined. A predator is a species that consumes another species, and the species that is eaten is referred to as prey. Bear and fish, tiger and cow, snake and mice, leopard and fox, fox and rabbit, and more animals are examples of predator and prey species. The terms ”predator”

and ”prey” are almost often used to refer to solely carnivorous animals. The same vision also includes many plant species at the same time, such as a bear and a fruit, a grasshopper and a leaf, a rabbit and a carrot, etc. Newly numerous mathematicians explain these relations with the help of modeling, bringing into report the populations of species and ecosystem situations that have evolved the increasing issue of analysis in diverse domains, particularly biology. The Lotka-Volterra equation, developed in biological mathematics [211, 212], plays a crucial part in creating a model for the population growth of biological organisms. It has been determined that these equations, which include the interspecific rival, are necessary for those involved in biology. These equations once more aid in understanding the effects of competitive relationships between distinct species; see [213–216]. Freedman [217] studied the famous classical model for predator-prey population and delivered it with the help of the Gaussian system. Recent research by Raw *et al.* [218] examined the effects of movement within the head predator species population and the defense mechanism of a prey species. In recent years, numerous scholars have published theoretical studies in biology and numerical studies in mathematics on these dynamics (refer to [15, 219–221]).

To solve time-fractional problems, several scholars have employed the ABC derivative. Akgul and Modanli have studied a third-order fractional differential equation with ABC derivative [222]. Later, using the Atangana-Baleanu derivative to solve the advection-diffusion equation, Tajadodi [223] proposed an approximation method based on Bernstein polynomials. Additionally, several real-world issues with the ABC derivative have been outlined by Bas and Ozarslan [224] and Gao *et al.* [225], where the macroeconomic model integrating ABC fractional derivatives was looked into before the viral infection models for AIDS and Zika were researched. However, after reading these articles, we learned that the ABC derivative has a nonsingular kernel that we initialize problems with. For more information, see [226]. Therefore, our research uses the MABC derivative mentioned in [39].

In this chapter, we suppose a system of equations of fractional order with carrying capacity K_1[1]

$$ {}^{MABC}D_0^{\gamma}\omega(t) = \omega(t)\left(\alpha_1 - \frac{\alpha_1}{K_1}\omega(t)\right) - \beta_1\omega(t)\phi(t), \tag{6.2.1a} $$

$$ {}^{MABC}D_0^{\gamma}\phi(t) = \phi(t)(-\alpha_2 + \beta_2\omega(t)),\ t > 0, \tag{6.2.1b} $$

with the initial-conditions

$$\omega(0) = \mu_1, \ \phi(0) = \mu_2. \tag{6.2.1c}$$

Here ${}^{MABC}D_0^{\gamma}$ symbolizes the modified Atanagana-Baleanu fractional derivative of order γ in the Caputo sense; $0 < \gamma \leq 1$, and α_1, α_2, K_1, β_1, β_2, μ_1, μ_2 are positive constants. The table provided in this document, namely Table 6.1, presents the physical interpretations of the parameters and variables used in (6.2.1).

Table 6.1: The variables and parameters considered in the problem (6.2.1)

Variables/Parameter	Description
$\omega(t)$	The density of the prey population
$\phi(t)$	The density of the predator population
α_1	Prey's intrinsic growth
α_2	Predator's growth rate
K_1	Carrying capacity
β_1	Positive competition coefficient
β_2	Positive competition coefficient

Only a few numerical schemes are available for [1], and there is no study where this model was examined by the Predictor-Corrector method (PCM). This approach has established efficiency in numerous practical applications [227–230]. To the best of our knowledge, to analyze a two-dimensional, fractional-order predator-prey system with carrying capacity K_1, we use the PCM for the first time in this wor. Fractional-order nonlinear differential equations characterize the model under consideration. The strengths of the predator-prey model presented in this study may be apprehended during this examination. This chapter explores the Predictor-Corrector Method (PCM) to solve a The primary objective of this study is to provide the PCM solution for the mathematical model represented by equation (6.2.1). The equation (6.2.1) was previously solved using the homotopy perturbation Sumudu transform method (HPSTM) [1], which offers a semi-analytical solution. The reproducing kernel Hilbert space method (RKHSM) [231] also was used. The authors of [232] have presented a novel approach in their study, wherein they propose using a fractional Bernstein series solution form to address the fractional-order biological population model that incorporates a carrying capacity.

6.3 Preliminaries

Definition 6.3.1. *Let* $f_1(t),\ f_2(t) : \mathbb{R} \longrightarrow \mathbb{R}$ *are integrable functions, then their Laplace convolution is given by*

$$(f_1 * f_2)(t) = \int_0^t f_1(t-s) f_2(s) ds,\ t > 0.$$

Definition 6.3.2. *The modified Atangana-Baleanu fractional integral of order* $\gamma \in (n-1, n),\ n \in \mathbb{N}$ *is determined for* $\omega(t) \in L^1(0,T)$ *and given by*

$${}^{MAB}I_0^{\gamma}\omega(t) = \frac{1-\delta}{N(\delta)}\left[{}^{RL}I_0^{n-1}\omega(t) + \frac{\delta}{1-\delta}{}^{RL}I_0^{\delta+n-1}\omega(t) - \omega(0)\left(\frac{t^{n-1}}{\Gamma(n)} + \frac{\delta}{1-\delta}\frac{t^{n+\delta-1}}{\Gamma(n+\delta)}\right)\right]$$

where $\gamma = \delta + n - 1$.

When $n = 1$

$${}^{MAB}I_0^{\gamma}\omega(t) = \frac{1-\gamma}{N(\gamma)}\left[\omega(t) + \frac{\gamma}{1-\gamma}{}^{RL}I_0^{\gamma}\omega(t) - \omega(0)\left(1 + \frac{\gamma}{1-\gamma}\frac{t^{\gamma}}{\Gamma(\gamma+1)}\right)\right]$$

Lemma 6.3.1. *[39] If* $\omega^{(n)}(t) \in L^1(0,\infty)$*, and* $\gamma \in (n-1, n),\ n \in \mathbb{N}$*;* $\gamma = \delta + n - 1$*. The following equality holds*

$${}^{MAB}I_0^{\gamma}{}^{MABC}D_0^{\gamma}\omega(t) = \omega(t) - \sum_{k=0}^{n-1}\omega^{(k)}(t)\frac{t^k}{k!},$$

$${}^{MABC}D_0^{\gamma}{}^{MAB}I_0^{\gamma}\omega(t) = \omega(t) - \omega(0).$$

When $n = 1$

$${}^{MAB}I_0^{\gamma}{}^{MABC}D_0^{\gamma}\omega(t) = \omega(t) - \omega(0),$$

$${}^{MABC}D_0^{\gamma}{}^{MAB}I_0^{\gamma}\omega(t) = \omega(t) - \omega(0).$$

6.4 Equilibrium Point Stability

To the stability of the system (6.2.1), it is sufficient to examine the stability of equilibrium points of the system (6.2.1). To see the equilibrium points of the system of fractional order, let

$$\omega(t)\left(\alpha_1 - \frac{\alpha_1}{K_1}\omega(t)\right) - \beta_1\omega(t)\phi(t) = 0, \tag{6.4.1}$$

$$\phi(t)(-\alpha_2 + \beta_2\omega(t)) = 0. \tag{6.4.2}$$

From (6.4.1) and (6.4.2) equilibrium points of system (6.2.1) are $E_1^* = (0,0)$, $E_2^* = (K_1, 0)$, and $E_3^* = \left(\frac{\alpha_2}{\beta_2}, \frac{\alpha_1}{\beta_1}\left(1 - \frac{\alpha_2}{K_1\beta_2}\right)\right)$. Let us examine the stability of the system (6.2.1) at the trivial equilibrium point $E_1^* = (0,0)$. Thus, the variational matrix at trivial equilibrium point $E_1^* = (0,0)$ is

$$A_1 = \begin{bmatrix} \alpha_1 & 0 \\ 0 & -\alpha_2 \end{bmatrix},$$

eigenvalues of A_1 are $\lambda_1(E_1^*) = \alpha_1$ and $\lambda_2(E_1^*) = -\alpha_2$ here $\lambda_1(E_1^*)$ is positive eigenvalue of A_1. Therefore, from Routh-Hurwitz conditions [233, 234] trivial equilibrium point $E_1^* = (0,0)$ is unstable.

Next, we examine the stability of the model (6.2.1) at the equilibrium point $E_2^* = (K_1, 0)$. Thus, the variational matrix at equilibrium point $E_2^* = (K_1, 0)$ is

$$A_2 = \begin{bmatrix} -\alpha_1 & -\beta_1 K_1 \\ 0 & K_1\beta_2 - \alpha_2 \end{bmatrix},$$

eigenvalues of A_2 are $\lambda_1(E_2^*) = -\alpha_1$ and $\lambda_2(E_2^*) = K_1\beta_2 - \alpha_2$ here $\lambda_1(E_2^*)$ is negative eigenvalue of A_1 and $\lambda_2(E_2^*) = K_1\beta_2 - \alpha_2$ is negative if $K_1\beta_2 \leq \alpha_2$. Therefore, from Routh-Hurwitz conditions [233, 234] equilibrium point $E_1^* = (0,0)$ is stable for system (6.2.1) if and only if $K_1\beta_2 \leq \alpha_2$.

Successively, we analyze the stability of the model (6.2.1) at the equilibrium point

$E_3^* = \left(\frac{\alpha_2}{\beta_2}, \frac{\alpha_1}{\beta_1}\left(1 - \frac{\alpha_2}{K_1\beta_2}\right)\right)$. Therefore, the variational matrix at equilibrium point E_3^* is

$$A_3 = \begin{bmatrix} \frac{-\alpha_1\alpha_2}{K_1\beta_2} & \frac{-\beta_1\alpha_2}{\beta_2} \\ \frac{\beta_2\alpha_1}{\beta_1} - \frac{\alpha_1\alpha_2}{K_1\beta_1} & 0 \end{bmatrix},$$

the eigenvalues of this matrix, delivered by the algebraic equation

$$det(A_3 - \lambda I) = \lambda^2 + \lambda\left(\frac{\alpha_1\alpha_2}{K_1\beta_2}\right) + \left(\alpha_1\alpha_2 - \frac{\alpha_1\alpha_2^2}{K_1\beta_2}\right) = 0,$$

are

$$\lambda_{1,2}(E_3^*) = \frac{-\frac{\alpha_1\alpha_2}{K_1\beta_2} \pm \sqrt{\left(\frac{\alpha_1\alpha_2}{K_1\beta_2}\right)^2 - 4\left(\alpha_1\alpha_2 - \frac{\alpha_1\alpha_2^2}{K_1\beta_2}\right)}}{2},$$

as α_1, α_2, K_1 and β_2 all are positive constants. When

$$\left(\frac{\alpha_1\alpha_2}{K_1\beta_2}\right)^2 - 4\left(\alpha_1\alpha_2 - \frac{\alpha_1\alpha_2^2}{K_1\beta_2}\right) \geq 0,$$

then

$$\left|\frac{\alpha_1\alpha_2}{K_1\beta_2}\right|^2 > \left(\frac{\alpha_1\alpha_2}{K_1\beta_2}\right)^2 - 4\left(\alpha_1\alpha_2 - \frac{\alpha_1\alpha_2^2}{K_1\beta_2}\right) \geq 0,$$

so the eigenvalues $\lambda_{1,2}(E_3^*)$ are negative, which suggests that the solution $\omega(t) = 0$, $\phi(t) = 0$ corresponding to the equilibrium point E_3^* is globally asymptotically stable.

When

$$\left(\frac{\alpha_1\alpha_2}{K_1\beta_2}\right)^2 - 4\left(\alpha_1\alpha_2 - \frac{\alpha_1\alpha_2^2}{K_1\beta_2}\right) \leq 0,$$

then, the eigenvalues $\lambda_{1,2}(E_3^*)$ has a negative real part, which suggests that the solution $\omega(t) = 0$, $\phi(t) = 0$ corresponding to the equilibrium point E_3^* is globally asymptotically stable.

6.5 An explanation of the technique

In this province, we suggest the Predictor-Corrector method to obtain the approximate solution of the two-dimensional predator-prey system of fractional order (6.2.1). To apply the predictor-corrector method, we first discretize the time interval $[0, T]$ into N subintervals with the use

of equidistance mesh $h = \frac{T}{N}$. Let $\Pi = \{t_j | j = 0, 1, 2, \ldots, N\}$ be the partition of the interval $[0, T]$ and x_j be the approximation of $x(t_j)$ *i.e.,* $x_j \approx x(t_j)$. Furthermore, let x_j^i represent the approximation $x(t_j)$ after i corrector actions, where $x(t_j)$ is the solution at t_j of the general initial value problem as pursued. Then

$$^{MABC}D_0^{\gamma} x(t) = F(t, x(t)),\ x(0) = x_0,\ 0 < \gamma \leq 1,\ 0 < t \leq T,$$

gives

$$\begin{aligned} x(t) &= x_0 + {}^{MABC}I_0^{\gamma} F(t, x(t)) \\ &= x_0 + \frac{1-\gamma}{N(\gamma)}\left[F(t, x(t)) + \frac{\gamma}{1-\gamma}\,{}^{RL}I_0^{\gamma} F(t, x(t)) - F(0, x_0)\left(1 + \frac{\gamma}{1-\gamma}\frac{t^{\gamma}}{\Gamma(\gamma+1)}\right)\right] \\ &= x_0 + \frac{1-\gamma}{N(\gamma)}\left[F(t, x(t)) + \frac{\gamma}{1-\gamma}\frac{1}{\Gamma(\gamma)}\int_0^t (t-s)^{\gamma-1} F(s, x(s))\, ds\right. \\ &\quad \left. - F(0, x_0)\left(1 + \frac{\gamma}{1-\gamma}\frac{t^{\gamma}}{\Gamma(\gamma+1)}\right)\right]. \end{aligned} \tag{6.5.1}$$

Therefore, the execution of corrector iterations for Predictor-Corrector is explained as follows:

$$\begin{aligned} x_{j+1}^i = x_0 + \frac{1-\gamma}{N(\gamma)}&\left[F(t_{j+1}, x_{j+1}^{i-1}) + \frac{\gamma}{1-\gamma}\frac{h^{\gamma}}{\Gamma(\gamma+2)}\left\{\sum_{k=0}^{j} \mu_{k,j+1} F(t_k, x_k^i) + F\left(t_{j+1}, x_{j+1}^{i-1}\right)\right.\right. \\ &\left.\left. - F(0, x_0)\left(1 + \frac{\gamma}{1-\gamma}\frac{t_{j+1}^{\gamma}}{\Gamma(\gamma+1)}\right)\right\}\right],\ (i = 1, 2, \ldots, Q), \end{aligned} \tag{6.5.2}$$

$$\begin{aligned} x_{j+1}^0 := x_{j+1}^P = x_0 + \frac{1-\gamma}{N(\gamma)}&\left[F(t_{j+1}, x_j) + \frac{\gamma}{1-\gamma}\frac{h^{\gamma}}{\Gamma(\gamma+2)}\left\{\sum_{k=0}^{j} \nu_{k,j+1} F(t_k, x_k)\right.\right. \\ &\left.\left. - F(0, x_0)\left(1 + \frac{\gamma}{1-\gamma}\frac{t_{j+1}^{\gamma}}{\Gamma(\gamma+1)}\right)\right\}\right], \end{aligned} \tag{6.5.3}$$

where

$$\mu_{k,j+1} = \begin{cases} j^{\gamma+1} - (j-\gamma)(j+1)^{\gamma}, & \text{if } k = 0, \\ (j-k+2)^{\gamma+1} + (j-k)^{\gamma+1} - 2(j-k+1)^{\gamma+1}, & \text{if } 1 \leq k \leq j, \\ 1, & \text{if } k = j+1, \end{cases} \tag{6.5.4}$$

and

$$\nu_{k,j+1} = (j+1-k)^{\gamma} - (j-k)^{\gamma},\ 0 \le k \le j. \tag{6.5.5}$$

Here, $x^0_{j+1} := x^P_{j+1}$ is predictor approximation and x^Q_{j+1} is the final approximation.

Theorem 6.5.1. *[235] If* $0 < \gamma < 1$ *and* $x \in C^2[0,T]$. *Then the approximation calculated by the method (6.5.2) and (6.5.3) pleasures*

$$\max_{0\le j\le N} |x(t_j) - x_j| = O(h^M),$$

where $M = \min\{2, 1+Q\gamma\}$.

Now, we execute this method for the fractional order system (6.2.1). We have

$$\begin{aligned}
\omega^i_{j+1} &= \mu_1 + \frac{1-\gamma}{N(\gamma)}\Bigg[\omega^{i-1}_{j+1}\left(\alpha_1 - \frac{\alpha_1}{K_1}\omega^{i-1}_{j+1}\right) - \beta_1\omega^{i-1}_{j+1}\phi^{i-1}_{j+1} \\
&\quad + \frac{\gamma}{1-\gamma}\frac{h^\gamma}{\Gamma(\gamma+2)}\Bigg\{\sum_{k=0}^{j}\mu_{k,j+1}\left(\omega^i_k\left(\alpha_1 - \frac{\alpha_1}{K_1}\omega^i_k\right) - \beta_1\omega^i_k\phi^i_k\right) + \omega^{i-1}_{j+1}\left(\alpha_1 - \frac{\alpha_1}{K_1}\omega^{i-1}_{j+1}\right) \\
&\quad - \beta_1\omega^{i-1}_{j+1}\phi^{i-1}_{j+1} - \left(\mu_1\left(\alpha_1 - \frac{\alpha_1}{K_1}\mu_1\right) - \beta_1\mu_1\mu_2\right)\left(1 + \frac{\gamma}{1-\gamma}\frac{t^\gamma_{j+1}}{\Gamma(\gamma+1)}\right)\Bigg\}\Bigg], \\
\phi^i_{j+1} &= \mu_2 + \frac{1-\gamma}{N(\gamma)}\Bigg[\phi^{i-1}_{j+1}(-\alpha_2 + \beta_2\omega^{i-1}_{j+1}) \\
&\quad + \frac{\gamma}{1-\gamma}\frac{h^\gamma}{\Gamma(\gamma+2)}\Bigg\{\sum_{k=0}^{j}\mu_{k,j+1}\left(\phi^i_k(-\alpha_2 + \beta_2\omega^i_k)\right) + \phi^{i-1}_{j+1}(-\alpha_2 + \beta_2\omega^{i-1}_{j+1}) \\
&\quad - (\mu_2(-\alpha_2 + \beta_2\mu_1))\left(1 + \frac{\gamma}{1-\gamma}\frac{t^\gamma_{j+1}}{\Gamma(\gamma+1)}\right)\Bigg\}\Bigg],
\end{aligned}$$

where

$$\begin{aligned}
\omega^0_{j+1} &= \mu_1 + \frac{1-\gamma}{N(\gamma)}\Bigg[\omega^0_{j-1}\left(\alpha_1 - \frac{\alpha_1}{K_1}\omega^0_{j-1}\right) - \beta_1\omega^0_{j-1}\phi^0_{j-1} \\
&\quad + \frac{\gamma}{1-\gamma}\frac{h^\gamma}{\Gamma(\gamma+1)}\Bigg\{\sum_{k=0}^{j}\nu_{k,j+1}\left(\omega^0_k\left(\alpha_1 - \frac{\alpha_1}{K_1}\omega^0_k\right) - \beta_1\omega^0_k\phi^0_k\right) \\
&\quad - \left(\mu_1\left(\alpha_1 - \frac{\alpha_1}{K_1}\mu_1\right) - \beta_1\mu_1\mu_2\right)\left(1 + \frac{\gamma}{1-\gamma}\frac{t^\gamma_{j+1}}{\Gamma(\gamma+1)}\right)\Bigg\}\Bigg], \\
\phi^0_{j+1} &= \mu_2 + \frac{1-\gamma}{N(\gamma)}\Bigg[\phi^0_{j-1}(-\alpha_2 + \beta_2\omega^0_{j-1}) + \frac{\gamma}{1-\gamma}\frac{h^\gamma}{\Gamma(\gamma+2)}\Bigg\{\sum_{k=0}^{j}\nu_{k,j+1}\left(\phi^0_k(-\alpha_2 + \beta_2\omega^0_k)\right)
\end{aligned}$$

$$- (\mu_2(-\alpha_2 + \beta_2\mu_1)) \left(1 + \frac{\gamma}{1-\gamma}\frac{t_{j+1}^{\gamma}}{\Gamma(\gamma+1)}\right)\Bigg\}\Bigg],$$

and the coefficients $\mu_{k,j+1}$ and $\nu_{k,j+1}$ are given by equations (6.5.4) and (6.5.5), respectively.

6.6 Numerical discussion and results

In this province, we propose the graphical analysis of the impact of the γ derivative on densities of the prey population density (ω) and predator population density (ϕ) at various times. The numerical investigation of a two-dimensional predator-prey system of fractional order through PCM for different values of the fractional parameter $\gamma = 0.25,\ 0.50,\ 0.75$, and one is carried into account. The numerical results of the population density of prey (ω) and the population density of predator (ϕ) are given in Tables 6.2 and 6.3 at different values of time t. In Figures 1 and 2, the effects of interpretations of parameter γ on predator and prey population density, respectively, have been investigated. Figure 1 clarifies that the prey's population dashingly declines with growing t and decreasing γ. Figure 2 explains that the predator's population nattily grows with growing t and declining γ. Figure 3 illustrates the relations of the predator and prey population for various values of γ concerning time t. In this portion, we carry the dimensionless parameters as $\alpha_1 = \alpha_2 = 5/100$, $\beta_1 = 4/100$, $\beta_2 = 1/100$, $K_1 = 20$, $\mu_1 = 20$, and $\mu_2 = 15$. We can see that plots drowned with the help of PCM match the plots given by HPSTM and HASTM, presented by Srivastava *et al.* in [1].

Table 6.2: Numerical results of the population density of prey

t	$\gamma = 0.25$	$\gamma = 0.50$	$\gamma = 0.75$	$\gamma = 1$
0	20	20	20	20
0.01	16.4234	18.7045	19.5916	19.8803
0.02	15.8669	18.2011	19.3183	19.7612
0.03	15.5120	17.8273	19.0820	19.6427
0.04	15.2470	17.5206	18.8678	19.5248
0.05	15.0340	17.2564	18.6691	19.4075
0.1	14.3318	16.2734	17.8172	18.8298
0.2	13.5720	15.0180	16.4808	17.7182
0.3	13.1037	14.1519	15.4035	16.6636
0.4	12.7622	13.4808	14.4868	15.6644
0.5	12.4925	12.9308	13.6858	14.7188
0.6	12.2695	12.4643	12.9744	13.8249
0.7	12.0792	12.0593	12.3354	12.9807
0.8	11.9132	11.7019	11.7567	12.1842
0.9	11.7660	11.3822	11.2292	11.4334
1.0	11.6338	11.0934	10.7458	10.7263

Table 6.3: Numerical results of the population density of predator

t	$\gamma = 0.25$	$\gamma = 0.50$	$\gamma = 0.75$	$\gamma = 1$
0	15	15	15	15
0.01	15.6342	15.2395	15.0763	15.0224
0.02	15.7241	15.3306	15.1271	15.0447
0.03	15.7798	15.3973	15.1708	15.0668
0.04	15.8204	15.4515	15.2102	15.0888
0.05	15.8524	15.4977	15.2467	15.1107
0.1	15.9539	15.6656	15.4012	15.2177
0.2	16.0553	15.8690	15.6370	15.4210
0.3	16.1129	16.0004	15.8200	15.6101
0.4	16.1521	16.0960	15.9696	15.7852
0.5	16.1813	16.1697	16.0949	15.9469
0.6	16.2042	16.2285	16.2011	16.0953
0.7	16.2228	16.2763	16.2919	16.2311
0.8	16.2382	16.3159	16.3697	16.3546
0.9	16.2513	16.3489	16.4365	16.4663
1.0	16.2625	16.3767	16.4938	16.5666

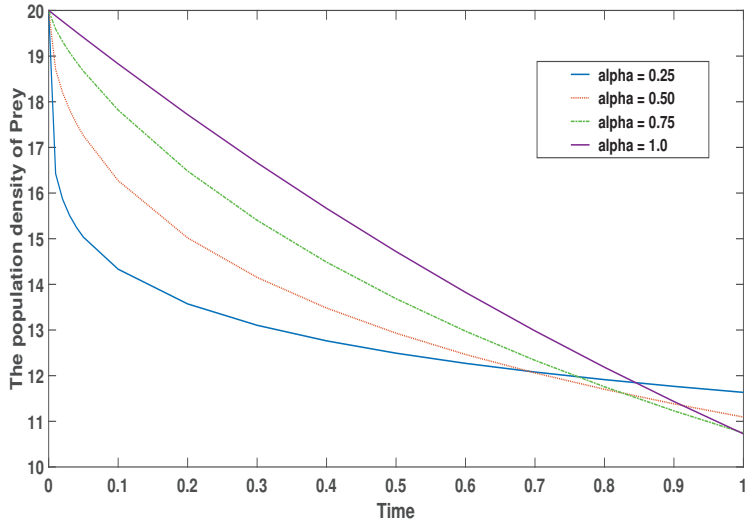

Figure 1: Graphs of Prey population density

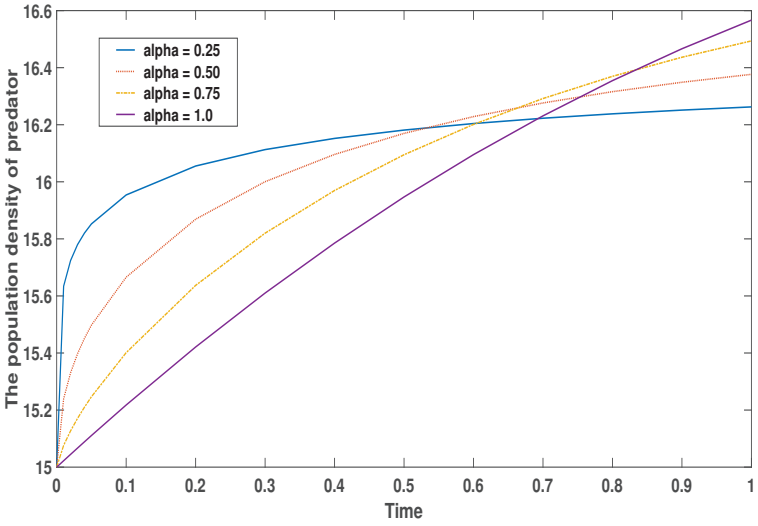

Figure 2: Graphs of Predator population density

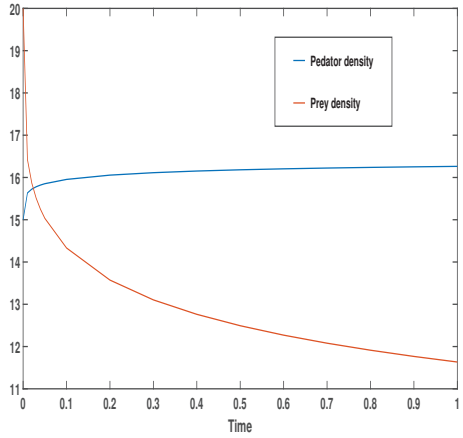

a $\alpha = 0.25$

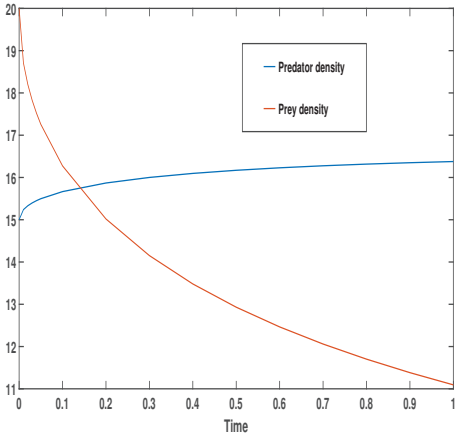

b $\alpha = 0.50$

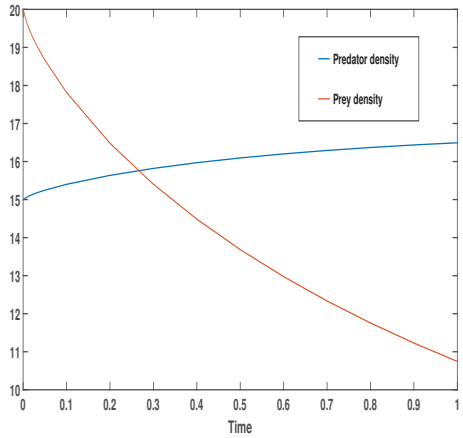

c $\alpha = 0.75$

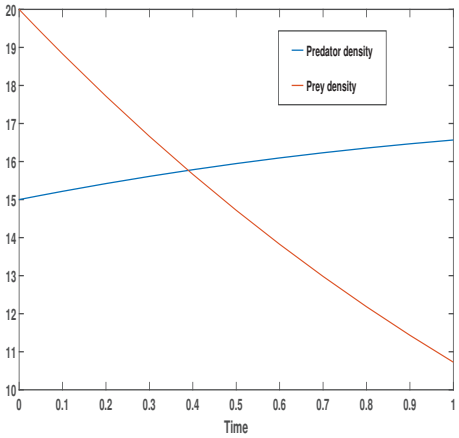

d $\alpha = 1$

Figure 3: Graphs of Prey population density and Predator population density

6.7 Conclusion

In this chapter, we used PCM to analyze the explanations of a nonlinear predator-prey model of fractional order. The derivative of fractional order is taken in the MABC sense. Several graphs are drawn to observe the effect of γ on the prey and predator population density. The comparisons show that the results are aligned with HPSTM and HASTM.

Chapter 7

Conclusion and Future Scopes

This chapter summarizes the conclusions of the research work completed throughout the thesis, emphasizing major points and innovations. Several concepts emerged throughout the current examination that have the potential to expand the study further. We also noted the possibility of subsequent research based on the outcomes of this investigation.

7.1 Description of the Submitted Research

A basic summary of fractional calculus and fraction-order partial differential equations is presented first in this thesis. Then, we come to the numerical solutions of fractional partial differential equations. This thesis aims to create numerical techniques for solving fractional partial differential equations. The stability, convergence, and error estimation of proposed schemes are presented in this work. There are numerical examples given to illustrate our theoretical results.

We covered the fundamentals of fractional calculus in Chapter 1. Some essential characteristics and definitions of fractional derivatives have also been provided. A literature review also contains the most recent discoveries and theoretical and methodological contributions to our research.

In Chapter 2, we propose a numerical technique for TF-DPDEs that combines the Crank-Nicolson scheme and a tension spline. The Caputo fractional derivative is used to discretize

the fractional-order time derivative. The approach is proven to be conditionally stable using Fourier series analysis. Furthermore, careful analysis demonstrates that the approach is second-order convergent for arbitrary acceptable selections of $\alpha\,(\alpha \neq 1/12)$, and β, with $2\alpha + \beta = 1$. Numerical examples illustrate the efficacy and applicability of the proposed strategy. The proposed approach may be extended to nonlinear TF-DPDEs and systems of FPDEs.

In Chapter 3, we suggested a highly accurate numerical approximation for the Caputo-type time-fractional fourth-order nonlinear KS problem, supported by multiple experimental data. The current $L1-2$ temporal approximation gives a higher precision in time at the exact computing cost as the $L1$ temporal approximation. The space derivatives are approximated using quintic $\mathfrak{B}$-spline polynomials to preserve quadratic convergence in space. The current method may also be applied to linear problems and Burgers equations, resulting in fourth-order precision in space. We have offered a concrete convergence analysis to support our theory and experimental data.

Chapter 4 describes a numerical methodology for time-fractional ACE that combines the Crank-Nicolson method with cubic B-splines. We employ consistent meshes in both directions to discretize the problem. By extensive examination, we demonstrated that the proposed technique is conditionally stable and produces good results for $\gamma \geq \log_3(3/2)$ and second-order convergent in all directions. Even though the L_2--norm is employed for error computation, error estimates are provided for the L_2 and L_∞ norms. The cubic B-spline approach is based on computational results. The cubic B-spline technique could not solve higher-order fractional partial differential equations.

Chapter 5 proposes a higher-order numerical approach in spatial direction for solving the generalized time-fractional Fisher's equation that requires much less computing time. The usual Euler backward approach was used to discretize the time-fractional derivative, whereas CFDS was used in the spatial direction. The numerical approach efficiently solves the GTFFE and delivers correct solutions with low computational error. The graphical findings show that the current method for determining the numerical solution of GTFFE is quite close to the precise solution. The tabular data support the theoretical characteristics of the spatial and temporal order of convergence.

We utilized PCM to investigate the explanations of a nonlinear predator-prey model of fractional order in Chapter 6. In the MABC meaning, the derivative of fractional order is taken. Several graphs are generated to examine the influence of γ on the density of prey and predator populations. The results are consistent with HPSTM and HASTM, according to the comparisons.

7.2 Future scope

We only studied the solution in one spatial dimension in this thesis, but this work might be expanded to two or three dimensions. We also examined the time-fractional partial differential equations; one can also solve space-fractional partial differential equations and time-space fractional partial differential equations using these numerical techniques. One can derive numerical techniques for these problems that will be more accurate. With the PCM method's help, one can numerically solve more fractional derivative models. The PCM method is easy to implement, and one can explore many other techniques for different models given in the literature survey. The author thinks fractional partial differential equations will become more prominent and used in more study domains. Then, by providing high-precision numerical computing tools, this thesis will aid in using and comprehending fractional partial differential equations.

Bibliography

[1] H. M. Srivastava, V. P. Dubey, R. Kumar, J. Singh, D. Kumar, and D. Baleanu. An efficient computational approach for a fractional-order biological population model with carrying capacity. *Chaos Solit. Fractals*, 138:10988, 2020.

[2] K. B. Oldham and J. Spanier. *The Fractional Calculus Theory and Applications of Differentiation and Integration to Arbitrary Order*. Academic Press, New York, 1974.

[3] A. A. Kilbas, H. M. Srivastava, and J. J. Trujillo. *Theory and Applications of Fractional Differential Equations*. North-Holland Mathematics Studies 204, Elsevier Science B.V., Amsterdam, 2006.

[4] C. P. Li and F. Zeng. *Numerical Methods for Fractional Calculus*. CRC Press, New York, 2015.

[5] K. S. Miller and B. Ross. *An Introduction to the Fractional Calculus and Fractional Differential Equations*. John Wiley & Sons, New York, 1993.

[6] I. Podlubny. *Fractional Differential Equations*. Academic Press, San Diego, 1999.

[7] M. Y. Xu and W. C. Tan. Intermediate processes and critical phenomena: theory method and progress of fractional operators and their applications to modern mechanics. *Sci. China Ser. G: Phys. Mech. Astron.*, 49:257–272, 2006.

[8] S. Kumar, A. Kumar, and D. Baleanu. Two analytical methods for time-fractional nonlinear coupled Boussinesq-Burger's equations arise in propagation of shallow water waves. *Nonlinear Dynam.*, 85:699–715, 2016.

[9] M. Dehghan, M. Safarpoor, and M. Abbaszadeh. Two high-order numerical algorithms for solving the multi-term time fractional diffusion-wave equations. *J. Comput. Appl. Math.*, 290:174–195, 2015.

[10] R. Matušů. Application of fractional order calculus to control theory. *Int. J. Math. Model. Methods Appl. Sci.*, 5:1162–1169, 2011.

[11] E. F. D. Koufos and J. J. Nieto. Attractors for fractional differential problems of transition to turbulent flows. *J. Comput. Appl. Math.*, 6:415–427, 2017.

[12] J. Liu, H. Li, and Y. Liu. A new fully discrete finite difference/element approximation for fractional cable equation. *J. Appl. Math. Comput.*, 52:345–361, 2016.

[13] Y. Li and M. Jiang. Spatial-fractional order diffusion filtering. *J. Math. Chem.*, 56: 257–267, 2018.

[14] Y. Li, M. Jiang, and F. Liu. Time fractional super-diffusion model and its application in peak-preserving smoothing. *Chemometr. Intell. Lab.*, 175:13–19, 2018.

[15] R. Choudhary, S. Singh, and D. Kumar. A second-order numerical scheme for the time-fractional partial differential equations with a time delay. *Comp. Appl. Math.*, 41: 114, 2022.

[16] A. Iomin. Fractional evolution in quantum mechanics. *Chaos Solitons Fractals: X*, 1: 100001, 2019.

[17] R. L. Bagley and P. J. Torvik. A theoretical basis for the application of fractional calculus to viscoelasticity. *J. Rheol*, 27:201–210, 1983.

[18] D. Benson, S. Wheatcraft, and M. Meerschaert. Application of a fractional advection-dispersion equation. *Water Resour. Res.*, 36:1403–1412, 2000.

[19] D. A. Benson, R. Schumer, M. M. Meerschaert, and S. W. Wheatcraft. Fractional dispersion, levy motion, and the made tracer tests. *Transp. Porous Media*, 42:211–240, 2001.

[20] A. D. Fitt, A. R. H. Goodwin, K. A. Ronaldson, and W. A. Wakeham. A fractional differential equation for a MEMS viscometer used in the oil industry. *J. Comput. Appl. Math.*, 229:373–381, 2009.

[21] L. Galue, S. L. Kalla, and B. N. Al-Saqabi. Fractional extensions of the temperature field problems in oil strata. *Appl. Math. Comput.*, 186:35–44, 2007.

[22] Y. Hatano and N. Hatano. Dispersive transport of ions in column experiments: An explanation of long-tailed profiles. *Water Resour. Res.*, 34:1027–1033, 1998.

[23] F. Höfling and T. Franosch. Anomalous transport in the crowded world of biological cells. *Rep. Progr. Phys.*, 76:46602, 2013.

[24] J. A. T. Machado. Discrete-time fractional-order controllers. *Fract. Calc. Appl. Anal.*, 4:47–66, 2001.

[25] M. Oeser and S. Freitag. Modeling of materials with fading memory using neural networks. *Int. J. Numer. Meth. Engng.*, 78:843–62, 2009.

[26] M. Raberto, E. Scalas, and F. Mainardi. Waiting-times returns in high frequency financial data: an empirical study. *Phys. A*, 314:749–755, 2002.

[27] E. Scalas, R. Gorenflo, and F. Mainardi. Fractional calculus and continuous-time finance. *Phys. A: Stat. Mech. Appl.*, 284:376–384, 2000.

[28] A. A. M. Arafa, S. Z. Rida, and M. Khalil. The effect of anti-viral drug treatment of human immunodeficiency virus type 1 (HIV-1) described by a fractional order model. *Appl. Math. Model*, 37:2189–2196, 2013.

[29] S. W. Wheatcraft and M. M. Meerschaert. Fractional conservation of mass. *Adv. Water. Resour.*, 31:1377–1381, 2008.

[30] L. Pospisil, M. Hromadova, R. Sokolova, and C. Lanza. Kinetics of radical dimerization. simple evaluation of rate constant from convolution voltammetry and faradaic phase angle data. *Electrochim. Acta*, 300:284–289, 2019.

[31] A. Atangana and N. Bildik. The use of fractional order derivative to predict the groundwater flow. *Math. Probl. Eng.*, 24(54302):6, 2013.

[32] A. Atangana and A. Kilicman. On the generalized mass transport equation to the concept of variable fractional derivative. *Math. Probl. Eng.*, 23(54280):9, 2014.

[33] S. Holm and S. P. Näsholm. A causal and fractional all-frequency wave equation for lossy media. *J. Acoust. Soc. Am.*, 130:2195–2201, 2011.

[34] S. P. Näsholm and S. Holm. Linking multiple relaxation, power-law attenuation, and fractional wave equations. *J. Acoust. Soc. Am.*, 130:3038–3045, 2011.

[35] S. P. Näsholm and S. Holm. On a fractional zener elastic wave equation. *Fract. Calc. Appl. Anal.*, 16:26–50, 2012.

[36] S. P. Näsholm and S. Holm. Comparison of fractional wave equations for power law attenuation in ultrasound and elastography. *Ultrasound Med Biol.*, 40:695–703, 2013.

[37] N. Laskin. Fractional Schrodinger equation. *Phys. Rev. E*, 66:056108, 2002.

[38] M. A. Zaky A. H. Bhrawy. An improved collocation method for multi-dimensional space–time variable-order fractional Schrodinger equations. *Appl. Numer. Math.*, 111: 197–218, 2017.

[39] M. Al-Refai. Proper inverse operators of fractional derivatives with nonsingular kernels. *Rend. Circ. Mat. Palermo*, 2, 2021. doi: 10.1007/s12215-021--00638-2.

[40] S. G. Samko, A. A. Kilbas, and O. I. Marichev. *Fractional Integrals and Derivative: Theory and Applications*. Gordonn and Breach Science Publishers, Yverdon, 1993.

[41] V. Kiryakova. *Generalised Fractional Calculus and Applications*. Pitman Research Notes in Mathematics 301, Longman, London, 1994.

[42] K. Shah, H. Khalil, and R. A. Khan. Investigation of positive solution to a coupled system of impulsive boundary value problems for nonlinear fractional order differential equations. *Chaos Solit. Fractals*, 77:240–246, 2015.

[43] T. A. Biala and S. N. Jator. Block implicit Adams methods for fractional differential equations. *Chaos Solit. Fractals*, 81:365–377, 2015.

[44] S. K. Ntouyas B. Ahmad and A. Alsaedi. On a coupled system of fractional differential equations with coupled nonlocal and integral boundary conditions. *Chaos Solit. Fractals*, 83:234–241, 2016.

[45] A. Atangana and D. Baleanu. New fractional derivatives with nonlocal and non-singular kernel: theory and application to heat transfer model. *Therm Sci.*, 20:763–769, 2016.

[46] M. Caputo and M. Fabrizio. A new definition of fractional derivative without singular kernel. *Progr. Fract. Differ. Appl.*, 1:73–85, 2015.

[47] A. Akgul. A novel method for a fractional derivative with non-local and non-singular kernel. *Chaos Solit. Fractals*, 114:478–82, 2018.

[48] K. B. Oldham. Fractional differential equations in electrochemistry. *Adv. Eng. Softw.*, 41:9–12, 2010.

[49] K. Mathiyalagan and G. Sangeetha. Second-order sliding mode control for nonlinear fractional-order systems. *Appl. Math. Comput.*, 383(12526):4, 2020.

[50] S. Pilipovic, T. M. Atanackovic, B. Stankovic, and D. Zorica. *Fractional Calculus With Applications In Mechanics: Vibrations And Diffusion Processes*. John Wiley Sons, London, 2014.

[51] N. Laskin. Fractional market dynamics. *Phys. A: Stat. Mech. Appl.*, 287:482–492, 2000.

[52] E. Ahmed and A. S. Elgazzar. On fractional order differential equations model for nonlocal epidemics. *Phys. A: Stat. Mech. Appl.*, 379:607–614, 2007.

[53] M. Z. Ullah, A. K. Alzahrani, and D. Baleanu. An efficient numerical technique for a new fractional tuberculosis model with nonsingular derivative operator. *J. Taibah. Univ. Sci.*, 13:1147–1157, 2019.

[54] F. Evirgen and M. Yavuz. An alternative approach for nonlinear optimization problem with Caputo-Fabrizio derivative. *ITM Web Conf.*, 22:01009, 2018.

[55] M. Yavuz. Novel recursive approximation for fractional nonlinear equations within Caputo-Fabrizio operator. *ITM Web Conf.*, 22:01008, 2018.

[56] B. Ghanbari and C. Cattani. On fractional predator and prey models with mutualistic predation including non-local and nonsingular kernels. *Chaos Solit. Fractals*, 136 (10982):3, 2020.

[57] N. H. Sweilam, S. M. AL-Mekhlafi, D. S. Alshomrani, and D. Baleanu. Comparative study for optimal control nonlinear variable-order fractional tumor model. *Chaos Solit. Fractals*, 136:10981, 2020.

[58] J. Danane, K. Allali, and Z. Hammouch. Mathematical analysis of a fractional differential model of HBV infection with antibody immune response. *Chaos Solit. Fractals*, 136(10978):7, 2020.

[59] D. Baleanu, A. Jajarmi, H. Mohammadi, and S. Rezapour. A new study on the mathematical modeling of human liver with Caputo-Fabrizio fractional derivative. *Chaos Solit. Fractals*, 134(10970):5, 2020.

[60] D. Kumar, J. Singh, M. Al Qurashi, and D. Baleanu. A new fractional SIRS-SI malaria disease model with application of vaccines, antimalarial drugs, and spraying. *Adv. Differ. Equ.*, 278, 2019. doi: 10.1186/s13662-019-2199-9.

[61] J. Singh, D. Kumar, and D. Baleanu. A new analysis of fractional fish farm model associated with Mittag-Leffler-type kernel. *Int. J. Biomath.*, 13(20500):10, 2020.

[62] X. J. Yang, M. Abdel-Aty, and C. Cattani. A new general fractional-order derivative with Rabotnov fractional-exponential kernel applied to model the anomalous heat transfer. *Therm Sci.*, 23:1677–1681, 2019.

[63] S. Kumar, R. Kumar, C. Cattani, and B. Samet. Chaotic behaviour of fractional predator-prey dynamical system. *Chaos Solit. Fractals*, 135(10981):1, 2020.

[64] Z. Sun G. Gao and H. Zhang. A new fractional numerical differentiation formula to approximate the Caputo fractional derivative and its applications. *J. Comput. Phys.*, 259:33–50, 2014.

[65] Y. M. Wang. A compact finite difference method for a class of time fractional convection-diffusion-wave equations with variable coefficients. *Numer. Algorithms*, 70 (3):625–651, 2015.

[66] S. B. Yuste and L. Acedo. An explicit finite difference method and a new Von Neumann-type stability analysis for fractional diffusion equations. *SIAM J. Numer. Anal.*, 42(5):1862–1874, 2005.

[67] G. H. Gao, Z. Z. Sun, and Y. N. Zhang. A finite difference scheme for fractional sub-diffusion equations on an unbounded domain using artificial boundary conditions. *J. Comput. Phys.*, 231(7):2865–2879, 2012.

[68] N. H. Sweilam, M. M. Khader, and A. M. Mahdy. Crank-Nicolson finite difference method for solving time-fractional diffusion equation. *J. Fractional Calc. Appl.*, 2(2): 1–9, 2012.

[69] M. Dehghan and M. Abbaszadeh. An efficient technique based on finite difference/finite element method for solution of two-dimensional space/multi-time fractional Bloch–Torrey equations. *Appl. Numer. Math.*, 131:190–206, 2018.

[70] B. Jin, R. Lazarov, Y. Liu, and Z. Zhou. The Galerkin finite element method for a multi-term time-fractional diffusion equation. *J. Comput. Phys.*, 281:825–843, 2015.

[71] Y. Jiang and J. Ma. High-order finite element methods for time-fractional partial differential equations. *J. Comput. Appl. Math.*, 235(11):3285–3290, 2011.

[72] D. Kumar, S. Chaudhary, and V. S. Kumar. Finite element analysis for coupled time-fractional nonlinear diffusion system. *Comput. Math. with Appl.*, 78(6):1919–1936, 2019.

[73] Y. Liu, Y. Du, H. Li, S. He, and W. Gao. Finite difference/finite element method for a nonlinear time-fractional fourth-order reaction–diffusion problem. *Comput. Math. with Appl.*, 70(4):573–591, 2015.

[74] A. Baseri, S. Abbasbandy, and E. Babolian. A collocation method for fractional diffusion equation in a long time with Chebyshev functions. *Appl. Math. Comput.*, 322: 55–65, 2018.

[75] A. Esen, O. Tasbozan, Y. Ucar, and N. M. Yagmurlu. A b-spline collocation method for solving fractional diffusion and fractional diffusion-wave equations. *Tbil. Math. J.*, 8:181–193, 2015.

[76] A. M. Nagy. Numerical solution of time fractional nonlinear Klein-Gordon equation using Sinc-Chebyshev collocation method. *Appl. Math. Comput.*, 310:139–148, 2017.

[77] F. Zhou and X. Xu. Numerical solution of time-fractional diffusion-wave equations via Chebyshev wavelets collocation method. *Adv. Math. Phys.*, 2017:17, 2017.

[78] A. Pirkhedri and H. H. Javadi. Solving the time-fractional diffusion equation via Sinc-Haar collocation method. *Appl. Math. Comput.*, 257:317–326, 2015.

[79] A. I. Aliyu, M. Inc, A. Yusuf, and D. Baleanu. A fractional model of vertical transmission and cure of vector-borne diseases pertaining to the Atangana-Baleanu fractional derivatives. *Chaos Solit. Fractals*, 116:268–277, 2018.

[80] K. M. Owolabi and A. Atangana. Analysis and application of new fractional Adams-Bashforth scheme with Caputo-Fabrizio derivative. *Chaos Solit. Fractals*, 105:111–119, 2017.

[81] Y. Yan and Ch. Kou. Stability analysis of a fractional differential model of HIV infection of $cd4^+$ t-cells with time delay. *Math. Comput. Simul.*, 82:1572–1585, 2012.

[82] Z. Ouyang. Existence and uniqueness of the solutions for a class of nonlinear fractional order partial differential equations with delay. *Comput. Math. Appl.*, 61:860–870, 2011.

[83] Y. Zhou, F. Jiao, and J. Li. Existence and uniqueness for fractional neutral differential equations with infinite delay. *Nonlinear Anal.*, 71:3249–3256, 2009.

[84] Q. Zhang, M. Ran, and D. Xu. Analysis of the compact difference scheme for the semilinear fractional partial differential equation with time delayl. *Appl. Anal.*, 11: 1867–1884, 2017.

[85] M. Sakara, F. Uludag, and F. Erdogan. Numerical solution of time-fractional nonlinear PDEs with proportional delays by homotopy perturbation method. *Appl. Math. Model*, 40:6639–6649, 2016.

[86] F. Rodriguez, M. Roales, and J. A. Martin. Exact solutions and numerical approximations of mixed problems for the wave equation with delay. *Appl. Math. Comput.*, 219: 3178–3186, 2012.

[87] A. Mohebbi. Finite difference and spectral collocation methods for the solution of semilinear time fractional convection-reaction-diffusion equations with time delay. *J. Appl. Math. Comput.*, 61:635–656, 2019.

[88] S. Nicaise and C. Pignotti. Stability and instability results of the wave equation with a delay term in the boundary or internal feedbacks. *SIAM J. Control Optim.*, 45: 1561–1585, 2006.

[89] M. P. Lazarević and A. M. Spasić. Finite-time stability analysis of fractional order time-delay systems: Gronwall's approach. *Math. Comput. Model*, 49:475–481, 2009.

[90] A. Si-Ammour, S. Djennoune, and M. Bettayeb. A sliding mode control for linear fractional systems with input and state delays. *Commun. Nonlinear Sci. Numer. Simul.*, 14:2310–2318, 2009.

[91] T. Ohira and J. Milton. *Delayed random walks: Investigating the interplay between delay and noise*. Springer-Verlag, Berlin, 2009.

[92] R. V. Culshaw, S. Ruan, and G. Webb. A mathematical model of cell-to-cell spread of HIV-1 that includes a time delay. *J. Math. Biol.*, 46:425–444, 2003.

[93] Z. Hao, K. Fan, W. Cao, and Z. Sun. A finite difference scheme for semilinear space-fractional diffusion equations with time delay. *Appl. Math. Comput.*, 275:238–254, 2016.

[94] A. Bellen and M. Zennaro. Numerical methods for delay differential equations. *Oxford University Press*, 2003.

[95] N. Guglielmi. Open issues in devising software for numerical solution of implicit delay differential equations. *J. Comput. Appl. Math.*, 185:261–277, 2006.

[96] N. Guglielmi and E. Hairer. Computing breaking points of implicit delay differential equations. In Leuven, editor, *Proceedings of 5th IFAC Workshop on Time-Delay Systems*, Belgium, 2004.

[97] N. Guglielmi and E. Hairer. Implementing radau IIA methods for stiff delay differential equations. *Computing*, 67:1–12, 2001.

[98] F. A. Rihan. *Numerical treatment of delay differential equations in bioscience*. PhD thesis, Ph.D. Thesis, University of Manchester, 2000.

[99] T. A. M. Langlands, B. I. Henry, and S. L. Wearne. Fractional cable equation models for anomalous electro-diffusion in nerve cells: finite domain solutions. *SIAM J. Appl. Math.*, 71:1168–1203, 2011.

[100] H. Jiang, F. Liu, I. Turner, and K. Burrage. Analytical solutions for the multi-term time-space Caputo-Riesz fractional advection-diffusion equations on a finite domain. *J. Appl. Math. Anal.*, 389:1117–1127, 2012.

[101] X. L. Ding and Y. L. Jiang. Analytical solutions for the multi-term time-space fractional advection-diffusion equations with mixed boundary conditions. *Nonlinear Anal. Real World Appl.*, 14:1026–1033, 2013.

[102] X. L. Ding and J. J. Nieto. Analytical solutions for the multi-term time-space fractional reaction-diffusion equations on an infinite domain. *Fract. Calc. Appl. Anal.*, 3:697–716, 2015.

[103] X. L. Ding and J. J. Nieto. Analytical solutions for coupling fractional partial differential equations with Dirichlet boundary conditions. *Commun. Nonlinear Sci. Numer. Simul.*, 52:165–176, 2017.

[104] P. Prakash, S. Choudhary, and V. D. Gejji. Exact solutions of generalized nonlinear time-fractional reaction-diffusion equations with time delay. *Eur. Phys. J. Plus.*, 135:490, 2020. URL https://doi.org/10.1140/epjp/s13360-020-00445-1.

[105] J. K. Hale and S. M. Verduyn Lunel. Introduction to functional differential equations. *Springer, New York*, 1993.

[106] U. Küchler and B. Mensch. Langevins stochastic differential equation extended by a time delayed term. *Stoch. stoch. rep.*, 40:23–42, 1992.

[107] V. Lakshmikantham. Theory of fractional functional differential equations. *Nonlinear Anal.*, 69:3337–3343, 2008.

[108] Y. Chen and K. L. Moore. Analytical stability bound for a class of delayed fractional-order dynamic systems. *Nonlinear Dyn.*, 29:191–200, 2002.

[109] W. Deng, C. Li, and J. Lü. Stability analysis of linear fractional differential system with multiple time delays. *Nonlinear Dyn.*, 48:409–416, 2007.

[110] C. Hwang and Y. C. Cheng. A numerical algorithm for stability testing of fractional delay systems. *Automatica*, 42:825–831, 2006.

[111] M. P. Lazarević. Finite time stability analysis of PD^{α} fractional control of robotic time-delay systems. *Mech. Res. Comm.*, 33:269–279, 2006.

[112] F. A. Rihan. Computational methods for delay parabolic and time-fractional partial differential equations. *Numer. Methods Partial Differ. Equ.*, 26:1556–1571, 2009.

[113] H. R. Marzban and H. R. Tabrizidooz. A hybrid approximation method for solving Hutchinson's equation. *Commun. Nonlinear Sci. Numer. Simul.*, 17:100–109, 2012.

[114] D. Li, C. Zhang, and J. Wen. A note on compact finite difference method for reaction-diffusion equations with delay. *Math. Comput. Model.*, 39:1749–1754, 2015.

[115] M. Garrido-Atienza and J. Real. Existence and uniqueness of solutions for delay evolution equations of second order in time. *J. Math. Anal. Appl.*, 283:582–609, 2003.

[116] R. Du, W. R. Cao, and Z. Z. Sun. A compact difference scheme for the fractional diffusion-wave equation. *Appl. Math. Model*, 34:2998–3007, 2010.

[117] T. Li, Q. Zhang, W. Niazi, Y. Xu, and M. Ran. An effective algorithm for delay fractional convection-diffusion wave equation based on reversible exponential recovery method. *IEEE Access*, 7:5554–5563, 2019.

[118] P. Li and C. Dai. Double loops and pitchfork symmetry breaking bifurcations of optical solitons in nonlinear fractional Schrodinger equation with competing cubic-quintic nonlinearities. *Ann. Phys.*, 532(20000):48, 2020.

[119] W. Weng, M. Zhang, G. Zhang, and Z. Yan. Dynamics of fractional N-soliton solutions with anomalous dispersions of integrable fractional higher-order nonlinear Schrodinger equations. *Chaos: An Interdisciplinary Journal of Nonlinear Science*, 32:12311, 2022.

[120] R. Chawla, K. Deswal, and D. Kumar. A new numerical formulation for the generalized time-fractional Benjamin Bona Mohany Burgers' equation. *Int. J. Nonlinear Sci. Numer. Simul.*, 2022. doi: https://doi.org/10.1515/ijnsns-2022-0209.

[121] P. Li, B. A. Malomed, and D. Mihalache. Symmetry-breaking bifurcations and ghost states in the fractional nonlinear Schrodinger equation with a PT-symmetric potential. *Optics Letters*, 46:3267–3270, 2021.

[122] A. P. Hooper and R. Grimshaw. Nonlinear instability at the interface between two viscous fluids. *Phys. Fluids.*, 28:37–45, 1985.

[123] M. A. Johnson and W. R. Perkins. Subharmonic dynamics of wave trains in the Korteweg-de-Vries/Kuramoto-Sivashinsky equation. *Stud. Appl. Math.*, 148:1274–1302, 2022.

[124] R. Conte. *Exact solutions of nonlinear partial differential equations by singularity analysis*. Springer Lecture notes in physics, Berlin, 2003.

[125] Y. Kuramoto. *Chemical Oscillations, Waves, and Turbulence*. Springer-Verlag, Berlin, 1984.

[126] G. Akrivis and Y. S. Smyrlis. Implicit-explicit BDF methods for the KS equation. *Appl. Numer. Math.*, 51:151–169, 2004.

[127] P. Das. An a posteriori based convergence analysis for a nonlinear singularly perturbed system of delay differential equations on an adaptive mesh. *Numer. Algorithms*, 81: 465–487, 2019.

[128] A. Larios and K. Yamazaki. On the well-posedness of an anisotropically-reduced two-dimensional KS equation. *Physica D.*, 411:13256, 2020.

[129] J. Gustafsson and B. Protas. Regularization of the backward-in-time KS equation. *J. Comput. Appl. Math.*, 234:398–406, 2010.

[130] A. V. Coward, D. T. Papageorgiou, Y. S. Smyrlis, and C. Nicosia. Nonlinear stability of oscillatory core-annular flow: a generalized KS equation with time periodic coefficients. *Z. Angew. Math. Phys.*, 46:1–39, 1995.

[131] B. Barker, M. L. Johnson, P. Noble, M. L. Rodrigues, and K. Zumbrun. Nonlinear modulational stability of periodic traveling-wave solutions of the generalized KS equation. *Physica D: Nonlinear Phenomena*, 258:11–46, 2013.

[132] F. Lu, K. K. Lin, and A. J. Chorin. Data-based stochastic model reduction for the KS equation. *Physica D: Nonlinear Phenomena*, 340:46–57, 2017.

[133] S. N. Gomes, S. Kalliadasis, D. T. Papageorgiou, G. A. Pavliotis, and M. Pradas. Controlling roughening processes in the stochastic Kuramoto Sivashinsky equation. *Physica D: Nonlinear Phenomena*, 348:33–43, 2017.

[134] R. C. Mittal and G. Arora. Quintic B-spline collocation method for numerical solution of the KS equation. *Commun. Nonlinear Sci. Numer. Simul.*, 15:2798–2808, 2010.

[135] S. Singh, D. Kumar, and V. Shanthi. Uniformly convergent scheme for fourth-order singularly perturbed convection-diffusion ODE. *Appl. Numer. Math.*, 186:334–357, 2023.

[136] A. H. Khater and R. S. Temsah. Numerical solutions of the generalized KS equation by Chebyshev spectral collocation methods. *Comput. Math. Appl.*, 56:1465–1472, 2008.

[137] J. Rashidinia and M. Jokar. Polynomial scaling functions for numerical solution of generalized KS equation. *Appl. Anal.*, 96:293–306, 2017.

[138] A. Mouloud, H. Fellouah, B. A. Wade, and M. Kessal. Time discretization and stability regions for dissipative-dispersive KS equation arising in turbulent gas flow over laminar liquid. *J. Comput. Appl. Math.*, 330:605–617, 2018.

[139] S. Haq, N. Bibi, T. Nagina, S. I. A. Tirmizi, and M. Usman. Meshless method of lines for the numerical solution of generalized KS equation. *Appl. Math. Comput.*, 217: 2404–2413, 2010.

[140] R. K. Mohanty and D. Kaur. Numerov type variable mesh approximations for 1D unsteady quasi-linear biharmonic problem: application to KS equation. *Numer. Algorithms*, 74:427–459, 2017.

[141] V. K. Srivastava M. Tamsir and R. Jiwari. An algorithm based on exponential modified cubic B-spline differential quadrature method for nonlinear Burgers' equation. *Appl. Math. Comput.*, 290:111–124, 2016.

[142] P. Das and S. Rana. Theoretical prospects of fractional order weakly singular Volterra integro differential equations and their approximations with convergence analysis. *Math. Methods Appl. Sci.*, 44:9419–9440, 2021.

[143] P. Das, S. Rana, and H. Ramos. On the approximate solutions of a class of fractional order nonlinear volterra integro-differential initial value problems and boundary value problems of first kind and their convergence analysis. *J. Comput. Appl. Math.*, 404 (11311):6, 2022.

[144] M. Hosseininia, M. H. Heydari, M. R. Hooshmandasl, G. Maalek, F. M. Ghaini, and Z. Avazzadeh. A numerical method based on the Chebyshev cardinal functions for variable-order fractional version of the fourth-order 2D KS equation. *Math. Methods Appl. Sci.*, 44:1831–1842, 2021.

[145] J. Zhang, J. Lv, J. Huang, and Y. Tang. A fast Euler Maruyama method for Riemann-Liouville stochastic fractional nonlinear differential equations. *Phys. D: Nonlinear Phenomena*, 446:13368, 2023.

[146] S. Saini, P. Das, and S. Kumar. Computational cost reduction for coupled system of multiple scale reaction diffusion problems with mixed type boundary conditions having boundary layers. *Rev. R. Acad. Cienc. Exactas Fisica. Nat. Ser. A Mat. RACSAM*, 117, 2023.

[147] Z. Z. Sun and X. N. Wu. A fully discrete difference scheme for a diffusion-wave system. *Appl. Numer. Math.*, 56:193–209, 2006.

[148] Y. Lin and C. Xu. Finite difference/spectral approximations for the time-fractional diffusion equation. *J. Comput. Phys.*, 225:1552–1553, 2007.

[149] S. G. Rubin and R. A. Graves. *A Cubic spline approximation for problems in fluid mechanics*. Nasa TR R–436, Washington, 1975.

[150] C. de Boor. *A Practical Guide to Splines*. Springer, New York, 2001.

[151] P. M. Prenter. *Splines and Variational Methods*. Wiley, New York, 1975.

[152] P. Roul, V. P. Goura, and R. Agarwal. A new high order numerical approach for a class of nonlinear derivative dependent singular boundary value problems. *Appl. Numer. Math.*, 145:315–341, 2019.

[153] C. A. Hall. On error bounds for spline interpolation. *J. Approx. Theory*, 1:209–218, 1968.

[154] A. Bekir, O. Guner, and A. C. Cevikel. Fractional complex transform and exp-function methods for fractional differential equations. *Abstr. Appl. Anal.*, 8:426–462, 2013.

[155] S. Zhang and H. Q. Zhang. Fractional sub-equation method and its applications to nonlinear fractional PDEs. *Phys. Lett. A*, 375:1069–1073, 2011.

[156] A. Bekir, O. Guner, and O. Unsal. The first integral method for exact solutions of nonlinear fractional differential equations. *J. Comput. Nonlinear Dyn.*, 10:210–221, 2015.

[157] B. Zheng. G'/G-expansion method for solving fractional partial differential equations in the theory of mathematical physics. *Commun. Theor. Phys.*, 58:623–630, 2012.

[158] R. K. Gazizov, A. A. Kasatkin, and S. Y. Lukashcuk. Symmetry properties of fractional diffusion equations. *Phys. Scr.*, T136:014016, 2009.

[159] W. Rui and X. Zhang. Lie symmetries and conservation laws for the time fractional Derrida-Lebowitz-Speer-Spohn equation. *Commun. Nonlinear Sci. Numer. Simul.*, 34: 38–44, 2016.

[160] H. Tariq and G. Akram. New approach for exact solutions of time fractional Cahn-Allen equation and time fractional phi-4 equation. *Physica A*, 2017. doi: http://dx.doi.org/10.1016/j.physa.2016.12.081.

[161] S. M. Allen and J. W. Cahn. A microscopic theory for antiphase boundary motion and its application to antiphase domain coarsening. *Acta Metall.*, 27:1085–1095, 1979.

[162] C. Liu and J. Shen. A phase field model for the mixture of two incompressible fluids and its approximation by a Fourier-spectral method. *Phys. D: Nonlinear Phenom.*, 179: 211–228, 2003.

[163] P. Yue, C. Zhou, J. J. Feng, C. F. Ollivier-Gooch, and H. H. Hu. Phase-field simulations of interfacial dynamics in viscoelastic fluids using finite elements with adaptive meshing. *J. Comput. Phys.*, 219:47–67, 2006.

[164] A. Atangana and A. Akgül. Can transfer function and Bode diagram be obtained from Sumudu transform. *Alex. Eng. J.*, 59:1971–1984, 2020.

[165] A. Esen, N. M. Yagmurlu, and O. Tasbozan. Approximate analytical solution to time-fractional damped Burger and Cahn-Allen equations. *Appl. Math. Inf. Sci.*, 7: 1951–1956, 2013.

[166] F. Tascan and A. Bekir. Travelling wave solutions of the Cahn-Allen equation by using first integral method. *Appl. Math. Comput.*, 207:279–282, 2009.

[167] A. M. Wazwaz. The tanh-coth method for solitons and kink solutions for nonlinear parabolic equations. *Appl. Math. Comput.*, 188:1467–1475, 2007.

[168] H. Jafari, H. Tajadodi, and D. Baleanu. Application of a homogeneous balance method to exact solutions of nonlinear fractional evolution equations. *J. Comput. Nonlinear Dyn.*, 9:2, 2014. URL https://doi.org/10.1115/1.4025770.

[169] S. Zhai, Z. Weng, and X. Feng. Fast explicit operator splitting method and time-step adaptivity for fractional nonlocal Allen-Cahn model. *Appl. Math. Model*, 40: 1315–1324, 2016.

[170] G. Akagi, G. Schimperna, and A. Segatti. Fractional Cahn-Hilliard, Allen-Cahn and porous medium equations. *J. Differ. Equ.*, 261:2935–2985, 2016.

[171] H. Liu, A. Cheng, and H. Wang. A fast Galerkin finite element method for a space-time fractional Allen-Cahn equation. *J. Comput. Appl. Math.*, 368(11248):2, 2020.

[172] C. Huang and M. Stynes. Optimal H^1 spatial convergence of a fully discrete finite element method for the time-fractional Allen-Cahn equation. *Adv. Comput. Math.*, 46, 2020. URL https://doi.org/10.1007/s10444-020-09805-y.

[173] B. Ji, H. L. Liao, and L. Zhang. Simple maximum principle preserving time-stepping methods for time-fractional Allen-Cahn equation. *Adv. Comput. Math.*, 46:37, 2020. URL https://doi.org/10.1007/s10444-020-09782-2.

[174] Z. Liu, X. Li, and J. Huang. Accurate and efficient algorithms with unconditional energy stability for the time fractional Cahn-Hilliard and Allen-Cahn equations. *Numer. Methods Partial Differ. Equ.*, 37:2613–2633, 2021.

[175] T. Hou, T. Tang, and J. Yang. Numerical analysis of fully discretized Crank-Nicolson scheme for fractional-in-space Allen-Cahn equations. *J. Sci. Comput.*, 72:1214–1231, 2017.

[176] M. G. Sakar, O. Saldir, and F. Erdogan. An iterative approximation for time-fractional Cahn-Allen equation with reproducing kernel method. *Comput. Appl. Math.*, 37: 5951–5964, 2018.

[177] H. Liu, A. Cheng, H. Wang, and J. Zhao. Time-fractional Allen-Cahn and Cahn-Hilliard phase-field models and their numerical investigation. *Comput. Math. Appl.*, 76:1876–1892, 2018.

[178] M. Inc, A. Yusuf, A. I. Aliyu, and D. Baleanu. Time-fractional Cahn-Allen and time-fractional Klein-Gordon equations: Lie symmetry analysis, explicit solutions and convergence analysis. *Phys. A*, 493:94–106, 2018.

[179] N. Khalid, M. Abbas, M. K. Iqbal, and D. Baleanu. A numerical investigation of Caputo time fractional Allen-Cahn equation using redefined cubic B-spline functions. *Adv. Differ. Equ.*, 2020:158, 2020. URL `https://doi.org/10.1186/s13662-020-02616-x`.

[180] R. Jiwari. Lagrange interpolation and modified cubic B-spline differential quadrature methods for solving hyperbolic partial differential equations with Dirichlet and Neumann boundary conditions. *Comput. Phys. Commun.*, 193:55–65, 2015.

[181] R. C. Mittal and S. Dahiya. Numerical simulation of three-dimensional telegraphic equation using cubic B-spline differential quadrature method. *Appl. Math. Comput.*, 313:442–452, 2017.

[182] R. C. Mittal and R. K. Jain. Cubic B-splines collocation method for solving nonlinear parabolic partial differential equations with neumann boundary conditions. *Commun. Nonlinear Sci. Numer. Simulat.*, 17:4616–4625, 2012.

[183] H. S. Shukla and M. Tamsir. Extended modified cubic B-spline algorithm for nonlinear Fisher's reaction-diffusion equation. *Alex. Eng. J.*, 55:2871–2879, 2016.

[184] H. Ramos, A. Kaur, and V. Kanwar. Using a cubic B-spline method in conjunction with a one-step optimized hybrid block approach to solve nonlinear partial differential equations. *Comput. Appl. Math.*, pages 41–34, 2022.

[185] R. Jiwari, S. Pandit, and M. E. Koksal. A class of numerical algorithms based on cubic trigonometric B-spline functions for numerical simulation of nonlinear parabolic problems. *Comput. Appl. Math.*, 38:140, 2019. URL https://doi.org/10.1007/s40314-019-0918-1.

[186] M. K. Kadalbajoo and P. Arora. B-spline collocation method for the singular-perturbation problem using artificial viscosity. *Comput. Math. Appl.*, 57:650–663, 2009.

[187] V. E. Tarasov and S. S. Tarasova. Fractional derivatives and integrals: What are they needed for? *Mathematics*, 8:164, 2020.

[188] R. A. Fisher. The wave of advance of advantageous genes. *Ann Eugenics*, 7:353–369, 1937.

[189] A. Majeed, M. Kamran, M. K. Iqbal, and D. Baleanu. Solving time fractional Burger's and Fisher's equations using cubic B-spline approximation method. *Adv. Differ. Equ.*, 175, 2020. URL https://doi.org/10.1186/s13662-020-02619-8.

[190] D. A. Frank. *Diffusion and Heat Exchange in Chemical Kinetics*. Princeton, Princeton University Press, 1955.

[191] H. C. Tuckwell. *Introduction to Theoretical Neurobiology*. Cambridge University Press, Cambridge, 1955.

[192] W. Malfict. Solitary wave solutions of nonlinear wave equations. *Am. J. Phys.*, 60: 650–654, 1992.

[193] M. D. Bramson. Maximal displacement of branching Brownian motion. *Commun. Pure Appl. Math.*, 31:531–581, 1978.

[194] A. K. Gupta and S. S. Ray. On the solutions of fractional Burgers Fisher and generalized Fishers equations using two reliable methods. *Int. J. Math. Math. Sci.*, 2014:68291, 2014.

[195] P. Veeresha, D. G. Prakasha, and H. M. Baskonus. Novel simulations to the time-fractional Fisher's equation. *Math. Sci.*, 13:33–42, 2019.

[196] M. M. A. Qurashi, Z. Korpinar, D. Baleanu, and M. Inc. A new iterative algorithm on the time-fractional fisher equation: Residual power series method. *Adv. Mech. Eng.*, 9: 1–8, 2017.

[197] S. S. Ray. The comparison of two reliable methods for the accurate solution of fractional Fisher type equation. *Eng. Comput.*, 34:2598–2613, 2017.

[198] A. Secer and M. Cinar. A jacobi wavelet collocation method for fractional Fisher's equation in time. *Thermal Sci.*, 24:S119–S129, 2020.

[199] X. D. Zhang, Y. N. He, L. L. Wei, B. Tang, and S. L. Wang. A fully discrete local discontinuous Galerkin method for one-dimensional time-fractional Fisher's equation. *Int. J. Comput. Math.*, 91:2021–2038, 2014.

[200] A. Majeed, M. Kamran, M. Abbas, and J. Singh. An efficient numerical technique for solving time fractional generalized Fisher's equation. *Front. Phys.*, 8:293, 2020.

[201] X. Qin, X. Yang, and P. Lyu. A class of explicit implicit alternating difference schemes for generalized time fractional fisher equation. *AIMS Math.*, 6:11449–11466, 2021.

[202] P. Roul and V. Rohil. A high order numerical technique and its analysis for nonlinear generalized Fisher's equation. *J. Comput. Appl. Math.*, 406(11404):7, 2022.

[203] A. Chen and C. Li. A novel compact ADI scheme for the time-fractional subdiffusion equation in two space dimensions. *Int. J. Comput. Math.*, 93:889–914, 2016.

[204] X. R. Lu, G. H. Gao, and Z. Z. Sun. Finite difference schemes for the fourth-order parabolic equations with different boundary value conditions. *Numer. Methods Partial Differential Equations*, 39:447–480, 2023.

[205] S. Chen, F. Liu, P. Zhuang, and V. Anh. Finite difference approximations for the fractional Fokker-Planck equation. *Appl. Math. Model*, 33:256–273, 2009.

[206] Q. Zhang and C. Zhang. A compact difference scheme combined with extrapolation techniques for solving a class of neutral delay parabolic differential equations. *Appl. Math. Lett.*, 26:306–312, 2013.

[207] A. Samarskii and B. Andreev. *Finite Difference Methods for Elliptic Equation*. Science Press, Beijing, 1984.

[208] Z. Sun. *The Numerical Methods for Partial Differential Equations*. Science Press, Beijing, 2005.

[209] Q. Zhang and C. Zhang. A new linearized compact multisplitting scheme for the nonlinear convection-reaction-diffusion equations with delay. *Commun. Nonlinear Sci. Numer. Simul.*, 18:3278–3288, 2013.

[210] J. M. Holte. Discrete Gronwall lemma and applications. *In MAA-NCS meeting at the University of North Dakota*, 24:1–7, 2009.

[211] A. J. Lotka. *Elements of physical biology*. Williams and Wilkins, USA, 1925.

[212] V. Volterra. Variazioni efluttuazioni del numero di individui in specie animali conviventi. *In: Memoria della Reale Accademia Nazionale dei Lince*, pages 31–113, 1927.

[213] B. Chakraborty and N. Bairagi. Complexity in a prey-predator model with prey refuge and diffusion. *Ecol. Complex*, 37:11–23, 2019.

[214] B. Mukhopadhyay and R. Bhattacharyya. Effects of harvesting and predator interference in a model of two-predators competing for a single prey. *Appl. Math. Model.*, 40: 3264–3274, 2016.

[215] C. C. Wu. The spreading speed for a predator-prey model with one predator and two preys. *Appl. Math. Lett.*, 91:9–14, 2019.

[216] A. Das and G. P. Samanta. Stochastic prey-predator model with additional food for predator. *Phys. A: Stat. Mech. Appl.*, 512:121–141, 2018.

[217] H. I. Freedman. *Deterministic Mathematical Models in Population Ecology: pure applied mathematics: a series of monographs and textbooks*. Marcel Dekker, New York, 1980.

[218] S. N. Raw, P. Mishra, R. Kumar, and S. Thakur. Complex behavior of prey-predator system exhibiting group defense: A mathematical modeling study. *Chaos Solit. Fractals*, 100:74–90, 2017.

[219] G. Buffoni, A. Griffa, Z. Li, and Mottoni P. d. Spatially distributed communities: the resource-consumer system. *J. Math. Bio.*, 33:723–743, 1995.

[220] G. Li, W. Wang, K. Wang, and Z. Jin. Dynamic behavior of a parasite-host model with general incidence. *J. Math. Anal. Appl.*, 331:631–643, 2007.

[221] A. Q. Khan, J. Ma, and D. Xiao. Bifurcations of a two-dimensional discrete time plant-herbivore system. *Commun. Nonlinear Sci. Numer. Simul.*, 39:185–198, 2016.

[222] A. Akgul and M. Modanli. Crank-nicholson difference method and reproducing kernel function for third order fractional differential equations in the sense of Atangana-Baleanu Caputo derivative. *Chaos Solit. Fractals*, 127:10–16, 2019.

[223] H. Tajadodi. A numerical approach of fractional advection-diffusion equation with Atangana-Baleanu derivative. *Chaos Solit. Fractals*, 130(10952):7, 2020.

[224] E. Bas and R. Ozarslan. Real world applications of fractional models by Atangana-Baleanu fractional derivative. *Chaos Solit. Fractals*, 116:121–125, 2018.

[225] W. Gao, B. Ghanbari, and H. M. Baskonus. New numerical simulations for some real world problems with Atangana-Baleanu fractional derivative. *Chaos Solit. Fractals*, 128:34–43, 2019.

[226] K. Diethelm, R. Garrappa, A. Giusti, and M. Stynes. Why fractional derivatives with nonsingular kernels should not be used. *Fract. Calc. Appl. Anal.*, 23:610–634, 2020.

[227] N. J. Ford and J. A. Connolly. Comparison of numerical methods for fractional differential equations. *Commun. Pure Appl. Anal.*, 5:289–307, 2006.

[228] M. S. Tavazoei. Comments on stability analysis of a class of nonlinear fractional-order systems. *IEEE Trans. Circ. Syst.*, 56:519–520, 2009.

[229] M. S. Tavazoei, M. Haeri, S. Bolouki, and M. Siami. Stability preservation analysis for frequency-based methods in numerical simulation of fractional-order systems. *SIAM J. Numer. Anal*, 47:321–328, 2008.

[230] K. Diethelm and J. Ford. Numerical solution of the Bagley-Torvik equation. *BIT Numer. Math.*, 42:490–507, 2002.

[231] N. Attia, A. Akgul, D. Seba, and A. Nour. An efficient numerical technique for a biological population model of fractional order. *Chaos Solit. Fractals*, 141(11034):9, 2020.

[232] E. Gokmen. A computational approach with residual error analysis for the fractional-order biological population model. *J. Taibah Univ.*, pages 218–225, 2021.

[233] J. J. Anagnost and C. A. Desoer. An elementary proof of the Routh-Hurwitz stability criterion. *Circuits Syst. Signal Process*, 10:101–114, 1991.

[234] M. Gopal. *Control Systems: Principles and and Design, 2nd edn*. Tata McGraw-Hill, New Delhi, 2002.

[235] K. Diethelm. Efficient solution of multi-term fractional differential equation using $P(EC)^m E$ methods. *Computing*, 71:289–307, 2003.

List of research publications

Journal Publications

1. R. Choudhary, S. Singh, D. Kumar, A second-order numerical scheme for the time-fractional partial differential equations with a time delay, Comput. Appl. Math., 41 (2022), 114.

2. R. Choudhary, S. Singh, D. Kumar, A high-order numerical technique for generalized time-fractional Fisher's equation, Math. Methods Appl. Sci. , 46 (2023), 16050-–16071.

3. R. Choudhary, D. Kumar, Collocation-based numerical simulation of fractional order Allen–Cahn equation, J. Math. Chem. , (2023), https://doi.org/10.1007/s10910-023-01525-0.

4. R. Choudhary, D. Kumar, Numerical solution of linear time-fractional Kuramoto-Sivashinsky equation via quintic B-splines, Int. J. Comput. Math. , (2023), 1–20.

5. S. Singh, R. Choudhary, D. Kumar, An efficient numerical technique for two-parameter singularly perturbed problems having discontinuity in convection coefficient and source term, Comput. Appl. Math., 42 (2023), 62.

6. R. Choudhary, D. Kumar, S. Singh, Second-order convergent scheme for time-fractional partial differential equations with a delay in time, J. Math. Chem. , 61 (2023), 21–46.

7. K. Deswal, R. Choudhary, D. Kumar, Modified Atangana-Baleanu Caputo Operator for Time-Fractional Kuramoto-Sivashinsky Equation via Quintic B-Splines, J. Comput. Nonlinear Dynam. , (2023), 1–19, https://doi.org/10.1115/1.4063554,

8. R. Choudhary, S. Singh, P. Das, D. Kumar, A higher-order stable numerical approximation for time-fractional non-linear Kuramoto-Sivashinsky equation based on quintic $\mathfrak{B}$-spline, **Math. Methods Appl. Sci.** (Accepted).

9. R. Choudhary, S. Singh, D. Kumar, A higher-order stable numerical approximation for time-fractional non-linear Kuramoto-Sivashinsky equation based on quintic $\mathfrak{B}$-spline. **Comput. Appl. Math.**(Accepted)

10. R. Choudhary, D. Kumar, A numerical method for solving the fractional-order predator-prey model. **(Communicated)**

Conferences /Workshops attended

Conferences

1. International conference on dynamical system, control and their applications, IIT Roorkee, 2022. **(Presented)**

2. 5th International conference on mathematical modelling, applied analysis and computation-2022 organized by department of Mathematics, Faculty of science, JECRC University, Jaipur (Raj.), 2022. **(Presented)**

3. International Conference on differential equations and control problems organized by department of School of mathematics & Statics science, IIT Mandi, 2023. **(Presented)**

Biography of the Candidate

Ms. Renu Choudhary has a B.Sc. (Honours) and an M.Sc. in Mathematics from Raj Rishi Government College Alwar, Rajasthan, India. She began working as a full-time Ph.D. student at the Department of Mathematics at Birla Institute of Technology and Science (BITS) Pilani, India, in 2020, under the supervision of Prof. Devendra Kumar. Her research interests include numerical methods for linear, and nonlinear fractional-order partial differential equations. She is also researching PDEs with single perturbations. She has worked as a mathematics teaching assistant at BITS Pilani's Pilani Campus. `scholar.google.com` has more information on her research efforts. `p20200048@pilani.bits-pilani.ac.in` is how to reach her.

Biography of the Supervisor

Prof. Devendra Kumar is the current head and professor of the Department of Mathematics at the Pilani campus of Birla Institute of Technology and Science. He received his Ph.D. from the Indian Institute of Technology, Kanpur's Department of Mathematics. His research interests include numerical methods for initial/boundary value problems for ordinary differential equations, partial differential equations, delay/advanced differential equations, singularly perturbed problems, fractional-order differential equations, fractional-order partial differential equations, etc.

More on his research contributions can be found at `https://www.bits-pilani.ac.in/pilani/dkumar/Profile`. Contact him at `dkumar@pilani.bits-pilani.ac.in`.